BIOOXIDATION OF SULFIDE-BASED REFRACTORY GOLD ORES AT LOW TEMPERATURE

MOHAMMAD HOSSEIN KARIMI DARVANJOOGHI

A DISSERTATION SUBMITTED TO THE
FACULTY OF GRADUATE STUDIES IN
PARTIAL FULFILLMENT OF THE
REQUIREMENTS FOR THE DEGREE OF
DOCTOR OF PHILOSOPHY

GRADUATE PROGRAM IN CIVIL
ENGINEERING YORK UNIVERSITY TORONTO,
ONTARIO

June 2025

ABSTRACT

Gold recovery from iron-sulfide-bearing refractory ores presents significant challenges, particularly at low temperatures where traditional pretreatment methods, such as microbial biooxidation, exhibit reduced efficiency. This research systematically investigates and compares two biooxidation strategies—microorganism-assisted biooxidation using *Ferroplasma acidiphilum* and an enzymatic biooxidation technology (EnBiTe) based on glucose oxidase (GO) immobilization—to enhance gold liberation from refractory ores. Bench-scale experiments demonstrated that microbial biooxidation achieved optimal pyrite dissolution (~75%) under controlled conditions, including a 15-day operating time, a pyrite content of 7.2 wt.%, and a pH of 1.47. However, microbial oxidation efficiency significantly decreased at temperatures below 10°C due to the metabolic limitations of acidophilic microorganisms. To mitigate these limitations, extracellular polymeric substances (EPS) overproduction was induced through monosaccharide supplementation, with D-sucrose yielding the highest ferric ion production and pyrite dissolution. Despite these improvements, the microbial biooxidation approach remained highly sensitive to environmental fluctuations and required precise control of pH, aeration, and nutrient availability to maintain microbial activity, making it less viable for cold-climate applications. Moreover, machine learning models, including Artificial Neural Networks (ANN) and Genetic Programming, were employed to predict biooxidation efficiency based on key parameters such as time, pH, oxidation-reduction potential (ORP), pyrite content, and monosaccharide concentrations. To address the limitations of microbial biooxidation in low-temperature environments, enzymatic biooxidation technology (EnBiTe) was developed as an alternative pretreatment strategy. This method employed glucose oxidase (GO) immobilized on modified sawdust to catalyze the oxidative dissolution of pyrite and arsenopyrite, thereby liberating encapsulated gold. The process optimization study revealed that EnBiTe achieved up to 89.2% pyrite dissolution for high-grade ore and 73.4% for low-grade ore under conditions including a 100 mM glucose substrate concentration, 5 g immobilized enzyme, and a pH range of 5–6. Unlike microbial biooxidation, EnBiTe functioned effectively at low temperatures (~5–10°C) without requiring extensive aeration or pH adjustments. Furthermore, a modular enzyme system incorporating catalase (CAT) was introduced to mitigate oxidative stress and enzyme degradation, extending process stability. Column test evaluations confirmed that EnBiTe not only enhanced pyrite oxidation but also facilitated faster gold liberation, demonstrating a significant advantage over microorganism-assisted methods. The controlled enzymatic approach also reduced operational uncertainties, providing a scalable and environmentally sustainable alternative to conventional biooxidation. A comparative analysis of the two biooxidation strategies indicated that enzymatic biooxidation significantly outperformed microbial biooxidation in low-temperature conditions, achieving higher pyrite oxidation rates and gold recovery efficiencies. Cyanidation trials following biooxidation showed that gold recovery reached 90% after EnBiTe pretreatment, compared to 60% following microbial biooxidation under optimized conditions. The findings of this research establish EnBiTe as a promising alternative to microbial biooxidation for gold recovery from refractory sulfide ores, particularly in cold regions where traditional methods struggle. By offering

a more efficient, scalable, and environmentally friendly approach, this research contributes to the advancement of biohydrometallurgical processing and provides a foundation for potential industrial applications of enzymatic biooxidation in the mining sector.

Key words: Gold Recovery, Biooxidation, Low temperature, Enzymatic process, Refractory sulfide ore.

GRAPHICAL ABSTRACT

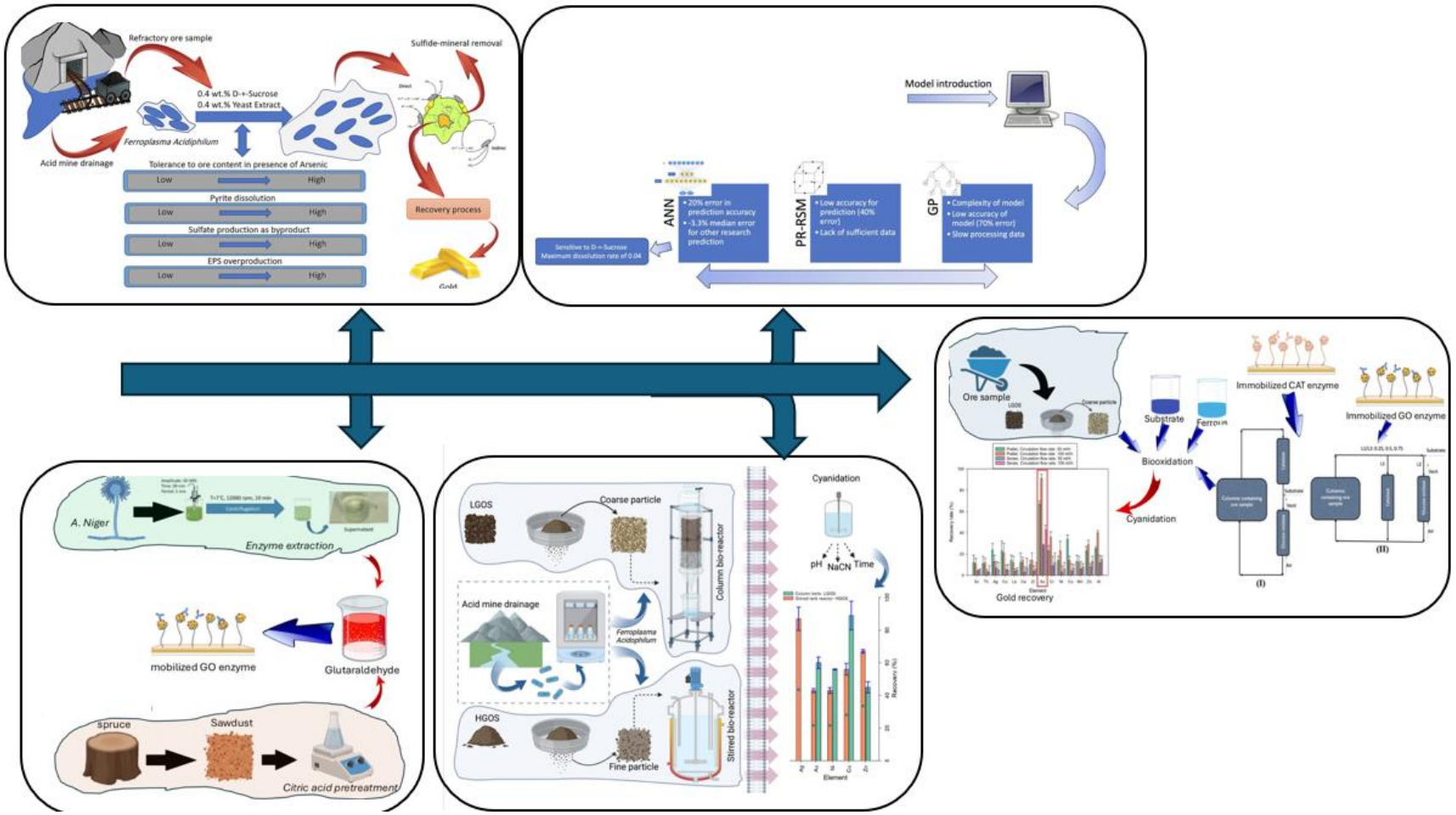

ACKNOWLEDGEMENT

First and foremost, I would like to express my deepest gratitude to my Ph.D. supervisor, Dr. Satinder Kaur Brar, for her unwavering guidance, mentorship, and support throughout this research journey. Her expertise, vision, and dedication were instrumental in shaping this work. I am equally thankful to my co-supervisor, Dr. Sara Magdouli, whose insightful feedback and continuous encouragement greatly enriched the quality of my research.

I would also like to extend my sincere thanks to the members of my supervisory committee and doctoral examination committee for their valuable time, critical insights, and constructive suggestions, which significantly contributed to the development and refinement of this thesis.

My sincere thanks to York University for providing the opportunity and academic environment to pursue this Ph.D. research. I am also grateful to the Centre Technologique des Résidus Industriels (CTRI) and Agnico Eagle for their collaboration and access to essential resources and data.

I acknowledge the generous financial support provided by Natural Sciences and Engineering Research Council of Canada (NSERC) and Mitacs Accelerate, James and Joanne Love Chair in Environmental Engineering, National Research Council Canada (NRC) without which this research would not have been possible.

A special note of appreciation to my colleagues and the members of Professor Brar's research team for their camaraderie, insightful discussions, and technical support throughout the course of this project.

Lastly, and most importantly, I am deeply thankful to my wife for her love, patience, and unwavering support during the highs and lows of this Ph.D. journey. Her encouragement has been my anchor throughout.

TABLE OF CONTENTS

LIST OF TABLES

LIST OF FIGURES

LIST OF ABBREVIATIONS

Abbreviation	Meaning
ABTS	2,2′-azino-bis(3-ethylbenzothiazoline-6-sulfonic acid)
AIC	Akaike Information Criterion
ATP	Adenosine triphosphate
AMD	Acid Mine Drainage
ANN	Artificial Neural Network
ANOVA	Analysis of variance
CAT	Catalase
CIP	Carbon in Pulp
CIL	Carbon in Leach
CLSM	Confocal Laser Scanning Microscope
D-F	D-(+)-Fructose
D-G	D-(+)-galactose
D-S	D-(+)-Sucrose
DO	Dissolved oxygen
EDTA	Ethylenediaminetetraacetic Acid
EnBiTe	Enzymatic Biooxidation Technology
EPS	Extracellular Polymeric Substances
FPI	Fluorescence Propidium Iodide
FWGA	Fluorescence Wheat Germ Agglutinin
FOP	Ferric Ions Production
FTIR	Fourier Transform Infrared Spectroscopy
GDP	Gross Domestic Product
GHG	Greenhouse gases
G3P	Glyceraldehyde-3-phosphate
GP	Genetic programming
GO	Glucose oxidase
HGOS	High grade ore sample
HPC	High pyrite concentration
HRP	Horseradish peroxidase
ICP	Inductive Couple Plasma
LCA	Life Cycle Analysis
LGOS	Low Grade Ore Sample
LPC	Low pyrite concentration
MP-AES	Microwave Plasma Atomic Emission Spectroscopy
NADPH	Nicotinamide adenine dinucleotide phosphate
OC	Ore content (%)
ORP	Oxidation-Reduction Potential
OS	Ore Sample
PC	Pyrite content (%)
PR-RSM	Polynomial Regression informed by Response Surface Methodology

RMSE	Root means square error
rpm	Revolutions per minute
RuBisCO	Ribulose-1,5-bisphosphate carboxylase/oxygenase
3PGA	3-phospho glycerate
XRD	X-ray Diffraction
XRF	X-ray Fluorescence
SEM	Scanning Electron Emission
TEA	Technoeconomic Analysis
TDI	Total dissolved iron (ppm)
YE	Yeast Extract

LIST OF PARAMETERS

Parameter	Definition
K_{la}	Mass Transfer Coefficient in Liquid
QP	Production rate (mg/l.h)
ϕ	Ore sample weight fraction (%)
ξ	Dimensionless parameter
N	Parameter
X	Transformed dimensionless input parameter
Y	Transformed dimensionless input parameter
$e1$	Pyrite dissolution model error %
$e2$	Ferric concentration model error %
k	Reaction kinetic constant l/mol.s
A	Ratio of active days to inactive days
Subscriptions	
min	minimum
max	maximum
exp	experimental

Chapter 1: Introduction

1.1. Overview

Biotechnology offers promising options to recover desired precious metal such as gold from refractory ores and complex structures (Karimi Darvanjooghi et al., 2024a; Kumar & Yaashikaa, 2020; Martell-Nevárez et al., 2025). There are wide range of precious metals and compounds which is needed to be recovered by using biotechnological methods for minimizing the environmental impacts and operational costs (Mohanty et al., 2017a, 2017b; Sanket et al., 2017; Ghosh et al., 2018). Among them, gold is usually disseminated in fine flakes (called placers), metal alloy with tellurium (Te, known as telluride), iron sulfide structures having a very small-sized of flakes (near to 500 to 200 micron), and arsenic pyrite (arsenic sulfide) (Karthikeyan et al., 2015). This metal is found also in the macron-size particle within the other sulfides-based minerals (such as marcasite, tetrahedrite sulfosalts, and sphalerite), chalcedony, sericite (in forms of silicate minerals, dolomite, calcite, barite, ankerite, gypsum), and carbonaceous matters (Haque, 1992; Olson & Clark, 2008). Accordingly, the abundance of gold and the geochemical structure of ores influence the recovery (Karthikeyan et al., 2015; Martell-Nevárez et al., 2025). To efficiently extract gold from various minerals structures, full knowledge about the mineralogical properties of ores in combination with minerals' particle size as well as the presence of alloy in minerals, cyanides consumers structures (including enargite, carbonaceous materials and clay deposits oxygen consumers especially preg-robbers materials in refractory mineral gold ores) is strongly required (J. Y. Zhou & Cabri, 2004).

Besides, conventional methods including cyanidation, pyrometallurgy, roasting, pressure oxidation are energy-consuming and present a potential source of greenhouse gases (GHG) emissions and environmental damage (Zolfaghari et al., 2020). Thus, biotechnology is recognized to be a sustainable, green method to extract metals from polymetallic (Garrido-Cardenas et al., 2020) and aligns with developed countries' action plan on climate change to reduce GHG emissions by 40-45%. Harnessing the abilities of some species of prokaryotic microorganisms to catalyze the oxidative dissolution of sulfide minerals (Olson, 1994; Olson et al., 2006; Olson & Clark, 2008) and to facilitate the extraction of metals is promising. The research currently focuses on the development of microbial consortia to carry out this biological process.

The biological oxidation of minerals has been established as a commercially viable primary treatment method for recovering gold trapped in sulfidic ores. Biooxidation can be implemented through two main approaches: stirred tank reactors or heap systems irrigated with an oxidizing solution containing minerals, bacteria, and supplemented with aeration to promote microbial activity (Burbank et al., 1990; Run & Clark, 2004a). For low-grade sulfide ores, heap biooxidation using microorganisms is particularly cost-effective. However, this method introduces operational complexities. Key to optimizing sulfide mineral oxidation is the regulation of bacterial growth across temperature ranges and the fine-tuning of parameters such as irrigation and aeration rates. Successful biooxidation relies on several critical factors: (i) transport of aqueous species within ore particles, (ii) transport, attachment, growth, and catalytic activity of microbial populations, (iii) oxygen and water transport through the ore bed, and (iv) efficient mass and heat transfer. Central to the process is maintaining high biological activity of selected microbes to enhance metal solubilization (Karimi Darvanjooghi et al., 2024a).

Chapter 2: Literature review*

(*some part extracted from these two published reviews)

*Mohammad Hossein Karimi Darvanjooghi, Sara Magdouli, Satinder Kaur Brar, Hadi Abdollahi, Mehdi Zolfaghari, *Geomicrobiology Journal* 39.3-5 (2022): 399-415.

*Mohammad Hossein Karimi Darvanjooghi, Sara Magdouli, Satinder Kaur Brar, Hadi Abdollahi, Mehdi Zolfaghari, *World Journal of Microbiology and Biotechnology* 40-67 (2024): 1-18.

Abstract

Biomining through bioleaching and biooxidation aims at recovering desired metals at the required specifications with lower environmental impact and costs from ores and waste streams. Research and developments related to the process technology and efficient implementation of this approach are advanced worldwide. Small particles of gold, a metal of higher interest, are mostly found in a matrix of sulfide-based mineral and not affordably recovered with conventional approaches encompassing cyanidation, pyrometallurgy, extreme heating (roasting), oxidation of ore sample at high pressure. Recently, advances in biooxidation have been made in addressing scientific and technical challenges that arise during the pilot and demonstration scales in the operations units in bioreactors and heaps. By incorporating high-throughput bacterial growth data and process understanding of the extraction and recovery approaches, the biooxidation becomes more economically feasible and efficient. More advancements are necessary to evaluate the wide-range of mineralogical structure of ores being processed, microbiological, and physicochemical that can significantly influence the biooxidation reaction within the different types of reactors (heap and continuously stirred tank reactors), the microbial interactions between metal and microbes, geographical localizations of mining sector, economic as well as data interpretation by using advanced artificial intelligence methods toward obtaining optimized operation and efficiency. This literature review covers important advances and developments and associated industrial and academic research and challenges from the past few years for the gold ore biooxidation.

2.1. Introduction

The global approach toward growth and development of industries is driving the increase in demand for precious metals such as gold (M. Qin et al., 2023). Furthermore, the global gold reserves of ore types that can be processed more facilely are becoming exhausted (Oktay et al., 2016). Complex ore deposits or abandoned mine waste piles and other residues have all received a lot of attention recently in this context toward enhanced recovery (Schneider & Greenberg, 2023). To properly utilize such ores and resources effectively and sustainably, efficient metal recovery techniques must be devised. Microorganism-assisted extraction, called "biohydrometallurgy", is a promising alternative method in this field. The "biohydrometallurgy" technique has many advantages over traditional extractive technologies, including less capital investment particularly for low-grade gold ores, less energy and labor utilization, and fewer adverse impacts on the environment (Schippers, 2007; Naseri et al., 2022; Chaerun et al., 2023). This process covers both the mineral's "bioleaching" and "biooxidation" operations (M. Chen & Schlömann, 2022; Saldaña et al., 2023).

Microorganisms-aided leaching processes have improved significantly over the last few years, with two primary process types including irrigation-type procedure which involves in situ, dump, heap, and vat leaching processes and stirred tank-type processes for utilization of high-grade ore containing the desired metal (Aylmore & Muir, 2001; M. Chen & Schlömann, 2022; Saldaña et al., 2023; Karimi Darvanjooghi et al., 2025). Both methods of leaching have been studied thoroughly and advanced in both laboratory and pilot scales (Saldaña et al., 2023). The extraction of gold from refractory (resistive) resources including complicated polymetallic concentrates, low-grade ores, and different oxides has been a significant challenge for biohydrometallurgy processes. These available ore types, which are mostly categorized as refractory ore, must be tailored to the bioleaching processes operation as they are not processed using conventional methods such as cyanidation (Darvanjooghi et al., 2021).

Gold is found in sulfide mineral phases such as pyrite, pyrrhotite, arsenopyrite, and chalcopyrite in refractory concentrates and these structures reduce the efficiency of the gold extraction process by direct cyanidation. Refractory concentrates can first be pretreated using a wide range of methods, one of which is the biooxidation process. Acidophile oxidant

microorganisms degrade the iron-sulfide matrix (by oxidizing iron or sulfide) and liberate the gold for cyanidation, enabling a greater level of gold recovery (J. Wang et al., 2021).

Therefore, this review discusses the key methods of biooxidation from lab to pilot scale with a major focus on various parameters (majorly related to biological, operational, mineralogical factors) and challenges to consider for efficient industrial-scale operation in heaps and stirred tank reactor for the extraction of gold-bearing sulfide ores.

2.2. Biooxidation: Current status, pros and cons

Microorganisms play a significant role in oxidizing metal sulfide compounds such as Fe_2S and sulfur-based molecules leading to the production of ferric iron and protons. The produced compounds are categorized as bio-agents that easily attack the sulfide matrix. In this method of microbial extraction, microorganisms are allowed to grow in a medium that should be effectively aerobic and highly or moderately acidic containing only inorganic compounds (Bonnefoy & Holmes, 2012; Ghosh & Das, 2018; Johnson, 2008; Kimura et al., 2011; Martinez et al., 2015; Mohanty et al., 2018). Acidophilus are mesophilic types that grow at temperatures ranging from 20 to 40℃, while moderately thermophilic microorganisms are active at a temperature range of 40-60℃, and extremely thermophilic bacteria grow at a temperature higher than 60℃ (Johnson, 2008; Kimura et al., 2011; Bonnefoy & Holmes, 2012; Martinez et al., 2015). List of common bacteria reported in the biooxidation of sulfur minerals as well as their biological activity are presented in **Table 2.1**. Although a wide range of microorganisms have been used for biooxidation and their performance has been investigated under different operating conditions, there is still a gap between the incorporated mechanisms as well as other external and internal factors. It has been reported that the effect of the addition of external compounds such as ions: Ag^{+}, Bi^{3+}, Co^{2+}, Hg^{2+}, NO^{3-}; surfactants: tween 80, tween 20, emulsifier OP have significant influence on the biooxidation rates. Normally, these factor and parameters are responsible for EPS production which influence the biooxidation rates positively. Some of these metal ions also can influence solubility of minerals in the media and influence the solubility of sulfide-based structures such as pyrite and arsenopyrite. They operate through cooperative mechanisms in combination with biooxidation, however their excess amount will decrease the biooxidation efficiency due to their inhibition properties (Deng et al., 2000; Liu et al., 2020; Saavedra et al., 2020). Effect of carbon

sources such as D-galactose, humic acid, and yeast extract has been studied on the biooxidation of ore sample in the presence of the mixture of different types of iron and sulfur-oxidizing bacteria (A. G. Bulaev, 2020a; Saavedra et al., 2020; D. Zhang et al., 2020). *Sulfobacillus thermosulfidooxidans* VKMB1269T, *Acidithiobacillus caldus* MBC-1, and *Acidiplasma sp.* MBA-1 were used to investigate the effect of yeast extract on the biooxdiation rate and performance. The results disclosed that the maximum biooxidation rate (~2.0%/day) for *S. thermosulfidooxidans* VKMV 1269T with the regular addition of carbon source (to keep its content at 0.02% at the first, 10th and 20th day) (A. G. Bulaev, 2020a). Furthermore, addition of humic acid modifies the surface's chemical and physical properties of ore sample (such as arsenopyrites) and influence the immobilization of produced ions such as iron and arsenic by speciation of the bacteria. Indeed, humic acid will be adsorbed by the bacteria's membrane, and this leads to the enhanced arsenic and jarosite uptake which increases the biooxidation rate and performance (D. Zhang et al., 2020; Yadollahi et al., 2021). The addition of D-galactose was investigated and the results indicated that it could affect extracellular polymeric substances (EPS) production of acidophilic (*At. ferrooxidans*) which is responsible for the enhanced biooxidation rate and the microorganism's tolerance to a high concentration of ferric ions (Saavedra et al., 2020).

In general, the biooxidation is often based on two different mechanisms of "direct" or "indirect" (Tributsch, 2001), which can be involved simultaneously (schematic mechanism is depicted in Appendix A **Fig.A1**). Also, galvanic corrosion, which is due to the electronic dissolution process mediated by bacteria (Appendix A **Fig.A2**), should be considered during biooxidation as well (Ballester et al., 2007; Ahmadi et al., 2012). Taken all together, the mechanisms are controversial. Other physical-mechanisms might also occur in addition to the chemical-biooxidation reactions involved in the metal sulfides microbial-assisted oxidation and should be well studied. For instance, the formation of mineral-precipitation that might cover the surface of minerals particles preventing the mass transfer has to be also overcome. Therefore, it is conclusively evident that the reaction rate is reduced due to the increase in resistance of reactants while mass transfer and products resulted from the interface between solid and liquid phases.

Table 2.1. Acidophilic microorganisms studied for biooxidation.

Type of microorganisms	Operation type	Temperature (℃)	Range of pH	Nutrition system	Ability for oxidation of MS‡-pyrite, MS‡, Fe^{2+}, S				References
Archaea									
Sulfolobus metallicus	Stirred Bio-Reactor	50-75 (65)*	1.0-4.5 (2.0-3.0)*	Autotroph	✓	✓	✓	✓	(Vera et al., 2013; Johnson, 2014)
Metallosphaera hakonensis	Stirred Bio-Reactor	50-80 (70)*	1-4 (3)*	Autotroph (facultative)	N.R.	✓	N.R.	✓	(Bromfield, 2011; Counts, 2019; Ghadiri et al., 2019; Sajjad et al., 2019a; Shiers et al., 2013)
Metallosphaera prunae	Stirred Bio-Reactor	55-80 (75)*	1-4.5 (2-3)*	Autotroph (facultative)	✓	✓	✓	✓	(Akcil & Gahan, 2015; Castro et al., 2023a; Norris, 1997; Panda, Mishra, et al., 2015; Vera et al., 2013)
Rawlings *Metallosphaera sedula*	Stirred Bio-Reactor	50-80 (75)*	1-4.5 (2-3)*	Autotroph (facultative)	✓	✓	✓	✓	(Brandl, 2001a; Rawlings, 2002a; Run & Clark, 2004b; Schippers, 2007b; Vera et al., 2013)
Ferroplasma acidiphilum	Stirred Bio-Reactor	15-45 (35)*	1.3-2.2 (1.7)*	Autotroph (facultative)	✓	N.R.	✓	✕	(Golyshina et al., 2000a; Golyshina & Timmis, 2005; Schippers, 2007c; Vera et al., 2013)
Acidianus infernus	Stirred Bio-Reactor	65-96 (90)*	1.0-5.5 (2.0)*	Autotroph	✓	✓	✓	✓	(Brandl, 2001a; Johnson, 2014; Rawlings, 2002a; Schippers, 2007c; Schippers et al., 2010; Segerer et al., 1986)
Sulfolobus yangmingensis	Stirred Bio-Reactor	65-95 (80)*	2.0-6.0 (4)*	Autotroph (facultative)	N.R.	✓	N.R.	✓	(Salo-Zieman et al., 2006; R. Zhang, 2016)
Sulfurococcus mirabilis	Stirred Bio-Reactor	50-86 (70-75)*	1.0-5.8 (2.0-2.6)*	Autotroph (facultative)	✓	✓	✓	✓	(Akcil & Gahan, 2015; Sajjad et al., 2019a; Schippers, 2007c; Vera et al., 2013)
Acidianus brierleyi	Stirred Bio-Reactor	45-75 (70)*	1.0-6.0 (1.5-2.0)*	Autotroph (facultative)	✓	✓	✓	✓	(C. L. Brierley & Brierley, 1973; Konishi et al., 1995, 1997; Larsson et al., 1990; Segerer et al., 1986)
Sulfurococcus yellowstonensis	Stirred Bio-Reactor	40-80 (60)*	1.0-5.5 (2.0-2.6)*	Autotroph (facultative)	✓	✓	✓	✓	(Duku, 2011a; Hallberg & Johnson, 2001; Sadowski & Pawlowska, 2018)
Bacteria									
Acidimicrobium ferrooxidans	Stirred Bio-Reactor	<30-55 (45-50)*	2.0 (2.0)*	Autotroph (facultative)	✓	N.R.	✓	✕	(Brandl, 2001b; D. A. Clark & Norris, 1996; Johnson, 2006, 2014; Norris, 2007a; Run & Clark, 2004b)
Leptospirillum ferrodiazotrophum	Stirred Bio-Reactor	N.R. (37)*	N.R. (1.2)*	Autotroph	N.R.	✓	N.R.	N.R.	(Akcil & Gahan, 2015; Mazuelos et al., 2012; Norris, 2007a; A. K. Vardanyan et al., 2013; X. Yuan et al., 2013)
Leptospirillum ferrooxidans	Stirred Bio-Reactor	(28-30)*	1.3-4.0 (1.5-3.0)*	Autotroph	✓	✓	✓	✕	(B. J. Baker & Banfield, 2003; Boon & Heijnen, 1998a; Brandl, 2001a; Johnson, 2006)
Caldibacillus ferrivorus	Stirred Bio-Reactor	35-55 (45)*	N.R. (1.8)*	Autotroph (facultative)	✓	N.R.	✓	✓	(Zahari et al., n.d.)
Sulfobacillus thermotolerans	Stirred Bio-Reactor	20-60 (40)*	1.2-5.0 (2.0-2.5)*	Autotroph (facultative)	✓	✓	✓	✓	(M. Muravyov & Panyushkina, 2020; Rathna & Nakkeeran, 2020; B. Wu et al., 2020a)

Ferrimicrobium acidiphilum	-	<37 (35)*	1.3-4.8 (2.0-2.5)*	Heterotroph	✓	N.R.	✓	✕	(Johnson, 2007; Norris, 2007b; Okibe et al., 2003; Run & Clark, 2004b; Schippers, 2007c; Vera et al., 2013)
Acidithiobacillus caldus	Stirred Bio-Reactor	32-52 (45)*	1.0-3.5 (2.0-2.5)*	Autotroph (facultative)	✕	✓	✕	✓	(Brandl, 2001a; Hallberg & Lindström, 1994; Johnson, 1998a; Norris, 2007a; Rawlings, 2002a, 2005; Schippers, 2007c; Schippers et al., 2010)
Sulfobacillus montserratensis	Stirred Bio-Reactor	<30-43 (37)*	0.7-2.0 (1.6)*	Autotroph (facultative)	✓	N.R.	✓	✓	(Bampole & Mulaba-Bafubiandi, 2020; A. G. Bulaev, 2020b)
Alicyclobacillus tolerans	-	<20-55 (37-42)*	1.5-5.0 (2.5-2.7)*	Autotroph (facultative)	✓	✓	✓	✓	(Brandl, 2001a; Johnson, 1998b; Karavaiko et al., 2005; Kovalenko & Malakhova, 1983; Rawlings, 2002a; Schippers, 2007c)
Acidithiobacillus ferrooxidans	Stirred Bio-Reactor	10-37 (30-35)*	1.3-4.5 (1.8-2.5)*	Autotroph	✓	✓	✓	✓	(Colmer & Hinkle, 1947; Fowler et al., 1999, 2001; Kelly & Wood, 2000; Krebs et al., 1997)
Acidithiobacillus albertensis	Stirred Bio-Reactor	(25-30)*	2.0-4.5 (3.5-4.0)*	Autotroph	✕	✓	✕	✓	(Banerjee et al., 2017; Dave & Tipre, 2019; FAZZINI & VALDECANTOS, 2016)
Sulfobacillus acidophilus	Stirred Bio-Reactor	<30-55 (45-50)*	(2.0)*	Autotroph (facultative)	✓	✓	✓	✓	(Brandl, 2001a; Johnson, 1998b; Norris et al., 1996; Rawlings, 2002a; Schippers, 2007c; Schippers et al., 2010)
Leptospirillum ferriphilum	Stirred Bio-Reactor	<45 (30-37)*	(1.3-1.8)*	Autotroph	✓	✓	✓	✕	(W. E. Baker, 1973; Coram & Rawlings, 2002; Okibe et al., 2003)
Sulfobacillus sibiricus	Stirred Bio-Reactor	17-60 (55)*	1.1-3.5 (2.2-2.5)*	Autotroph (facultative)	✓	✓	✓	✓	(S.-Y. Chen & Cheng, 2019; Christel et al., 2018)
Alicyclobacillus disulfidooxidans	Stirred Bio-Reactor	4-40 (35)*	0.5-6.0 (1.5-2.5)*	Autotroph (facultative)	✓	N.R.	✓	✓	(FAZZINI & VALDECANTOS, 2016; Kondrat'eva et al., 2012; Panda, Akcil, et al., 2015)
Acidithiobacillus thiooxidans	Stirred Bio-Reactor	10-37 (28-30)*	0.5-5.5 (2.0-3.0)*	Autotroph	✕	✓	✕	✓	(Bacelar-Nicolau & Johnson, 1999; Norris, 2007a; Rawlings, 2002a; Schippers, 2007c; Schippers et al., 2010; Vera et al., 2013)
Sulfobacillus thermosulfidooxidans	Stirred Bio-Reactor	20-60 (45-48)*	1.5-5.5 (2.0)*	Autotroph (facultative)	✓	✓	✓	✓	(D. A. Clark & Norris, 1996; Johnson, 1998b; Rawlings, 2002a; Run & Clark, 2004b; Schippers, 2007c; Schippers et al., 2010; Vera et al., 2013)
Sulfobacillus thermosulfidooxidans	Stirred Bio-Reactor	20-60 (45-48)*	1.5-5.5 (2.0)*	Autotroph (facultative)	✓	✓	✓	✓	(A. G. Bulaev, 2020b; M. Muravyov & Panyushkina, 2020; Noguchi & Okibe, 2020; Shen et al., 2020)

*Optimum operating condition
‡ Metal sulfide
N.R.: Not reported

The tendency of bacteria for attaching to the surface of sulfide-based mineral as well as the temperature fluctuation should be studied further for understanding the biooxidation mechanism and effects of different variables on its efficiency. For instance, EPS play an important role in biooxidation (Sand et al., 2001; Rawlings, 2002) through the indirect mechanism that includes the non-contact and the contact approaches which is explained thoroughly in the supplementary information (Appendix A **Fig.A3**). These approaches are likely important in biooxidation, and a single mechanism is not sufficient to comprehend the overall reaction. Although large numbers of studies have been conducted to underline mechanisms related to the biological activity of microorganisms in the biooxidation of sulfide-based minerals, the direct reaction of biooxidation and the interaction between microbial strains with dissolved molecular oxygen is doubtful yet and needs to be profoundly investigated to better optimize the process flowsheet. Although, the ability of the fungi such as *Phanerochaete chrysosporium* for the elimination of perg-robbing compounds has been reported widely, its ability to oxidize sulfur andiron (II) is another point that can be used in direction of biooxidation (Jennings et al., 2000; Ofori-Sarpong et al., 2011; Karthikeyan et al., 2015). Indeed, these fungi produce lignin peroxidase and manganese peroxidase that are used for degrading aromatic and carbon-based materials that inhibit the gold recovery process. *P. chrysosporium* also can produce hydrogen peroxide which leads to the enhanced oxidation of sulfur andiron (II) resulting in the destruction of pyrite or arsenopyrite structures (Ofori-Sarpong et al., 2011; Karthikeyan et al., 2015).

Different types of microorganisms are used and reported as capable of handling biooxidation process. There are no comprehensive mechanisms involved in the biooxidation by acidophilic and each of them is entitled to be involved in pyrite and arsenopyrite biooxidation via different types of mechanisms (Karthikeyan et al., 2015). These mechanisms are dependent on the following factors that should be optimized to achieve the maximum biooxidation rate:

I) Microbial: diversity of the microbial population, the population density, and the microorganisms' tolerance to the metal ions concentrations.

II) Metabolic activity: enhanced and reduced production of EPS in combination with the alteration in EPS structure that leads to the efficient biooxidation.

III) Reaction parameters: pH, temperature, types and content of nutrients, ore particle size distribution, the addition of ions (cation or anion) and carbon sources, oxygen and oxidative compounds, other heavy metals that are categorized as antibacterial materials.

Till date, various processes are developed and commercialized and get in scope for various mines worldwide. In 1986, Fairview Mine in South Africa initiated the first biooxidation plant. Other countries have followed suite, such as Australia, Peru, Czech Republic, China, Brazil, Uganda, Uzbekistan and Russia, and Kazakhstan. Commercial plants of biooxidation are presented in **Table 2.2**. Remarkably, no demonstration plants or commercial units of operations are shown up in North America despite associated academic research in different research entities. The absence of industrial operations can be related to geographical and geochemical structures of ores and other climatic challenges that burden their scalability. Thus, biooxidation is inherently demanding owing to the elaborate structure of sulfide ores encompassing a complex matrix embedding the gold, equally broad in its mineralogical property. This complexity arises from the historically geochemical formations of different rocks. Besides, successful biooxidation industrial trials have been applied for high concentrate in bioreactor tanks. Conversely, pretreating gold ores within biooxidation remains a complicated task compared to the easy processing of concentrate. The data presented in **Table 2.2** indicate that most of the biooxidation can be performed stirred tank reactor. Accordingly, to make the process affordable and feasible, the concentration of both pyrite and arsenopyrite (as main precursors containing a major amount of gold), is higher than 10% on an average and high grade of gold as a result.

Table 2.2. Commercial biooxidation plants for the extraction of gold from the refractory ore (P: pyrite, AsP: arsenopyrite, PH: Pyrrhotite) (Bhakta & Arthur, 2002a; Olson et al., 2003; Rawlings et al., 2003; du Plessis et al., 2007; Logan et al., 2007; Ndlovu, 2008; C. L. Brierley & Brierley, 2013; Kaksonen et al., 2014; Darvanjooghi et al., 2021)

Mine name	Fairview	São Bento	Harbour Lights	Wiluna	Ashanti-Shansu	Youanmi	Coricancha	Beaconsfield	Chuqui-camata	Olympiada	Suzdal	Fosterville	Bogoso	Jinfeng	Kokpatas	Au quarry mine	Agnes
Country	South Africa	Brazil	Australia	Australia	Ghana	Australia	Peru	Australia	Chile	Russia	Kazakhsan	Australia	Ghana	China	Uzbekistan	USA	South Africa
Method & design	Stirred bio-reactor	Stirred bio-reactor	Stirred bio-reactor	Stirred bio-reactor	Stirred bio-reactor	Stirred bio-reactor	Stirred bio-reactor	Stirred bio-reactor	Heap (dump)	Stirred bio-reactor	Stirred bio-reactor	Stirred bio-reactor	Stirred bio-reactor	Stirred bio-reactor	Stirred bio-reactor	Heap (dump)	Heap (dump)
Ore characterization	P[1]: 28%, AsP[2]: 10%	P: 16%, AsP: 38%, PH: 46%	P: 28%, AsP: 18%	P: 37%, AsP: 22%	P: 6.5%, AsP: 17%, PH[3]: 14%	P: 43%, AsP: 5%	P: 35%, AsP: 56%	P: 54%, AsP: 10%,	P: 33%	-	P: 35%, AsP: 42%,	P: 26%, AsP: 18%	P: 52%, AsP: 2%	P: 3%, AsP: 12%, PH: 1%	P: 46%, AsP: 3%	P: 23%, AsP: 12%	P: 31%, AsP: 5%
Reactor size (m^3)	1415	1487	980	4230	21600	3000	1001	2310	-	-	-	1385	19800	18000	2340	-	-
Operational capacity (tones/day)	55	380	40	158	960	120	60	68	20,000	1000	196	211	750	790	1069	10,400	50
Duration of operation	1986-current	1991-current	1986-1994	1993-current	1994-current	1986-1998	1998-current	2000-current	2015-current	2001-current	2005-current	2005-current	2006-current	2006-current	2008-current	2000-current	2009-current

1: P=Pyrite, 2: AsP=Aspiryte, 3: PH=Pyrrhotite

2.3. Stirred tank reactor biooxidation

The frequently employed reactors for biooxidation in the laboratory, in batch and continuous modes, include the stirred tank reactors, the pneumatic reactors, bubble-column for continuous use, airlifting reactors. In order to keep the biooxidation rate constant, different types of minerals and gasses such as nitrogen, potassium salts, phosphorus, and carbonate (roughly 2%) should be added to the primary reactors and then the aeration must be continuously supplied to put the concentration of dissolved oxygen fixed (Konadu et al., 2020;A. Bulaev et al., 2021a; Karimi Darvanjooghi et al., 2025a). Since the biooxidation produces heat, it is often required to set the temperature of the bioreactor constant with a cooling-jacket at desired temperature (Choi & Gharelar, 2020; H. Li, Li, et al., 2020; Rao et al., 2020; B. Wu et al., 2020b). For excess carbon dioxide supply, this latter should be introduced by using air to the first bio-reactors for microorganisms (Astudillo & Acevedo, 2009). To facilitate the growth of various biooxidizing microorganisms, other organic carbon source such as yeast extract can be introduced to the bioreactor (M. I. Muravyov & Bulaev, 2013). Among other parameters to be also well optimized in any developed process, the morphological and the rheological behavior of the bacterial consortia (Magdouli et al., 2018; Brar et al., 2020) and their ecological diversity should be studied to avoid any potential contamination with indigenous and native microbes. According to **Table 2.1.**, the control of pH solution within the bioreactor through the addition of sulfuric acid and alkali compounds such as limestone to keep it at certain value ranging from 1.2 to 1.8 is crucial (Van Aswegen & Van Niekerk, 2004). Moreover, for successful biooxidation operation, required speciation (minimum costs and environmental burden) should be considered. This attention should be given to the overall flowsheet of gold processing. Thus, enabling synergy between the upstream and the downstream processes with particular attention to overall production costs is essential and needed to be considered (Van Aswegen & Van Niekerk, 2004). Among the additional major concerns, the treatment of solids and their washing to remove the dissolved iron, which acts as a cyanide consumption agent, is another point which needs to be considered and may lead to waste and product quality concerns. Moreover, the commercial recovery of gold requires efficient recovery processes at a low price and investment costs particularly on energy consumption and facilities establishment.

Accordingly, the broadening of recovery processes with innovative technologies such as super adsorbents to recover remains a potential area of investigation (Xing et al., 2020; H. Abdollahi et al., 2021) and may help to complete the flowsheet and improve the process efficiency leading to wider applicability of biooxidation technology. The optimized protocols and parameters are of paramount importance for developing a basis related to the life cycle analysis (LCA) as well as techno-economic analysis (TEA) of the process, making the assessment of the potential applicable for implementing bioprocesses in general (Sara et al., 2016) and biooxidation in particular as practical way to extract metals from ores (Elomaa et al., 2020).

Further, as the cost of operation in a bioreactor is high, the implementation of bioreactors and continuous extraction process is not affordable for the low-grade refractory gold ores (usually less than 2 g/ton). Therefore, another method of pre-treatment, heap biooxidation, can be proposed (C. L. Brierley & Brierley, 2013). One of the successful and excellent examples of the installation of heap biooxidation for the pretreatment of refractory gold ores was applied in Agnes Gold Mine, South Africa (Rawlings & Johnson, 2007a; Ndlovu, 2008; C. L. Brierley & Brierley, 2013). The sulfide concentrates containing gold particles (a slurry combined with nutrients and microorganisms) is mixed with a small-sized crushed rock to cover its surface. Afterward, the crushed rock concentrate is introduced to a flat surface for *in-situ* biooxidation (Rawlings & Johnson, 2007a; Ndlovu, 2008; C. L. Brierley & Brierley, 2013). A large scale of heap biooxidation (demonstration scale with a capacity of approximately 4-million tons per year) has been finalized by Newmont Mining, Gold Quarry Mine (J. Brierley, 2000; Bhakta & Arthur, 2002a; Kaksonen et al., 2014). The overall oxidation of sulfide ores to sulfur and other byproducts was estimated to be up to 50% for one period of biooxidation (i.e. 5 months of operation). This biooxidation unit was complemented with a cyanidation step (J. Brierley, 2000; Bhakta & Arthur, 2002a; C. L. Brierley & Brierley, 2013; Kaksonen et al., 2014; Elomaa et al., 2020). Regardless of these successful stories, North American mines have not yet reproduced these operations in their sites and no industrial-scale methods for gold extraction from the refractory ores can be found. Herein, *in-situ* biooxidation is strongly recommended and preferred over conventional approaches and underground processing techniques may be used in future in different mining industries; however, additional focus on technical challenges, enhanced the reproducibility of assays from lab to pilot scale should be targeted. To succeed *in-situ* biooxidation, hydrology and the morphology of mine sites should be studied to control the environmental impacts of the *in-situ* extraction

method. Conclusions are drawn from Carlin New Mont operations, GECOAT^{TM}, BIOX^{TM} should be carefully analyzed to translate towards potential application in a northern climate in North America (Chapman et al., 1993; Mousaid & Kaya, 2020; Vriens et al., 2020). Such studies are helpful as proof of principle to bring an extensible understanding of different challenges that encounter the bioprocess to be developed. Among the drawbacks to being carefully addressed the microbiological aspects of biooxidation is required to fully understood and studied toward obtaining the best way for optimization of the process. A recent development in this field including metagenomics, proteomics and transcriptomic and bacterial nutrient requirements are of higher necessity. For example, Kaksonen et al. performed literature review research to carefully study the oxidation of sulfide-bearing minerals utilizing microbially-produced ferric iron (Kaksonen et al., 2014). They indicated that the underground aeration as well as the activity of microorganisms in biooxidation reaction intensified the rate of sulfide-bearing minerals oxidation and, thus, declined the piling up of sulfur within the ore sample. Both sulfide-bearing ores such as pyrite or arsenopyrite and the presence of elemental sulfur decline the rate of extraction and reduce the efficiency of solvent extraction in the ongoing gold recovery process (Kaksonen et al., 2014). Additionally, the reagents component of the lixiviant solution including ferric ions, microbes, sulfuric acid plays a crucial role in biooxidation. Diffusion mechanisms and the reactional equations should be well defined and optimized towards better process monitoring (Holmes & Crundwell, 2000).

Although many research and industrial development centers recommend the implementation of continuous stirred tank reactors for biohydrometallurgy rather than heaps, their implementation and utilization tend to be limited due to the operations costs and the high technical level of engineering and process control. Furthermore, the solids loading adversely influence biooxidation including nutrients and dissolved oxygen availability. To increase the capacity of biooxidation, different researches have been conducted on the adaptation of moderate thermophilic bacteria to make it possible for tolerating the solids loading near to 30 wt.% without any significant declination in the biooxidation efficiency. Garcia-Ochoa et al. also suggested using slurry bubble columns, (which is known as an efficient alternative thanks to the significant decrease in operating and power costs of agitation as well as a decline in the produced agitation stress on the microorganisms), for overcoming this issue and increasing the solid loadings in biooxidation

(Garcia-Ochoa et al., 1997). The process design of such bubble column reactors remains a new challenge for ongoing research (Mäkinen et al., 2015).

Microbiological, physicochemical, and mineralogical factors (as shown in **Figure 2.1)** can significantly influence the biooxidation reaction within the continuous stirred tank reactors (C. L. Brierley, 2008; C. L. Brierley & Brierley, 2013; M. E. Clark et al., 2006; Mäkinen et al., 2015; Rawlings et al., 2003; Rawlings & Johnson, 2007b). To keep the biooxidation reaction at optimized condition within the stirred tank reactor, monitoring and controlling important factors such as mass transfer rate within the liquid and gas phases, temperature and pH, nutrients and minerals availability, the solids content in bioreactors, and particle ore sizes should be checked and adjusted accurately. Also, to the operational factors, heat transfer and the uniformity of temperature must be considered as another crucial parameter. The low amount of solid content in bioreactors limits the ultimate efficiency of the process; therefore, to find efficient and suitable types of stirred tank reactors, research as well as modelling and experimental studies are still required for the optimization of operating conditions. It is needed to focus on finding a new and low-cost type of stirred tank bioreactor with various key parameters toward obtaining optimized control. This would be very useful to maximize heat and gas flow with much higher solid content within the bioreactors to open new prospects for applications of biooxidation in gold recovery. Also, further fundamental experiments and mathematical modelling are needed to gather data for the estimation of biooxidation output and render it more efficient. Hence, investigational improvements are a must to affect the profitability of stirred tank bioreactors in biomining processes and the efficient design of the process.

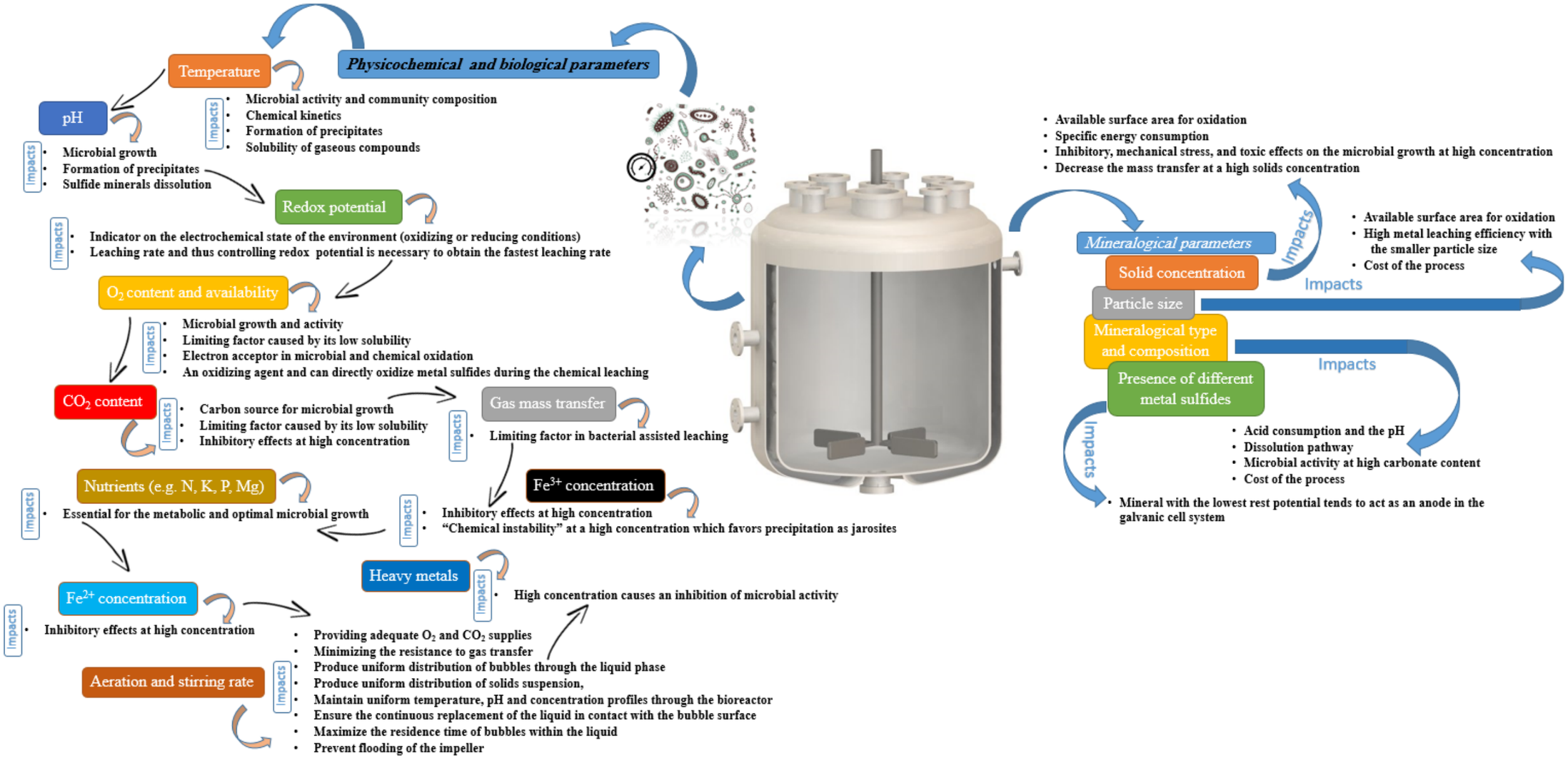

Figure 2.1. The parameters that directly influence the biooxidation reaction in continuous tank reactors.

2.4. Heap and dump biooxidation

While heap extraction is a beneficial approach for mining companies, serious issues and complexities often remain throughout this procedure (Ghadiri, 2020; Kremser et al., 2020b). Most of the workers and operators would not be able to design the affordable form of the heap for biooxidation of refractory gold ores or address issues that may arise along with insufficient knowledge mostly on related physicochemical and biological processes (J. Petersen & Dixon, 2002; Thiel & Smith, 2004). Other useful operating parameters including ores particle sizes, the rate of liquid and airflow through the heap, the acidity and minerals in the reagent solution, the degree of ore particles agglomeration, and the time of irrigation should be also introduced as crucial parameters to be optimized in column and heaps (**Table 2.3**).

Generally, the rate of oxidation in arsenopyrite and pyrite in heaps is low, (needs at least 6 months to remove almost 35% of the barrier matrix from refractory gold ores containing only 3% of the sulfidic barrier) and various operating parameters should be well understood to guarantee successful operation units such as the chemical and mineralogical properties of sulfide ores, biooxidation kinetics rate, the mass transfer within the gas and liquid phase, the biooxidation temperature, redox potential and the barrier of diffusion through the mineral ore particles and void space (Ghorbani et al., 2011; Wan et al., 1995). Thus, the biooxidation kinetics rate of sulfide mineral ores as well as any transport factors of compounds inside the gas and liquid phases should be noticed in order to interpret the modelling and experimental data profoundly. In this regard, the use of phenomenological models may help and the elaborate physicochemical interaction of the gas, liquid, and solid components at interfaces inside the heap structure which is easily predicted for responding to the operational and environmental changes.

The acidic leachate solution, which contains a high amount of iron, will be collected at the base of the heap and then it will be reused again from the top of the biooxidation heap after adjusting pH and other minerals concentrations. The primary components that directly influence the efficiency are the advective flows of solution through the heap, which directly affect the distribution of reaction-points within the heap and the rate of corresponding biochemical reaction (BOUFFARD & DIXON, 2004a; Ghorbani et al., 2011). Two factors including the amount of ores, near to a million tons, and the roughly one-year time of one batch reaction should be considered in heap biooxidation. The parameters to be adjusted to control the heap efficiency in optimized conditions

are the geometry of heap and its height; particle ore sizes and the stability of agglomerated particles; aeration of heap during the biooxidation; the iron content, bacteria activity, and pH of recycling solution; rest time, rates of recycling solution during biooxidation (Bennett et al., 2012a). These parameters should be optimized to maximize the interaction of the solution with the ore particles, providing a perfect environment for reactions and guaranteeing the targeted metals to be entirely extracted.

The hydraulic properties as a function of pore sizes and particle size distribution, as well as flow motion of solution (which significantly influence the capillary motion forces and gravitational forces), are reported to affect the contact of ore particles with the acidic solution. Although very fine ores particles produce a large surface area which leads to a high reaction rate, the passage of gas and oxygen will be limited and adversely influence the reaction efficiency (Kaksonen et al., 2014). The reactions of metal dissolution depend on kinetics, diffusion of reactants to the surface of ores particles, the amount of reagents, and temperature. Recently, it has been reported that higher temperatures effectively promote the reaction rates; although, this temperature enhancement may negatively influence the growth rate of bacteria that are responsible for the production of ferrous ions (BOUFFARD & DIXON, 2004a).

The diffusion of reagents into the ore particles is as a function of particles sizes; therefore, optimum particle sizes should be considered by which reagents can easily permeate into the ores particles and the extracted metal can quickly diffuse out (BOUFFARD & DIXON, 2004a). Both experimental and modeling results can demonstrate the biooxidation efficiency and high performance of the heap process. Also, accurate results correspondence to the heap conditions (temperature, pH, irons ions concentration, bacterial activity in a controlled condition), will be obtained by implementation of biooxidation column tests (0.5m height by 5cm diameter for laboratory scale and 10m height by 2m diameter for pilot scale) (Bennett et al., 2012a).

Recent works on the diffusion of oxygen through mathematical modelling showed that the diffusion of oxygen from the bottom/top of the heap through its void space would be the process that limits the rate of biooxidation without the natural convection of air within the heap biooxidation. The diffusion layer of the oxidization zone reached up to 4 m after 3 consecutive years of operation (with void space of up to 30 vol.% and pyrite concentration of up to 2.0 wt.%). Among the recommendations is to increase the bulk flow of gas produced from the water

evaporation and consumption of oxygen simultaneously (Bartlett & Prisbrey, 1996). To do so, Milayhov and Hendrix studied the impacts of particle size and solution in the columns with small geometry (Mihaylov & Hendrix, 1993). Results showed that the recovery of gold and its concentration were affected by the regenerating acidic solution and the decrease of particle size from 19.3 to 1.7 directly influences the redox potential, pH, and iron ions concentration (Mihaylov & Hendrix, 1993).

Other researchers also introduced a new kinetics model that includes biological kinetics of oxidation reaction. Results obtained by the model's equation were near to the experimental results and the low iron extraction can be triggered by the limitation of diffusion for oxygen within the heap biooxidation. These kinetics equations were helpful to carry large scale heap biooxidation (Wan et al., 1995). However, more attention should be taken into consideration such as temperature, pH, nature of the sulfide matrix of gold ores. For example, while carrying out the biooxidation in Quarry mine site, located in Carlin, results showed that the value of pH for the leaching solution increased up to 2.7 within the 8 months of biooxidation operation. Also, the results of heat production showed that the average temperature of the heap was set at 49-52℃, with a maximum temperature of 75℃. The value of redox potentials enhanced up to 685 mV and the efficiency of bioheap was not significantly as high as it was estimated (oxidization of 35% of the siliceous-sulfide barriers within the 8 months of operation and 28% of carbonaceous-sulfide barriers in 5 months).

Effective implementation of emerging biooxidation heap technology, as well as the creation of the best available methods for the processing and its transportation, would finally need a reasonable technological principle (Bennett et al., 2012a; J. Petersen, 2010; J. Petersen & Dixon, 2002; Renman et al., 2006). It should also be noted that research on column tests and pilot heap biooxidation focused particularly on studying the enhanced gold extraction from refractory gold ores with a wide range of biochemical and mineralogical characteristics. Also, shortage of essential detailed information on oxidation profiles through the heap depth, oxygen concentrations in different layers of the heap, bacterial growth and counts, and temperature profiles and heat loss lead to bringing limitations on investigating the effect of important parameters on efficient extraction of gold from refractory ores inside bioheap processes (Darvanjooghi et al., 2024; Phyo et al., 2020). Furthermore, the high value of costs for studying the operational parameters must be

reasonable by introducing a suitable plan, operation, and design. The information provided in **Table 2.2** indicates that most of the column test for biooxidation takes a longer time and the final pyrite dissolution will range from 38 to 98%. The key factor for this phenomenon is attributed to the particle and agglomerate distribution of ore samples in the column test (Kremser et al., 2020a). Accordingly, the following factor should be considered for achieving an efficient heap biooxidation:

I) Ore sample characterization: mineral content and their structure, compounds that consume acid, particle size and agglomerates morphology, available surface area and the porosity, mineral precipitation and inhibition factors.

II) Biological parameters: microorganisms' diversity and their population densities, adaptation to ore sample, tolerance to other heavy metals and antibacterial compounds, attachment to ore sample and efficient production of EPS.

III) Operational parameters: temperature, pH, nutrients and their component concentrations, carbon source, oxygen and carbon dioxide, heat transfer and its effect of inhibition of bacterial growth, mass transfer resistance due to precipitation or pore diffusion phenomena.

Table 2.3. Column test results for biooxidation of refractory gold ores.

Researchers / Parameters	(Mihaylov & Hendrix, 1993)	(H. Li, Li, et al., 2020)	(Bouffard & Dixon, 2002)	(Holtum & Murray, 1994a)	(Burbank et al., 1990)	(Groudev, Spasova, Groudeva, et al., 1995)	(Epiforov et al., 2017)	(Langhans et al., 1995)
Biooxidation process	Inoculation Biooxidation	Inoculation Biooxidation	Agglomeration Two steps Inoculation Biooxidation	Acidification+ Inoculation Biooxidation	Inoculation Biooxidation	Biooxidation	Agglomeration+ Inoculation Biooxidation	Agglomeration+ Inoculation Biooxidation
Diameter of column (cm)	8.9	-	24	31.5	15.2	24	10	20.3
Height of column (m)	0.9	-	1.7	2	1.2	1.8	110	6
Ores particle size (mm)	19	10	12.5	12	19	10	0.071	19
Temperature (initial/final) (℃)	32/32	-	20/20	–	–	20/–	14/32-42	–
Maximum total iron (g/l)	0.7	1.23	5.5	24	14	–	24	23
pH (initial/final)	2.0/2.75	-	2.7/1.9	1.0/1.7	3.5/2.0	1.9/1.3	1.2-1.9/2.2-2.7	6.6/1.5
Redox potential (initial/final)	460/580	420/460	250/450	–	800/600	–/600	400/525	–/700
Time of biooxidation (d)	62	80	365	180	90	365	450	300
Population of cell (initial/final) (cells/ml)	$-/3\times10^{7}$	9×10^{8}	$10^{5}/8\times10^{7}$	–	$10^{7}/-$	$-/10^{8}$	-	$-/10^{8}$
Gold extraction (initial/final) (%)	20/41	36/87	50/50	26/52	25/75	15/84	65/85	–
Initial grade of Gold (g/t)	0.84	0.85	–	4.2	–	3.2	1.6	–
Formation solid sulfur and jarosite	–	-	Yes	–	–	Yes	-	Yes
Final sulfide oxidation (%)	–	38	–	–	–	68	98	–

2.5. Biooxidation: Challenges in process technology

Before the deployment of biooxidation for metal extraction, a wide range of challenges that directly influence the biooxidation reaction and metal recovery should be considered.

2.5.1. Preg robbing materials

The carbon-based perg robbing issues need to be evaluated. Thus, more elaborative studies are required to understand the effect of long-chained hydrocarbons and organic acids in the biooxidation efficiency (J. A. Brierley & Kulpa Jr, 1993). To remove carbon-based materials from the ore sample for the elimination of perg robbing factors different physicochemical approaches such as high-pressure roasting, pressure oxidation, blinding, flotation, and microbial treatment can be implemented. However, the cost of microbial treatment is lower in comparison to these methods (Azizitorghabeh et al., 2021; Feng & Van Deventer, 2001; Nanthakumar et al., 2007; Ng et al., 2020; Xu, Li, et al., 2020a). To do so, simultaneous or consecutive microbial-based treatment processes can be implemented for the elimination of the carbon-based compounds within the ores. Recent attempts have been carried out and different microbial species consortiums including *P. fluorescens, P. stutzeri*, *P. oryzihabitans*, *Pseudomonas (P.) maltophila, Achromobacter* spp*., Rhodococcus* spp, *P. putida,* and *Arthrobacter* spp could offer a promising perspective (J. A. Brierley & Kulpa Jr, 1993). Fungal agents and/or culture media including *Phanerochaete spp., Cyathus* spp., *Tyromyces* spp., *Trametes* spp., and *Phlebia spp* are also proposed as an alternative method to remove the carbon source within the ore sample (Yen et al., 2009).

2.5.2. Permeability and porosity

The permeability and porosity of minerals during the biooxidation are among the bottlenecks that restrict the biooxidation of gold from low-grade ores especially in bioheaps. Therefore, enhancing the permeability of ores is highly required to increase the efficiency of the recovery process (Brehm et al., 2005). Spreading microscopic fungi within the ores crack, particularly in the in-situ method can help in breaking down the rock and mineral ores (Brehm et al., 2005). Microorganisms directly produce chemical agents including nitric acid, sulfuric acid, citric acid, oxalic, and gluconic acids as well as pyruvic acid, succinic, acetic acid, lactic acid, formic acid, and 2-

ketogluconic acid that are documented to influence the crack formation within the rock and help in corroding the rock by reducing its components (Brehm et al., 2005).

Furthermore, these microorganisms may produce ferric iron-complexing agents that directly increase the promote rock weathering (Brehm et al., 2005; Burford et al., 2003). Besides, microorganisms can produce biological solutions (containing surfactants), that influence the wettability of ores due to their hydrophilic properties (Aitimbetov et al., 2005). In the circulation of leachate solution, the implementation of wells and spray allows for an efficient increase in mass transfer and development of ores oxidation rate. While these technologies have been shown to enhance leachate circulation and higher oxidation rates, the permeability of ores remains a big challenge. Thus, integrated processes combining spray and wells can enhance the circulation of leachate. Equipment sizing and optimizing the dimensions of wells, the sequence of units, the selection of operational settings is further required for better process performance. Besides, mathematical-based models implemented for simulation of biooxidation and developing more algorithms to deal with the complex nature of the reaction, thermodynamic models are again a key mandate to enable the prediction of the system behavior within the inherent variations of operating conditions. This approach may help to reduce the time of experimentation and model the nutrient requirements of microbial strains especially in the presence of complex sulfidic ores in bioreactors and heaps (Hold et al., 2009).

2.5.3. Silicate barriers

The presence of silicate-based barriers is among other compounds that can decrease the gold recovery after performing biooxidation on refractory gold ores. For this attempt, the disintegration of the silicate structure within the biological action should be considered.

Generally, silicate dissolution may happen due to the production of acids, alkaline products from NH_3, and acid polysaccharides which form complexes with silicate and led to the dissolution of silicate structure. For instance, it is reported that 2-ketogluconic acid produced by bacteria as well as citric and oxalic acids which are produced by fungi are categorized as the most effective agents that effectively contribute to the dissolution of silicates minerals. The produced acids may also separate the cations from the crystal structure of silicates and, then, lead to the breakage of silicates structure.

Furthermore, it is reported that the rate of quartz dissolution is extremely insignificant at neutral pH owing to the breakage of Si–O bonds with corrosive agents (Ehrlich, 2004). The solubility of quartz structure increases at alkaline conditions (Ehrlich, 2004). Thus, harnessing the ability of microorganisms performing photosynthesis, urea hydrolysis, denitrification, methanogenesis and ammonification to produce alkaline compounds can effectively lead to the dissolution of quartz structure. These statements are in accordance with Brehm et al. who investigated the effect of biological breakdown of quartz sand, crystalline quartz, and commercial glass (Brehm et al., 2005). They observed that diatoms, heterotrophic bacteria and cyanobacteria can change the pH of the solution from 3.4 to 9.0 and destroy the quartz and glass structure (Brehm et al., 2005). *Bacillus* spp. was also reported to disband the microscopic structure of quartz and dissolve the iron (as iron oxyhydroxides), silica, and aluminum compounds from quartz sands and offers a potential application at a large scale. **Figure 2.2** shows microbial reactions that produce alkaline compounds for the degradation of silicate and quartz compounds.

2.5.4. Passivation and precipitation

The passivating layers on mineral ores should be removed. Generally, these layers are constituted of solid sulfur and polymorphic structures as well asiron (II) oxide and form jarosite, at pH higher than 2.0 (Stott et al., 2000). Some microorganisms such as *At. Ferrooxidans* (i.e. elemental sulfur oxidizer) and other microorganisms such as *At. ferrivorans, Ferrimicrobium acidiphilum, Acidiferrobacter thiooxydans, Ferrithrix thermotolerans, Acidimicrobium ferrooxidans, Acidocella spp., Acidiphilum spp., Alicyclobacillus spp., Acidobacterium spp., Ferroplasma spp., Acidiplasma spp.* and *Sulfobacillus spp.* are capable to overcome these barriers and destroy the jarosite structure, eliminate and destroy the passivating layers, leading to a significant increase in the permeability of ores and mineral particles (Coupland & Johnson, 2008; Johnson et al., 2012).

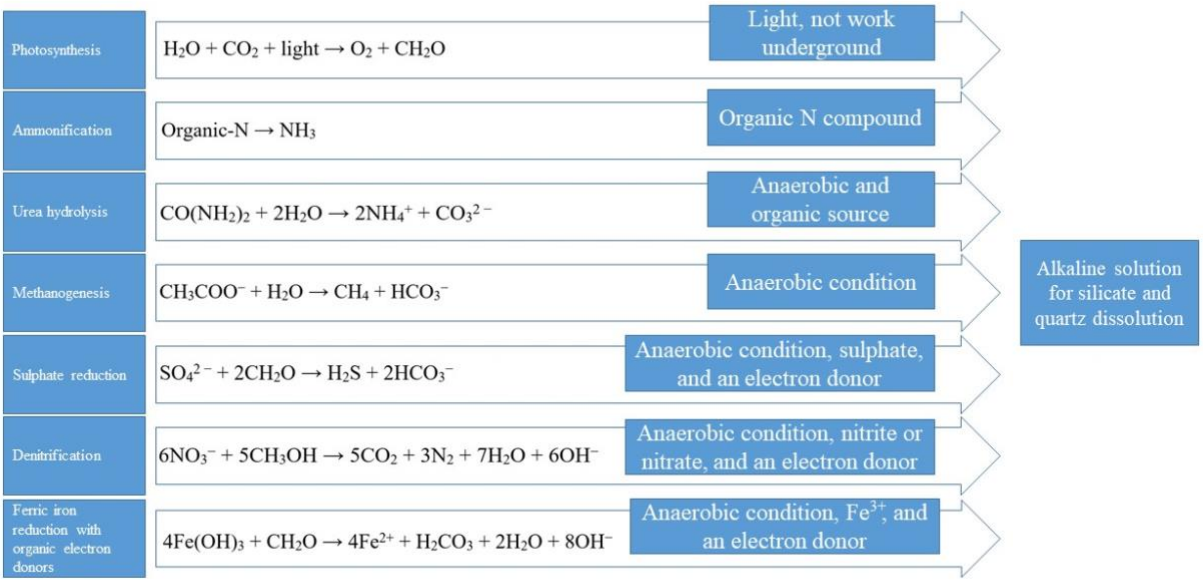

Figure 2.2. Microbial reactions that produce alkaline compounds for degradation of silicate and quartz compounds.

2.5.5. Impurities and heavy metals

The presence of impurities is also among the drawbacks that can restrain the potential applications of biooxidation approach to economically recover gold metal. Further, impurities such as (Cu, As, Sb, Zn, etc.) can adversely affect the recovery process and become problematic for the operation in question. Biooxidation was highly recommended to dissolve and remove these impurities, especially arsenic. Despite its reduced efficiency, this latter fails to meet industrial requirements and measurements should be taken to reduce arsenic content from the liquor. The co-precipitation approach with the iron and sulfate as well as washing steps are frequently suggested (Johnson, 2013; Kaksonen et al., 2014). Besides, the neutralized liquor with an acceptable level of arsenic after purification can be easily re-utilized in the other recovery processes, such as milling and flotation or even the biooxidation circuits redundantly (Johnson, 2013; Kaksonen et al., 2014). Furthermore, it was observed that a neutralized solid precipitate comprises a large amount of calcium sulfate,iron (III) arsenate that is stable and insoluble in water and requires safe management. In spite, biooxidation is a suitable approach for the metal extraction from calcium-based sulfide ores, the formation of calcium sulfate dehydrates, (gypsum) is a major concern. This

problem is more pronounced in heaps and can negatively influence the contact between mineral particles and the acid solution to be injected as well as the permeability of air causing a significant decrease in the efficiency of metal extraction as well as the solution circulation within the heap (Bouffard et al., 2009; Langhans et al., 1995).

2.5.6. Operational and transport properties

Mass transfer

The mass transfer of components in the gas-liquid interface is significantly affected by different factors including type of biooxidation reactors (heap and stirred tank reactor), mineral ores particle size and the sphericity of ores, the agitation speed and aeration flow rate, pulp density of ores in stirred tank reactor as well as the rate of leachate production in heaps. Because mass transfer rate at the interface of gas-liquid plays an essential role in the kinetics of the interfacial reaction and can influence the experimentations, more profound studies and research-based considerations must be taken. As mentioned above, oxygen, carbon dioxide as well as pyrite and sulfides compounds are generally involved in the interfacial biochemical reactions and affect the gas-liquid mass transfer rate. Thus, it is required to provide higher values of O_2 and CO_2 to overcome both limitations of mass transfer within the gas-liquid interface as well as their consumption rates (i.e. the amount of oxygen must be higher than the maximum rate of oxygen transfer and consumption in liquid and similarly the amount of carbon dioxide should exceed the maximum consumption and transfer rate to eliminate the limiting criteria of biooxidation) (Boon & Heijnen, 1998b). Since bacterial assisted oxidation occurs at the surface of the gas-liquid interface, the availability of the surface influences the rate of biooxidation (Boon & Heijnen, 1998b). To determine the constant rate of biooxidation, the first-order reaction can be considered since it is not affected by the particle size of minerals. Moreover, it is essential to determine when the deficiency of mass transfer rate at gas-liquid interface in biological oxidation occurs to well monitor the process. Thus, the calculation of mass transfer coefficients, $(k_La)_{Oxygen}$ and $(k_La)_{Carbon\ dioxide}$, is a must and should be done. The mean transport levels of oxygen and carbon dioxide were measured using 10 percent of the concentrations of air equilibrium as measurements of the true amounts of O_2 and CO_2. It disregards the influence of the dissolved salts. The amounts of saturation shall be calculated in equilibrium with the gas-phase with a water-phase (Boon & Heijnen, 1998b).

More other parameters including slurry density must be included among the numerous factors that can impact the bio-oxidation of sulfide minerals. Generally, the bacterial oxidation rate of pyrite declined with the enhancement in the densities of slurry, and the supply of carbon dioxide and yeast extract enhances the rate of oxidation as a result (Rawlings & Johnson, 2007a). The increase in slurry density decreases the biooxidation rate in reactors and the addition of carbon dioxide to the aeration flow leads generally to an increase in the biooxidation rate (Rawlings & Johnson, 2007a). Therefore, more attention should be paid to these factors while scaling the process. Harnessing the biological activity of *T. ferrooxydans* as well as *Sulfolobus* in pretreating refractory gold ores containing sulfide minerals can be always suggested as a better alternative (Boon & Heijnen, 1998b; Rawlings & Johnson, 2007a). In contrast with thermophilic bacteria, mesophilic bacteria showed that the leaching kinetics rate is obtained in higher slurry densities. This difference is possibly induced by an enhancement in the mass transfer rate combined with the temperature rise. Generally, dissolved carbon dioxide and oxygen balance decline at higher temperatures. It must be mentioned that the amounts of oxygen and carbon dioxide in the gas phase are rising as the content of water in the gas phase enhances at higher temperatures. On the other hand, thermophilic bacteria absorb far more oxygen and carbon dioxide than *T. ferrooxidans*. Further care is required to prevent carbon dioxide limits by utilizing thermophilic bacteria. In the stirred tank with the air-lift reactor, Norris and Barr examined pyrite dissolution with *Sulfolobus*, they claimed that improved mass transfer can be seen in an air-lift reactor in laboratory-scale, presumably by the greater rate of airflow preventing the gas stage from being exhausted (Norris et al., 1988; Norris & Barr, 1988).

Heat transfer

Due to the exothermic nature of mineral oxidation, sulfide biooxidation produces heat in heap biooxidation at operating temperature of 30-35 °C (A. Bulaev et al., 2017; J. Li, Zhong, et al., 2020; Zhao et al., 2020). A heap biooxidation is nearly assumed to be an adiabatic process with heat lost primarily through the temperature increase in the leaching solution passing through it (Kremser et al., 2020b). The rate of mineral oxidation and heat generation depends on numerous factors such as the rate of air supply or intrinsic heterogeneous kinetics of sulfide mineral oxidation (Bennett et al., 2012b; Panda, Akcil, et al., 2015). The transport of oxidant (ferric ions) in the

solution-filled rock pores to the internal locked minerals can also be a rate-limiting factor. Therefore, optimizing the ore crushing to the desired granulometry is recommended (Bartlett, 1996, 1998) and will help to control the heat transfer and hence energy costs. Fortunately, heat can also be controlled at moderate environment temperature of 30-35 °C in the heap while controlling the leaching solution to be percolated through at temperature of 20-30 °C. The heat control generally depends on the flow rate, heat capacity and temperature profile of the solution (J. Li, Tong, et al., 2020). At a steady heap temperature, the biooxidation rate cannot exceed the heat removal rate by the draining solution. Using the heat released from oxidizing pyrite, the time required for complete ore biooxidation can be determined especially if the heat removal is the rate-limiting process.

In the absence of forced air ventilation, effective percolation systems are required, and the percolation solution should be used intermittently. The major causes of heat loss in sulfide heap are related to the evaporation of solutions from the heap surface and the sensible heat loss with the effluent solution (Bartlett, 1996, 1998). Therefore, several options can be used for compensating this heat lost, and thereby increasing the temperature of the heap, including (Bartlett, 1996, 1998): i) Reducing the rate of solution irrigation; ii) Enhancement in the rate of aeration; iii) Implementing iii) Heating the solution; iv) Heating the air, with or/and without humidification. The most effective means of achieving a high degree of heat conservation within a sulfide heap is to blow air into the heap above a certain critical rate while maintaining a low rate of solution irrigation (Bartlett, 1998, 1996). In this case, other means of conserving heat will bring additional effects and probably would not justify the related expenses.

For more efficiency, modelling the heat transfer is needed while considering hundreds to thousands of variables of different parameters, process systems engineering that encompasses model-based process simulation, optimization and control. Model management and a better understanding of the underlying computational problems should receive more proper attention at an early stage of biooxidation development, though. Therefore, modeling the experimentation can be easily adopted by both academic and industrial research. Independent of the biooxidation design, modeling aims to generate large data with a limited amount of material and tests, data on kinetics reaction, thermodynamic properties, modelling biphasic and triphasic systems interaction between solid,

liquid-gas, reactors and heaps design for better screening of a broad range of operating conditions and overall accelerated process development and performance.

The challenges which are mentioned in the previous research are related to the heap biooxidation at high temperature (usually higher than 20℃) (Bouffard & Dixon, 2003; J. Li, Tong, et al., 2020; J. Li, Zhong, et al., 2020; Zhao et al., 2020). The heat transfer process plays an important role on the biooxidation rate since it influences the absorption of gases (oxygen and carbon dioxide) into the ore sample and circulating solution. In fact, these phenomena influence the growth and activity of bacteria as it is dependent on temperature (Kaksonen et al., 2014), the formation of mineral precipitates such as jarosite, scorodite, and arsenic compounds which inhibits the biooxidation process. This leads to lower growth rate of bacteria during biooxidation particularly in the heap leaching process (Escobar et al., 2010).

2.6. Research Gaps

Different potential approaches for the biooxidation of refractory gold ores have been investigated so far; some of the relevant problems associated with the current biotechnology-based metal recovery methods that need timely attention are as follows:

2.6.1. Microorganisms' activity: rate limiting factor

The oxidation of pyrite and pyrrhotite is involved in a microorganism-assisted method where their population and growth rate depend on known factors. The production of ferric ions and the participation of microorganisms in the electron transfer chain is highly dependent on sufficient nutrients, temperature, oxygen, and pH. Besides the low production of biomass will enhance the sensitivity and growth rate of microorganisms in the solution (Run & Clark, 2004a). Although the presence of ferrous ions might be effective for the microorganism as it assists to provide electrons for their metabolism, the iron excess and other metal presence may reduce the growth rate of microorganism due to toxicity to the acidophil microorganism. All these factors lead to a decrease in the rate of microorganisms' growth and then we can consider this as the rate-limiting factor in gold recovery (Langhans et al., 1995).

2.6.2. Low temperature

Most of the acidophil microorganisms (including both archaea and bacteria) are adapted to high temperatures and their growth rate is optimum at a temperature higher than 15 ℃. The psychrophile acidophil microorganisms' growth rate is very low compared to the mesophilic and thermophilic. Therefore, it is required to find a solution for this issue to make the biooxidation applicable and affordable in both heap and reactor at low temperatures since most of the mine sites in Canada are placed in northern regions (Escobar et al., 2010).

2.6.3. Toxic metals

The presence of other toxic metals in the microorganism growth environment leads to the low growth rate of acidophil microorganisms. In the pyrite structure, the presence of arsenic might reduce the activity of bacteria and EPS production. Therefore, for some ore sample with a high concentration of arsenic the method of biooxidation might not be applicable and other pre-treatment method is required that increase the investment cost for the metal recovery (Langhans et al., 1995).

2.7. Hypotheses

Hypothesis I

One of the most critical elements of biofilms is extracellular polymeric molecules. Proteins, carbohydrates, lipids, nucleic acids, and cell fragments comprise their makeup, which varies based on microorganisms and environmental factors. The EPS (extracellular polymeric substance) involves various processes, including providing a reaction area for oxidation, generating an active and absorbent surface, promoting bacterial adhesion, contributing to biofilm structural stability, and building a protective layer against biocides and other media inhibitors. EPS is formed primarily by secretion mechanisms and cell lysis, and it is then stored on cell surfaces or distributed in the media. In microorganisms, the production of EPS is generally a cellular reaction to adverse environmental factors such as temperature fluctuation, the presence of metal ions, and inhibitors, among others, and it is also one of the approaches in the adaptation process. The development of EPS in biohydrometallurgical processes would enhance bacterial attachment to minerals and, as a result, its participation in the creation of biofilm on minerals, enhancing biochemical attack on the mineral and, as a result, the process improvement.

Considering that different types of monosaccharide sources for microorganisms are an important factor that influences the biooxidation rate, the addition of different types of sugars including D-galactose, D-fructose, and D-sucrose will enhance and modify the activity of bacteria in the biooxidation. Therefore, it is expected that microorganisms' activity differs by the addition of these carbon sources as they are participating in the formation of EPS. On the other hand, monitoring and characterization of the oxidant acidophil microbial populations (consortium) in environmental samples is important and needed to be studied. *Therefore, implementing community profiling will be a helpful approach for determining the specific strains which are associated with relevant metabolic activities and EPS production by the addition of monosaccharides.*

Hypothesis II

Despite the connected academic research being conducted in a variety of research institutions, there are notably no demonstration plants or commercial units of operation on the biooxidation of refractory gold ores. The lack of industrial activities may be ascribed to the geographical and geochemical structures of the ore, as well as other climate constraints that hinder the scalability of the operations. Because of the intricate structure of sulfide ores, which includes a complicated matrix that contains gold and is similarly diverse in its mineralogical characteristic, biooxidation is naturally challenging. This is since the gold is embedded within the matrix. The historically geochemical formations of the various rocks lead to intricacy. Biooxidation may be done in stirred tank reactors or heaps. To measure heap biooxidation in industries, column tests will be used on a pilot level heap. The ore sample will be placed in a column of approximately 1 m in height and 15 cm in diameter, and air and carbon dioxide will be bubbled from the bottom of the column. *It is finally assumed that the optimized condition from the previous objectives can positively influence the biooxidation rate and the bacteria growth; therefore, implementing both stirred tank reactor for high-grade ore and column tests for low-grade ore will be another significant and novel purpose of this research that is covered in this objective.*

Hypothesis III

The biooxidation (heap and reactor) needs to be an integrated process because of complexity and efficiency; therefore, enzyme immobilization methods will be an efficient option to increase feasibility. Since the activity and oxidation rate of biooxidation via microorganisms is strongly

dependent on the environmental temperature, it is required to develop a new method for heap leaching or oxidation process (especially for refractory sulfide-based gold ore) independent of the temperature. Therefore, understanding the mechanism and enzymatic activity will be a novel technique to separate the oxidation rate and efficiency from the activity and growth of the microorganisms, which is dependent on the temperature. *To do so, the immobilization of enzymes (biological catalysts) on the porous media is a very novel option to provide an oxidizing agent for the destruction of Pyrites, Chalcopyrite, and Arsenopyrites (that might contain gold fine particles) toward the recovery of gold from refractory ores.*

2.8. Objectives

The primary objective of this Ph.D. thesis is to enhance biooxidation efficiency by introducing innovative concepts in bioheap and bioreactor design, along with integrated extraction strategies for both low- and high-grade gold-bearing sulfide ores—specifically tailored to Canada's cold climate. The novelty of this research lies in four key areas:
I) **Process optimization** at the laboratory scale through the application of effective nutrients and carbon sources to promote microbial growth and improve biooxidation rates under optimal experimental conditions.

II) **Reactor and heap biooxidation trials**, including semi-pilot scale column tests designed to simulate heap conditions and serve as case studies for future scale-up and novel implementation strategies.

III) **Development of an integrated bio-enzymatic extraction process** aimed at achieving cost-effective gold recovery from refractory ores under cold climate conditions and Implementation of modular EnBiTe in column test and optimization of process configuration.

2.9. Thesis originality

The thesis comprises the following original studies:

✓ This research presents a comparative and systematic evaluation of microbial versus enzymatic biooxidation strategies for gold recovery from refractory sulfide ores under low-temperature conditions. The enzymatic method (EnBiTe), incorporating glucose oxidase and catalase, is

introduced as a novel, scalable alternative capable of overcoming microbial limitations in cold climates.

✓ A pioneering approach is proposed through the immobilization of glucose oxidase on modified cellulosic supports to enhance enzymatic activity at low-temperature environments. This platform provides a temperature-independent oxidation route for pyrite and arsenopyrite matrices, enabling efficient liberation of gold.

✓ This thesis uniquely integrates bench-scale microbial experiments with machine learning techniques—including artificial neural networks and genetic programming—to model and optimize biooxidation performance based on operational parameters such as pH, ORP, nutrient concentration, and pyrite content.

✓ To date, no studies have applied enzyme-based column systems for continuous, low-cost oxidative treatment of refractory ores. This work validates the fixed-bed enzymatic columns using real ore samples, achieving over 89% pyrite dissolution and up to 90% gold recovery under cold conditions.

✓ The dual enzymatic module—GO and CAT—designed in this research represents a novel configuration for maintaining oxidative stability and enzyme longevity. This enables continuous operation with reduced oxidative stress, a previously unaddressed limitation in enzymatic oxidation processes.

✓ This study offers a practical, cost-effective, and environmentally sustainable solution tailored for cold region mining operations in Canada. Its outcomes provide a foundation for transitioning from energy-intensive microbial biooxidation to industrial-scale enzymatic pretreatment processes for gold extraction.

2.10. Summary of the different aspects of research

The body of research presented herein reflects a systematic and incremental approach to overcoming the critical limitations of refractory gold ore processing under cold-climate and low-grade ore conditions. The progression from microbial enhancement to enzymatic innovation is underpinned by empirical data, experimental optimization, and a clear identification of

technological gaps. The following subsections summarize each major investigation while establishing the rationale for the subsequent research phase.

2.10.1. Monosaccharides impact in refractory gold ore biooxidation using *Acidiphilum Ferroplasma*

The initial study investigated the influence of monosaccharides, particularly glucose, fructose, and sucrose, on the enhancement of biooxidation activity by *Ferroplasma acidiphilum*. The supplementation of glucose significantly increased the secretion of extracellular polymeric substances (EPS), which facilitated microbial adhesion to pyrite surfaces and moderately improved biooxidation rates. Compared to D-galactose and D-fructose, D-sucrose produced the most EPS with the most pyrite dissolution (69%). For an ore load of 20%, 0.8 wt. % D-sucrose increased ferric ion production by 65%, while 0.4 wt.% increased it to 95%. Adding yeast extract and D-sucrose at 0.4 wt.% increased the EPS biovolume fraction from 7.5 to 32.5 v/v%.

Rationale for next phase: The research shifted towards broader performance evaluation and predictive modeling of microbial-assisted biooxidation, incorporating a wider range of operational variables in bench scale study

2.10.2. Microorganisms-assisted Biooxidation: Efficiency assessment and machine learning based prediction

In this phase of the research, the impact of critical operational factors on the biooxidation efficacy of *Ferroplasma acidiphilum*, sourced from native Acid Mine Drainage (AMD) was investigated. The concurrent impacts of monosaccharide type, ore content, pyrite concentration, and operating time were evaluated. The optimal parameters for achieving maximal pyrite dissolving (~75%) comprised: 15 days of operation, 7.2 wt.% pyrite content, 5 wt.% ore content, pH 1.47, oxidation-reduction potential (ORP) of 562 mV, and concentrations of D-+-sucrose (0.52 wt.%), D-+-galactose (0.09 wt.%), and D-+-fructose (0.12 wt.%). The Artificial Neural Network (ANN) surpassed Genetic Programming and Polynomial Regression (RSM-informed) in predictive modelling methodologies, exhibiting more accuracy in forecasting experimental results. Sensitivity analysis indicated that fluctuations in sucrose content significantly influenced ferric ion generation and pyrite dissolution, whereas alterations in galactose and fructose had little impacts.

Rationale for next phase: The predictive modeling not only validated experimental trends but also identified an optimum condition—15 days operation, 7.2 wt.% pyrite, 5 wt.% ore, pH 1.47, and ORP 562 mV—with sucrose exerting the most significant impact on process efficiency. This modeling approach facilitated the design of optimal parameters for subsequent bench-scale biooxidation studies, supporting the system's robustness under toxic conditions by enhancing microbial resilience and activity through carbohydrate-based bio-stimulation.

2.10.3. Biooxidation of refractory gold ore using *Ferroplasma acidophilum*: a bench scale case study

In this step of the research project stirred tank reactor demonstrated enhanced performance relative to the column test, achieving much greater recovery rates for essential components. Gold recovery in high grade ore sample (HGOS) treated with a stirred tank reactor achieved 55% after 14 days, whilst low grade ore sample (LGOS) treated with the column test attained 40% after 60-70 days of operation. The recovery rates for silver and copper in the stirred tank reactor were roughly 60% and 80%, respectively. The enhancements are ascribed to superior mixing, oxidation, and overall pretreatment efficacy in the stirred tank reactor. Optimal conditions for biooxidation included precise aeration flow rates and agitation velocities, which enhanced microbial activity and pyrite breakdown, essential for extracting gold from complicated ores.
The research emphasizes the significance of pH and cyanide concentration in the cyanidation process. Optimal gold recovery occurred at a pH of around 10.5, with elevated cyanide concentrations (up to 8 g/L) facilitating increased dissolving rates. Gold recovery reached around 60% at a pH of 10.5 and a concentration of 8 g/L NaCN.

Rationale for next phase: This phase of study confirmed that microbial methods are unsuitable for efficient and scalable application and the time of operation is significantly high for a single batch operation of column test. Therefore, the next phase sought to eliminate biological dependence by implementing an enzyme-based system capable of operating under controlled, modular conditions: Enzymatic Biooxidation Technology (EnBiTe).

2.10.4. Enzymatic Biooxidation Technology (EnBiTe) of gold from refractory sulfide low/high grade ores

The novel low-temperature Enzymatic Biooxidation Technology (EnBiTe) recovers gold from refractory sulphide ores in this phase of this research. Glucose oxidase (GO) immobilized on modified sawdust improves pyrite breakdown and gold liberation. Citric acid carboxylation increased enzyme activity to 80 μmol/min at 1 wt.% glutaraldehyde concentration, with hydrogen peroxide generation peaking at 20-24°C. The optimized biooxidation conditions—100 mM substrate, 5 g immobilized enzyme, 1 g/Liron (II), and 20% ore content—dissolved 89.2% pyrite for high-grade ore sample (HGOS) and 73.4% for low-grade samples. In 20 hours at pH 10–11, cyanidation recovered maximal gold, with HGOS recovering more. These findings suggest that EnBiTe might replace standard pretreatment procedures in colder climates as an effective and environmentally acceptable alternative.

Rationale for next phase: To confirm the industrial feasibility of EnBiTe, especially under operationally relevant flow conditions, the next research phase applied the enzymatic modules to column systems simulating heap leach environments.

2.10.5. Enzymatic Biooxidation Technology (EnBiTe): Column test for recovery of gold from refractory sulfide ores

This research examined Enzymatic Biooxidation Technology (EnBiTe) for gold recovery from refractory sulphide ores using modular enzymatic systems. Optimal biooxidation conditions included substrate flow rates of 5–10 mL/h, circulation flow rates of 50–200 mL/h, and aeration flow rates of 1.0–2.0 L/min. EnBiTe used two immobilized enzyme modules: a glucose oxidase (GO) module to create oxidizing agents and a catalase (CAT) module to consume hydrogen peroxide and reduce oxidative stress. The parallel configuration of these modules outperformed the serries arrangement. Pyrite dissolution attained 91% under optimum circumstances with a substrate flow rate of 10 mL/h and a circulation flow rate of 100 mL/h. Cyanidation recovered 90% more gold (Au) in parallel with a circulation flow rate of 100 mL/h. This study shows that modular EnBiTe systems are controlled and effective gold recovery technologies that outperform microorganism-assisted biooxidation.

2.11. Thesis Layout

This dissertation consists of Seven chapters, hypotheses and objectives as described below.

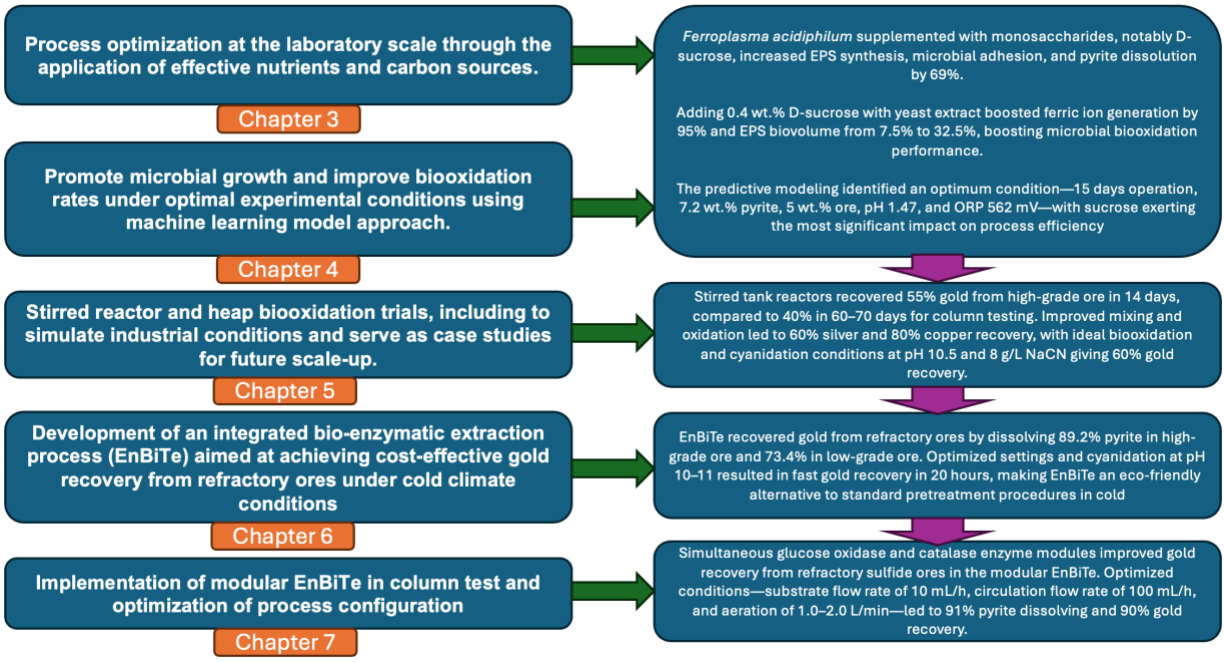

Figure 2.3. Schematic of objectives (left) and summary (right).

2.12. Conclusion

This research progression delineates a clear trajectory from biological augmentation to engineered enzyme systems. The consistent limitations of microbial-assisted biooxidation, including sensitivity to environmental stress, long adaptation periods, and poor performance in low temperatures, necessitated the exploration of non-biological alternatives. The EnBiTe system, through its modular enzymatic approach, will demonstrate high pyrite dissolution and gold recovery efficiency in both lab-scale and operational-scale experiments, establishing it as a scalable and robust solution for refractory gold ore treatment in cold and variable environments.

Chapter 3: Biooxidation of low-grade gold bearing ore using *ferroplasma acidiphilum**

*Mohammad Hossein Karimi Darvanjooghi[1], Kamalpreet Kaur[2], Sara Magdouli[3], Satinder Kaur Brar[4], *Bioresource Technology* 369 (2023): 128476.

Authors' contributions:

[1] Conceptualization, Methodology, Software, Investigation, Formal analysis

2 Genomic and metagenomic analysis, community profiling

3 Supervision, Writing - Review & Editing, Material supports

4 Project administration, Funding acquisition, Supervision, Material supports

Abstract

The adhesion of microorganisms to surfaces and the affecting factors is important in biomining pretreatment. In this chapter of research, the novelty is focused on studying the monosaccharide's impact on the adaptability and adhesivity of *Ferroplasma acidiphilum* for oxidization of sulfide-bearing ore containing pyrite harboring 98 % of gold in its crystal lattice. D-sucrose increased EPS production with the highest amount of pyrite dissolution (69%) as compared to the other types of monosaccharides (D-galactose and D-fructose). Addition of 0.8 wt. % D-sucrose enhanced the production of ferric ions 65% for the ore load of 20 wt.% while for the addition of 0.4 wt.%, the ferric ions concentration was maximum up to 95 %. The results indicated that the addition of both yeast extract and D-sucrose with the concentration of 0.4 wt.% enhanced the EPS (Extracellular Polymeric Substances) biovolume fraction from 7.5 to 32.5 v/v%.

3.1. Introduction

To extract metals from polymetallic ore, biotechnology is an environmentally friendly method that aligns with Canada's climate change action plan (Garrido-Cardenas et al., 2020; Ofori-Sarpong et al., 2011; Pakostova et al., 2020; Zhao et al., n.d.). Thus, the ability of certain acidophilic bacteria to aid the oxidative dissolution of sulfide minerals is very promising as well as the extraction of precious metals within assisted microbial activity is a trend (Jerez Guevara, 2011; Johnson, 1998c, 2008; Johnson & Bangor, 2009).

It has been reported that the ore sample that gold content higher than 2~2.5 g/ton the ore sample is classified as a high-grade sample and below this range, the matrix is known as low-grade gold ore. These criteria are reported based on the techno-economic analysis for the pretreatment of a wide range of ore samples (Darvanjooghi et al., 2021; Rohwerder et al., 2003). The presence of pyrite, pyrrhotite, chalcopyrite, and arsenopyrite which enclose the gold particles restricts the recovery of gold from ore sample using conventional methods such as cyanidation; therefore, implementation of a pretreatment is wise to remove the minerals that surround the gold particles (Rossi, 1990). Also, for a recovery higher than 80~85% using cyanidation, the ore is categorized as non-refractory and for a recovery less than this criterion, the ore is classified as refractory.

Proteobacteria, *Actinobacteria*, and *Firmicutes* bacteria have been shown to oxidize and dissolve metal sulfide minerals, such as ferrous iron (Fe_2S) and sulfur compounds, such as sulfur dioxide (SO_2) to produce ferric ions and protons (Garrido-Cardenas et al., 2020; Mahmoud et al., 2017; Pakostova et al., 2020; Zhao et al., n.d.). These microorganisms can grow under conditions with sufficient inorganic compounds by providing sufficient oxygen in an acidic environment (Mahmoud et al., 2017; Yadollahi et al., 2021). Optimizing heat transfer and operational parameters such as irrigation and oxygenation rates are critical to enhancing the oxidation of sulfide minerals over a wide temperature range. The contact of bacterial populations and surface's minerals play a crucial role in growth conditions changesets as well as the microbial activity of these microorganisms (Bobadilla-Fazzini & Poblete-Castro, 2021; J. Chen et al., 2022; Ulya, 2022). Therefore, bacterial adhesion to sulfide-based minerals and the inorganic compounds should be taken into account as a critical factor to better understand the biooxidation and its efficacy in laboratory and pilot scale experiments. The presence of toxic minerals such as arsenopyrite and elements such as ferric and arsenic ions inhibit the growth of acidophilus

microorganisms that play important roles in the biooxidation and biomining in general (Jung et al., 2022; Makaula et al., 2020; Pham et al., 2022; N. Vardanyan et al., 2020). Thus, the presence of pyrite and arsenopyrite structures that are present in refractory ore samples may reduce the microorganism's activity and the rate of biooxidation.

Employing monosaccharides to trigger the formation of extracellular polymeric substances (EPS) in chemolithoautotrophic bacteria does not hinder bacterial activity when the microorganisms are adapted to the arsenic-based mineral substances and available ions that generally lead to the declination of bacterial activity (Bellenberg et al., 2012; Saavedra et al., 2020). It is evident from the previous study that gal operon is majorly found in bacteria cells (particularly in *Acidothiobacillus ferrooxidans*), where the ferrous ions act as an energy source (energy substrate) throughout the biological mechanisms in relation to those that use sulfur.

The different types of carbon sources (D-Galactose, D-Fructose, and D-sucrose) influence the biooxidation rate by modifying bacterial activity in the presence of ions, and other types of inhibitors. Therefore, monitoring and characterizing the acidophilic microbial populations (consortium) in environmental samples is vital for the optimization of biooxidation of refractory gold ores. Biooxidation of refractory gold ore at an industrial scale needs to work with the mixed consortium since working with pure culture/consortium cultures is challenging due to the complexity of the minerals. In this regard, implementing sequencing analysis is another scope of this research paper in which determining the specific strains, associated with relevant metabolic activities, will aid to understand the effect of the sugar types on the community profiling of the microorganisms. Taken all together, the main scope of this research chapter is to understand the effect of different monosaccharides and their concentrations on the activity of acidophilic microorganisms which are obtained from acid mine drainage (AMD, from Hammond reef mine site in Canada) in the presence of different concentrations of real refractory gold ore samples in the solution, which also contains other toxic metals such as arsenic. Also, monitoring and measuring EPS biosynthesis, responsible for any change in the biooxidation of refractory gold ores, will help to establish the effect of it on the growth and activity of other acidophiles.

3.2. Materials and methods

$(NH_4)\ SO_4$, $MgSO_4.7H2O$, K_2HPO_4, KCl, $FeSO_4.7H2O$, sulfur powder and $Ca(NO_3)_2.H_2O$ with high purity (>98 wt.% from Merch Co. Canada) were used for the preparation of media and inoculation of microorganisms. Also, ore samples were collected from the gold mine site and the samples were ground to obtain particles size of 100-200 μm. To understand the effect of monosaccharides on the biooxidation rate, D-galactose (99.95 wt.% from Merck Co.), D-sucrose (99.9 wt.% from Merch Co.), and D-sucrose (99.99 wt.% from Merch Co.) was prepared and added to the solution with three different quantities. $BaCl_2$ (99.6 wt.%), glycerol (99.9 wt.%), and HCl (37 wt.%) were used for the measurement of sulfate concentration. Also, the concentration of sulfite was measured using a titration of iodide/iodate with high purity (99.5 wt.%) in the presence of Ethylenediaminetetraacetic acid (EDTA, with 98 wt.% purity) and starch as an indicator. Wheat Germ Agglutinin (WGA), Alexa Fluor™ 488 Conjugate (purity of 99.99 wt.%) and Fluorescence Propidium iodide, Millipore Sigma, (FPI, with 90.0% purity) were used for labelling the EPS and nucleic acids macromolecules during the biooxidation of the ore sample.

3.2.1. Characterization of low-grade ore samples (LGOS)

Different types of analysis were carried out for the characterization of mineral ores and microbial populations. X-Ray Diffraction (XRD) and X-Ray Fluorescence (XRF) tests were performed for the determination of the crystals and minerals in the ore. The results of XRD data were gathered by using the radiation of CuKα. To do so, the mineral samples were ground into small particles of 10-50 μm and then introduced to the XRD test. The measurements were performed on the samples in a 2θ range between 5° and 70°. To measure oxides-based minerals, XRF tests also were carried out on samples. The gold inclusion in the minerals (pyrite and other minerals) was determined using a photo-micrograph study. To do so, the mineral engagement determination in fine-grained sizes of the samples was carried out using analysis of polished sections. The results and related microscopic images of the polished section were collected by Zeis Microscope, 2000. The elemental composition of the gold, other metals, and non-metals inside the ore sample was determined using the Inductive Couple Plasma (ICP) test. To measure the concentration of total iron in the solution, Microwave Plasma Atomic Emission Spectroscopy (MP-AES) with a standard

absorption curve of different iron concentrations was used in the experiment. For MP-AES, the maximum amount of emission was achieved at the wavelength of 440 nm.

A confocal laser scanning microscope (CLSM) was used to examine the EPS. For each study, 1 mL of sample was obtained and stored at 5°C in 2% glycerol for preparation. About 10 µL of samples were placed on a circular reverse glass slide for 10 minutes before being submerged in methanol for 10 minutes. The EPS carbohydrates were labelled with wheat germ agglutinin (WGA) as a fluorophore and propidium iodide (PI) for labelling the nucleic acids. The fluorophore was incubated with the specimen for 2 hours before being observed using suitable laser excitation wavelengths and optical filters (argon laser: 488 nm, 505-550 nm bandpass filter). Image J software was used to determine the bio-volume fraction (v/v %), the relative quantity of cells, and EPS to the sample's image volume.

3.2.2. Consortium inoculation and biooxidation

The experiments run for different concentrations of monosaccharides (0, 0.4, and 0.8 wt.%) in the presence of 0.4 wt.% of yeast extract as an inducer to produce EPS. To understand the effect of various monosaccharides on the microorganism's adaptation to the refractory ore sample, the ore content was introduced to the flasks at the loading rate of 5, 10, and 20 wt.%. The source of the microorganisms was the acid mine drainage from the Hammond reef mine site. To inoculate the microorganisms, 9K media with salts compositions of 3 g/l $(NH_4)_2SO_4$, 0.5g/l $MgSO_4$.7H2O, 0.5g/l K_2HPO4, 0.1g/l KCl, 0.01g/l $Ca(NO_3)_2.2H_2O$ was used. The temperature of inoculation was fixed at 37.1℃ for an incubation period of 22 days at 180 rpm in a rotary incubator. The initial ferrous and sulfur concentration was kept at 0.2 and 0.1 g/l to activate the growth of both sulfur and iron oxidizing microorganisms. During the inoculation, pH and Oxidation-Reduction Potential (ORP) were measured using commercial electrodes. Ferric and ferrous ions concentrations were measured to understand the activity of bacteria during biooxidation. The level of ferrous ions concentration was measured using titration with potassium dichromate and the total concentration of iron in the solution was measured using MP-AES. Finally, the concentration of ferric ions was calculated from the difference in total iron and ferrous ions concentrations. After the inoculation, the samples were collected at a regular interval of 24 hours for 22 days to measure the efficiency of biooxidation and gold recovery.

3.2.3. Genomics Analysis

3.2.3.1 Sample preparation and DNA isolation

To identify the types of microorganisms influenced by the addition of different monosaccharides during biooxidation, 16s sequencing was performed for community profiling. Nucleic acid (DNA) was isolated from the samples using the Quick-DNA Fecal/Soil Microbe MidiPrep kit from Zymo Research (Cedarlane, Burlington, ON, Canada). DL-Dithiothreitol (Sigma-Aldrich, Oakville, ON, Canada) was added to the Genomic lysis buffer instead of beta-mercaptoethanol.

3.3. Results and discussion

3.3.1. Element analysis (XRD and ICP)

ICP and Fire assay, XRF, and XRD were performed to identify the elemental composition, metal oxides, and mineral phases in the representative sample (LGOS), respectively. **Table B1** (in Appendix B) shows the result of XRF, elemental ICP analysis. According to the XRF data in **Table B1** (in Appendix B), SiO_2 with 66.2%, and Al_2O_3 with 13.2% are the main components of the sample. The gold grade was also determined around 477 ppb (0.477 ppm) which is classified as a low-grade gold-bearing (refractory) sample. In addition, it is shown that the amount of arsenic in the ore sample is 4.1 ppm (adversely influencing the bacteria growth) is higher compared to the grade of gold in the ore sample and it can play an inhibitory role in microorganisms' growth.

Two samples were introduced for XRD analysis. Quartz at 44.6%, plagioclase at 22.5% and mica at 20% were the dominant minerals in the raw ore. Due to the small amount of the sulfide mineral, the detection was not possible (Appendix B **Table B2**). To increase the concentration of pyrite and sulfide minerals in the ore sample, bromoform (density of 2.89 g/cm^3) as a heavy liquid was used to separate light minerals and increase the concentration of pyrite (5 g/cm^3) in the bottom of the solution. According to the result, Ankerite with 58.1% was the dominant phase rather than other minerals (Appendix B **Table B2**). In the sample concentrated with bromoform, pyrite content was measured. The results of (Appendix B **Table B2**) indicate that pyrite is the only sulfide mineral in the ore sample that contains the major portion of gold particles.

A summary of the distribution of gold associations in the sample is presented in (Appendix B **Table B3**). According to this data, it is concluded that most of the gold is present in sulfide-based

minerals. Therefore, less than 0.4% of the gold in the sample is associated with other non-opaque gangue minerals.

According to the results presented in Appendix B **Table B3**, it is concluded that for the most part, gold particles are very fine- to extremely fine-grained (overall particle average 4.3 μm); gold particles are entirely or partly associated with other minerals (mainly sulfides); approximately 75% of the gold particles present a mode of occurrence that would separate readily under milling stresses (at grain boundaries or along thin fractures); roughly 25% of the gold particles occurs entirely locked in sulfides.

The micrograph images were used to visualize the inclusion of gold in different minerals in the ore samples (Appendix A **Fig. A4**). According to these images, it is concluded that gold can be found mostly in sulfides minerals and chalcopyrite. However, some of the gold fractions might be in association with silicate minerals and the form of electrum (associated with other metal alloys). These results indicate that the native gold inclusion in pyrite and the gold is likely occurring at the pyrite cleavage limit and for some samples native gold inclusion in pyrite. The results of the gold inclusion image indicate that gold is associated with chalcopyrite partly occurring at the pyrite cleavage limit while other image shows the presence of native gold in lead-sulfosalt. This portion of gold occurs as inclusion, and at sulfosalt silicate grain boundaries (circle on the right) as well as galena and chalcopyrite. Moreover, an uncommon occurrence of gold occurring as inclusion in chalcopyrite as well as the gold grain at chalcopyrite-pyrite grain boundaries are also observed during studying mineralogical phases and gold inclusion of the sample. The results reveal the electrum inclusion of gold in galena (or Au-Pb Telluride) which is uncommon very low compared to the other types of gold occurrence in the ore sample.

3.3.2. Biooxidation

The pH and ORP fluctuations during biooxidation are the key factors that indicate the changes in microorganisms' activity due to the addition of carbohydrate sources such as yeast extract and monosaccharides (Appendix B, **Fig. B5**). Results showed that the addition of just yeast extract does not influence the pH and ORP in the absence of the monosaccharides throughout the biooxidation period. However, the addition of yeast extract increased the ORP of the solution just after 9 days indicating the positive effect on biooxidation and the bacteria growth. On the other

hand, yeast extract reduced the pH of the solution faster compared to its absence in the sample. Furthermore, the value of pH was maximum after passing 20 days for the highest ore loading sample. A similar trend was also followed by the other samples containing monosaccharides for both pH and ORP. However, the competition for obtaining the highest value of ORP and pH at the early biooxidation stage in all the samples was different. To understand the efficiency of biooxidation, further tests including the measurement of total iron concentration, ferric and ferrous ions concentration, as well as pyrite dissolution efficiency needs to be carried out.

To understand the effect of yeast extract on the biooxidation with an increase in ore loading rates, the amount of pyrite dissolution was calculated at the end of the experiment and the results were compared with the control devoid of yeast extract (**Figure 3.1**). The results indicated that the addition of yeast extract enhanced the ability of pyrite dissolution by improving microbial cell concentration at a low ore loading rate of 5 (wt.%) and for the higher concentration of 20 (wt.%) the ability of microorganisms for pyrite removal decreases. Furthermore, when no yeast extract is added to the sample, the efficiency of biooxidation does not change at any ore loading rate i.e. less than 20% (**Figure 3.1**).

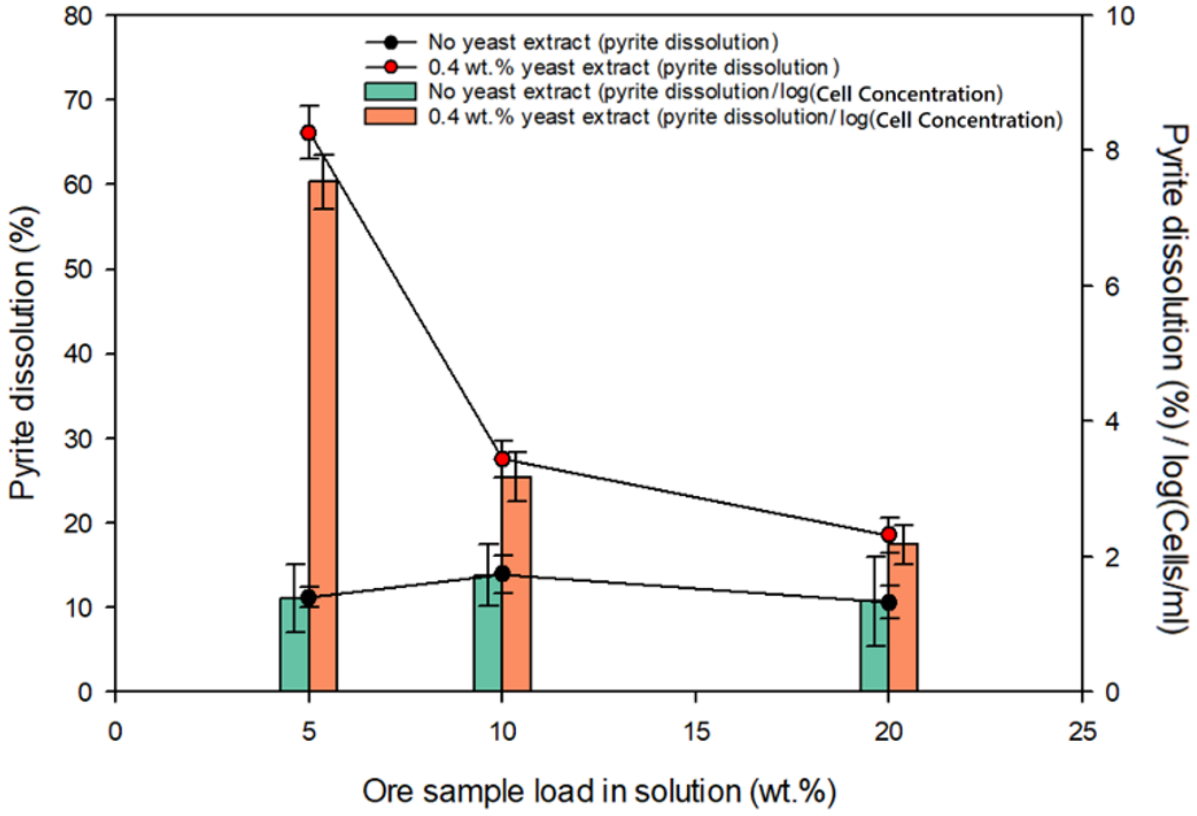

Figure 3.1. Pyrite dissolution in the presence and absence of yeast extract.

Since the amount of ferric ions concentration in the biooxidation plays an important role in the dissolution of pyrites and is an indicator for the activity of the microorganisms and their efficiency in the process, the plot of ferric ions concentration will help to understand the effect of monosaccharides concentration and types on the biooxidation rate (**Figure 3.2**). The results represented the amount of ferric ions production in the process vs the time of incubation. The maximum value of ferric production was attributed to the sample containing D-sucrose (0.4 wt.%) at an ore loading rate of 20 wt.%. However, the addition of other types of monosaccharides (D-galactose and D-fructose) positively regulated the production of ferric ions in the solution. Based on collected data (**Figure 3.2**), it is evaluated that the addition of 0.8 wt.% D-galactose, D-fructose, and D-sucrose improve the production of ferric ions 33.5%, 49%, and 65% at an ore loading rate of 20 wt.% and while for the addition of 0.4 wt.% the ferric ions production is maximum corresponding to 95 % recovery efficiency. Finally, it is concluded that the addition of 0.4 wt.% of D-sucrose regulates the microbial ability to overproduce ferric ions as well as to get acclimatize

to the high ore loading concentrations. The results of the ferrous ions concentration ales are shown in **Figure 3.3**. According to this figure, the concentration of ferrous ions drops from roughly 0.18 to 0.2 g/L after passing 9 days to 0.05 g/L. Moreover, these results indicate the reaching of a high concentration of ferrous ions when 5 wt.% of ore sample is added to the solution in the presence of 0.4 and 0.8 wt.% of D-sucrose.

Another parameter that aid to understand the efficiency of biooxidation is the ferric ions production (FOP) with respect to the microorganism's cell concentration in solution. The results of ferric ions on cells concentration for different conditions and the presence of D-galactose, D-fructose, and D-sucrose are shown in **Figure 3.4 a**. By the addition of D-sucrose, the amount of FOC increased when the ore loading rate was higher in the solutions. The addition of D-galactose and D-fructose does not influence the FOP for samples having ore loading rates lower than 10 wt.%. This study revealed that D-galactose and D-fructose have a low positive effect on the tolerance of the microorganisms to the high ore concentrations in the solution. Furthermore, the increase of D-sucrose from 0.4 to 0.8 wt.% decreased the amount of FOP which represents the negative effect of high D-sucrose concentration. The results of **Figure 3.4 b** also showed that the maximum pyrite dissolution was attributed to the condition where 0.4 wt.% D-sucrose added to the sample with 20 wt.% ore loading rate.

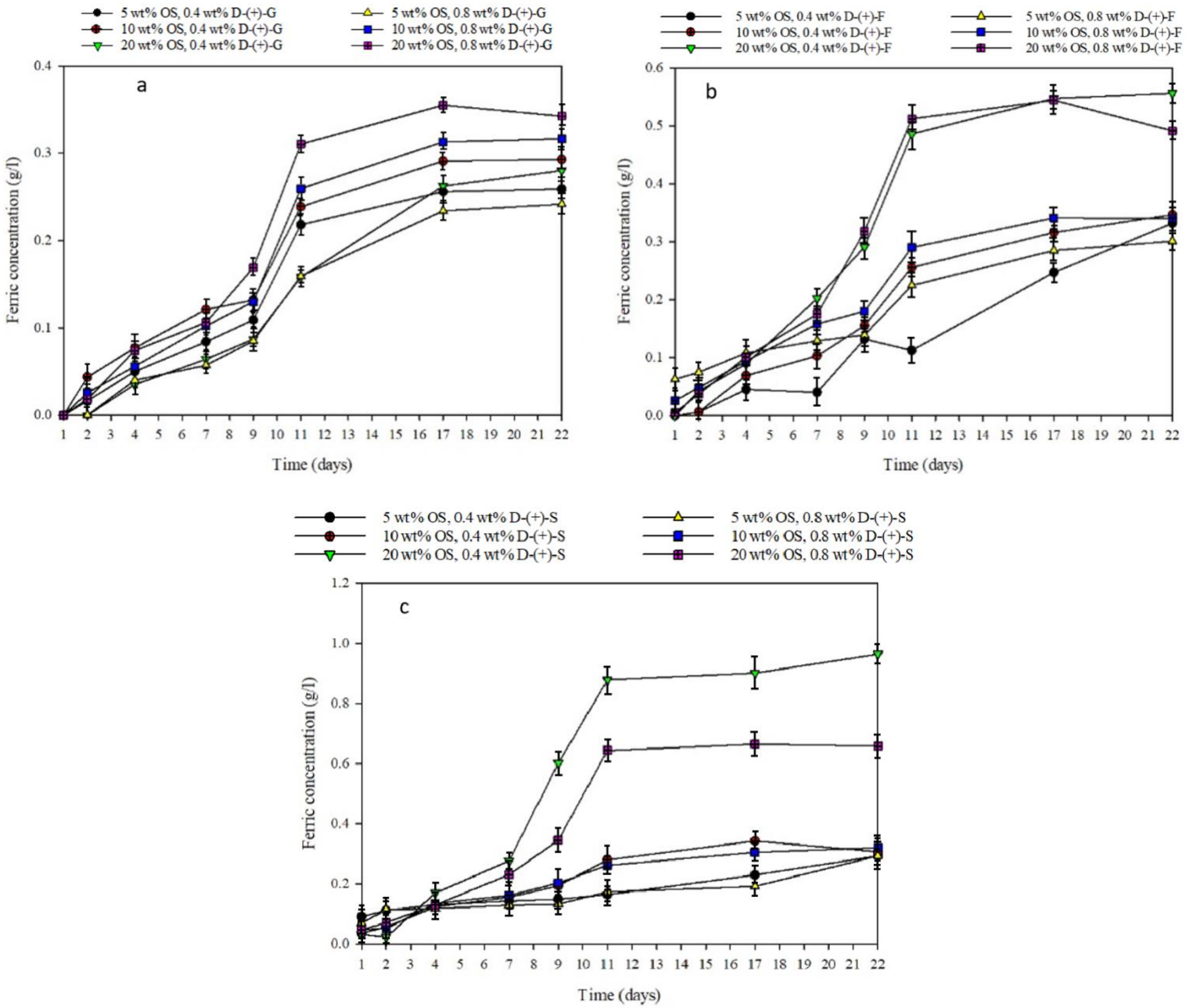

Figure 3.2. Ferric production in presence of: a), D-galactose, b), D-fructose, c), D-sucrose (OS: ore sample, D-+-G: D-galactose, D-+-F: D-fructose, D-+-S: D-sucrose).

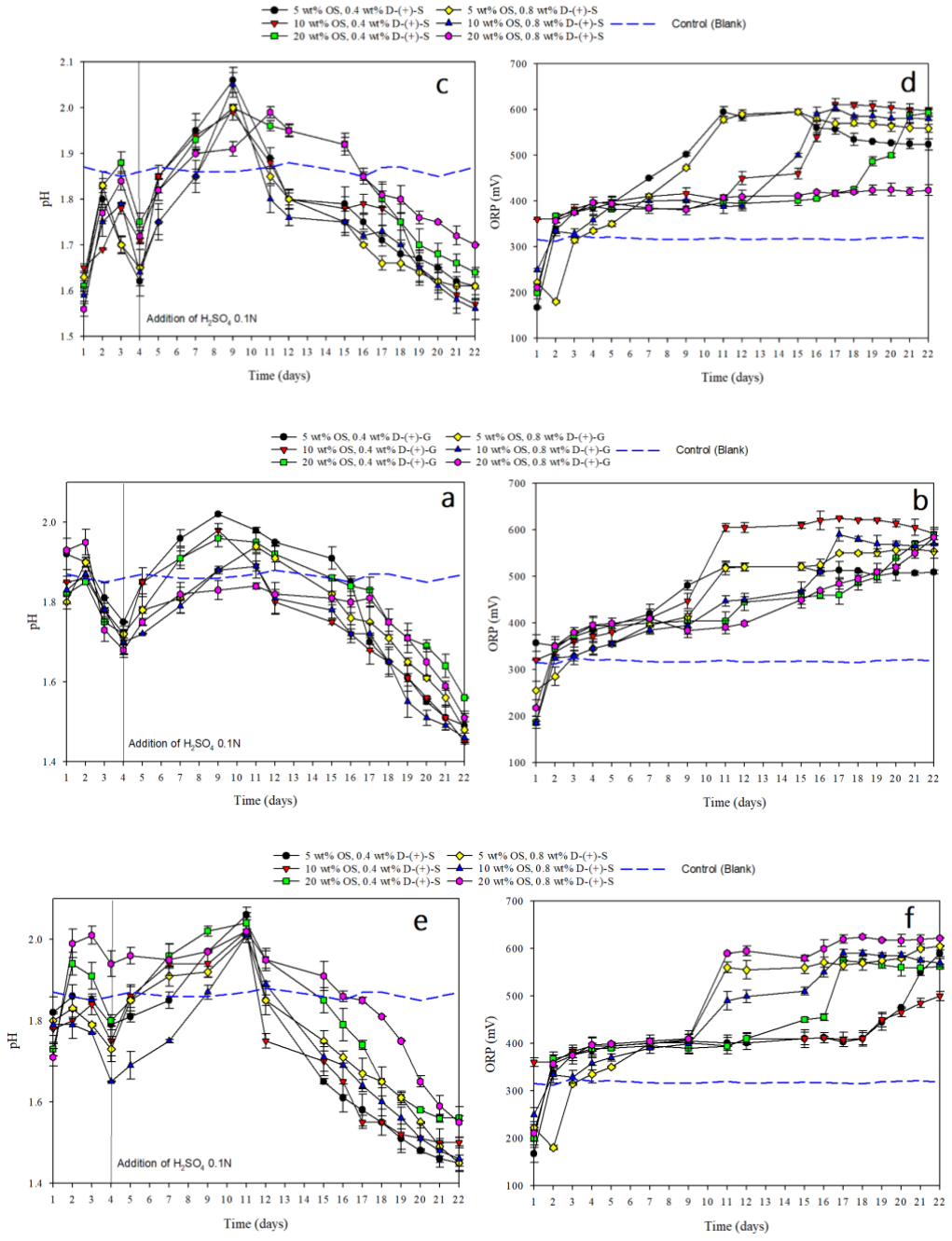

Figure 3.3. pH and ORP of biooxidation of ore sample in the presence of monosaccharides (a and b, D-+-G, c and d, D-+-F, e and f, D-+-S) and yeast extract (OS: ore sample, D-+-G: D-galactose, D-+-F: D-fructose, D-+-S: D-sucrose)- reference condition: Ag/AgCl 1 M KCl.

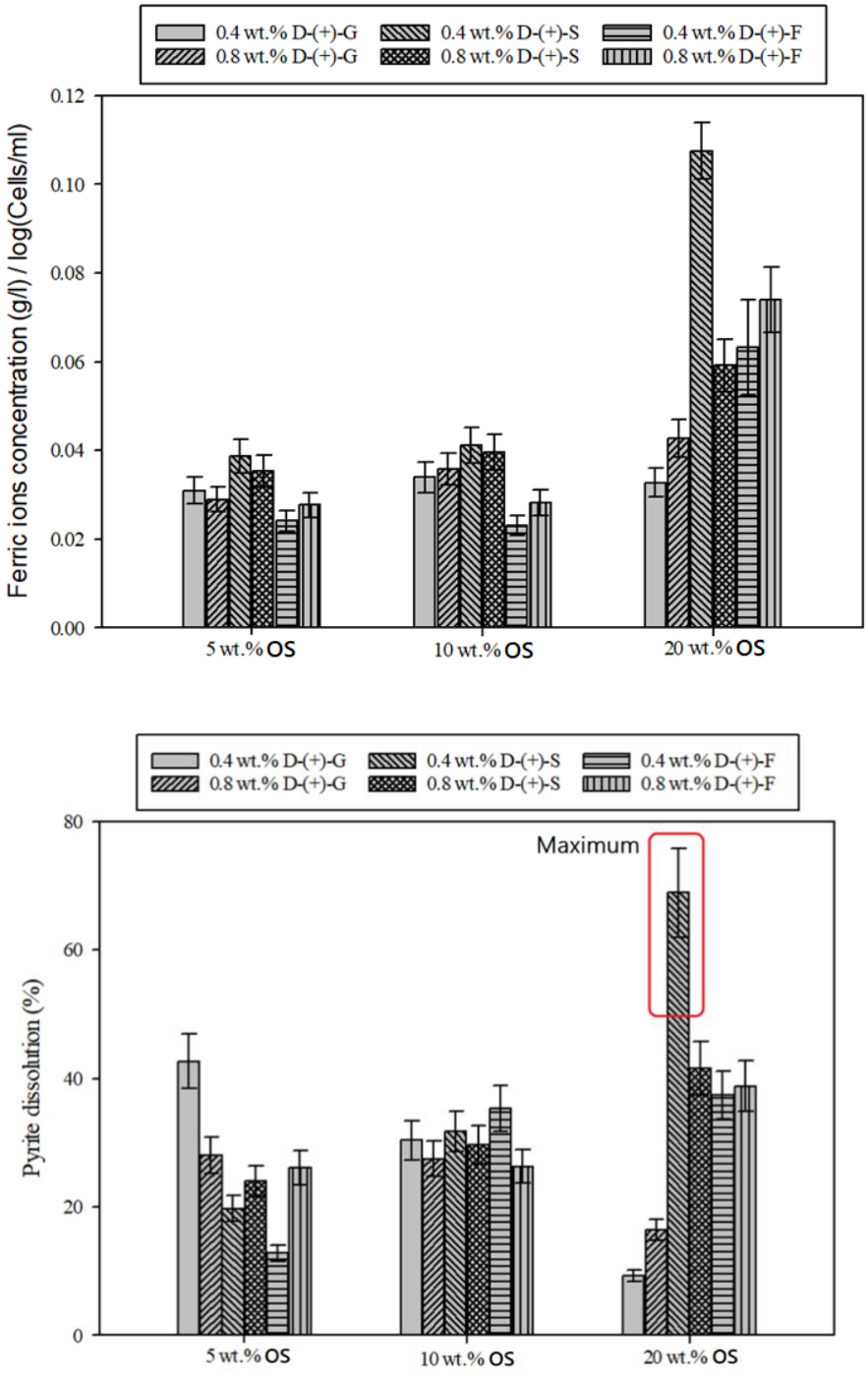

Figure 3.4. Ferrous ions consumption (a), pyrite dissolution (b) in the presence of different monosaccharide types (OS: ore sample, D-+-G: D-galactose, D-+-F: D-fructose, D-+-S: D-sucrose).

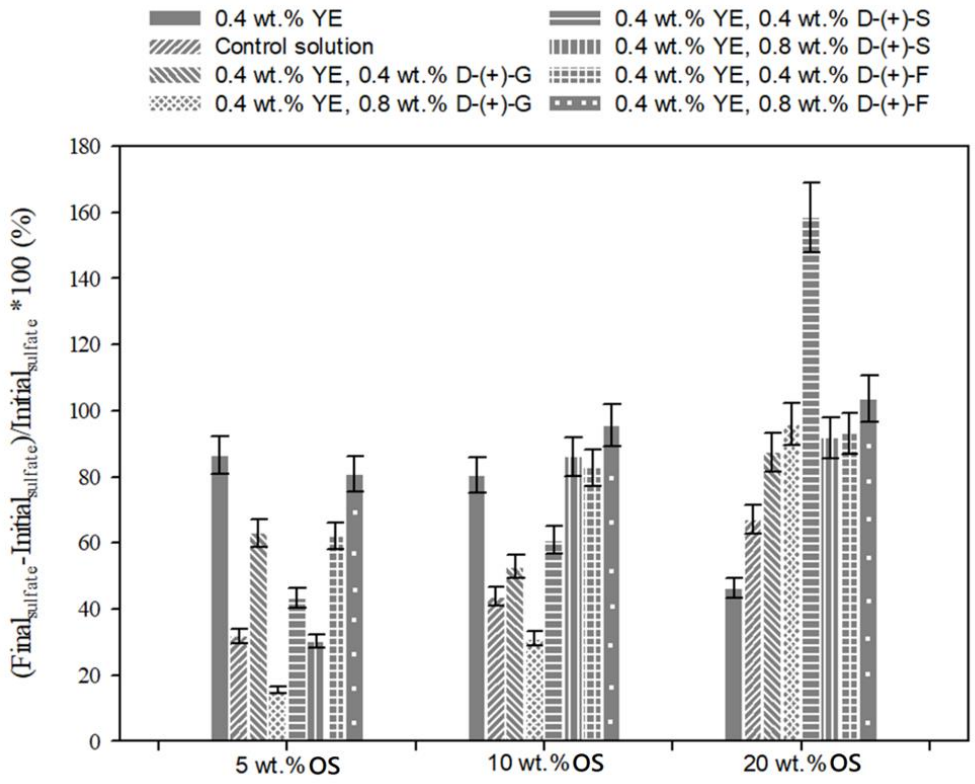

Figure 3.5. Sulfate production in presence of different types (OS: ore sample, D-+-G: D-galactose, D-+-F: D-fructose, D-+-S: D-sucrose) of monosaccharides and yeast extract.

The results of sulfate production where D-sucrose (0.4 wt.%) was added to the solution were correlated with 20 wt.% of ore sample in the solution (**Figure 3.5**). This indicated that a higher amount of pyrite destruction leads to the production of sulfate as a by-product.

Current results were compared with the previous study on the implementation of two microorganisms of *At. thiooxidans* DSM 14887T and *L. ferrooxidans* DSM 2705T (with different portions of 30:70, 50:50, and 70:30) in the presence of an optimum concentration of D-galactose (Aguirre et al., 2021). The value of $Q_p.\emptyset$ (production rate multiplied by ore sample weight fraction) was used for both sulfate and ferric ions production to compare different results. It is concluded that this parameter is higher for the *Ferroplasma acidiphilum* used in the current study ($(Q_p.\emptyset)_{Fe(III)}$= 0.659 $\frac{mg}{l.h}$, for literature data: $(Q_p.\emptyset)_{Fe(III),30:70}$= 0.007 $\frac{mg}{l.h}$, $(Q_p.\emptyset)_{Fe(III),50:50}$= 0.194 $\frac{mg}{l.h}$, and $(Q_p.\emptyset)_{Fe(III),70:30}$= 0.182 $\frac{mg}{l.h}$); however, the value of pH reduction for *Ferroplasma Acidiphilum* (ΔpH=0.27) was lower than the mixture of microorganisms with any

portion ($\Delta pH_{30:70}$=0.32, $\Delta pH_{50:50}$=0.38, $\Delta pH_{70:30}$=0.36) from the literature. The value of sulfate production for *Ferroplasma Acidiphilum* was higher ($(Q_p.\emptyset)_{Sulfate}$= 0.276 $\frac{mg}{l.h}$) as by-product compared to the mixture of *At. thiooxidans* DSM 14887T and *L. ferrooxidans* ($(Q_p.\emptyset)_{Sulfate,30:70}$= 0.130 $\frac{mg}{l.h}$, $(Q_p.\emptyset)_{Sulfate,50:50}$= 0.234 $\frac{mg}{l.h}$, and $(Q_p.\emptyset)_{Sulfate,70:30}$= 0.114 $\frac{mg}{l.h}$). Although the production of sulfate may affect the production and recovery rate adversely; yet the amount of ferric ions concentration production is tangible for *Ferroplasma acidiphilum* and compensates the adverse impact of sulfate production as a pollutant in environment.

3.3.2.1. SEM analysis of samples

The results of Scanning Electron Emission (SEM) analysis also are shown used to understand the pyrite dissolution in ore samples (Appendix B, **Fig. B6**). According to these results, the particles of raw ores are larger than the processed ones and by the addition of D-sucrose, the smallest ore particles are achieved. The results of SEM analysis for the raw (unprocessed) samples are shows that the average particle sizes are up to 50-60 μm, showing large particle sizes. For the condition where the samples underwent biooxidation in the absence and presence of yeast extract the same results are achieved and large particle sizes ranging from 5 to 50 μm are seen in the images. However, the average particle sizes are smaller than the raw sample indicating the dissolution of the portion of pyrite in the ore sample. The presence of fine particles with larger visual quantity is obtained in the promoted biooxidation in the presence of both yeast extract and D-sucrose. This indicated that the addition of the monosaccharides enhanced the ability of microorganisms to the dissolution of pyrites in the ore sample and reduced the size of the ore grains. For all samples the rotation speed of the incubation period was 180 rpm in shake flask tests and the ore sample concentration was kept at 5 wt.%. To bring a more accurate comparison between the different conditions, Image Plus software was used to measure the average sizes of the grains before and after the biooxidation at different conditions.

The distribution curves for ore particles are shown in **Figure 3.6 a**. The smallest ore particles were obtained after biooxidation when 0.4 wt.% D-sucrose was added to the solution and the addition of yeast extract enhanced the pyrite destruction and reduced the ore sample particle size. Therefore, the particle size with maximum distribution (%) were 600, 1000, 1750, and 2000 nm for the

condition where 0.4 wt.% D-sucrose added to the solution, in the presence of yeast extract, absence of yeast extract, and raw sample, respectively.

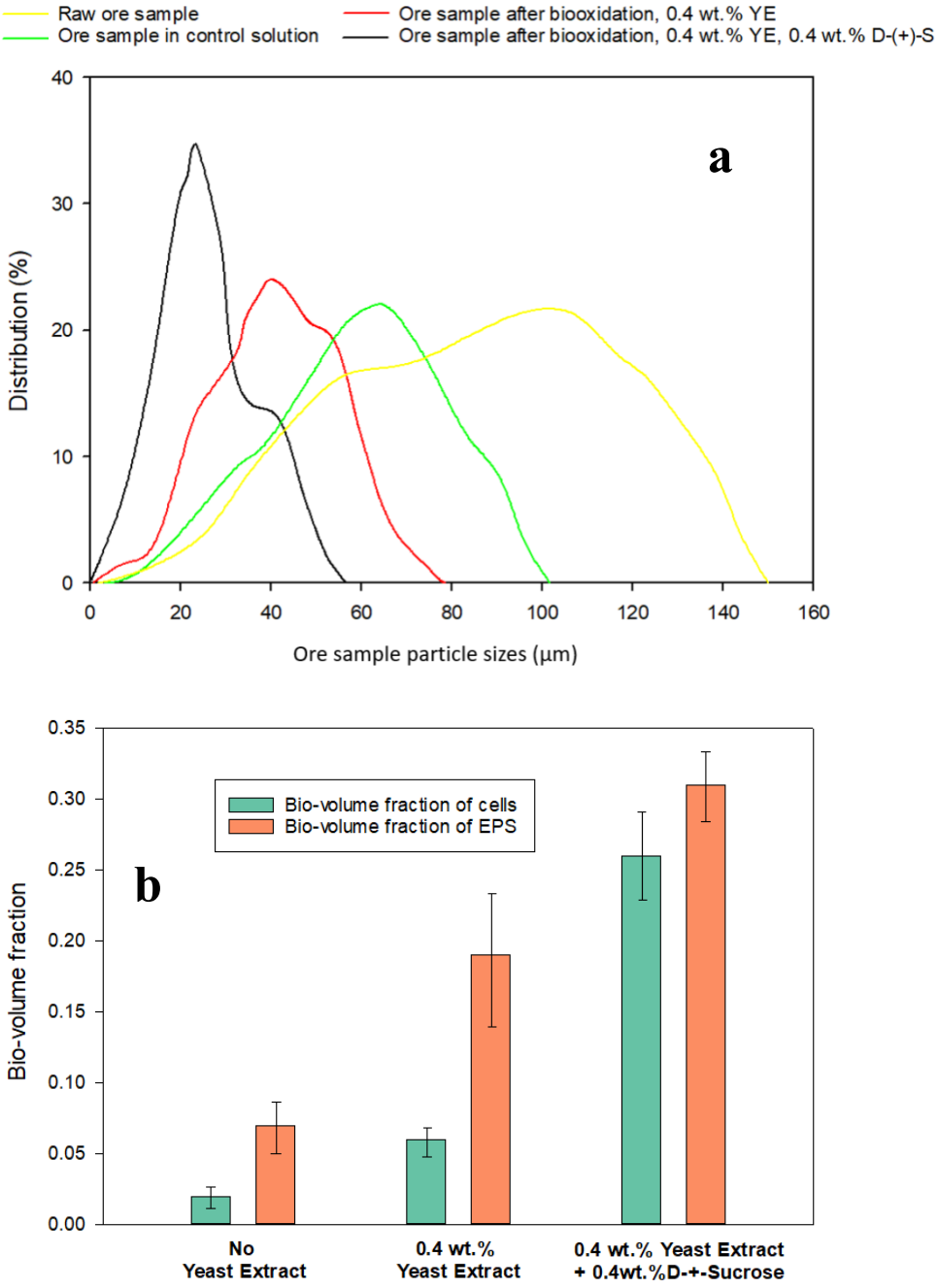

Figure 3.6. a), Particle size distribution of ore sample before and after biooxidation, and b), quantitative bio-volume of cells and EPS (extracellular polymeric substances) for the different conditions after biooxidation; YE: Yeast extract.

3.3.2.2. Role of EPS

Extracellular Polymer Substances (EPS) play a significant role in biooxidation through the "*indirect mechanism*" which comprises both "*non-contact*" and "*contact*" ways (Rawlings, 2002b; Sand et al., 2001). Several techniques are probably important in biooxidation, and a single mechanism is not adequate to understand the complete response. It is still uncertain whether microorganisms directly react with dissolved molecular oxygen during biooxidation of sulphur-based minerals despite numerous studies that have been carried out to highlight mechanisms related to their biological activity.

To name a few of its roles, EPS provide an active and absorbing surface, aid in stabilizing of the biofilm's structural integrity, and serve as a barrier against biocides and other media inhibitors. The microbial cells produce EPS and secret it into the surrounding environment (Wenbin et al., 2011; R. Yu et al., 2013). The broken microbial cells also contribute to EPS release, where it might build up on cell surfaces or be dispersed throughout the environment. One of the mechanisms reported in the adaptation process of microorganisms is the synthesis of EPS, which is generally a cell reaction to adverse environmental circumstances such as high and low temperatures, metal ions, inhibitors, etc. (Geyik & Çeçen, 2015). The inclusion of EPS in biohydrometallurgical processes would promote bacterial adhesion to the mineral and its subsequent role in the production of biofilm on minerals, enhancing chemical reaction on the mineral and hence process efficiency (Gehrke et al., 1998). As a result, the synthesis of EPS in planktonic cells may result in improved cell attachment capacity as well as protection against harsh environments (Saavedra et al., 2020).

Figure 3.6 b shows the results of EPS and cell bio-volume production for different conditions. The EPS is viewed separately, evidently in a homogenous dispersion, surrounding each cell in images that were obtained from Confocal Laser Scanning Microscopy. As it is shown in this figure, the EPS and cell bio-volume are comparable in the presence of D-sucrose (0.4 wt.%) and yeast extract (0.4 wt.%) while the amount of cell bio-volume is 80% less for the condition that no monosaccharides are added to the solution. According to the results obtained, the addition of both D-sucrose and yeast extract with concentrations of 0.4 wt.% leads to enhancement in the EPS biovolume from 7.5 (v/v %) to 32.5 (v/v %). Moreover, this increase is also seen for the biovolume fraction of cells when they are exposed to the 0.4 wt.% of both D-sucrose and yeast extract. This

clearly stated that the microorganism's biovolume was larger compared to the control sample. Previous literature reported that bacterial EPS increased under stressful situations, including being exposed to excessive copper and other heavy metal concentrations (R. Yu et al., 2013). On the other hand, bacteria are known to undergo morphological alterations under stressful situations (Young, 2006; R. Yu et al., 2013). Barreto et al.(2005a) reported this shift in the biovolume of acidophilic microorganisms and ascribed it to EPS overproduction (Barreto, Gehrke, et al., 2005).
The results of fluorescence microscopic imaging from the consortium indicate that the addition of D-sucrose and yeast extract with the same weight concentration of 0.4 wt.% leads to the maximum amount of EPS overproduction and cell growth (Appendix B, **Fig. B7**). Accordingly, it is concluded that for the condition that no yeast extract and D-sucrose are added the numbers of microorganisms are less compared as a result.

The higher amount of EPS will enhance the adaptability of bacteria to the presence of elements and ions that are toxic for their growth. The higher EPS production helps bacteria to tolerate higher concentration of arsenic ions in the solution and act as a shield that keeps microorganism from deactivation and death (Saavedra et al., 2020). Due to the high oxidizing potential of ferric ions, other types of minerals (which do not enclose gold) may be dissolved and this leads to a significant reduction in biooxidation rate of desired minerals (pyrite). Production of a higher amount of EPS will help to keep the concentration of ferric and ferrous ions high in the EPS matrix and lead to higher biooxidation efficiency (Beech & Cheung, 1995; Bhaskar & Bhosle, 2006; Sheng et al., 2013).

The nucleic acids inside the microorganisms were labeled using PI during the preparation of the sample for CLSM imaging. The implementation of this compound as a dye is used to understand the results of higher concentration of nucleic acids macromolecules when both yeast extract and D-sucrose is used. Finally, the content of carbohydrates inside the produced EPS during biooxidation was visualized using CLSM similarly. These results indicated that the addition of both yeast extract and D-sucrose with the similar concentration of 0.4 wt.% leads to enhanced EPS production which is responsible for higher efficiency in biooxidation. It has been reported that glucose has an inducing effect on the growth of iron and sulfur-oxidizing acidophilus microorganisms. This carbohydrate stimulates EPS production; however, their high concentration limits the growth rate of microorganisms (Silver et al., 1967). In this research, D-sucrose is more

effective in EPS over-production as it consists of one glucose and one fructose structure and after deformation in the microorganism's metabolism pathway, the same carbohydrate molecules are produced. As an example, the protein-precursors (i.e. UDP-glucose, UDP-galactose, and dTDP-rhamnose) in *At. ferrooxidans* are known to be involved in the biosynthesizes of EPS, transformation of monosaccharides molecules, and the production of more complex polysaccharides (Barreto, Jedlicki, et al., 2005). Therefore, not only does the addition of D-sucrose enhances the production of EPS due to the galactose formation, but also it helps with the overproduction of polysaccharides with a more elaborate form because of fructose molecular structure and engagement in the polysaccharides chain. This helps to intensify the adhesion property of microorganisms to ore sample and increase in biooxidation rate.

3.3.3. Community profiling

The results of the microbial community profiling were used to understand the community profiling before and after biooxidation and their role in gold recovery (Appendix B, **Fig. B8**). According to these results, it is concluded that before performing the biooxidation, roughly less than 15% of the microbial community was *Ferroplasma acidiphilum*. Acid mine drainage (highly acidic pH ≤ 2.0 and heavy metal-laden) harbor acidophiles which actively participate in geochemical cycles. Bacterium *F. acidiphilum* plays a significant role in the recycling of iron and sulfur compounds (Golyshina et al., 2000b). The results of community profiling for the sample with the highest pyrite dissolution indicate the significant growth of *F.acidiphilum* compared to the other microorganisms. The addition of D-sucrose leads to an increase in the EPS production of *F. acidiphilum* (mentioned in section 3.3.5.).

3.4. Conclusion

The impact of different types and concentrations of monosaccharides were investigated on the adaptability of microorganisms to different ore sample loads. The bacterial profiling study revealed the presence of *Ferroplasma acidiphilum* responsible for the biooxidation. The findings indicated that the addition of 0.4 wt.% D-galactose, D-fructose, and D-sucrose enhanced the production of ferric ions 33.5%, 49%, and 65% for the ore sample load of 20 wt.%. After the addition of D-

sucrose (0.4 wt.%) as a source for polysaccharide and EPS production, the highest amount of pyrite dissolution (69%) was obtained compared to the other types of monosaccharides.

Interface* 1: This phase of the study aimed to evaluate the role of monosaccharides in enhancing the adaptability and surface adhesion of *Ferroplasma acidiphilum* during the biooxidation of pyrite-dominant sulfide ores containing 98% of gold encapsulated within the crystal lattice. Among the tested sugars, D-sucrose proved most effective, achieving 69% pyrite dissolution and elevating ferric ion production to 95% at a concentration of 0.4 wt.%. Additionally, the combined addition of yeast extract and D-sucrose significantly increased EPS biovolume from 7.5% to 32.5%, leading to improved microbial adhesion and oxidation performance. In the subsequent phase, these findings were applied to define and optimize operational parameters for implementation in bench-scale experiments targeting specific ore types.

Chapter 4: Machine learning based prediction of biooxidation of refractory sulfide-bearing*

*Mohammad Hossein Karimi Darvanjooghi, Usman T. Khan, Sara Magdouli, Satinder Kaur Brar, *Current Research in Biotechnology* 7 (2024): 100179.

Abstract

In this chapter, the simultaneous effects of monosaccharides, ore content, pyrite content, and time on the activity and growth rate of *Ferroplasma acidiphilum* from native Acid Mine Drainage (AMD) was investigated during biooxidation alongside finding the best machine learning approach for the prediction of process efficiency using the independent variables. The results revealed that the optimum condition for reaching the highest pyrite dissolution (~75%) is 15 days of operating time, pyrite content of 7.2 wt.%, and ore content of 5 wt.%, pH of 1.47, and D-+-sucrose, D-+-galactose, and D-+-fructose concentrations of 0.52, 0.09, and 0.12 wt.%, respectively. The results of the model comparison indicated that the Artificial Neural Network (ANN) model was able to predict the experimental results of this study with acceptable accuracy and better than Genetic Programming (GP) and Polynomial Regression informed by Response Surface Methodology (PR-RSM) from experimental data. Finally, the results showed that the change in D-+-fructose and D-+-galactose concentration has no significant effect on ferric ions concentration and pyrite dissolution content, while the influence of alteration in D-+-sucrose concentration is significantly high.

4.1. Introduction

The use of monosaccharides, as a promoting factor for the synthesis of EPS, was reported and confirmed in previous chapter and literature as an important approach that affects bacterial activity positively when toxic metals are found in the minerals (Bellenberg et al., 2012; Saavedra et al., 2020). For example, D-+-galactose was shown to enhance EPS production in a *Lactobacillus ferrooxidans* culture, and this enhancement leads to protecting microorganisms from toxic elements present in the ore (Aguirre et al., 2018). An increased biofilm growth (which is due to higher EPS production) on minerals was also observed when D-+-galactose and D-+-glucose were present during biooxidation (Bellenberg et al., 2012). *L. ferrooxidans* ability to thrive in environments with a high concentration of ferric ions was also due to the presence of 0.35 wt% D-+-galactose leading to the overproduction of EPS (Saavedra et al., 2020). Yu et al. investigated the overproduction of Extracellular Polymeric Substances (EPS) in *At. ferrooxidans* lead to higher tolerance of these microorganisms in high concentrations of copper and ferric ions (Z. Yu et al., 2017). Ouyang et al. and Cruz et al. also showed that higher EPS production will give the results of higher tolerance to toxic nanoparticles and mercury (Cruz et al., 2017; Ouyang et al., 2017). The adhesivity of *Ferroplasma acidiphilum* for oxidization of pyrite using EPS overproduction is enhanced by 69% by the addition of 0.4 wt.% D-+-sucrose (Darvanjooghi et al., 2023a). Also, the maximum amount of cell attachment of *At. ferrooxidans* were observed by the addition of 18 g/L D-+-galactose and the reason was due to the high volume of EPS production (Moncayo et al., 2022). Various carbon sources such as D-+-galactose, D-+-fructose, and D-+-sucrose as key factors can be implemented for enhancing the biooxidation rate and microorganism's community profile due to their influence in the overproduction of polysaccharides, as a compound that forms EPS (Limoli et al., 2015).

Although the impacts of different types of monosaccharides on various microorganisms' activity in the presence of toxic metals and ions have been reported widely (Aguirre et al., 2018; Darvanjooghi et al., 2023a; Moncayo et al., 2022; Saavedra et al., 2020), there is still a gap to develop an accurate prediction of biooxidation when different types of ore samples (with different pyrite contents in ore) are introduced to the biooxidation process (Ganjkhanlou, 2012; Kang et al., 2020; Trivedi & Hait, 2023; Vyas et al., 2020). The biooxidation process efficiency is solely dependent on the acidophilic microbial populations (consortium) and their adaptability to harsh conditions when exposed to different operational conditions. The presence of different types of

microorganisms in the AMD and the complexity of pyrite dissolution influenced by various parameters necessitate to use a data-driven modelling approach to explain the growth and activity of microorganisms under critical environment and find the condition for each independent variable at the maximum biooxidation efficiency. Additionally, the simultaneous effect of monosaccharides has not been reported yet as these compounds are crucial factors influencing the production of EPS made up of polysaccharides and proteins (Limoli et al., 2015). The overarching goal of this chapter is to learn how the simultaneous implementation of various concentrations of monosaccharides and other parameters (including time, pH, ORP, ore content, pyrite content, and gold grade) affect the activity of acidophilic microorganisms from raw AMD sample (obtained from the Hammond Reef gold mine site, Ontario, Canada). Finally, the development of machine learning approach for the prediction of biooxidation extent and rate in the presence of different refractory gold ore samples is another goal of this research. To do so, three different methods of modeling (Artificial Neural Network, Genetic Programming, and Polynomial Regression informed by Response Surface Methodology) were used to model the experimental data. After choosing the best model, the sensitivity analysis of parameters at optimum conditions and output prediction are also explored. The sensitivity analysis is used to understand the effect of the variable that has the highest effect on biooxidation efficiency; therefore, changing the determined parameters with the highest sensitivity leads to understanding their impacts on biooxidation rate alteration. This part of the study is used for determining the most significant parameters in controlling the biooxidation process in continuous state and pilot scale mode. Finally, the model was used to predict the results of other studies.

4.2. Materials and Methods

In this research, two different ore samples with high (concentrate, High Grade Ore Sample, HGOS) and low amounts (Low Grade Ore Sample) of pyrite (which is corresponding to the gold grade) were used to prepare the solid content of the aqueous biooxidation. The ore sample was obtained from the Hammond Reef gold mine site (Ontario, Canada) and the fine particles of samples (100-200 μm) were introduced to the experiment. The concentrate of pyrite also was prepared by using the floatation technique provided by AgnicoEagle Co. To prepare the 9K media for the growth of the microorganisms, $(NH_4)_2SO_4$, $MgSO_4.7H_2O$, K_2HPO_4, KCl, and $Ca(NO_3)_2.H_2O$ (purity > 98 wt.%, provided by Merck Inc. Canada) were used. Finally, D-+-galactose (purchased from Merck

Inc. Canada, 99.95 wt.%), D-+-sucrose (purchased from Merck Inc. Canada, 99.9 wt.%), and D-+-fructose (purchased from Merck Inc. Canada, 99.99 wt.%) were purchased for understanding the simultaneous effect of monosaccharides.

4.2.1. Characterization

The identification of the mineral ores and the population of microorganisms in this study was completed by employing different methods of analysis. The XRD and XRF analyses, as well as the photo-microgram tests, were employed in determining the gold particles and minerals present in the ore. The presence of gold inclusions in the particles was verified by the implementation of the photo-microgram test. The ICP analyses were used to quantify the extent of gold and other elements in ore. Microwave Plasma Atomic Emission Spectrometer (MP-AES), fitted with a standard absorption curve, was employed to facilitate the measurement of the total iron concentration in the solution. 16s genomic sequencing analysis was employed to determine the bacterial profile before and after the experiment for understanding of the predominant forms of microorganisms.

4.2.2. Consortium inoculation and biooxidation

Each experiment ran with different concentrations of monosaccharides, ore content, and pyrite content for 24 days. To prepare the inoculum, 9K media (3 g/l $(NH_4)_2SO_4$, 0.5g/l $MgSO_4$.7H2O, 0.5g/l K_2HPO4, 0.1g/l KCl, 0.01g/l $Ca(NO_3)_2.2H_2O$) was added to 500 ml of water and 30 ml of AMD was added to the solution. Afterward, 3.27 g of ferrous sulfate heptahydrate and 0.625 g of sulfur was added to activate the growth of both iron and sulfur oxidizing microorganisms. Finally, the prepared solution was volumed up to reach 1000 ml. The solution was incubated for 24 days at 37.1 °C at a rotation speed of 180 rpm and pH~1.4. Finally, 100 ml of solution was prepared by the addition of 1 ml of prepared inoculum, the initial pH of the solution was kept at 1.8 and ferrous sulfate was added to the solution to keep the initial ferrous concentration around 1 g/l. The inoculations were carried out in shake flask experiments with rotation speed of 180 rpm at 37.1 °C. The levels of parameters for the experiment are shown in **Table 4.1**. To get a better understanding of the microorganism's activity during biooxidation, measurements of pH and ORP were taken throughout the inoculation using commercial electrodes. The concentrations of ferric

and ferrous ions were also measured using titration with potassium dichromate and MP-AES, respectively. The values of ORP, pH, total iron, and ferrous ions concentrations were measured daily during the experiment.

Table 4.1. Conditions for inoculation of strains and applying biooxidation on refractory ore sample.

	Time (day)	gold content (g/ton)	Pyrite-content in ore (wt.%)	Ore content in solution (wt.%)	pH*	ORP*	D-G (wt.%)	D-S (wt.%)	D-F (wt.%)
No.	24	6	6	3	-	-	3	3	3
Levels	1 to 24 (everyday)	0.5 5.4 10.4 15.3 20.2 25.2	1.5 7.1 13.2 19.4 25.6 30.6	5 10 20	-	-	0.01 0.1 1	0.01 0.1 1	0.01 0.1 1

*Measured parameters

In order to understand the extent of biooxidation, two parameters of pyrite dissolution (%) and ferric ions concentration (g/l) were calculated and measured during the experiment. Due to the difficulty and low accuracy in the daily measurement of pyrite content in the ore sample using XRD, it is assumed that all the pyrite crystals are oxidized during the biooxidation using microorganisms and the production of ferric and ferrous ions from the dissolution of other iron-reach minerals is negligible. Therefore, the quantitative pyrite dissolution is calculated using the following equation1:

$$Pyrite\ dissolution\ (\%) = \frac{TDI_{final} - TDI_{initial}}{0.465 \times \frac{PC}{100} \times \frac{OC}{100}} \times 100 \quad (4.1)$$

Here, TDI represents the total dissolved iron in the water phase, PC indicates the amount of pyrite content (%) in the ore sample, and OC represents the ore content (%) in the flask. 16s sequencing was employed for species profiling and discovering their abundance by the addition of monosaccharides during biooxidation.

4.2.3. Modelling and optimization

To keep input and output data within the range of -1 to +1, the following transformation was employed (**Eq. 4.2**). This assists in fast convergence of loss function in model training in estimating the model parameters. To find the best models and optimize the variables in the model, the different cost functions (**Eq. 4.3** to 4.**5**) were implemented during optimization. Akaike Information Criterion (AIC) is a score-based parameter which is defined to predict the performance of complex machine learning approach (Kubara & Kopczewska, 2024). The value of *M* represents the number of available data and p represents the numbers of model parameters in **Eq. 4.5**.

$$\xi_N = \frac{N - N_{average}}{N_{max} - N_{min}} \quad , \quad N: parameter \tag{4.2}$$

$$RMSE = \sqrt{\frac{\sum_{i=1}^{M}(\xi_{N,model} - \xi_{N,exp})^2}{M}} \tag{4.3}$$

$$R = \frac{\sum_{i=1}^{M}(\xi_{N,model,i} - \xi_{N,exp,average})}{\sum_{i=1}^{M}(\xi_{N,exp,i} - \xi_{N,exp,average})} \tag{4.4}$$

$$AIC = \mathrm{M}\log\left(\frac{\sum_{i=1}^{M}\left(\xi_{N,model} - \xi_{N,exp,average}\right)}{M}\right) + 2p \tag{4.5}$$

4.2.3.1. Genetic programming

Genetic programming (GP) is one of the intelligent approaches which can be employed effectively in nonlinear problems. Mandal et al. used an evolutionary genetic programming model for predicting the adsorption of arsenic (III) from aqueous solution (Mandal et al., 2015). Amar et al. also used a genetic programming approach for the prediction of Pb(II) removal for clinoptilolite-rich tuffs (Amar et al., 2022). In the present research, the GP algorithm was employed using Python programming, the PySR library, to predict the output data by considering the data from independent input variables. The GP model develops equations for predicting pyrite dissolution (%) as well as the ferric ions concentration using dimensionless input variables (obtained from **Eq.**

4.2) including time (day), pyrite content (wt.%), ore content in solution (wt.%), D-+-galactose (wt.%), D-+-sucrose (wt.%), D-+-fructose (wt.%). The flowchart for obtaining the best equations is presented in **Figure C.1** (Appendix C).

In this method, the initial population is comprised of numerous mathematical operations for input parameters. The combination step employs two primary common procedures of crossover and mutation from the initial population and then the repeated operation is employed to obtain the final equation by the algorithm after satisfying the iteration criteria (cost function). The following transformation functions were employed to derive the best model using GP.

$$X_l = sigmoid\left(\frac{\xi_l}{(\sum_l \xi_l)^2}\right) \quad , \quad sigmoid(a) = \frac{1}{1+e^{-a}} \tag{4.6}$$

$$Y_m = sigmoid(\xi_m) \quad , \quad sigmoid(a) = \frac{1}{1+e^{-a}} \tag{4.7}$$

In this equation *l* represents pH, ORP, Monosaccharides concentration, time, pyrite content, and ore content and *m* represent pyrite dissolution and ferric ions concentration (output parameters). The numbers of iteration and the numbers of population running were 30 and 10, respectively. The mean square was used as a loss function, and the binary and unary operators were "+", "-", "×", "/" as well as "sinh", and "cosh" for the correlation production, respectively.

4.2.3.2. Polynomial Regression Informed by Response Surface Methodology (PR-RSM)

Response surface methodology (PR-RSM) is a popular mathematical and statistical tool for modelling and improving the biotechnology-based process with the minimum number of experiments (Weremfo et al., 2023). In this research, to formulate a 2nd order predictive model, the Box-Behnken design of response surface methodology was employed to construct six components at three distinct levels. The experiments were designed using Python programming and with the assistance of pyDOE, Numpy, Scikit and Scipy libraries. These six different parameters including time (day), pyrite content (wt.%), ore content in solution (wt.%), D-+-galactose (wt.%), D-+-sucrose (wt.%), D-+-fructose (wt.%) were employed in three distinct levels listed in **Table C.1** (Appendix A). In this table, the values of D-+-galactose (wt.%), D-+-sucrose (wt.%), D-+-fructose (wt.%) were presented in logarithmic form to be used in Response surface methodology (RSM) experiment design. The results of the experiment design indicated a total number of 60 tests for measuring both pyrite dissolution (%) and ferric ions concentration (g/L) in the solution with 6

central points. To get results with high accuracy, the experiments were repeated three times, and the average amounts of output were employed to assess the pyrite dissolution (%) as well as ferric ions concentration (g/L) as dependent parameters. The resultant independent (input) and dependent (output, which are ferric ions concentration and pyrite dissolution) data were used for obtaining the second-order polynomial correlation that fit best to the experimental data by considering the correlation coefficient as a cost function. Furthermore, ANOVA table was used to understand the significance and importance of each term in the polynomial correlation and show the accuracy of the model for the prediction of experimental data.

4.2.3.3. Artificial Neural Networks

Recently, Artificial Neural Network (ANN) models have been employed to determine the nonlinear, complex, and uncertain relations between input and output parameters (Chung et al., 2023; Mahmood et al., 2007; Xu, Nan, et al., 2020; X. Zhou et al., 2022). In these models, a network of nodes including an input layer followed by one or more hidden layers, and finally one output layer for estimating the output parameters is constructed (LeCun et al., 2015)(Chakraborty & Mali, 2020)(T. Jia et al., 2023). Here, the complexity of the effect of monosaccharides and other parameters such as ore load, pyrite concentration, time, and the community profiling of microorganisms in the consortium limit the implementation of analytical models; therefore, the utilization of ANN model helps to estimate the pyrite dissolution and ferric ions concentration by considering the complex hidden pathways of microorganisms-assisted biooxidation. In this experiment, Python and SciKit were used to find the best model for the prediction of dimensionless pyrite dissolution and ferric ions concentration.

To optimize the model, the ANN model with two hidden layers was considered and the number of nodes in each layer was optimized by considering the loss function of RMSE. The performance of the model was also studied using correlation coefficient and AIC. To understand the effect of input parameters and their selection on the loss functions, different sets of input parameters were introduced to the ANN model according to **Table C.2** (Appendix C). The model parameters (weights and biases) were optimized by using a gradient descendent algorithm. Furthermore, for optimizing the data partitioning, different data portion selections for training (ranging from 10 to 95%) and testing (ranging from 5 to 90%) were chosen. In this part of modelling the hyperparameters of the model were adaptative learning rate (Adam), sigmoid function as activation

function, batch size of 23,328, and maximum epoch numbers of 1000 (the early stop method was used to eliminate overfitting of the model by considering validation loss).

4.3. Results and discussion

4.3.1. Characterization and community profiling

The results of elemental analysis for two types of ore samples with high pyrite concentration (HPC, 30.6 wt.%) and low pyrite concentration (LPC, 1.5 wt.%) are presented in **Table C.3** (Appendix C). The results of XRD analysis for both HPC and LPC samples are presented in **Table C.4** (Appendix C). According to these results, both ore samples contain arsenic compounds that might affect the microorganisms' activity due to their high toxicity. Also, the results indicated that the major parts of the HPC and LPC (after separation by Bromoform) samples are made of Quartz (62.5 wt.%) and Ankerite (58.1 wt.%). The results of XRF (**Table C.3** (Appendix A)) and XRD (**Table C.4** (Appendix C)) showed that the major parts of LPC are made of SiO_2 with 66.2% and Al_2O_3 with 13.2%. The grade of gold for both LPC and HPC samples were found to be 0.477, and 25.2 ppm, respectively.

As HPC samples are the concentrated form of LPC samples with a higher amount of pyrite, the inclusion of gold in the crystal structures (pyrite, chalcopyrite, silicate, and alloys) are same for both samples. This concentrate was obtained by using a single-step floatation process to separate pyrites from the LPC ore sample. The microscopic images of polished LPC samples were used to visualize the presence of gold in various minerals (Appendix B **Figure B.4**).

The findings of the microbial community profiling were employed to determine the community profiling prior to and following biooxidation. These results are shown in **Figure 4.1**. In this figure, the microbial community profiling was carried out before biooxidation and after biooxidation in the presence of D-+-galactose, D-+-fructose, and D-+-sucrose. The results presented in this figure indicate that for the AMD sample before biooxidation the presence of microorganisms including *Yersinia pestis*, *Marinobacter*, *Alcanivorax*, *Psuedomonas*, *Ferroplasma acidiphilum* is significant. However, the presence of *Ferroplasma acidiphilum*, which is responsible for biooxidation of refractory gold ore after the addition of all types of monosaccharides, is vivid.

4.3.2. Biooxidation and statistical analysis

The effect of time on the biooxidation of refractory-sulfide ore with different pyrite content are shown in **Figure 4.2 b**. According to our previous research, the maximum biooxidation rate is achieved when D-+-sucrose is added to the solution leading to an increase in EPS. However, the simultaneous effects of the three types of monosaccharides were not reported. Therefore, the results of **Figure 4.2 a** and **b** were obtained at maximum concentration of D-+-sucrose (1 wt.%) and minimum concentrations of D-+-galactose and D-+-fructose (0.01 wt.%). The results of this figure indicate that maximum pyrite dissolution of 30 % and ferric concentration of 14.5 g/L were achieved for the ore sample with the highest pyrite content (30.6 wt.%) and this is because of the high amount of iron (in the form of pyrite) in ore sample. Also, the values of pyrite dissolution and ferric concentration reached the maximum amount for all samples after passing 12 days and then remained constant over time.

Figures 4.2 c and **d** also indicate the amount of pyrite dissolution and ferric production versus pyrite content for different ore content in the solutions. These results (the average values and the error bars) were obtained from the time (12 days or more) that indicates the biooxidation reached the maximum extent. According to these results, for pyrite content of 12.7 wt.% the maximum amount of pyrite dissolution of 25, 22, and 17 % was observed for different ore contents of 5, 10, 20 wt.%. The higher ore content in the solution leads to the lower amount of average pyrite dissolution indicating that the microorganisms could not tolerate the higher amount of ore content possibly due to the increase in the arsenic or cadmium concentration in the solution or tension applied to microorganism's membrane by high pulp density (Darvanjooghi et al., 2023a).

The results of **Figure 4.2 d** indicate that a rise in pyrite content and ore content leads to a higher number of ferric ions due to the availability of pyrite source. **Figure 4.2 e** and **f** also indicate that for pyrite content of 18.7 wt.% the maximum pyrite dissolution was observed at D-+-sucrose concentration of 0.1 wt.%. However, an increase is observed in the D-+-sucrose concentration for other pyrite contents in the ore sample. The results of **Figure 4.2 f** show that with the increase in D-+-sucrose concentration in the solution a slight change in the ferric ions concentration is observed. This result indicates that for the higher amount of pyrite in the ore sample, higher ferric ions are produced which is related to the abundance of iron in the pyrite structure. To better understand the trends in the experimental data, routine statistical properties were computed and presented in **Table C.5** (Appendix C). The standard deviation to mean ratio is higher than 0.5 for

ferric concentration, gold grade, pyrite content, ore content, and pyrite dissolution, while this parameter is less than 0.25 for pH, and ORP. Also, the change in ORP and pH is low compared to the other parameters and most of the data for ORP and pH is distributed between 475 mV to 508 mV and 2.1 to 2.6, respectively.

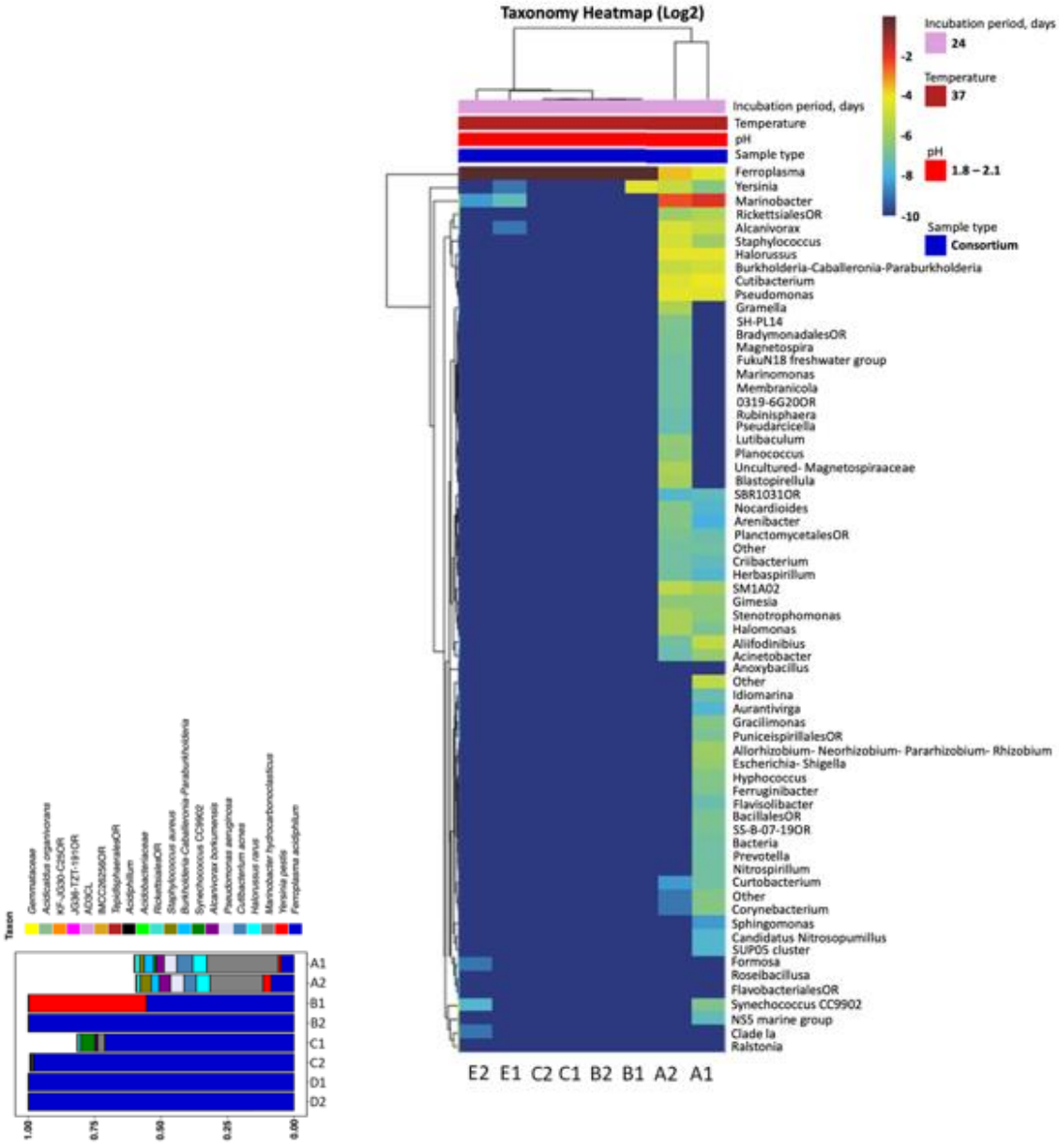

Figure 4.1. Results of microorganisms' community profiling before (A1, A2) and after biooxidation in the presence of D-+-fructose (B1, B2), D-+-galactose (C1, C2), D-+-Sucrose (D1, D2).

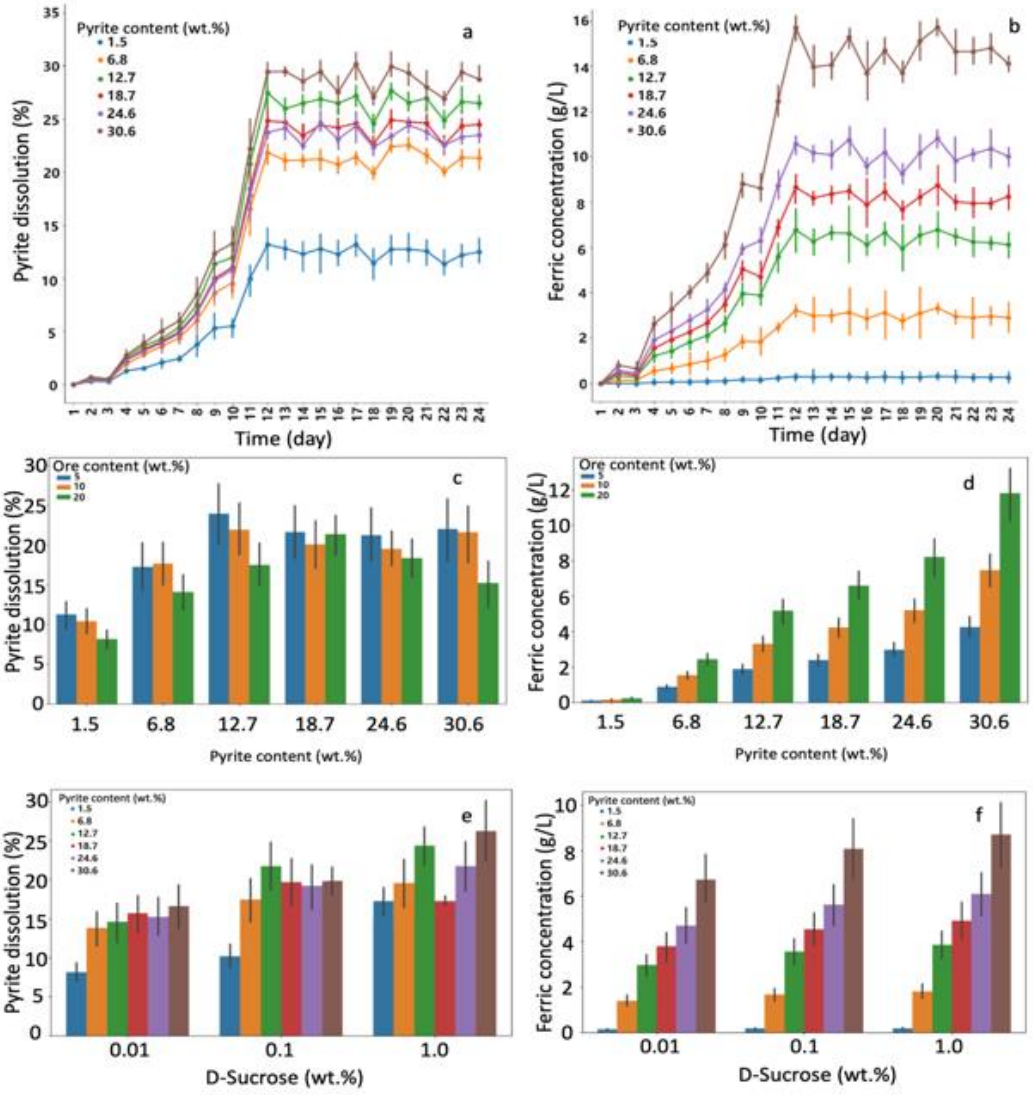

Figure 4.2. Biooxidation of refractory sulfide ore. Effect of time on: a) pyrite dissolution; b) ferric concentration (D-+-sucrose 1 wt.%, D-+-galactose 0.01 wt.%, D-+-fructose 0.01 wt.%, and ore content 10 wt.%). Effect of pyrite content on c, pyrite dissolution and d, ferric concentration (time higher than 12 days, D-+-sucrose 1 wt.%, D-+-galactose 0.01 wt.% and D-+-fructose 0.01 wt.%,). Effect of D-+-sucrose content on c, pyrite dissolution and d, ferric concentration (time higher than 12 days, D-+-galactose 0.01 wt.%, D-+-fructose 0.01 wt.%, and ore content 10 wt.%).

It is wise to use the best parameters for the model with the lowest dependency on other parameters. Thus, **Figure C.2** (Appendix C) helps to understand the auto and cross-correlation coefficient for parameters and the trends of change. The dimensionless pyrite content is highly correlated with the gold grade, and this is because the major parts of gold particles are surrounded by the pyrite crystals. Thus, the gold grade parameter should be eliminated from the set of input parameters in deriving the models' fitting values. Although the correlation coefficient for ORP with time and pyrite dissolution is higher than 0.8, it is appropriate to keep this parameter as input since this parameter represents the potential of oxidant-redox in the solution which is correspondence to the ratio of ferric to ferrous contents. The inter-item plot of parameters indicates that with the increase in gold grade in ore samples the trend of data is unique and significant. The plot of dimensionless ferric concentration versus pyrite dissolution indicates non-linear relation between them, indicating that for the constant values of pH, ORP, D-+-galactose, D-+-fructose, D-+-sucrose, and time, higher amount of ferric concentration is produced with the increase in gold grade in ore sample (data shift to the right side of the diagram). The schematic diagram of the data preprocessing is shown in **Figure C.3** (Appendix C).

4.3.3. Models and comparison

In this part of the research, the results of GP-based model were studied, and the best equation was chosen for the prediction of both pyrite dissolution (**Eq. C.1** (Appendix C)) and ferric ions concentration (**Eq. C.1** (Appendix C)). To find the best correlation for the prediction of outputs, the values of RMSE and correlation coefficient were calculated for different data portioning as presented in **Figure C.4** (Appendix C). The best equation was chosen for pyrite dissolution where the values of RMSE were minimum (4.03×10^4 for training and 3.97×10^4 for testing data) and the correlation coefficient was maximum (0.94 for training and 0.94 for testing)— here the portion of testing was 10%. Furthermore, the best correlation for the prediction of pyrite dissolution was found with RMSE of 2.25×10^4 for training and 2.77×10^4 for testing and a correlation coefficient of 0.95 for training and 0.94 for testing.

The relation of the input parameters including time (day), pyrite content (wt.%), ore content in solution (wt.%), D-+-galactose (wt.%), D-+-sucrose (wt.%), D-+-fructose (wt.%) with output parameters was also studied using the framework of PR-RSM. Finally, a second-order polynomial equation was proposed by using regression analysis for both outputs as a function of input

parameters by fitting the experimental data obtained from the Box-Behnken design of the experiment. The experimental data were collected for given levels of input parameters and presented in **Table C.6** (Appendix C). The proposed polynomial equations for PR-RSM model are represented as **Eq. C.3** and **Eq. C.5** (Appendix C).

The results and significance of the components in the PR-RSM regression model were investigated using an ANOVA. **Table C.7** (Appendix C) provides a summary of the findings. The results indicated that the model is significant for ferric concentration prediction (F = 7.4) and the proposed model for pyrite dissolution prediction is not significant (F = 0.6). On the other hand, the lack-of-fit for both concentrations of ferric ions and pyrite dissolution prediction is significant (P >0.05); therefore, it is concluded that this method of modeling cannot provide a satisfactory prediction and explanation of the data trend. Also, both time and pyrite content are significant for the prediction of both output parameters (ferric ions concentration and pyrite dissolution) and parameter of ore content is just significant for the prediction of pyrite dissolution as $p < 0.05$. The results also indicate that the multiplying of time by other parameters (pyrite content, ore content, D-+-sucrose, D-+-galactose, D-+-fructose) is categorized as a significant term in the models for predictions of both outputs; however, multiplying of pyrite content and other parameters (ore content, D-+-sucrose, D-+-galactose, D-+-fructose) can be observed to be just significant for pyrite dissolution prediction.

The response surface plot, showing the effect of input parameters on pyrite dissolution and ferric ions concentrations, is shown in **Figure C.5** (Appendix C). According to this plot, pyrite dissolution will be maximum for the condition where ξ_{time} and $\xi_{pyrite\ content}$ are 0.21 and 0.38, respectively. However, the maximum ferric ions concentration is observed at ξ_{time} and $\xi_{pyrite\ content}$ higher than 0.4. Increase in both $\xi_{D-Sucrose}$ and $\xi_{D-Galactose}$ leads to higher pyrite dissolution while the minimum values of ferric ions concentration are at 0.3 and -0.1, respectively. The results presented in this figure also indicate that for higher $\xi_{D-Fructose}$ and lower $\xi_{Ore\ content}$ an increase in pyrite dissolution is observed which is related to the lower toleration of microorganisms to high amounts of ore content and consequently toxic metals such as arsenic. However, the effect of ore content ($\xi_{Ore\ content}$) is more vivid on the ferric ion concentrations alteration compared to $\xi_{D-Fructose}$.

In the last step of modeling, the adjusting variables of an Artificial Neural Network model with two hidden layers were optimized to predict both outputs. To select the best input variables set,

the values of correlation coefficient, RMSE, and AIC were calculated for all four sets of input by considering the change in second-layer neuron numbers in the ANN model (**Table C.8** (Appendix C)). The results indicated that for the fixed 3 neurons in the first layer; by considering 9 neurons in the second layer and input variable set of No. 4 the values of correlation coefficient are maximum (0.996) while the values of RMSE and AIC are minimum (0.0269 and 1629, respectively). The results of optimization (by considering 3 nodes in the first hidden layer and 9 in the second hidden layer and data portion of 30% and 70% for testing and training, respectively) indicated that for input sets presented in **Figure C.6** (Appendix C) the best condition (R^2=0.996, RMSE=0.0269, AIC=1669) was for input set of No. 4 (inputs: time, pyrite content, ore content, pH, ORP, concentrations of D-+-galactose, D-+-fructose, and D-+-sucrose) while the input set of No. 1 (inputs: time and gold content) indicated the lowest satisfactory of the outputs predictions (R^2=0.760, RMSE=0.1245, AIC=11900) using the proposed ANN model. According to the results presented in **Figure C.6** (Appendix C), with the increase of test data portion up to 25% higher correlation coefficient (~0.99) and lower RMSE (~0.002) for both pyrite dissolution (training and testing data) and ferric ions concentration (training and testing data) prediction is observed while for higher than 25%, the values of correlation factors fall below 0.94 and RMSE would be higher than 0.008.

To finalize the numbers of nodes in both hidden layers the results of the correlation factor and RMSE calculation are depicted in the form of a heatmap graph in **Figure 4.3 a** for both training and testing data (the relative values, i.e. the ratio of correlation coefficient to the maximum correlation coefficient and ratio of RMSE to maximum RMSE, were used for these graphs). According to these results, the configuration of the model with the 3 nodes in the first hidden layer and 9 nodes in the second hidden layer leads to the maximum relative correlation factor (1.00) and minimum relative RMSE (0.024). Finally, the ANN model was proposed with the structure presented in **Figure 4.3 b**. This model includes 8 inputs, 3 nodes of calculation in the first layer 9 nodes of calculation for the second layer (with specific weights and biases for each node), and two outputs. The weights and biases are presented in **Table C.9** (Appendix C).

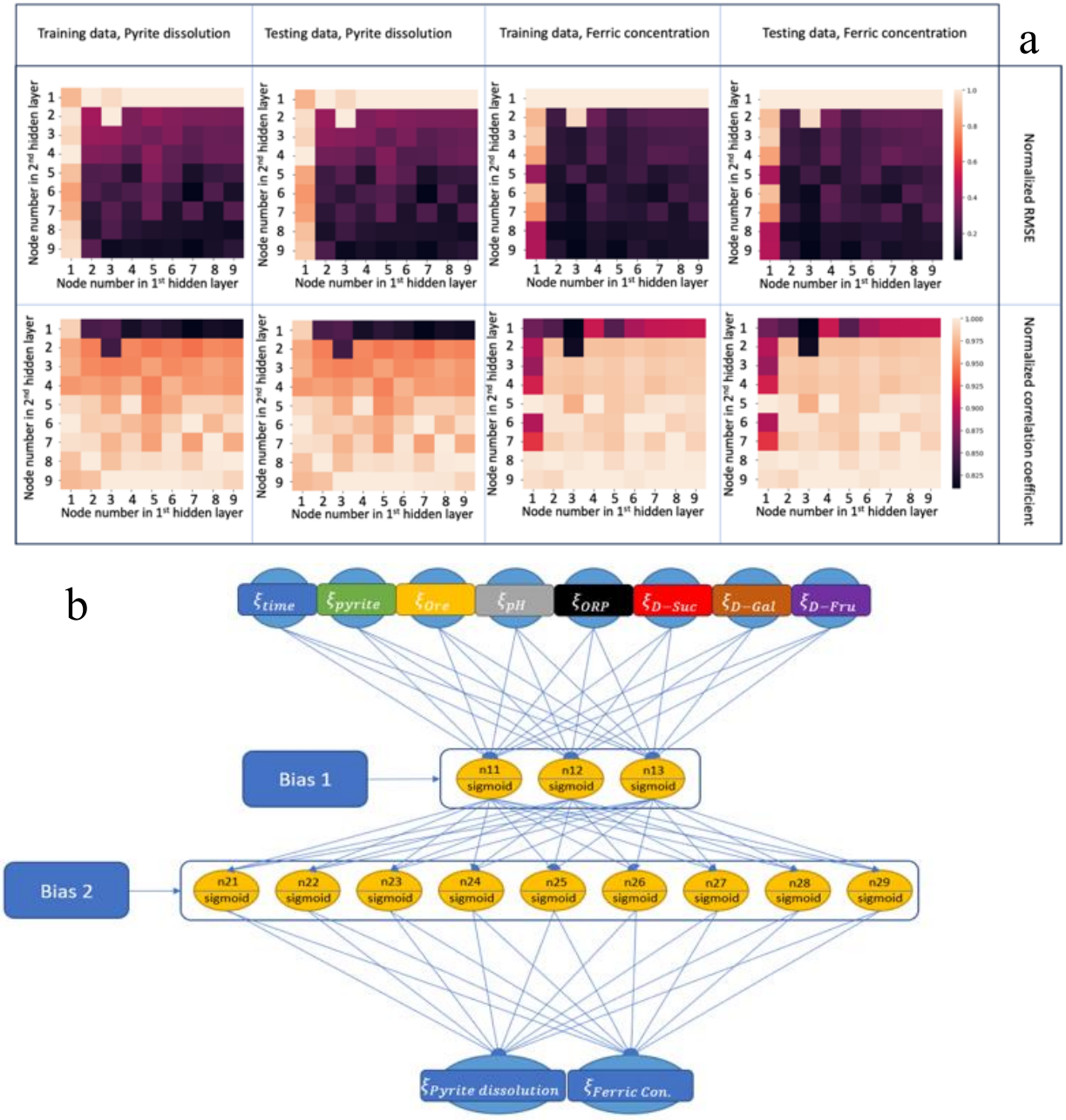

Figure 4.3. A heatmap plot of RMSE and correlation coefficient, b, ANN model structure.

Finally, to perform a comparison between the models and choosing the best one, the output from each model (i.e., GP, PR-RSM, and ANN) for pyrite dissolution and ferric ions concentration are plotted against the experimental values in **Figure 4.4**. According to these results, the GP model can predict data with correlation coefficients of 0.94 and 0.95 for pyrite dissolution and ferric ions concentrations. The plot of data indicated that the deviation of some modeled data from experimental data is less than -20% for pyrite dissolution ranging from 0.01 to 0.55 and the deviation would be higher than +20% for higher values of this parameter in the GP model. In addition, the deviation of the major portion of modeled data from experimental data would be higher than +20% in PR-RSM model for the pyrite dissolution range of 0.0 to 0.1 and ferric ions concentration between 0.0 to 0.2. Finally, it is concluded that the ANN model can be used for the prediction of both outputs with a deviation of less than 10% for the major portion of data and 20% for the entire data.

The plots in **Figure 4.5** also indicate the extent of pyrite dissolution at different ore contents vs the input parameters including pyrite content, monosaccharides concentrations, and time for the experimental data and the data obtained by ANN, PR-RSM, and GP models. According to the results of this figure, the distribution of experimental data (for each parameter and every level) is like those obtained from ANN model and there is a vivid difference between experimental data with GP and PR-RSM model data. In this figure, the trend of the graph and the distribution of data for both experimental and modeled data are plotted at every level of experiment. It is observed that the distribution of experimental data is close to the predicted data by using ANN and for the data obtained from PR-RSM, the distribution of data does not match with the experimental data. Furthermore, the results indicate that with the increase in D-+-sucrose concentration there is a slight increase in pyrite dissolution extent for both ANN model and experimental data; however, the addition of other types of monosaccharides does not influence the pyrite dissolution extent tangibly. The results obtained from PR-RSM and GP models showed a significant decrease of pyrite dissolution with time after 20 days which is in contradiction to those obtained experimentally. Also, all the models and experimental data indicate that with the increase in pyrite content, higher values of pyrite dissolution are observed.

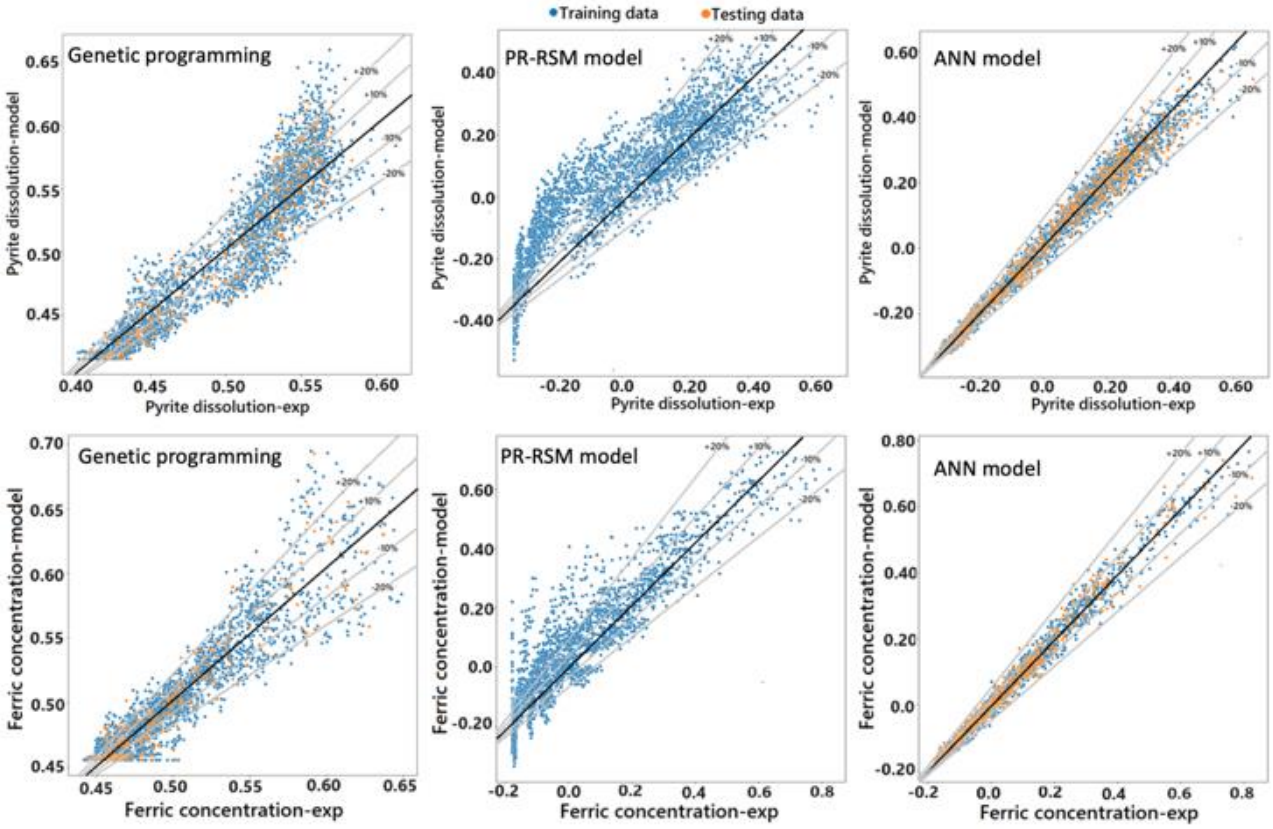

Figure 4.4. Plot of dimensionless model's data vs experimental values (ξ_i) for pyrite dissolution and ferric ions concentration in GP, PR-RSM, and ANN

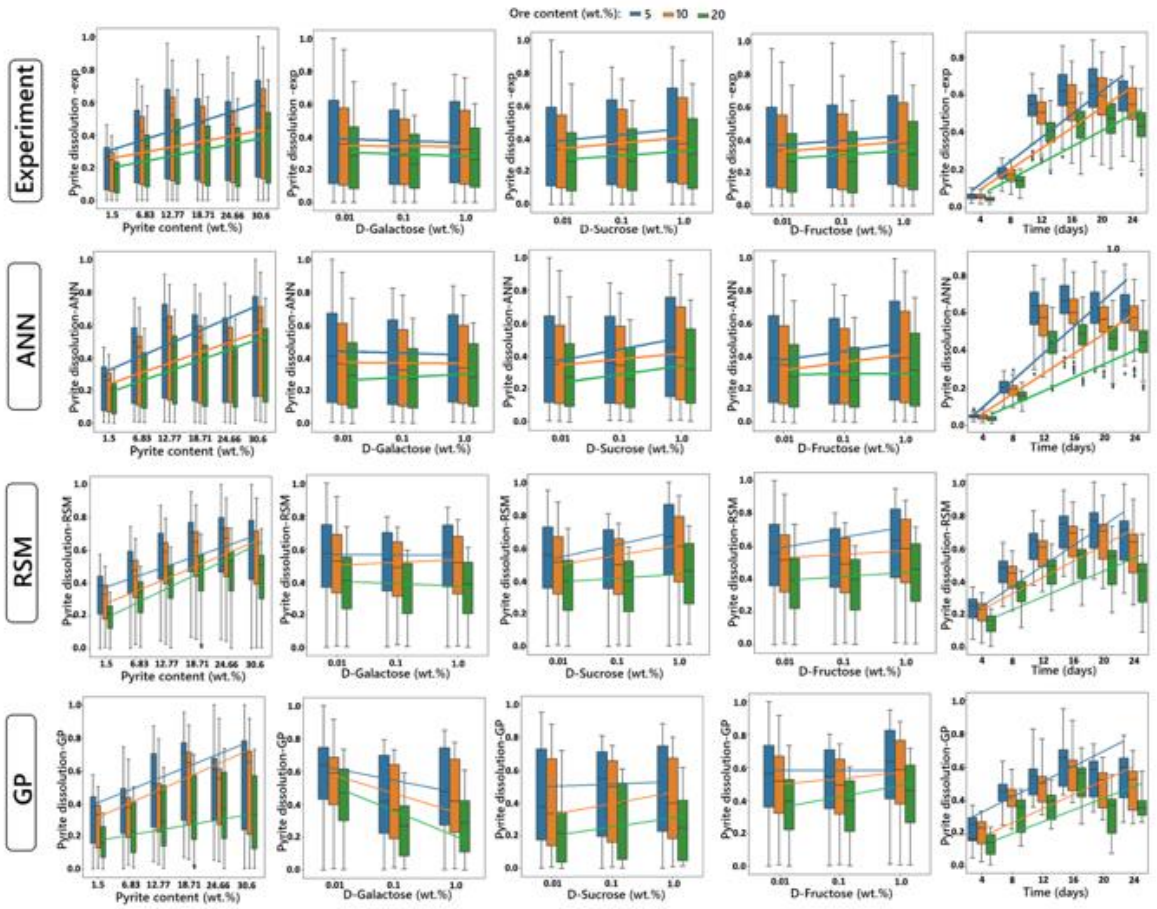

Figure 4.5. A plot of dimensionless relative pyrite dissolution data ($\xi_{pyrite\ dissolution}/\xi_{pyrite\ dissolution,max}$) vs input parameters vaues (ξ_i) for GP, PR-RSM, and ANN models as well as real experimental data.

4.3.3. Sensitivity analysis

A sensitivity analysis may be performed to determine which processing or targeted parameter has the most impacts on the final outputs of the model (A. Abdollahi et al., 2018; Karimipour et al., 2018; Miri et al., 2021; Salimpour et al., 2019). The understanding of the operational parameter levels which leads to the maximum values of change on outputs is crucial. Therefore, implementation of a genetic algorithm helps to find the best condition where the values of ferric concentration and pyrite dissolution are maximum (Rafie et al., 2023). In the algorithm, the population of genes was chosen as input parameter values, and the fitness function was the minimum value of inverse output parameters. The modelling findings of this study suggest that the highest value of pyrite dissolution is achieved from the ANN model (due to the highest accuracy in prediction of data) under the condition where time is 15 days, pyrite content is 7.2 wt.%, ore content is 5 wt.%, pH is 1.47, ORP is 562 mV, and D-+-sucrose, D-+-galactose, and D-+-fructose concentrations are 0.52, 0.09, and 0.12 wt.%, respectively.

The sensitivity of output parameters was measured by changing (±30, ±20, ±10 %) in input parameters at optimum conditions. The results of the sensitivity analysis of the model are shown in **Figure 4.6**. According to these results, the effect of time and D-+-sucrose concentration on the pyrite dissolution and ferric ions concentration is tangible and decreasing the time affects the output parameters significantly while an increase in this parameter results in a slight change in the output parameters. An increase in both pyrite and ore content enhance the effect of these parameters on outputs and the sensitivity of the model to the concentrations of two other monosaccharides is majorly less than 5%.

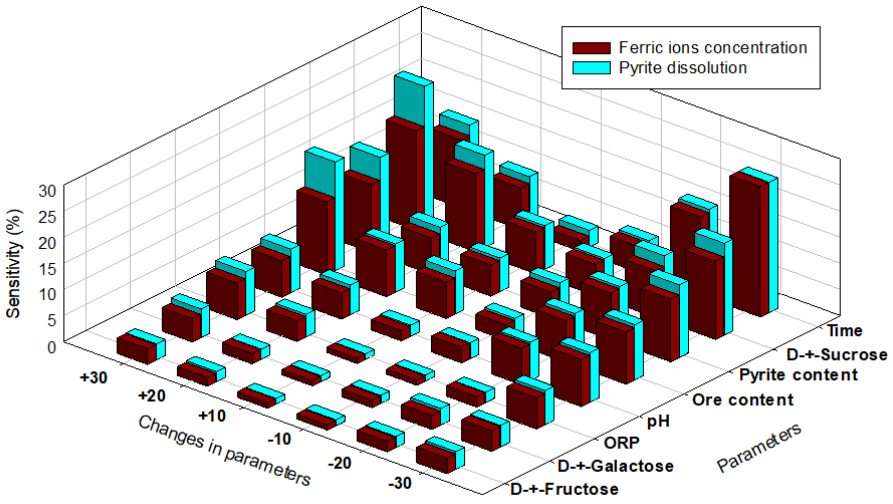

Figure 4.6. Sensitivity analysis of ANN model outputs vs the input parameters.

4.3.4. Validation

To better validate the model and assess the accuracy of the model for prediction of data from other research sources, the values of pyrite dissolution and ferric ions concentration were collected from literature and the corresponding data were calculated using the ANN model. The data were gathered from research articles where diverse types of microorganisms with different portions of pyrite content, monosaccharides' concentrations, as well as pH and ORP were employed to report the extent of biooxidation (Castro et al., 2023b; Darvanjooghi et al., 2023a; Moncayo et al., 2022; Saavedra et al., 2020; N. Vardanyan et al., 2020; YU et al., 2008). The results of the comparison between the experimental and the model data are presented in **Table C10** in appendix C. and for the inputs parameters that are not presented in the literature data the value was set to zero. According to these results, the minimum and maximum deviation values of model data from experimental results are -48.4% and 33.8, respectively, for pyrite dissolution and these values for ferric ions concentration are -44% and 25.7%, respectively. Although the results indicate that the model prediction accuracy is low, the major portion of the data (55%) is estimated using the model with a deviation of less than 20%. This indicates that the model performance for the prediction of other data is in the acceptable range and further studies are required to develop the model by considering other influential factors. One suggestion is that the model can be advanced by considering the data from different published research sources and several types of microorganisms as well as understanding the most important parameters.

Table 4.2. Comparison between experimental data from different sources and model data.

Source	Experimental		Model prediction		Deviation (%)	
	$\xi_{Pyrite\ dissolution}$	$\xi_{Ferric\ concentration}$	$\xi_{Pyrite\ dissolution}$	$\xi_{Ferric\ concentration}$	e_1[‡]	e_2[†]
(Darvanjooghi et al., 2023a)	-0.213	-0.518	-0.213	-0.462	0.2	10.8
(Darvanjooghi et al., 2023a)	-0.182	-0.494	-0.174	-0.544	4.4	-10.1
(Darvanjooghi et al., 2023a)	-0.084	-0.356	-0.089	-0.323	-5.4	9.2
(Darvanjooghi et al., 2023a)	-0.015	-0.124	-0.017	-0.109	-13.8	12.1
(Darvanjooghi et al., 2023a)	0.076	0.187	0.09	0.221	-19	-18.4
(Darvanjooghi et al., 2023a)	0.137	0.241	0.151	0.198	-10	18
(Darvanjooghi et al., 2023a)	0.192	0.499	0.156	0.442	18.7	11.4
(Saavedra et al., 2020)	-0.680	-0.672	-0.764	-0.802	-12.4	-19.3
(Saavedra et al., 2020)	-0.634	-0.402	-0.538	-0.353	15.2	12.2
(Saavedra et al., 2020)	-0.546	-0.035	-0.564	-0.043	-3.3	-23.7
(Saavedra et al., 2020)	-0.039	0.085	-0.048	0.09	-22.7	-5.6
(Saavedra et al., 2020)	0.174	0.148	0.196	0.119	-12.6	19.4
(Saavedra et al., 2020)	0.314	0.175	0.292	0.177	6.9	-1.3
(Saavedra et al., 2020)	0.509	0.282	0.492	0.25	3.3	11.5
(Moncayo et al., 2022)	-0.846	-0.884	-0.779	-1.079	7.9	-22.1

(Moncayo et al., 2022)	-0.722	-0.621	-0.833	-0.621	-15.4	0
(Moncayo et al., 2022)	-0.628	-0.472	-0.932	-0.479	-48.4	-1.4
(Moncayo et al., 2022)	-0.566	-0.095	-0.375	-0.072	33.8	24
(Moncayo et al., 2022)	-0.521	0.056	-0.618	0.065	-18.6	-16.7
(Moncayo et al., 2022)	-0.434	0.103	-0.608	0.108	-40	-4.5
(Castro et al., 2023b)	-0.569	-0.649	-0.58	-0.489	-1.9	24.6
(Castro et al., 2023b)	-0.442	-0.482	-0.435	-0.358	1.5	25.7
(Castro et al., 2023b)	0.011	0.039	0.016	0.052	-43.4	-34.6
(Castro et al., 2023b)	0.330	0.436	0.221	0.628	33	-44
(N. Vardanyan et al., 2020)	-0.322	-0.458	-0.29	-0.498	9.8	-8.8
(N. Vardanyan et al., 2020)	0.237	-0.200	0.212	-0.205	10.6	-2.4
(N. Vardanyan et al., 2020)	0.525	-0.156	0.453	-0.218	13.7	-39.7
(YU et al., 2008)	-0.026	0.069	-0.037	0.091	-40.6	-32.2
(YU et al., 2008)	0.03	0.114	0.04	0.128	-33.9	-12.3
				Median	-3.3	-2.4
Data of this study				Median	1.2	1.1

‡ $e_1 : (\xi_{Pyrite\ dissolution,exp} - \xi_{Pyrite\ dissolution,model})/\xi_{Pyrite\ dissolution,exp} \times 100$

† $e_2 : (\xi_{Ferric\ concentration,exp} - \xi_{Ferric\ concentration,model})/\xi_{Ferric\ concentration,exp} \times 100$

4.4. Conclusions

Microbial community profiling, conducted both before and after biooxidation in the presence of monosaccharides, revealed the initial presence of microorganisms like *Yersinia pestis*, *Marinobacter*, *Alcanivorax*, *Pseudomonas*, and *Ferroplasma acidiphilum* in the AMD sample. Post-biooxidation, profiling indicated the persistence of *Ferroplasma acidiphilum*, crucial for the biooxidation of refractory gold ore, following the addition of all types of monosaccharides. The intricacies associated with the growth of *Ferroplasma acidiphilum* in a consortium, coupled with the pivotal role of monosaccharides in EPS production, pose challenges for analytically developed mathematical models. Consequently, the application of a machine learning approach proves invaluable in formulating a model that exhibits acceptable accuracy when predicting biooxidation efficiency and rate. This involves considering variables such as the concurrent impact of monosaccharides, ore content, pyrite content, and time. In this context, Artificial Neural Network outperformed Genetic Programming and Polynomial Regression informed by Response Surface Methodology, in predicting biooxidation efficiency with deviation below 20% in the studied conditions. Moreover, the proposed model extended its utilization for forecasting the rate of biooxidation and ferric content, parameters that are inherently difficult to measure experimentally. While the model demonstrated satisfactory performance in predicting other data points, it is acknowledged that further research is imperative to refine the model by incorporating additional influential factors. One such recommendation involves enhancing the model through the integration of data from diverse published research sources and various microorganism types that can play a vital role in biooxidation of sulfidic refractory gold ore.

Interface 2: The synergistic effects of monosaccharides, ore composition, pyrite concentration, and operating time on the biooxidation efficiency and proliferation of *Ferroplasma acidiphilum* (derived from indigenous Acid Mine Drainage) were methodically assessed. Furthermore, machine learning models were used to forecast process performance. The optimal conditions for maximal pyrite dissolving (~75%) were identified as 15 days of operation, 7.2 wt.% pyrite, 5 wt.% ore, pH 1.47, and monosaccharide concentrations of 0.52 wt.% D-sucrose, 0.09 wt.% D-galactose, and 0.12 wt.% D-fructose. Among the evaluated models, the Artificial Neural Network (ANN) demonstrated greater predictive accuracy than Genetic Programming (GP) and Polynomial Regression using Response Surface Methodology (PR-RSM). Sensitivity analysis revealed that D-sucrose significantly affected ferric ion production and pyrite dissolution, whereas D-galactose and D-fructose had less effect.

The predictive modelling corroborated experimental trends and indicated sucrose having the most substantial effect on process efficiency. This modelling technique enabled the selection of appropriate parameters and their values for subsequent bench-scale biooxidation tests. In the next chapter the optimum condition from the best models is introduced to the experimental bench-scale setup and the effect of each parameter will be assessed separately in both column test and stirred tank reactor configurations.

Chapter 5: Microorganism-assisted biooxidation of refractory gold ore: bench scale case study*

*Mohammad Hossein Karimi Darvanjooghi, Sara Magdouli, Satinder Kaur Brar, *Chemical Engineering and Processing - Process Intensification*, submitted.

Abstract

This chapter investigates the effects of biooxidation using *Ferroplasma acidiphilum* on gold recovery from high-grade (HGOS) and low-grade ore samples (LGOS). Pretreatment methods included stirred tank reactors and column tests. Results showed that the stirred tank reactor yielded higher recovery rates for key elements, with gold recovery reaching 55% for HGOS compared to 40% for LGOS using the column test. Optimal conditions for biooxidation were identified, including aeration flow rates of 1.0-1.5 l/min and agitation speeds of 300-450 rpm, which facilitated effective microbial activity and pyrite dissolution. During cyanidation, gold recovery was highest at a pH of 10.5, with up to 60% recovery at 8 (g/l) NaCN. However, at pH levels above 11, gold recovery decreased to around 40% due to competing chemical species and metal hydroxide precipitation. The study also found that extending cyanidation time enhanced gold recovery, with significant increases observed within the first 10 hours.

5.1. Introduction

Studies on the biooxidation of resistant gold ores have made progress, with an emphasis on developing ecologically sustainable and economically efficient methods to improve gold extraction. The BIOX process, designed by Gencor, employs bacteria to catalyze the oxidation of sulfide minerals, hence enhancing the availability of gold (Free, 2024). This method has been successfully used in various mines, including the Fairview Gold Mine in South Africa. Newmont Mining's heap biooxidation process at the Carlin Mine in Nevada is renowned for its ability to effectively treat low-grade ores (Karimi Darvanjooghi et al., 2024b). In addition, the MesoTHERM and ASTER processes enhance the effectiveness of biooxidation and purify process fluids after treatment.

There are still a few gaps in the biooxidation procedures for refractory gold ores, despite recent developments. Although the BIOX process works well, it is sensitive to operating circumstances since it needs exact control over temperature, pH, and oxygen levels. In colder areas or with very refractory ores, heap biooxidation is less effective and slower than tank biooxidation. Furthermore, these procedures frequently call for pre-treatment stages and have trouble effectively scaling up for larger operations (van Niekerk et al., 2022).

Although there has been much research on the beneficial effects of supplemental compounds on microbial activity in the presence of harmful metals, there is still a lack of understanding regarding the biooxidation process when the ore sample is subjected to larger scale (bench scale) methods for gold recovery particularly when exposed to low temperature (Ganjkhanlou, 2012; Trivedi & Hait, 2023; Vyas et al., 2020). Biooxidation effectiveness depends on acidophilic bacteria populations' adaptability to different operating conditions. For biooxidation processes, pilot-scale studies imitate real-world settings better than laboratory trials, identifying operational problems. Aeration rates, temperature, pH, and nutrient delivery may be optimized using this data for optimal efficiency (Busch et al., 1961).

In this work, the research explores the biooxidation of refractory gold ore using the acidophilic microorganism *Ferroplasma acidiphilum*. Two pretreatment methods, column tests, and stirred tank reactors were employed to prepare low-grade ore samples (LGOS) and high-grade ore samples (HGOS) respectively. The study investigates the effects of various parameters including time, pH, ORP (oxidation-reduction potential), ore content, pyrite content, and gold grade on the biooxidation process. Finally, the pretreated samples from both stirred tank reactor and column

test biooxidation were introduced to cyanidation to determine the efficiency of gold recovery and other element extraction.

5.2. Materials and methods

The microorganisms were grown in 9K media incorporating $(NH_4)_2SO_4$, $MgSO_4.7H_2O$, K_2HPO_4, KCl, and $Ca(NO_3)_2.H_2O$ with acceptable purity of higher than 98 wt.%, provided by Merck Inc. Germany. Also, D-+-galactose, D-+-sucrose, and D-+-fructose with a high purity of 99.99 % (Merck Inc. Germany) were finally employed in a stirred tank reactor and column tests with yeast extract (BioBasic Co.). Within this research, two distinct ore samples were employed to make up the different solid portions in the aqueous biooxidation. One of the samples had a high concentration of pyrite (~31 wt.%), which is directly correlated to the gold grade in the sample (25 g/ton), while the other sample had a low concentration of pyrite (1.5 wt.%) and gold grade of 0.5 g/ton. The low-grade ore sample (LGOS) was collected at the Hammond Reef gold mine site which is situated in Ontario, Canada. As the high-grade ore sample (HGOS) represents a concentrated form of the LGOS with a higher pyrite content, the inclusion of gold within the crystal structures (pyrite, chalcopyrite, silicate, and alloys) remains consistent across both samples. This concentrate was produced using a single-step flotation process to isolate pyrite from the LGOS ore sample. The experiment incorporated the introduction of small particles of the specimens, ranging from 100 to 200 μm in particle average diameters. The flotation method supplied by Agnico Eagle Co. was also used for producing the pyrite concentrate sample. Finally, sodium cyanide was purchased (with a purity of 98%, Merck Inc. Germany) and used for the dissolution of gold after pretreatment.

5.2.1. Characterization

Different techniques of analysis were utilized to identify mineral ores and the microorganism population (Darvanjooghi et al., 2023b) in the previously published article. Photomicrograph tests, X-ray diffraction (XRD), and X-ray fluorescence (XRF) analyses were among the methods used to identify the presence of minerals and gold particles as well as their morphology in the ore showing majorly presenting in pyrite crystals (Darvanjooghi et al., 2024). ICP was utilized to determine the initial concentration of gold and other metals in the ore, (Appendix D, **Table D.1**). The utilization of a Microwave Plasma Atomic Emission Spectrometer (MP-AES) equipped with

a standard absorption curve enabled the precise determination of the solution's total iron concentration and gold concentration after cyanidation for the calculation of total recovery.

5.2.2. Pretreatment: Biooxidation

5.2.2.1. Microorganisms

The native microorganisms from the Hammond Reef mine site were obtained for this investigation by using acid mine drainage. After a period of incubation (14 days), a notable growth of *Ferroplasma acidiphilum* was found in an acid solution with the addition of iron (II). This growth suggests that the bacteria might thrive in these circumstances. During the mechanisms of growth ferric ions, which function as oxidizing agents and dissolve pyrite and pyrrhotite compounds, are produced and *Ferroplasma acidiphilum* is essential to the iron and sulphur cycle by accepting electrons from produced ferrous ions in the pyrite dissolution reaction. This discovery emphasizes how crucial these microbes are to the biogeochemical processes that affect mining settings. Other microorganisms that showed notable multiplication beyond the first growth phase also included *Marinobacter*, *Alcanivorax*, and *Yersinia pestis*. The findings of the microbial community profiling are shown in Figure **B8** in Appendix B.

5.2.2.2. Inoculation and sample preparation

The inoculum was prepared by adding 30 ml of AMD to 500 ml of water, which included 9K media (3 g/l $(NH_4)_2SO_4$, 0.5g/l $MgSO_4.7H2O$, 0.5g/l K_2HPO4, 0.1g/l KCl, 0.01g/l $Ca(NO_3)_2.2H_2O$). The mixture was then placed under stirring of 180 rpm for an hour. To boost microorganisms' growth that can oxidize iron, 3.27 g of ferrous sulfate heptahydrate was added thereafter. The produced solution (containing microorganisms, 9K media, and sulfur and iron) was then filled up to 1000 ml. The final solution was incubated for 24 days at 37.1 °C, 180 rpm, and pH~1.8.

Pyrite dissolution (%) and ferric ions concentration (g/l) have been determined and monitored to evaluate biooxidation. All pyrite crystals are assumed to be oxidized during the microorganisms' biooxidation process and the dissolution of iron from other mineral sources in ore samples is negligible. Therefore, the quantitative pyrite dissolution is calculated using **Eq. 5.1** which is used in previous research (Darvanjooghi et al., 2024):

$$Pyrite\ dissolution\ (\%) = 2.15 \times 10^6 \frac{\alpha_{final} - \alpha_{initial}}{X.Y} \quad (5.1)$$

In this context, α denotes the concentration of dissolved iron in the liquid phase, X defines the percentage of pyrite found in the ore specimen, and Y represents the percentage of ore in the container.

In this chapter, two different ore samples were utilized for biooxidation using a column test and a stirred tank reactor. The low-grade ore sample (LGOS, containing 1.5 wt.% pyrite and 0.5 g/ton of gold in pyrite inclusions) was employed for the column test, as heap biooxidation is commonly reported to be feasible for ores with a gold grade of less than 2 g/ton (Darvanjooghi et al., 2022; Fernando et al., 2024; Karimi Darvanjooghi et al., 2024b). On the other hand, the high-grade ore sample (HGOS, containing 7.2 wt.% pyrite and 5.4 g/ton of gold in pyrite inclusions) was employed for the stirred tank reactor.

5.2.3. Stirred tank reactor biooxidation

In conducting the bench scale experiment, a jacketed reactor of 1000 ml volume was employed. Maintaining a constant temperature (37.5 °C) was ensured using a thermal circulator bath, while parameters such as pH, ORP, and dissolved oxygen were monitored within the reactor. The optimum condition of pyrite content (7.2 wt.%), ore content (5 wt.%), maintaining pH at constant value of 1.47, D-+sucrose (0.52 wt.%), D-+-galactose (0.09 wt.%), and D-+-fructose (0.12 wt.%) were obtained from previous research and applied for stirred tank using the data-driven model (Darvanjooghi et al., 2024). Varied levels of aeration flow rates (0.5, 1.5, and 3 l/min) were considered to oxygenate the solution. Also, calcium carbonate (~0.05 M) daily makeup (5, 10, and 20 ml/day) was introduced to analyze the impact of inorganic carbon sources on biooxidation efficiency. Additionally, differing agitation speeds (300, 450, and 600 rpm) were investigated to find the optimum condition for reaching the highest biooxidation efficiency. The values of ORP, pH, total iron, and ferrous ions concentrations were measured daily during the experiment to monitor the biooxidation performance. A process flow diagram and an image of the stirred reactor are depicted in **Figure 5.1 a** and **b**, respectively.

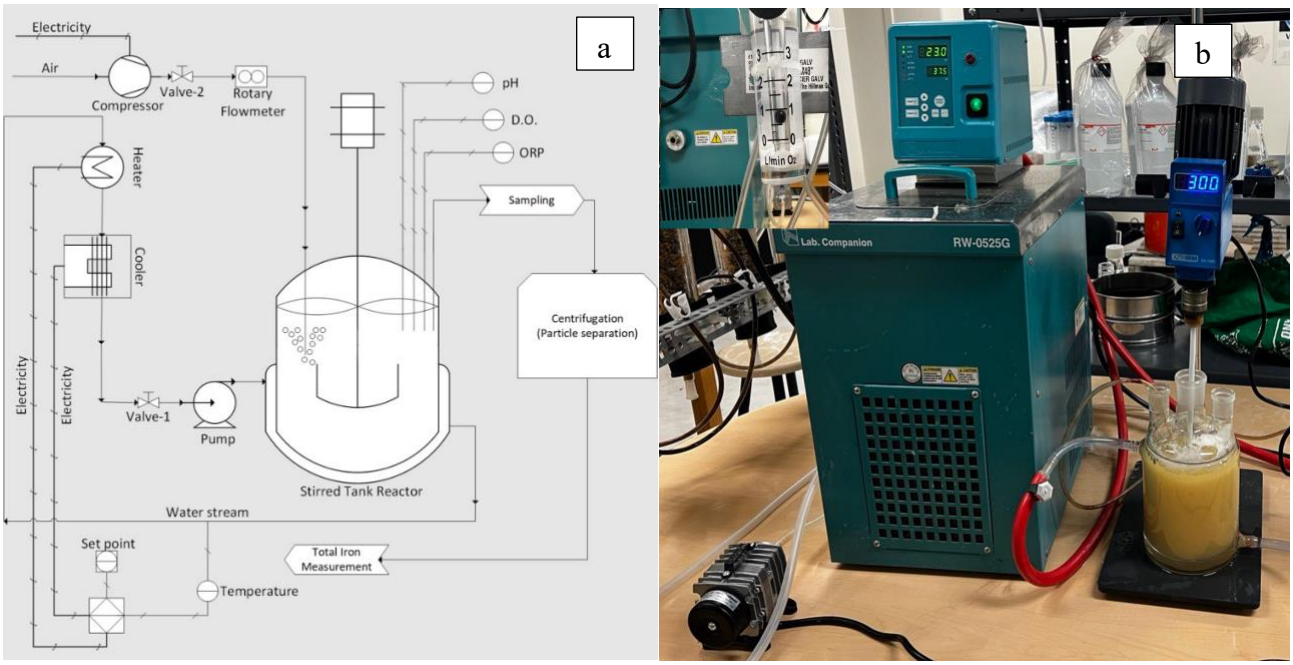

Figure 5.1 a) process flow diagram of stirred tank reactor biooxidation, and b) experimental setup image.

In **Figure 5.1 a**, a water stream was utilized to maintain the temperature of the stirred reactor at a constant 37.5°C. Throughout the experimentation, key parameters including pH, dissolved oxygen (DO), and oxidation-reduction potential (ORP) were closely monitored to evaluate the reactivity of the microorganisms involved in the biooxidation. Samples were periodically collected during the biooxidation and subjected to centrifugation at 1500 rpm to remove fine particles. Following this, the total iron content was measured to determine the efficiency of the biooxidation.

5.2.4. Column biooxidation

A column test was employed as a representative model for heap biooxidation. The experimentation focused on investigating the effects of various operational parameters, specifically aeration flow rate and recycling solution flow rate, on the biooxidation performance. The column test setup was designed to simulate the conditions of a heap biooxidation system, allowing for controlled variations and precise measurement of outcomes.

To investigate the biooxidation of low-grade ore, a 9K medium (Darvanjooghi et al., 2024) with a concentration of 5 g/l Fe (II) was prepared in 900 ml of solution, supplemented with 0.4 wt.% D-Sucrose and 0.4 wt.% yeast extract (Darvanjooghi et al., 2024). Subsequently, 100 ml of AMD was added to this medium. The resulting mixture was kept under stirring conditions at 37.5 °C and an agitation speed of 300 rpm for 22 days. Following this period, 500 ml of inoculum was sprayed onto 45 kg of low-grade ore, which contained 1.5 wt.% pyrite and a total of ~0.5 g/ton gold inclusions within the pyrite structure. The inoculated ore was mixed for five minutes three times, with each mixing interval separated by a one-hour resting period. This prepared sample was then placed into a jacketed column with a diameter of 6 cm, filling it to a height of 1 m. During the biooxidation, the iron-rich recycling solution was maintained at flow rates of 5 and 10 ml/h, while the temperature of the jacketed column was kept constant at 37.5 °C. To achieve optimal biooxidation efficiency, various aeration rates (0.5, 1, 1.5, 2, and 3 l/min) were tested to determine the appropriate oxygen level required for the process. The experiment included daily measurements of ORP, pH, total iron, and ferrous ion concentrations. **Fig. 5.2.** shows a process flow diagram and a picture of the column testing, respectively.

5.2.5. Cyanidation

To find the optimal conditions for the pretreated samples from both column and stirred tank biooxidation, cyanidation procedures were performed. In this part of the experiment, leaching duration (up to 30 h), cyanide concentration (ranging from 2 to 8 g/l) as well and pH (ranging from 9 to 12) were manipulated to find the optimum gold leaching from pretreated samples (Karimi et al., 2010). The efficiency of gold recovery after pretreatment was calculated using **Eq. 5.2.**:

$$Gold\ recovery\ (\%) = \frac{Recovered\ gold/1\ kg\ ore}{Present\ gold/1\ kg\ ore} \times 100 \quad (5.2)$$

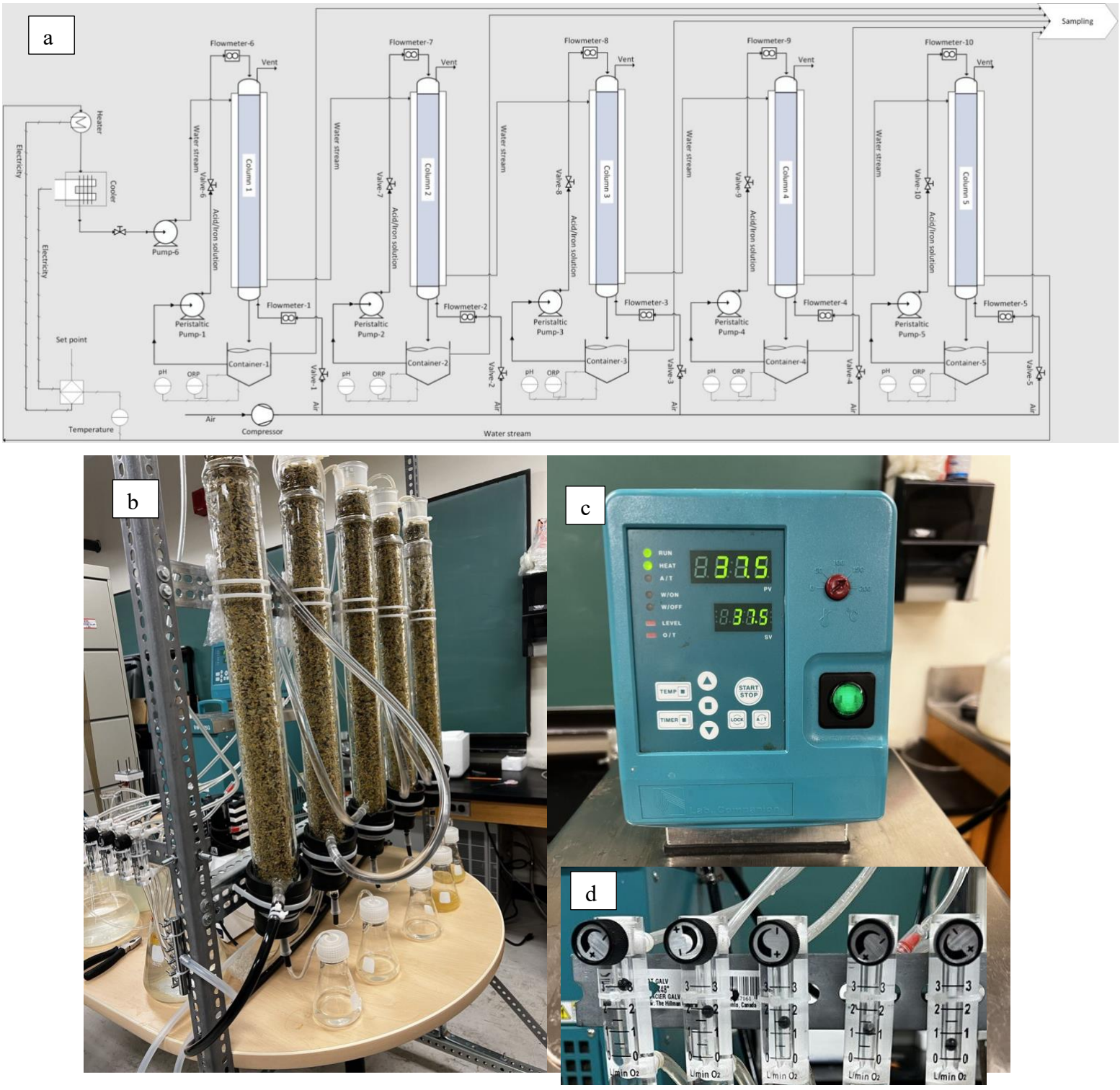

Figure 5.2. a) process flow diagram of column test biooxidation; b) experimental setup; c) temperature control system;and, d) aeration flowmeter and controlling valve for each column.

5.3. Results and discussion

5.3.1. Characterization

The results of elemental analysis from the ICP test for these two types of ore samples (LGOS and HGOS) are presented in **Table D1** (Appendix D). The results of the XRD analysis and the plot of the pattern for both LGOS and HGOS are also presented in **Table D2 and Figure D1** (Appendix D), respectively. The results indicate that both ore samples contain arsenic (1.16×10^4 g/ton and 4.1 g/ton for HGOS and LGOS, respectively), which could potentially affect microbial activity due to their high toxicity. Additionally, the analysis revealed that the primary minerals in these samples are ankerite and quartz, with weight fractions of 23% and 48% for the high-grade ore sample (HGOS), and 58.1% and 10.5% for the low-grade ore sample (LGOS), respectively.

In this study, XRF was utilized to determine the weight fractions of metal oxides in the ore samples. The results (**Table D3**, Appendix D) revealed that the major components of LGOS are SiO_2 (66.2 wt.%) and Al_2O_3 (13.2 wt.%), while HGOS is predominantly composed of SiO_2 (36.93 wt.%), Fe_2O_3 (12.02 wt.%), and Na_2O (11.02 wt.%). The gold grades of 0.477 g/ton and 25.2 g/ton, respectively, were determined for the LGOS and HGOS samples.

5.3.2. Column tests

5.3.2.1 Effect of aeration

Figure 5.3 a illustrates the change in oxidation-reduction potential (ORP) in a recycling acid solution through a column test biooxidation of refractory gold ore. The ORP remained relatively stable and low (around 370-400 mV) throughout the experiment for the negative control sample. This stability indicated minimal microbial activity affecting the ORP in the absence of additional aeration. For the aeration rate of 0.5 l/min, the ORP increased gradually, indicating a slow rise to approximately 450 mV around day 60. There was a sharp increase in ORP afterward, peaking just above 500 mV by day 80 before it started to decline. On the other hand, for an aeration rate of 3.0 l/min, the ORP increased rapidly and reached above 600 mV by day 30, then stabilized slightly below the peak. Similar to the 2.0 l/min rate, this increase indicated very high microbial activity, but the stabilization suggested that beyond a certain point, further increases in aeration rate did not significantly enhance activity. It is also concluded from other literature that heap biooxidation is largely affected by aeration. Aeration increases oxygen availability to biooxidizing

microorganisms, speeding sulfide mineral oxidation and gold recovery (J. Li et al., 2024). Studies reveal that forced aeration improves biooxidation and gold leaching efficiency compared to spontaneous convection. The expense and challenges of installing and maintaining aeration systems in heap biooxidation remain problematic (Logan et al., 2007).

In **Figure 5.3 b** it is concluded that the initial increase in pH across all column test configurations is attributed to the presence of acid-consuming substances in the LGOS. This is a common initial response as these substances neutralize some of the acidity in the solution leading to higher pH at the initial steps of biooxidation. Also, due to the nature of *Ferroplasma acidiphilum* (Ferrer et al., 2007), the subsequent decrease in pH indicated increased microbial activity and acid production. Higher aeration rates generally correlate with a more rapid and significant decrease in pH showing more oxidation of ferrous and production of ferric (Ofori-Sarpong et al., n.d.), reflecting enhanced microbial activity. Furthermore, the most efficient aeration rates for microbial activity and acid production appear to be between 1.5 and 3.0 l/min. These conditions resulted in the lowest and most stable pH levels, suggesting optimal conditions for the activity of *Ferroplasma acidiphilum*.

Figure 5.3 c shows that lower aeration rates (0.5 l/min) cause a lower gradual increase in ferric ion concentration, indicating slow microbial activity. In contrast, higher aeration rates (1.0, 1.5, 2.0, and 3.0 l/min) resulted in more substantial and rapid increases in ferric ion concentration, with the most pronounced rises at 2.0 and 3.0 l/min, peaking around day 80. Therefore, with the increase in aeration rates, the microbial oxidation process intensified, facilitating a more effective conversion of ferrous to ferric ions which is an important factor for the pyrite biooxidation.

The most significant reductions in ferrous ion concentration occurred at aeration rates of 2.0 l/min and 3.0 l/min (**Figure 5.3 d**). These exhibited a sharp decline starting around day 30, continuing to decrease rapidly and nearing depletion by day 80. The higher aeration rates enhanced the biooxidation, likely by providing optimal oxygen levels that facilitated microbial metabolism and activity. The reduction in ferrous ion concentration over time was primarily attributed to the biooxidation of pyrite. *Ferroplasma acidiphilum* oxidized ferrous ions to ferric ions, which then attacked the pyrite structure, further producing ferrous ions. This cyclical process of oxidation and reduction resulted in a net decrease in ferrous ion concentration as ferric ions continued to break down pyrite.

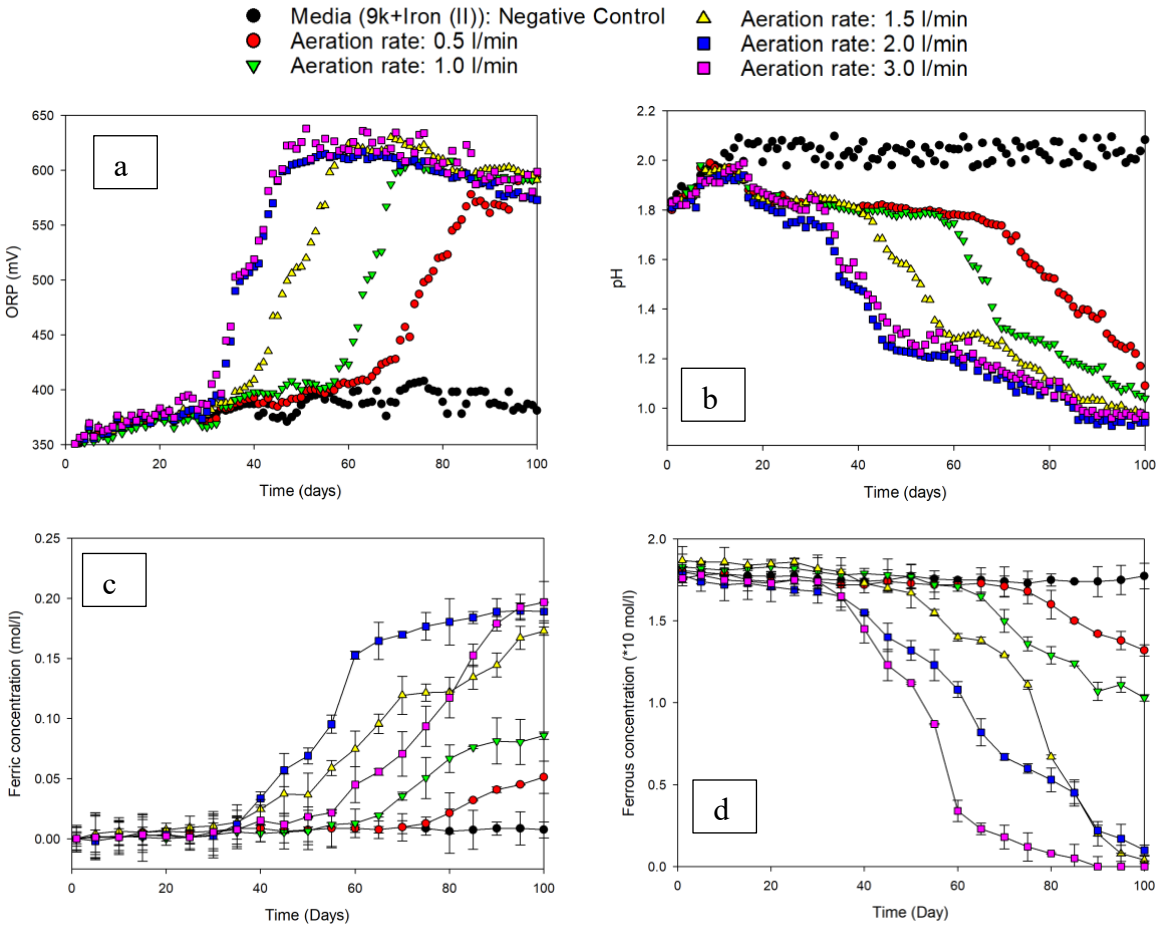

Figure 5.3. a) ORP; b), pH; c) ferric concentration; and d), ferrous concentration vs time for ore sample under column test biooxidation condition (aeration rate of negative control: 3.0 l/min).

5.3.2.2. Effect of solution flow rate

The average pyrite dissolving rate and the amount of recycling solution lost to evaporation in column biooxidation are both highly influenced by the aeration flow rate (**Figure 5.4 a**). The recycling solution loss increased noticeably as the aeration flow rate rose from 0.5 to 3.0 l/min, suggesting faster evaporation rates at higher aeration levels. This phenomenon holds for acid solution flow rates of 5 ml/h and 10 ml/h; however, solution loss is typically higher at the higher flow rate of 10 ml/h. In a similar vein, the average rate of pyrite dissolution rises as the aeration flow rate does, reaching its maximum dissolution at 3.0 l/min. Higher aeration and acid solution flow rates improved the biooxidation, but with greater evaporation losses. The flow rate of 10 ml/h

acid solution continuously produces a higher pyrite dissolving rate compared to the 5 ml/h flow rate.

The reduction in pyrite dissolution rate observed in **Figure 5.4 a** is primarily attributed to the aeration rate of 3 L/min, which leads to a significant decrease in humidity levels. This reduction in humidity impacted the microbial activity of *Ferroplasma acidiphilum*. This drier environment inhibited the growth and metabolic functions of *Ferroplasma acidiphilum*, as these microorganisms thrived in moist conditions resulting in keeping the osmotic stress as low as possible (Rohwerder et al., 2003). Consequently, the efficiency of pyrite oxidation diminished, resulting in a lower dissolution rate.

Figure 5.4 b shows the average pyrite dissolution rate for the recycling solution flow rate of 5 ml/hr. It is illustrated that the aeration rate significantly influences the pyrite dissolution rate. The aeration rate of 2.0 l/min consistently shows the highest pyrite dissolution rate, peaking around 0.9 %/5 days at 50 days and maintaining relatively high rates until around 70 days. The aeration rate of 3.0 l/min also showed a substantial pyrite dissolution rate but slightly lower than the 2.0 l/min rate, peaking at around 0.8. %/5days. The lower aeration rates (1.5, 1.0, and 0.5 l/min) exhibited significantly lower dissolution rates, with the 0.5 l/min rate showing the least dissolution, peaking at around 0.2 %/5 days. The negative control consistently demonstrated the lowest pyrite dissolution rates, barely exceeding 0.1 %/5 days, highlighting the critical role of aeration in enhancing pyrite biooxidation using *Ferroplasma Acidiphilum* at this flow rate. The total pyrite dissolution rates for 3.0, 2.0, 1.5, 1.0, and 0.5 l/min aeration rates are 33.1%, 42.8%, 29.3%, 20.8%, and 16.6%, respectively.

Increasing the aeration in heap biooxidation results in more evaporation of the liquid phase as a result of improved airflow and transfer of heat. This leads to higher temperatures and increased moisture loss (BOUFFARD and DIXON, 2004). The decrease in moisture content has a detrimental effect on microbial activity, which is crucial for the oxidation of sulfide minerals (Bailey & Hansford, 1993). As a result, the effectiveness of the biooxidation process is reduced. In addition, a reduction in the amount of liquid decreases the ability to transport metal ions that have been used in biooxidation, resulting in a further fall in the efficiency of pretreatment. As a result, it becomes difficult to maintain the ideal moisture levels, leading to higher operating expenses due to the need for more water to compensate for evaporation (Hansford & Miller, 1993).

For the recycling solution flow rate of 10 ml/h (**Figure 4 c**), the pattern was similar but with generally higher pyrite dissolution rates compared to the 5 ml/h flow rate. The aeration rate of 2.0 l/min again shows the highest pyrite dissolution rate, peaking around 1.1 %/5 days at approximately 50 days. Also, lower aeration rates (1.5, 1.0, and 0.5 l/min) show reduced effectiveness, with the 0.5 l/min rate peaking at around 0.3 %/5 days. The total pyrite dissolution rates for 3.0, 2.0, 1.5, 1.0, and 0.5 l/min aeration rates were 42.1%, 51.4%, 31.0%, 25.2%, and 19.1%, respectively.

5.3.3. Stirred tank reactor

Stirred tank reactor biooxidation for HGOS was explored using three key variables: aeration flow rate, organic carbon source, and agitation. It was observed that varying the aeration flow rate significantly influenced the biooxidation efficiency, with optimal oxygen transfer rates enhancing microbial activity and pyrite dissolution rates in HGOS. The concentration and continuous addition of organic carbon sources to the solution during the *Ferroplasma Acidiphilum* growth also played a crucial role, with certain sources leading to more efficient biooxidation. Additionally, the level of agitation can affect the homogeneity of the reactor environment, the contact between microorganisms and substrates, and shear stress on microorganisms' wall.

5.3.3.1. Effect of aeration

Figure D2 a, (Appendix D) illustrates the pH changes vs time in a stirred tank reactor during the biooxidation of HGOS using the same microorganism over 14 days. The results indicated that the pH values remain relatively stable at initial days and a gradual decrease in pH is observed in all aerated conditions, indicating the production of acid due to microbial activity. However, around day 6, the pH began to rise in reactors, likely due to the presence of acid-consuming substances in the ore sample. The reactor with 1.5 l/min aeration shows the most significant increase in pH. In contrast, the negative control maintains a relatively stable and higher pH throughout the experiment, demonstrating the absence of microbial biooxidation activity.

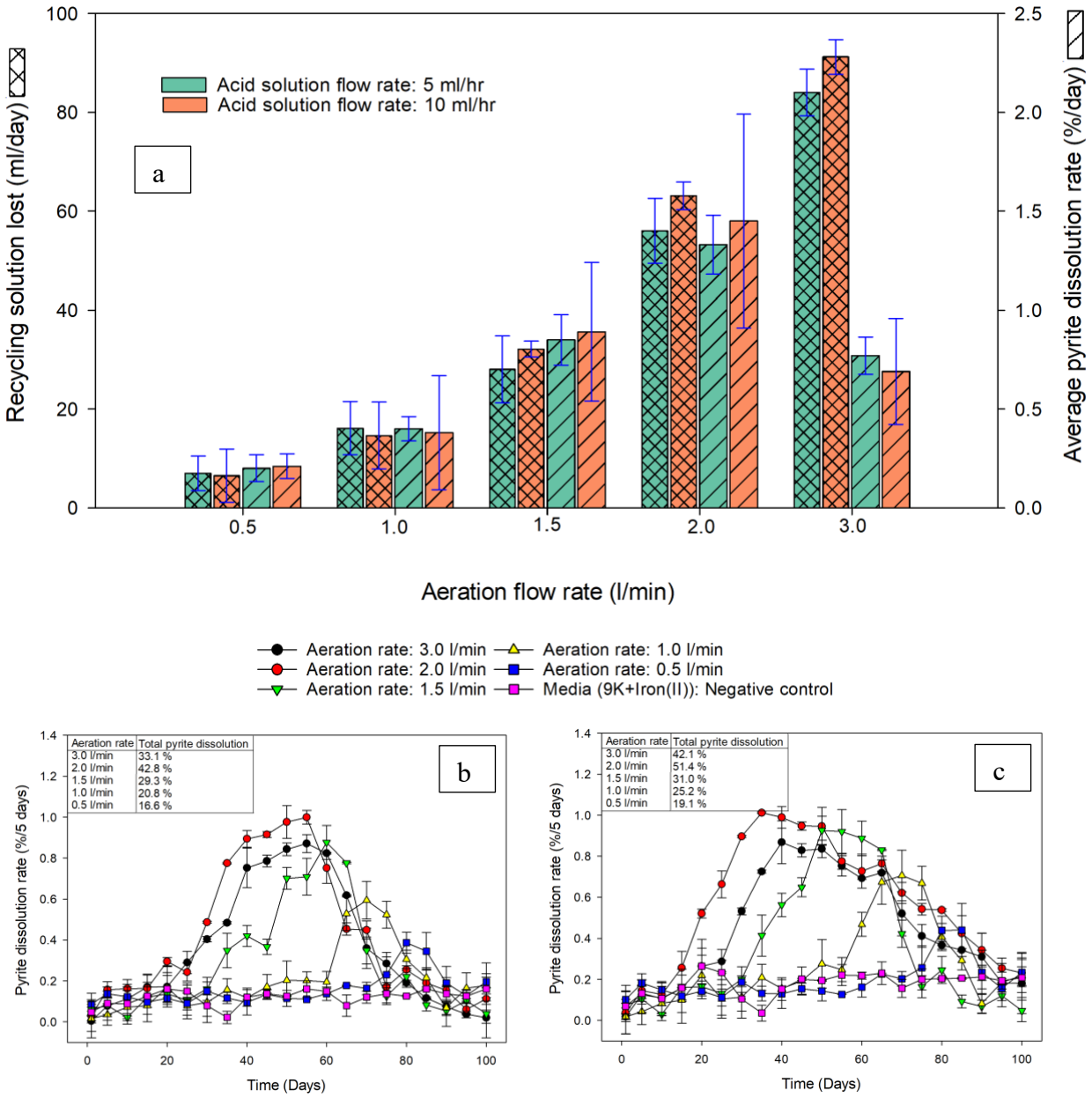

Figure 5.4. a, plot of average pyrite dissolution rate and solvent lost for various aeration in column test. Plot of pyrite dissolution rate for recycling solution flow rates of b, 5 ml/h, c, 10 ml/h, (aeration rate of negative control: 3.0 l/min).

Figure D2 b, (Appendix D) also shows the change in ORP within the stirred tank reactor. Initially, ORP values start at around 300 mV for all conditions and this parameter increases which indicates the progression of oxidation reactions by microbial activity. The reactors with higher aeration flow

rates (1.5 l/min and 1.0 l/min) show a more significant increase in ORP, reaching around 600 mV by the end of the experiment. Also, dissolved oxygen (DO) levels generally increased and after passing 4 days stabilized between 6.0 and 7.5 ppm (**Figure D2 c,** Appendix D). Higher aeration rates (1.5 l/min and 1.0 l/min) showed higher and more stable D.O. levels, indicating better oxygen transfer and availability for microbial activity.

Figure D2 d, (Appendix D) also shows the changes in pyrite oxidation rate normalized to microorganism counts (CFU) over 14 days during the biooxidation process for HGOS. The pyrite oxidation rate was highest across all conditions in the initial days but gradually decreased over time, suggesting a reduction in microbial activity or substrate availability (here pyrite). Aeration rate of 1.5 l/min maintained a relatively higher oxidation rate compared to the other aeration rates which indicated higher aeration flow rates support sustained microbial activity and oxidation efficiency. The pyrite dissolution rate per microorganism count reduced to 99% for 14 days for all aeration flow rates.

According to the results presented in **Figure D2 e, (**Appendix D), ferric ion concentration (Fe^{3+}) increased steadily over 14 days in aerated reactors, reaching around 0.3 mM by day 14, particularly in the 1.5 l/min and 1.0 l/min conditions. This increase supported the rise in ORP values and indicated active microbial oxidation of ferrous ions to ferric ions. Furthermore, pyrite dissolution rates exhibit a marked increase under aerated conditions, achieving up to 40% by day 14, particularly in the conditions where aeration flow rates were 1.5 /min and 1.0 l/min (**Figure D2 f,** Appendix D). This observation aligned with the trends in D.O. levels and ferric ion concentrations, corroborating that higher aeration rates boosted microbial activity and biooxidation efficiency. Conversely, the negative control demonstrated minimal pyrite dissolution, indicating a significant microbial oxidation activity in other samples.

5.3.3.2. Effect of organic carbon sources

The results presented in **Table 5.1** show HGOS pyrite dissolution in a stirred tank reactor by varying aeration flow rates and calcium carbonate make-up rates over 14 days. The data shows that higher aeration flow rates generally lead to greater pyrite dissolution. For instance, at 1.5 l/min aeration and 10 ml/day $CaCO_3$ make-up, the dissolution rate reaches 50.81% by day 14. However, the addition of more calcium carbonate increases the pH, which can reduce the growth rate of

microorganisms. Higher aeration and an optimal level of calcium carbonate supplementation were crucial for enhancing pyrite dissolution in biooxidation. During the bio-oxidation, carbon dioxide (CO_2) from the environment was incorporated into the organism's cellular metabolism through the enzyme ribulose-1,5-bisphosphate carboxylase/oxygenase (RuBisCO). RuBisCO catalyzes the reaction between CO_2 and ribulose-1,5-bisphosphate (RuBP), producing two molecules of 3-phosphoglycerate (3-PGA). Finally, the 3-PGA molecules are then converted into glyceraldehyde-3-phosphate (G3P) using ATP and NADPH produced by the organism's energy-generating pathways (e.g., through the oxidation of ferrous iron, Fe^{2+}) (Golyshina et al., 2000b; Z. Li, Xin, et al., 2020).

5.3.3.3. Effect of agitation

Figure D3 (Appendix D), demonstrates the effect of agitation speed on pyrite dissolution vs time. These results indicate that mixing speed significantly affects the biooxidation efficiency of HGOS in a stirred tank reactor. An agitation speed of 300 rpm is optimum and it achieves high biooxidation efficiency faster than the other speeds due to its balance of low shear tension and optimal mixing, which promotes effective gas-liquid-solid contact. Furthermore, the increase in pyrite dissolution is modest across all agitation speeds during the initial days. This phase likely corresponds to the adaptation period where microorganisms are acclimatizing to the conditions and starting to colonize the pyrite surfaces. At the end of the process duration, pyrite dissolution continues to increase but at a slower rate compared to the middle phase. This plateau effect could be due to the depletion of easily accessible pyrite or the accumulation of inhibitory byproducts.

Figure D4 (Appendix D), also illustrates the pyrite dissolution rate per microorganism count over 14 days at different agitation speeds in a stirred tank reactor during the biooxidation of high-grade ore samples (HGOS). Initially, all conditions start with high dissolution rates around 1×10^{-7} %.ml/day.cells, which significantly drop to around 1×10^{-8} %.ml/day.cells by day 2, suggesting rapid initial substrate consumption. From days 2 to 8, the dissolution rates stabilized across all speeds, indicating a steady state of microbial activity where agitation speed does not significantly influence the rate per cell concentration. However, from day 8 onwards, a gradual decline in dissolution rates is observed, especially pronounced at 600 rpm, dropping to 1×10^{-10} %.ml/day.cells by day 14.

Table 5.1. Effect of aeration flow rate and organic carbon source make up on the bio-oxidation of HGOS in stirred tank reactor.

		Aeration flow rate								
		0.5 l/min			1 l/min			1.5 l/min		
	Carbonate make up*	5 ml/day	10 ml/day	20 ml/day	5 ml/day	10 ml/day	20 ml/day	5 ml/day	10 ml/day	20 ml/day
Time (days)	1	1.21±0.12	1.53±0.32	1.42±0.55	1.34±0.65	1.71±0.54	1.62±0.45	1.32±0.45	1.84±0.53	1.65±1.12
	2	2.31±0.21	3.00±0.89	2.78±0.23	2.43±0.76	3.55±0.76	3.04±0.77	2.55±0.86	3.49±1.99	3.04±0.35
	3	5.67±0.22	7.28±0.13	7.19±0.65	5.99±0.15	8.27±0.15	7.60±0.43	6.03±0.37	8.38±0.87	7.17±1.67
	4	7.23±0.34	9.49±0.45	8.74±0.67	7.50±0.16	10.00±0.18	10.04±0.48	7.90±0.85	11.36±0.57	9.79±0.23
	5	12.23±0.21	16.33±0.76	13.97±0.86	13.14±0.37	17.56±0.15	15.14±0.27	13.06±0.97	17.48±1.17	17.34±0.86
	6	15.65±0.18	21.82±0.34	19.50±0.23	16.41±0.18	23.87±0.36	19.99±0.48	17.87±0.26	23.66±1.26	22.17±1.52
	7	18.85±0.37	26.62±0.88	23.39±0.95	20.34±0.78	26.99±0.39	23.20±0.38	21.41±0.84	28.69±0.57	22.85±1.86
	8	20.98±0.64	27.39±0.56	23.72±0.45	21.71±0.36	29.73±0.37	26.46±0.37	23.87±0.47	30.31±0.57	27.11±0.88
	9	25.81±0.81	34.23±0.23	30.63±0.87	26.92±0.85	34.80±0.58	35.26±0.26	29.04±0.27	40.64±0.76	34.21±0.99
	10	29.82±0.91	37.31±0.98	36.50±0.46	32.50±0.63	39.86±0.85	37.02±0.95	32.59±0.99	45.89±0.54	38.55±0.27
	11	31.67±0.39	40.39±0.87	38.10±0.35	35.00±0.06	49.46±0.64	40.49±0.89	34.34±0.47	44.24±0.46	40.95±1.04
	12	32.56±0.14	42.54±0.66	38.49±0.28	34.68±0.37	44.53±0.36	43.33±0.36	35.11±1.64	47.06±1.11	41.36±0.67
	13	32.18±0.19	43.20±0.76	40.54±0.28	33.64±0.39	42.62±0.49	40.20±0.18	36.47±1.54	43.98±0.24	43.44±0.77
	14	33.63±0.59	42.31±0.54	38.38±0.18	37.15±0.20	46.93±0.68	47.32±0.87	37.87±0.75	50.81±1.46	47.32±1.08

* 0.05 M $CaCO_3$ solution

5.3.4. Gold recovery

Figure D5 (Appendix D), illustrates the effect of time and pH on the cyanidation process for gold recovery from low-grade ore samples (LGOS) pretreated using column biooxidation with *Ferroplasma acidiphilum*. The data shows gold recovery percentages over 30 hours at various pH levels using a sodium cyanide solution. The results indicated that both pH and time significantly influenced gold recovery. Higher pH levels led to increased gold recovery, with the highest recovery rates observed at pH 10.5 to 11.0. Over time, gold recovery increased for all pH levels, with a rapid initial rise followed by a plateau phase. At lower pH levels (9.0 and 9.5), the gold recovery is substantially lower and slower compared to higher pH levels. This suggests that an

alkaline environment (higher pH) enhances the efficiency of the cyanidation process, likely due to improved stability of the cyanide complex and reduced interference from other ions.

At a pH higher than 11, the stability of the cyanide-gold complex is compromised. This can occur because high pH levels favored the formation of other chemical species, such as cyanate (CNO^-) and carbonate complexes, which compete with cyanide for the gold ions absorption. Additionally, this condition can also cause the precipitation of metal hydroxides, which can encapsulate the gold particles and prevent them from coming into contact with the cyanide solution (ref to A Review of the Cyanidation Treatment of Copper-Gold Ores and Concentrates).

Figure D6 a and **b (**Appendix D), illustrate the effects of pH and sodium cyanide (NaCN) concentration on gold recovery using cyanidation for two different ore samples and pretreatment methods.

In **Figure D6 a**, **(**Appendix D), representing LGOS pretreated with a column test, gold recovery increases with pH up to about 10.5 and with higher NaCN concentrations, highlighting the importance of an alkaline environment and sufficient cyanide availability for effective gold dissolution. However, at very high pH levels, the recovery rates tend to plateau or slightly decrease. In **Figure D6 b (**Appendix D), representing HGOS pretreated with a stirred tank reactor, the trends are similar, with optimal gold recovery achieved around pH 10.5 and higher NaCN concentrations. Notably, the stirred tank reactor pretreatment for HGOS results in higher overall gold recovery rates compared to the column test pretreatment for LGOS, suggesting more efficient oxidation and better gold exposure in the stirred tank reactor. This highlighted the significance of both optimizing chemical conditions and selecting effective pretreatment methods to maximize gold recovery during cyanidation.

Figure D6 c (Appendix D), also presents the results of an ICP (Inductively Coupled Plasma) test on the leachate solution following the cyanidation process, showing the recovery of various elements. The results indicate that the stirred tank reactor pretreatment (for HGOS) generally leads to higher recovery rates for most elements, especially Ag, Au, Zr, Cu, Mn, and Zn, compared to the column test (for LGOS). While the amount of gold recovery for untreated ore sample was less than 20%. This suggests that the stirred tank reactor method provides more effective exposure and liberation of these elements, enhancing their recovery during the cyanidation process. The higher recovery rates in the stirred tank reactor are likely due to better mixing, oxidation, presence of fine

particles compared to column test, and overall in-liquid pretreatment efficiency, making it a more effective method for preparing ore samples for cyanidation (A. Bulaev et al., 2021b; Mazuelos et al., 2000; Tavakoli et al., 2017).

5.4. Conclusion

Biooxidation using *Ferroplasma acidiphilum* is a highly effective pretreatment method for enhancing gold recovery from both high-grade (HGOS) and low-grade ore samples (LGOS). The stirred tank reactor showed superior performance compared to the column test, yielding significantly higher recovery rates for key elements. Gold recovery in HGOS pretreated with a stirred tank reactor reached up to 55%, compared to 40% in LGOS pretreated with the column test. Additionally, the recovery rates for silver and copper were also higher in the stirred tank reactor, reaching approximately 60% and 80%, respectively. These improvements are attributed to better mixing, oxidation, and overall pretreatment efficiency in the stirred tank reactor. Optimal conditions for biooxidation included specific aeration flow rates and agitation speeds, which facilitated effective microbial activity and pyrite dissolution, crucial for liberating gold from complex ores.

Interface 3: This chapter examines how *Ferroplasma acidiphilum* biooxidation affects gold recovery from HGOS and LGOS ore samples. Column tests and stirred tank reactors pretreated. Results indicated that the stirred tank reactor recovered critical elements better than the column test, with HGOS recovering 55% gold and LGOS 40%. Biooxidation was optimized using aeration flow rates of 1.0-1.5 L/min and agitation speeds of 300-450 rpm for microbial activity and pyrite dissolution. Gold recovery was best at pH 10.5, with up to 60% recovery at 8 (g/L) NaCN during cyanidation. At pH values over 11, competing chemical species and metal hydroxide precipitation reduced gold recovery to 40%. Increasing cyanidation time increased gold recovery, with considerable increases within 10 hours.

This research showed that microbiological approaches are inadequate for efficient and scalable and take a long time for a single batch column test. Next, an enzyme-based system called Enzymatic Biooxidation Technology (EnBiTe) was used to reduce biological reliance under regulated, modular settings.

Chapter 6: Enzymatic Biooxidation Technology (EnBiTe) for gold recovery from refractory sulfide ore*

*Mohammad Hossein Karimi Darvanjooghi, Sara Magdouli, Satinder Kaur Brar, *Bioresource Technology Journal*, submitted.

Abstract

This chapter also introduces an innovative low-temperature-adapted process, Enzymatic Biooxidation Technology (EnBiTe), for recovering gold from refractory sulfide ores. Utilizing glucose oxidase (GO) immobilized on modified sawdust, the process enhances pyrite dissolution and gold liberation under suboptimal conditions for traditional biooxidation methods. Experiments demonstrated that citric acid carboxylation improved enzyme activity, achieving a maximum of 80 µmol/min at 1 wt.% glutaraldehyde concentration, while hydrogen peroxide production peaked at 20–24°C. Optimized biooxidation conditions—100 mM substrate, 5 g immobilized enzyme, 1 g/l Iron(II), and 20% ore content—resulted in 89.2% pyrite dissolution for high-grade ore sample (HGOS) and 73.4% for low-grade ore sample (LGOS). Subsequent cyanidation achieved maximum gold recovery within 20 hours at pH 10–11, with HGOS exhibiting superior recovery of gold. These results underscore EnBiTe's potential as an effective and eco-friendly alternative to traditional pretreatment methods, particularly in colder climate.

6.1. Introduction

Typically, in regions where temperatures regularly drop below 10°C, essential microbial activity for biooxidation is significantly reduced, leading to slower rates of oxidation and incomplete mineral breakdown (Escobar et al., 2010). The biooxidation of high-grade refractory gold ore in a subarctic region can achieve only 35% gold recovery (Chowdhury & Ojumu, 2014; Ongendangenda & Ojumu, 2011; Z. L. Wu et al., 2013) , compared to 85% in temperate climates under similar conditions (Erüst et al., 2013; Hol et al., 2011). Research on the ASTER™ process, a biological thiocyanate and cyanide destruction method often integrated with biooxidation circuits, indicates that while optimal operation occurs between 18–28 °C, the process can function at temperatures as low as 12 °C. However, a significant reduction in degradation rates is observed at these lower temperatures, suggesting that microbial activity diminishes as temperature decreases (van Niekerk et al., 2022).

In order to overcome the issue of low-temperature limitation wide range of psychrophilic microorganisms including *Acidothiobacillus ferrivorans* and *Leptospirillum spp.* can be implemented for biooxidation at temperatures below 10 °C. Two factors directly affect the biooxidation process efficiency at low temperatures (less than 5 °C). The first factor is that the reduction in temperature reduces the chemical reaction rate which may influence the production rate of ferric ions in pyrite dissolution (Holmes & Crundwell, 2000). The second factor is that psychrophilic microorganisms become highly active at this temperature and less active as the temperature goes up and they are susceptible to temperature fluctuation (Sajjad et al., 2019b). When mesophiles and psychrophiles are used, this battle gets tougher. To keep conditions stable for bacteria growth and reactions, the right temperature range should be selected for bioleaching/oxidation, making it more costly for heap biooxidation (Sajjad et al., 2019b). However, maintaining the maximum efficiency in a wide range of temperature fluctuation would be operationally and physically difficult (Karimi Darvanjooghi et al., 2024b; Sajjad et al., 2019b). In addition to having a low temperature effect on biooxidation efficiency, these microorganisms' growth is significantly influenced by their interactions with mineral surfaces, which is a key mechanism for biological metal extraction. Higher concentrations of some ions and the presence of toxic minerals, however, may also negatively affect this interaction. As a result, the efficiency of bioleaching or biooxidation may be lowered since the capacity of microorganisms for effectively oxidizing metal sulphides may be doubled (J. Chen et al., 2022; Saavedra et al., 2020).

To address the challenges associated with microorganism-based biooxidation of sulfide-iron refractory gold ores at low temperatures, this research chapter explores the implementation of Enzymatic Biooxidation Technology (EnBiTe) based on high oxidative by-product of Glucose Oxidase (GO). Two distinct ore samples, designated as High-Grade Ore Sample (HGOS) and Low-Grade Ore Sample (LGOS), each with varying pyrite and gold contents, were utilized to assess the efficiency of EnBiTe. The study systematically examined the impact of several parameters on the biooxidation, including pH levels, temperature variations, enzyme activity, substrate type and concentration, and ore content (fraction) by considering the immobilization techniques. In the final phase, the effects of time, pH, and sodium cyanide concentration during the cyanidation of pretreated ore were investigated to optimize gold recovery.

6.2. Materials and Methods

6.2.1. Enzyme preparation

To extract glucose oxidase, *Aspergillus Niger* was used as a source of microorganisms. Potato dextrose broth, sucrose (99%, purchased from Merck Inc.), yeast extract, and Iron(II) with a purity of 99.6 (purchased from Merck Inc., USA) was used for the proliferation of *Aspergillus niger*. To perform an enzyme activity test, (2,2′-Azinobis-(3-Ethylbenzthiazolin-6-Sulfonic Acid) ABTS (purity 99.99%, purchased from Merck Co.), Horseradish peroxidase. D-β-glucose, D-+-galactose, D-+-sucrose, D-+-fructose (all with a purity of 99.6% and purchased from Merck Inc., USA) and molasses were used as substrates for enzyme activity tests. To preserve the produced enzyme, spruce sawdust was used as support with average particle size distribution presented in **Table E1** (Appendix E). Citric acid (purity 95%, purchased from Merck Inc.), sulfuric acid (purity 99.6%, purchased from Merck Inc.), and hydrochloric acid (purity 99.99%, purchased from Merck Inc.) were used for surface modification of support and optimize carboxylation. Glutaraldehyde (purity 99.9% and purchased from Merck Inc.) was used as la inking agent for the immobilization of Glucose Oxidase (GO) on pretreated support.

6.2.2. Sample preparation

Within this research, two distinct ore samples from a gold mine in the North of Quebec, Canada were employed to make up the different solid portions in the aqueous biooxidation. One of the samples had a high concentration of pyrite (~31 wt.%), which is directly correlated to the gold

grade in the sample (25 g/ton), while the other sample had a low concentration of pyrite (1.5 wt.%) and gold grade of 0.5 g/ton. The low-grade ore sample (LGOS) was collected at the Hammond Reef gold mine site which is situated in Ontario, Canada. As the high-grade ore sample (HGOS) represents a concentrated form of the LGOS with a higher pyrite content, the inclusion of gold within the crystal structures (pyrite, chalcopyrite, silicate, and alloys) remains consistent across both samples. Finally, sodium cyanide was purchased (with purity of 98%, Merck Inc. Germany) and used for dissolution of gold after pretreatment. Sodium hydroxide and sulfuric acid were used for adjusting pH. In all experiments, acetic acid (purity 99.9%, Merck Inc.) and sodium acetate (99.9% purchased from merck Inc.) were used to prepare the buffer solution for reaching the maximum GO enzyme activity.

6.2.3. Glucose Oxidase production

6.2.3.1. Incubation

The preparation of *Aspergillus Niger* cultures was carried out using a custom nutrient medium. The medium consisted of Potato Dextrose Broth (6.1 g/200 ml), sucrose (1 g/200 ml), yeast extract (1 g/200 ml), and an Iron (II) compound (10 g/200 ml) (Hamad et al., 2014). All components were dissolved in sterile distilled water and mixed thoroughly to ensure homogeneity. The pH of the medium was adjusted to a range of 5.0–6.5 to support optimal fungal growth. The prepared medium was transferred into a flask and sterilized in an autoclave at 121°C for 60 minutes. After sterilization, the medium was allowed to cool to approximately 50°C, before further use.

The sterile medium was poured into Petri dishes under aseptic conditions within a laminar flow hood. Each dish was filled with approximately 15–20 ml of the medium, which was left to solidify at room temperature. Once the medium had solidified, the plates were inoculated with *Aspergillus Niger* spores. The spores were either transferred directly to the center of the plates using a sterile inoculating loop or spread evenly across the surface using a spore suspension prepared in sterile distilled water. Spreading was accomplished with a sterile glass spreader to ensure even distribution of the spores.

The inoculated plates were incubated at 25–30°C for 3–5 days to promote fungal growth. Plates were monitored daily, and the development of characteristic black colonies was observed as an indicator of successful growth. Post-incubation, the plates were used for experimental analysis or

stored at 4°C for short-term use. To ensure sterility and prevent contamination, all equipment and materials were sterilized before use.

To extract glucose oxidase from the cultured *Aspergillus Niger*, the solid fungal content was harvested and subjected to sonication under controlled conditions. The fungal biomass was placed in an ice-cooled sonication bath set to 0°C to ensure enzyme stability throughout the process. Sonication was performed at an amplitude of 25% for a total duration of 30 minutes, with intermittent cycles of 1 minute on and 1 minute off to prevent overheating and minimize enzyme degradation. Following sonication, the resulting suspension was transferred into sterile centrifuge tubes. The tubes were centrifuged at 12,000 rpm for 10 minutes at 7°C to separate the cellular debris from the soluble components. The supernatant was carefully collected and used as the enzyme source for subsequent experimental procedures. The extracted enzyme solution was immediately stored on ice to maintain its activity and stability prior to utilization.

6.2.3.2. Enzyme activity determination

The activity of glucose oxidase was determined using a coupled enzymatic assay involving ABTS (2,2'-azino-bis(3-ethylbenzothiazoline-6-sulfonic acid)) and horseradish peroxidase (HRP). In this assay, glucose oxidase catalyzes the oxidation of glucose to gluconic acid and hydrogen peroxide (H_2O_2). The produced H_2O_2 is subsequently used by HRP to oxidize ABTS, generating a green-colored ABTS radical cation ($ABTS^{\bullet+}$), which can be quantified spectrophotometrically (Bankar et al., 2009a).

To prepare the reaction mixture, a buffer solution (commonly 0.1 M sodium acetate, pH 5.0–6.0) was used to maintain the optimal pH for the enzymes. The solution contained a defined concentration of substrate (here D-β-glucose 17–139 mM), a fixed amount of ABTS (200 mM), and an appropriate amount of HRP (5 U/ml). The glucose oxidase enzyme solution (e.g., 100 µl) was added to initiate the reaction. The reaction was conducted at a controlled temperature (25–30°C) in a final volume of 1 ml.

The enzymatic activity was monitored by measuring the increase in absorbance at 420 nm, corresponding to the formation of $ABTS^{\bullet+}$. The absorbance was recorded using a spectrophotometer at regular intervals (every 1 minute) for 13 minutes. One unit of glucose oxidase activity was defined as the amount of enzyme required to produce 1 µmol of H_2O_2 per minute under the assay conditions. To determine the correlation between hydrogen peroxide concentration

and the formation of ABTS•$^{+}$, a test was conducted using commercially obtained hydrogen peroxide. A standard curve was prepared and utilized to estimate hydrogen peroxide concentration based on absorbance. Negative controls (without glucose oxidase or substrate) were included to correct for background absorbance or non-specific oxidation of ABTS. The enzyme activity assay was used to measure the enzyme activity of obtained GO at different temperature, pH, and various types of substrates (**Figure E1** and **E2**, Appendix E).

6.2.4. Enzyme immobilization

To remove lignin and hydrolyze the sawdust, concentrated sodium hydroxide (10 M) and hydrochloric acid (98%) were used for pre-treatment. Following this process, the prepared samples underwent further treatment to enhance carboxylic acid functionalization on the sawdust surface.

Two methods were employed to achieve carboxylation of the sawdust surface to determine the most effective approach for maximum surface modification. In the first method, a citric acid solution with a concentration of 5 M was used to functionalize the sawdust, facilitating the introduction of carboxylic groups onto the surface through esterification. In the second method, a combination of hydrogen peroxide (3 v/w%) and hypochloric acid (6 wt.%) was utilized as the carboxylation agent, promoting surface modification through oxidation and chemical activation. These two approaches were compared to evaluate their efficiency in enhancing carboxylic acid functionalization, which is critical for improving the reactivity and surface properties of the sawdust.

After the pre-treatment and carboxylation, different concentrations of glutaraldehyde (0.1, 0.5, 1, and 2 wt.%) were added to 1 gram of the modified sawdust as a support material. Subsequently, 5 mL of a glucose oxidase (GO) enzyme cocktail was added to each sample. The total volume of the mixture was adjusted to 25 ml, and the resulting solutions were placed on a shaker for mixing at 180 rpm at 4 °C for 24 hours.

6.2.5. Biooxidation experiments

Following the immobilization of the enzyme onto the support and optimization of conditions to achieve maximum enzyme activity, experiments were conducted to evaluate the efficiency of the enzyme on biooxidation. Different types of substrates, including D-β-glucose, D-(+)-galactose, D-(+)-sucrose, D-(+)-fructose, and natural sugar (molasses), were used across multiple experimental

sets. Each set was performed with varying ore contents of 5, 10, 15, 20, and 25 wt.% (for both HGOS and LGOS). For each experiment, a 100 ml sample containing ore, immobilized enzyme, and the respective substrate was prepared in a flask. The flasks were incubated under rotational conditions at 180 rpm and a temperature of 22°C to facilitate biooxidation.

6.3. Results and discussion

6.3.1. Mineral characterization

In this experiment, two different ore samples were utilized for enzymatic biooxidation. The low-grade ore sample (LGOS, containing 1.5 wt.% pyrite and 0.5 g/ton of gold in pyrite inclusions) and the high-grade ore sample (HGOS, containing 7.2 wt.% pyrite and 5.4 g/ton of gold in pyrite inclusions) were separately characterized. The results of elemental analysis from ICP test for these two types of ore samples (LGOS and HGOS) are presented in **Table D1** (Appendix D). The results of XRD analysis and the plot of pattern for both LGOS and HGOS are also presented in **Table D2 and Figure D1** (Appendix D), respectively.

In this study, XRF was utilized to determine the weight fractions of metal oxides in the ore samples. The results (**Table D3**, Appendix D) revealed that the major components of LGOS are SiO_2 (66.2 wt.%) and Al_2O_3 (13.2 wt.%), while HGOS is predominantly composed of SiO_2 (36.93 wt.%), Fe_2O_3 (12.02 wt.%), and Na_2O (11.02 wt.%).

6.3.2. Immobilization approach

The enzyme activity of glucose oxidase (GO) immobilized using glutaraldehyde cross-linking was compared between two distinct pretreatment strategies using citric acid carboxylation and $NaClO/H_2O_2$ carboxylation. The results demonstrated that the citric acid carboxylation pretreatment led to significantly higher enzyme activity across all tested glutaraldehyde concentrations, with the peak observed at 1 wt.% glutaraldehyde (**Figure E3,** Appendix E). For instance, enzyme activity using D-β-glucose as the substrate reached approximately 35 µmol/min in the $NaClO/H_2O_2$-pretreated samples, compared to around 80 µmol/min in the citric acid-pretreated samples at a similar concentration of glutaraldehyde. These findings suggest that the citric acid pretreatment produces a higher density of reactive carboxyl groups on the enzyme

support, facilitating improved covalent binding with glutaraldehyde and resulting in enhanced enzyme activity due to higher chemical adsorption of enzyme of support's active surface.

However, in both methods, enzyme activity declined as glutaraldehyde concentration increased beyond 1 wt.%. At 5 wt.%, enzyme activity dropped to approximately 30–40% of the peak value across all substrates tested. This decline can be attributed to excessive cross-linking, which increases the rigidity of the enzyme-support matrix. Over-crosslinking can hinder the flexibility of enzyme molecules and limit substrate access to the active sites, reducing overall catalytic efficiency. Moreover, excessive glutaraldehyde may react non-specifically with amino groups of the enzyme, leading to partial denaturation or blockage of active sites.

6.3.3. Temperature effects

Figure E4 a (Appendix E), illustrates the hydrogen peroxide production over time at different temperatures (0–4°C, 10–12°C, and 20–24°C) using 30 mM D-β-glucose as the substrate and 1 ml of enzyme cocktail after extraction from *Aspergillus Niger*. Hydrogen peroxide production was negligible at 0–4°C, while it increased significantly at higher temperatures, with the highest production observed at 20–24°C after 120 minutes. This indicates that the catalytic activity of glucose oxidase (GO) is highly temperature-dependent, with limited reaction progress occurring at lower temperatures. In **Figure E4 b (**Appendix E), the enzyme activity of GO is plotted across the same temperature ranges. At 0–4°C, enzyme activity is effectively zero, whereas it reaches its maximum at 20–24°C, showing a sharp increase in enzymatic efficiency with rising temperature.

The absence of enzyme activity at 0–4°C can be attributed to the low molecular movement and reduced kinetic energy at such temperatures. Enzymatic reactions rely on the collision between the enzyme and the substrate, and at low temperatures, the molecular motion is significantly hindered, preventing sufficient substrate binding and catalysis. Additionally, the enzyme's flexibility, crucial for substrate recognition and catalysis, is restricted at low temperatures, rendering the enzyme inactive.

In contrast, the enzyme activity peaks at 20–24°C, which is close to the optimal temperature range for glucose oxidase extracted from *Aspergillus Niger*. At this temperature range, the enzyme achieves an ideal balance between structural flexibility and stability, enabling efficient substrate binding and catalytic turnover. The higher enzyme activity correlates directly with increased

hydrogen peroxide production, as observed in **Figure E4 a** in appendix E, due to the rapid conversion of glucose to gluconic acid and hydrogen peroxide under optimal conditions.

6.3.4. pH effects on enzyme activity

Figure 6.1 demonstrates the rate of hydrogen peroxide (H_2O_2) production as a function of time at various pH levels and different initial concentrations of D-galactose as the substrate: 80 mM (**Figure 6.1 a**) and 18 mM (**Figure 6.1 b**).

In **Figure 6.1 a**, at a higher substrate concentration of 80 mM, hydrogen peroxide production is significantly influenced by pH, with the highest production observed at pH 5 and pH 6. The rate of production increases rapidly during the initial phase (0–6 minutes) and gradually plateaus around 14–16 minutes, suggesting substrate saturation or equilibrium in enzyme activity. At more acidic conditions (pH 1–3), hydrogen peroxide production is notably lower, with minimal rates observed at pH 1. This trend indicates that the enzyme responsible for catalyzing D-galactose oxidation has optimal activity in slightly acidic conditions (pH 5–6), consistent with the properties of glucose oxidase enzymes from *Aspergillus Niger*.

In **Figure 6.1 b**, at a lower substrate concentration of 18 mM, hydrogen peroxide production follows a similar trend but at significantly lower levels. At pH 5 and pH 6, H_2O_2 production increases steadily over time, reaching approximately 6–7 mM at 30 minutes. However, at lower pH values (pH 1–3), the production remains negligible throughout the experiment. The reduced substrate concentration limits the availability of D-galactose for enzymatic conversion, leading to slower reaction kinetics and lower hydrogen peroxide yield.

Figure E5 (Appendix E), illustrates the effect of pH on enzyme activity at two initial D-galactose concentrations: 18 mM and 80 mM. The enzyme activity, represented in terms of hydrogen peroxide production, reveals a strong dependence on pH, with clear differences observed between the two substrate concentrations.

At 80 mM D-galactose, enzyme activity increases sharply with pH, reaching a peak at pH 5, where the activity reaches approximately 32 μM H_2O_2/min/ml enzyme. The activity remains relatively stable between pH 4–6, suggesting that the enzyme retains its optimal catalytic efficiency in this slightly acidic range. Below pH 4, enzyme activity drops drastically, particularly at pH 1–2, where

it is negligible. This steep decline indicates that the enzyme becomes denatured or structurally impaired in highly acidic environments.

At the lower substrate concentration of 18 mM D-galactose, a similar trend is observed, but the enzyme activity is significantly reduced. The maximum enzyme activity is again observed at pH 5, albeit at a much lower value (~0.8 µM H_2O_2/min/mL enzyme), due to substrate limitation. At pH 1–3, enzyme activity remains close to zero, consistent with enzyme inactivation under highly acidic conditions.

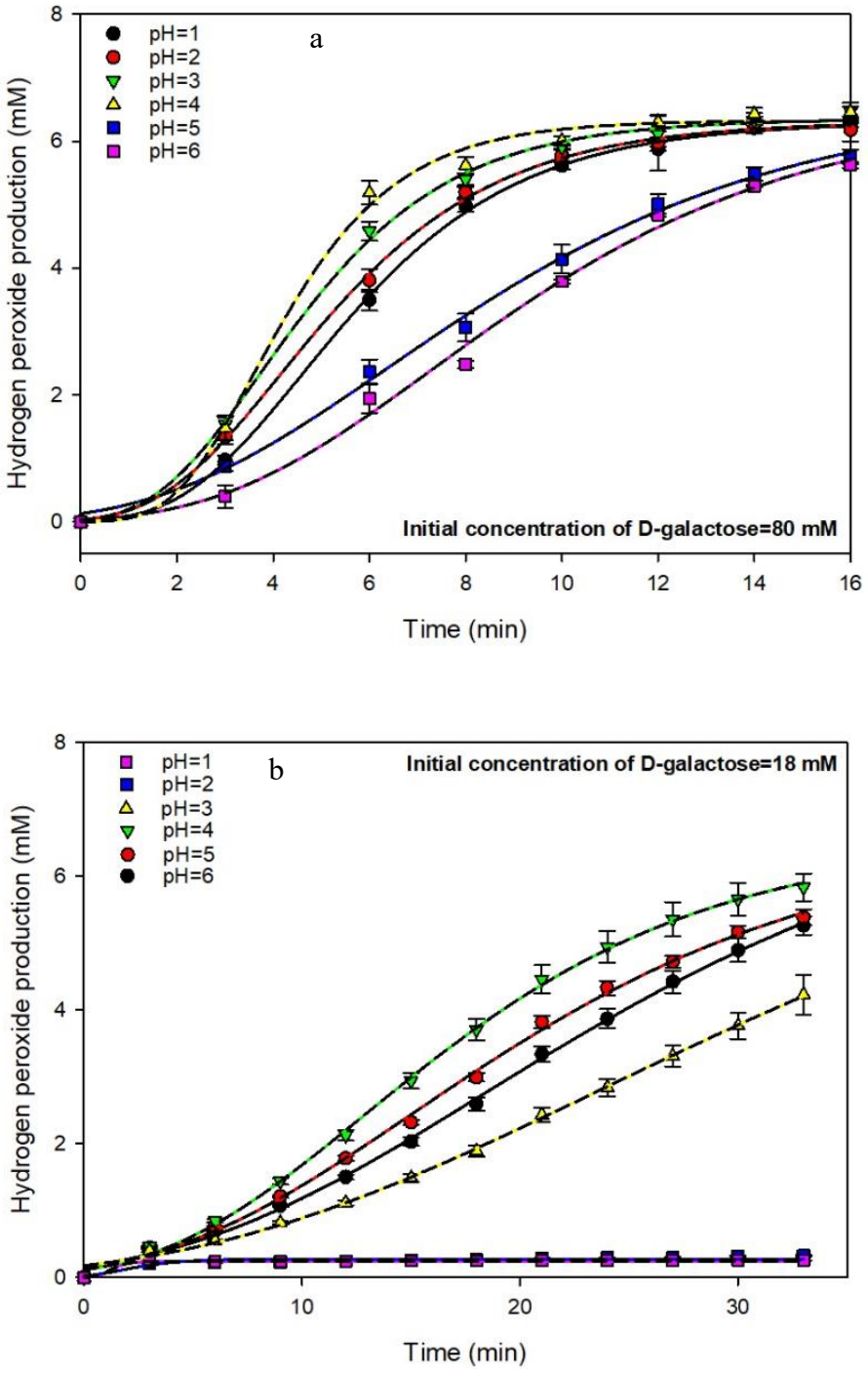

Figure 6.1. Rate of hydrogen peroxide production vs time for different pH and initial D-galactose concentration of a, 80 mM and b, 18 mM (100 ml of enzyme cocktail).

The observed pH dependence highlights the importance of maintaining an optimal pH range for enzyme functionality. At pH 5, the enzyme achieves its highest activity, likely due to the preservation of its structural integrity and the protonation state of critical amino acid residues in the active site. This pH range aligns with the optimal pH reported for glucose oxidase and other related oxidases derived from *Aspergillus Niger*. At highly acidic pH levels (1–3), the enzyme activity approaches zero due to protonation of essential residues in the active site, disrupting substrate binding and catalytic turnover. Enzyme denaturation may also occur under such acidic conditions, leading to irreversible loss of activity. Conversely, at higher pH values (6 and above), enzyme activity begins to decline, indicating a deviation from the enzyme's optimal stability range. The differences in enzyme activity between the two substrate concentrations (80 mM vs. 18 mM) further emphasize the role of substrate availability. At 80 mM, the enzyme operates closer to saturation, maximizing catalytic efficiency, whereas at 18 mM, substrate limitation reduces the overall reaction rate.

The observed pH dependence of glucose oxidase (GO) activity, with optimal performance at pH 5, aligns with findings in the literature (Bankar et al., 2009a; Guo et al., 2025; Khatami et al., 2022a; Mayel et al., 2025a; Vogt et al., 2014). For instance, a study on a cold-active GO from *Penicillium* sp. reported an optimal pH of 5.5, with the enzyme retaining more than 50% activity over a pH range of 3.0 to 7.0. This optimal pH range is crucial for preserving the enzyme's structural integrity and the proper protonation state of amino acid residues at the active site, which are essential for effective catalysis (M. Yuan et al., 2020a).

The significant decline in enzyme activity at highly acidic conditions (pH 1–3), as noted in the data, is consistent with findings that extreme pH levels can lead to enzyme denaturation or structural impairments. Such conditions can disrupt the hydrogen bonding and electrostatic interactions that maintain the enzyme's three-dimensional structure, thereby hindering substrate binding and catalytic efficiency. Conversely, at higher pH values (above 6), a decrease in activity has been observed, indicating that deviations from the optimal pH range can adversely affect enzyme stability and function (EFSA Panel on Food Contact Materials Flavourings and Processing Aids (CEF) et al., 2018).

6.3.5. Substrate effects on enzyme activity

The enzyme activity for glucose oxidase (GO) was measured with various substrates—D-β-glucose, D-galactose, D-sucrose, and D-fructose—at increasing substrate concentrations. The results demonstrate that D-β-glucose exhibits the highest enzyme activity among all substrates, reaching a maximum activity of approximately 90 μmol/min at higher substrate concentrations (~120–140 mM). This outcome aligns with the enzyme's natural specificity toward glucose, making it the most efficient substrate for glucose oxidase (**Figure 6.2 a**).

In contrast, D-galactose and D-sucrose showed significantly lower enzyme activity, even at higher substrate concentrations, with D-galactose peaking at around 40 μmol/min and D-sucrose at approximately 50 μmol/min. The lower activities observed with these substrates suggest that glucose oxidase has a reduced affinity and catalytic efficiency for sugars other than glucose, likely due to differences in molecular structure that hinder optimal binding to the enzyme's active site. D-fructose exhibited intermediate enzyme activity (~60 μmol/min) at higher concentrations, highlighting its partial compatibility as a substrate. The trend observed in Figure 5a emphasizes that substrate specificity plays a critical role in determining enzyme activity. Enzymatic efficiency decreases when substrates deviate structurally from glucose, limiting their recognition and conversion by the enzyme.

Figure 6.2 b illustrates hydrogen peroxide (H_2O_2) production as a function of time for various initial concentrations of D-galactose (17 mM to 139 mM). A clear positive correlation is observed between substrate concentration and H_2O_2 production. At the lowest concentration of 17 mM, H_2O_2 production remains minimal over the 12-minute period, indicating substrate limitation. As the D-galactose concentration increases, the rate of H_2O_2 production accelerates, with the highest production observed at 139 mM.

The increase in H_2O_2 production with substrate concentration can be attributed to the availability of more substrate molecules for enzymatic conversion. At higher concentrations, the enzyme active sites are saturated, resulting in maximum turnover rates and increased production of H_2O_2. However, a slight plateau can be observed at later time points, suggesting the system approaches equilibrium or that enzyme activity becomes constrained by product accumulation or substrate diffusion limitations.

The observed substrate specificity of glucose oxidase (GO), with D-β-glucose exhibiting the highest enzyme activity, aligns with findings in the literature. GO catalyzes the oxidation of β-D-glucose to D-glucono-δ-lactone and hydrogen peroxide, demonstrating a natural preference for β-D-glucopyranose due to its active site's structural configuration. This specificity is attributed to the enzyme's active site, which is tailored to accommodate the β-D-glucopyranose form of glucose, facilitating efficient catalysis (Bauer et al., 2022a).

In contrast, substrates such as D-galactose and D-sucrose exhibit significantly lower enzyme activity, as noted in the provided data. This reduced activity is likely due to structural differences that hinder optimal binding to the enzyme's active site. For instance, D-galactose differs from D-glucose in the orientation of the hydroxyl group on the fourth carbon, which may impede proper alignment within the active site. Similarly, D-sucrose, being a disaccharide composed of glucose and fructose, presents a more complex structure that may not fit efficiently into the active site of GO. These structural variations result in decreased affinity and catalytic efficiency for these substrates (Y. Wang et al., 2024).

Figure E6 a and **b** (Appendix E) show the flasks containing ferrous ions and various substrates (D-galactose, D-sucrose, D-β-glucose, D-fructose, and molasses) before and after the bio-Fenton reaction. Prior to the reaction (**Figure E6 a**), all solutions appeared colorless, indicating no initial production of Fe^{3+}. After the reaction (**Figure E6 b**), varying intensities of brown coloration are observed across the flasks. The D-β-glucose sample exhibits the darkest brown coloration, suggesting the highest H_2O_2 production and thus the most efficient ferric ion generation. In contrast, substrates like D-galactose, D-sucrose, D-fructose, and molasses result in lighter brown coloration, reflecting lower H_2O_2 production due to reduced enzymatic efficiency.

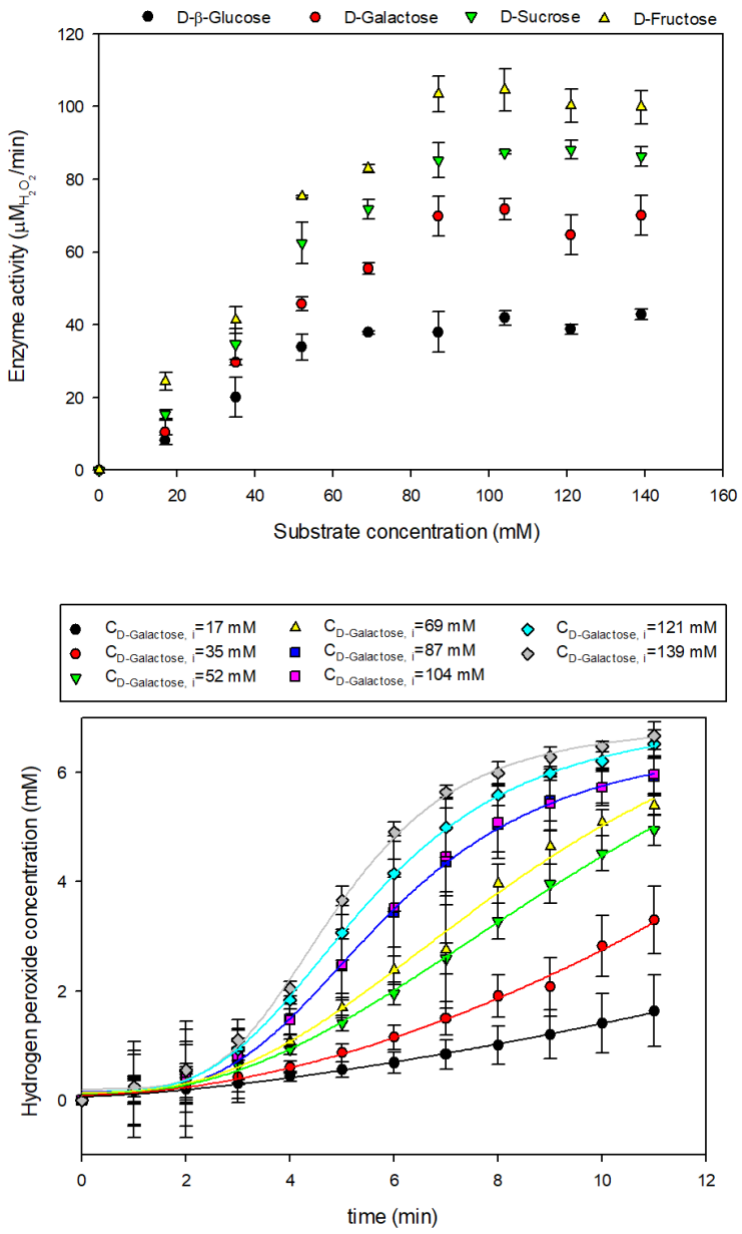

Figure 6.2. a, Enzyme activity (100 ml of enzyme cocktail) vs concentration for different types of substrates and b, hydrogen peroxide production for different initial concentration of D-+-galactose as a substrate.

Substrate Influence on GO Activity and Bio-Fenton Efficiency

The observed differences in ferric ion production can be attributed to the substrate specificity of glucose oxidase. D-β-glucose, as the preferred substrate, enables the highest catalytic activity, leading to maximum H_2O_2 generation and ferric ion conversion. Other substrates, such as D-

galactose and D-sucrose, exhibit lower compatibility with the enzyme's active site, resulting in reduced H_2O_2 production and consequently lower ferric ion formation. These results highlight the critical role of substrate selection in optimizing bio-Fenton reactions, as the extent of ferric ion production is directly dependent on the amount of H_2O_2 generated through enzymatic activity.

Glucose oxidase (GO) catalyzes the oxidation of glucose or similar substrates, producing gluconic acid and hydrogen peroxide (H_2O_2). The reaction is expressed as (Bankar et al., 2009b; Bauer et al., 2022b; Khatami et al., 2022b; Mayel et al., 2025b; M. Yuan et al., 2020b):

$$D-\beta-Glucose+O_2 \xrightarrow{Glucose\ Oxidase} Gluconic\ Acid+H_2O \tag{6.2}$$

In the presence of ferrous ions (Fe^{2+}), H_2O_2 facilitates a bio-Fenton reaction, converting Fe^{2+} to ferric ions (Fe^{3+}) and generating hydroxyl radicals (·OH)

$$Fe^{2+}+H_2O_2 \rightarrow Fe^{3+}+OH^{\bullet}+OH^{-} \qquad k=40-80\frac{L}{mol.s} \tag{6.3}$$

$$Fe^{3+}+H_2O_2 \rightarrow Fe^{2+}+OH_2^{\bullet}+H^{+} \qquad k=90\times10^{-7}\frac{L}{mol.s} \tag{6.4}$$

$$Fe^{3+}+OH_2^{\bullet} \rightarrow Fe^{2+}+O_2+H^{+} \qquad k=0.3-2\times10^{6}\frac{L}{mol.s} \tag{6.5}$$

This reaction results in the formation of ferric ions, which manifest as a brown coloration in solution, providing a visual indication of the extent of H_2O_2 production and its subsequent reaction with Fe^{2+}. According to reaction in **Eq. 6.3**, we can conclude that the rate of ferric ions production is comparable with its consumption rate, and this led to the high concentration of ferric ions in the solution. Although, reaction in **Eq. 6.5** is faster that **Eq. 6.3**, the rate limiting reaction here is **Eq. 6.4** and leads to low production of $OH_2^{\bullet}$ which is consumed in **Eq. 6.5**.

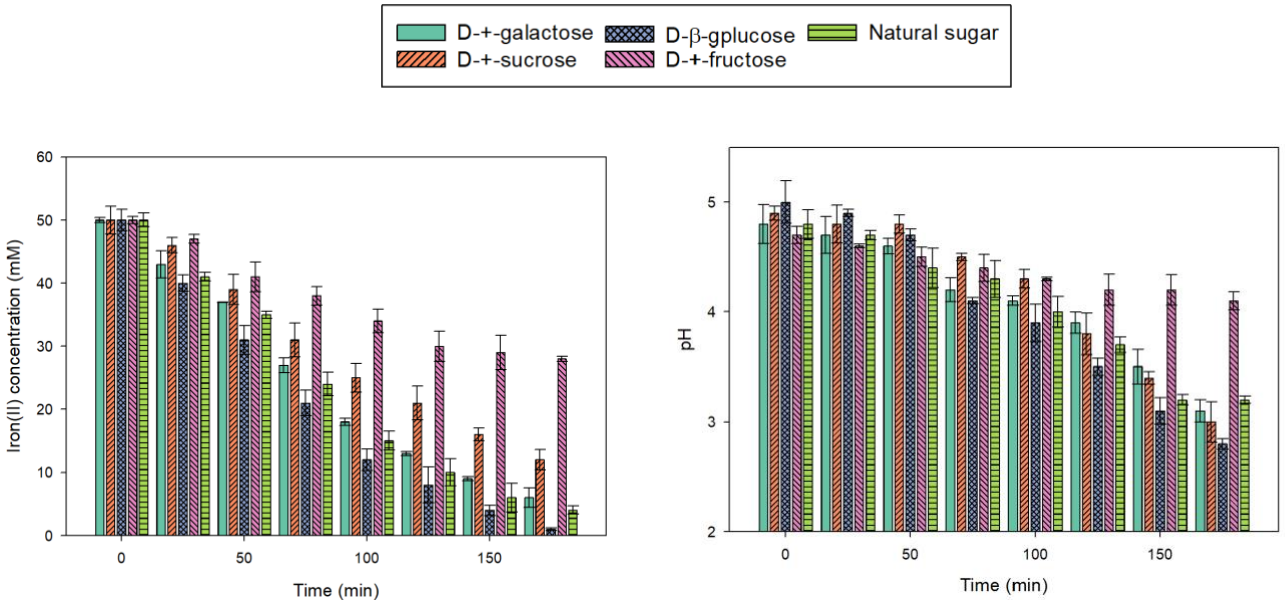

Figure 6.3. a,iron (II) consumption and, b, pH changes vs time for different substrate in the presence of GO enzyme (80 mM substrate and 1 ml of enzyme cocktail in 100 ml of solution).

The consumption of iron (II) (Fe^{2+}) was assessed over time in the presence of various substrates to evaluate their efficiency in promoting hydrogen peroxide (H_2O_2) production and subsequent oxidation to iron (III) (Fe^{3+}). The data presented in **Figure 6.3 a** indicate that D-β-glucose and natural sugar (molasses) are the effective substrates, exhibiting the maximum iron (II) consumption and consequent iron (III) production. Within 150 minutes, these substrates nearly depleted the available iron (II), highlighting their superior capacity to generate H_2O_2, which facilitates the oxidation process. In contrast, D-+-galactose and D-+-sucrose demonstrated moderate iron (II) consumption, with D-+-fructose being the least effective among all tested substrates.

The superior performance of D-β-glucose and molasses (due to high amount of glucose) can be attributed to their structural properties, which may enhance the catalytic activity of the GO enzyme, leading to increased H_2O_2 production. The results suggest that these substrates interact favorably with the enzymatic system, enabling a more rapid and complete oxidation of iron (II) to iron (III). On the other hand, the slower iron (II) consumption observed with D-+-fructose indicates its limited efficacy in supporting the enzymatic reaction, likely due to its less favorable molecular interactions with the enzyme.

The pH changes over time, shown in **Figure 6.3 b**, reflect the production of gluconic acid as a byproduct of the enzymatic reaction in the buffer system. D-β-glucose exhibited the most pronounced pH reduction, reaching approximately pH 3.5, followed by D-fructose and D-sucrose. This significant drop in pH suggests that D-β-glucose is the most effective substrate for gluconic acid production which leads to inactivation of GO enzyme. The lesser pH changes observed with D-galactose and natural sugar (molasses) align with their lower enzymatic activity, resulting in reduced acid production.

6.3.6. Biooxidation

This approach allowed for the quantification of pyrite oxidation efficiency under different experimental conditions. The immobilized GO enzyme facilitated the generation of H_2O_2, promoting the oxidation of iron (II) to iron (III), which subsequently enhanced the dissolution of pyrite.

In this section of the study, the effects of various parameters, including ore content, substrate concentration, andiron (II) concentration, were investigated on pyrite dissolution using immobilized glucose oxidase (GO) enzyme on cellulosic support. The pyrite dissolution was calculated based on the initial and final total iron concentrations in the system, applying the following equation:

$$Pyrite\ dissolution\ (\%) = 2.15 \times 10^{6} \frac{\alpha_{final} - \alpha_{initial}}{X.Y} \tag{6.6}$$

In this context, α denotes the concentration of dissolved iron in the liquid phase (wt.%), X defines the percentage of pyrite found in the ore specimen (wt.%), and Y represents the percentage of ore in the container (wt.%).

The duration of the pyrite dissolution process was standardized at 180 minutes, as this time frame ensured that the reaction proceeded until the pH of the solution reached its minimum value. The decline in pH is indicative of gluconic acid production, a byproduct of the enzymatic reaction catalyzed by the immobilized glucose oxidase (GO) enzyme. However, the significant drop in pH also corresponds to the eventual inactivation of the enzyme, as the acidic environment adversely affects its catalytic activity. By limiting the process to 180 minutes, the study captured the

maximum efficiency of pyrite dissolution before enzyme deactivation occurred, ensuring consistent and reliable comparisons across different experimental conditions.

6.3.6.1. Ore content effect

Figure 6.4 illustrates the relationship between pyrite dissolution (%) and ore content (wt.%) using molasses as the substrate for both low-grade ore samples (LGOS) and high-grade ore samples (HGOS). Three concentrations of molasses (20 mM, 40 mM, and 100 mM) were tested to evaluate their effect on pyrite dissolution across varying ore contents.

For LGOS, pyrite dissolution increases progressively with higher ore content and molasses concentration. At 20 mM molasses, the dissolution remains relatively low across all ore contents, indicating limited catalytic efficiency. However, with increasing molasses concentrations (40 mM and 100 mM), a substantial improvement in dissolution is observed, particularly at higher ore contents (20 wt.% and 25 wt.%). This trend highlights the importance of substrate concentration in enhancing the enzymatic activity for low-grade ores.

For HGOS, a similar trend is observed, with pyrite dissolution increasing with ore content and molasses concentration. However, the dissolution percentages for HGOS are consistently higher than those for LGOS under equivalent conditions. At 100 mM molasses and 25 wt.% ore content, HGOS achieves the highest dissolution, nearing 90%, compared to approximately 75% for LGOS. This indicates that high-grade ore samples are more responsive to the enzymatic reaction, likely due to their greater pyrite content and reactivity.

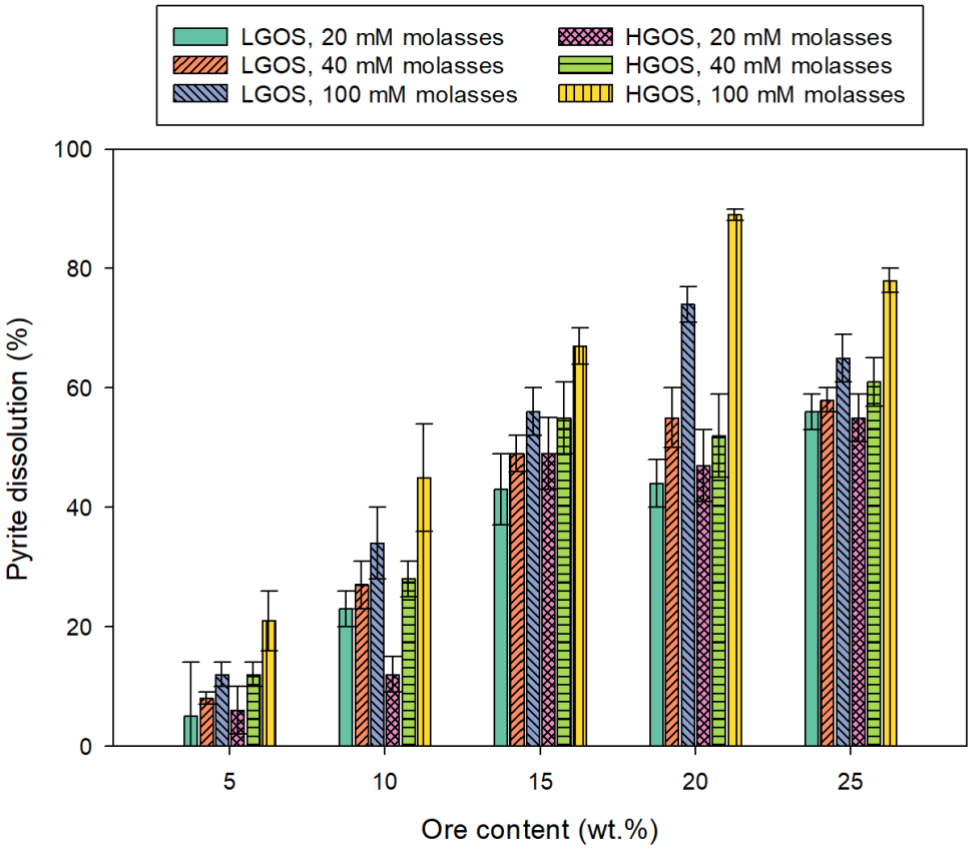

Figure 6.4. Pyrite dissolution vs different ore content (5 g of immobilized enzyme in 200 ml experiment solution and 1 g/L Iron(II)).

6.3.6.2. iron (II) concentration effect

Figure 6.5 illustrates the relationship between pyrite dissolution (%), final average pH, and initial iron (II) concentration (g/l) for various enzyme masses (1 g, 2 g, and 5 g) immobilized on cellulosic supports, applied to low-grade (LGOS) and high-grade (HGOS) ore samples. Pyrite dissolution increases consistently with initial iron (II) concentration up to 1 g/l, with a peak dissolution efficiency observed at this point for all experimental conditions. For HGOS, dissolution percentages are higher compared to LGOS across all tested concentrations, which reflects the greater pyrite content and reactivity of the high-grade ore. However, beyond 1 g/l, a significant decline in dissolution is observed, especially at 5 g/l and 10 g/l iron (II), for both ore types.

At low iron (II) concentrations (0.01–1 g/l), the final pH of the solution consistently drops below 4, indicating the active catalytic performance of the GO enzyme. This pH reduction is due to the production of gluconic acid as a byproduct of the oxidation of the substrate (molasses) by the immobilized enzyme. The acidification effect is particularly pronounced for samples with higher enzyme loading (5 g), as the increased enzyme mass enhances the catalytic reaction and gluconic acid production, contributing to the observed decrease in pH. This reduction in pH is a strong indicator of effective enzyme functionality, which correlates with the high pyrite dissolution rates under these conditions.

For higher iron (II) concentrations (5 g/l and 10 g/l), the final pH averages above 4.5, indicating significantly reduced gluconic acid production. This reduced acid production suggests partial or complete inactivation of the immobilized GO enzyme, likely due to the accumulation of hydroxyl radicals generated during the oxidation of iron (II). Hydroxyl radicals are highly reactive species that can damage the enzyme structure, leading to a marked decline in its catalytic efficiency. This phenomenon is accompanied by a corresponding reduction in pyrite dissolution percentages, reinforcing the critical impact of enzyme inactivation at elevated iron (II) levels.

Across all conditions, HGOS achieves consistently higher pyrite dissolution than LGOS, reflecting the enhanced reactivity and higher pyrite content of the high-grade ore. However, the trends in pH variation for both LGOS and HGOS are similar, demonstrating that the catalytic behavior of the immobilized enzyme is influenced more by iron (II) concentration and enzyme mass than by ore grade. These observations emphasize the delicate balance between substrate concentration and enzymatic activity, with excessive iron (II) concentrations causing enzyme inactivation and a subsequent decrease in pyrite dissolution efficiency.

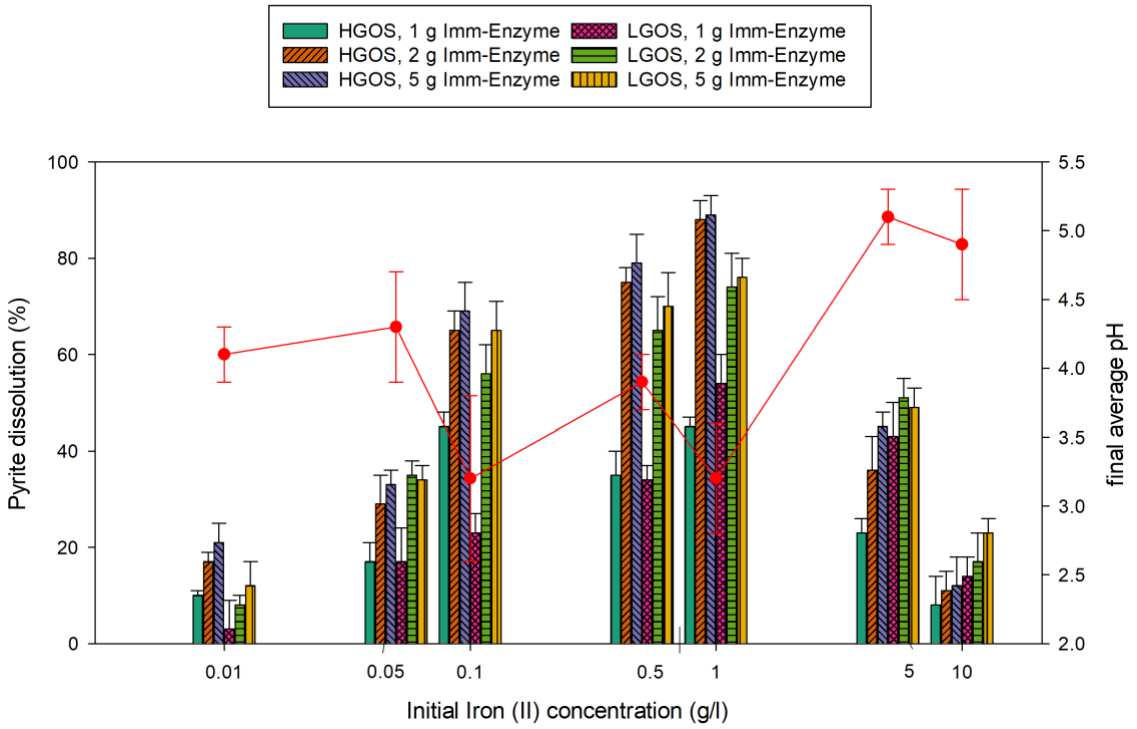

Figure 6.5. Pyrite dissolution vs initial iron (II) concentration for LGOS and HGOS and different amount of immobilized enzyme (1, 2, and 5 g) and 100 mM of substrate (natural sugar: molasses).

The observed relationship between pyrite dissolution, final pH, and initial iron (II) concentration in the presence of immobilized glucose oxidase (GO) aligns with findings in related studies. At lower iron (II) concentrations (0.01–1 g/l), the significant decrease in final pH below 4 indicates active catalytic performance of the immobilized GO, leading to increased pyrite dissolution. This acidification is attributed to the production of gluconic acid during the oxidation of glucose by GO, a phenomenon also reported in studies where gluconic acid production resulted in pH reductions, thereby enhancing the dissolution of metal sulfides (M. Wang et al., 2023).

However, at higher iron (II) concentrations (5–10 g/l), the observed reduction in pyrite dissolution and higher final pH values suggest enzyme inactivation. This is likely due to the accumulation of reactive oxygen species, such as hydroxyl radicals, generated during iron (II) oxidation. These radicals can damage the enzyme's structure, leading to decreased catalytic efficiency. Similar inhibitory effects of high iron (II) concentrations on enzymatic activity have been documented,

where excessive iron (II) led to the generation of reactive species that inactivate enzymes involved in oxidative processes (Forney et al., 1982).

6.3.6.3. Optimized condition

The analysis reveals that the maximum pyrite dissolution for both LGOS and HGOS is achieved under specific optimal conditions: a substrate concentration of 100 mM (molasses), 5 g of immobilized glucose oxidase (GO) enzyme on cellulosic support, an initial iron (II) concentration of 1 g/l, an ore content of 20%, and a biooxidation time of 200 minutes. Under these conditions, HGOS exhibits a superior pyrite dissolution rate of 89.2%, reflecting its higher reactivity and efficiency in the biooxidation process. In comparison, LGOS achieves a maximum pyrite dissolution rate of 73.4%, which, while lower than HGOS, still demonstrates the effectiveness of the enzymatic system. These findings emphasize the critical role of substrate concentration, enzyme loading, and iron concentration in optimizing the biooxidation of pyrite for both ore grades.

The lower pyrite dissolution observed in LGOS can be attributed to the presence of interfering elements, such as copper, which are known to inhibit the enzymatic activity and the biooxidation process. Copper and similar elements can compete with iron (II) during the catalytic reaction, reducing the efficiency of pyrite oxidation. In contrast, HGOS, which is a concentrated form of LGOS, has undergone processes to eliminate these inhibitory elements during the concentration stage. As a result, HGOS exhibits a higher pyrite dissolution rate, benefiting from a purer ore composition that enhances the enzymatic reaction and maximizes the oxidation efficiency. This distinction highlights the importance of ore purity in achieving optimal pyrite dissolution.

6.3.4. Gold recovery

The optimized time for cyanidation in gold recovery is detailed in the supplementary information, providing critical insights into process efficiency. According to the reported data, the maximum duration for effective cyanidation is approximately 20 hours, conducted under alkaline conditions with a pH range of 10-11 (**Figure D5**, Appendix D). This operational window ensures optimal dissolution of gold while minimizing cyanide consumption and potential side reactions. These

findings serve as a guideline for enhancing the recovery process by balancing reaction kinetics and chemical stability during cyanidation.

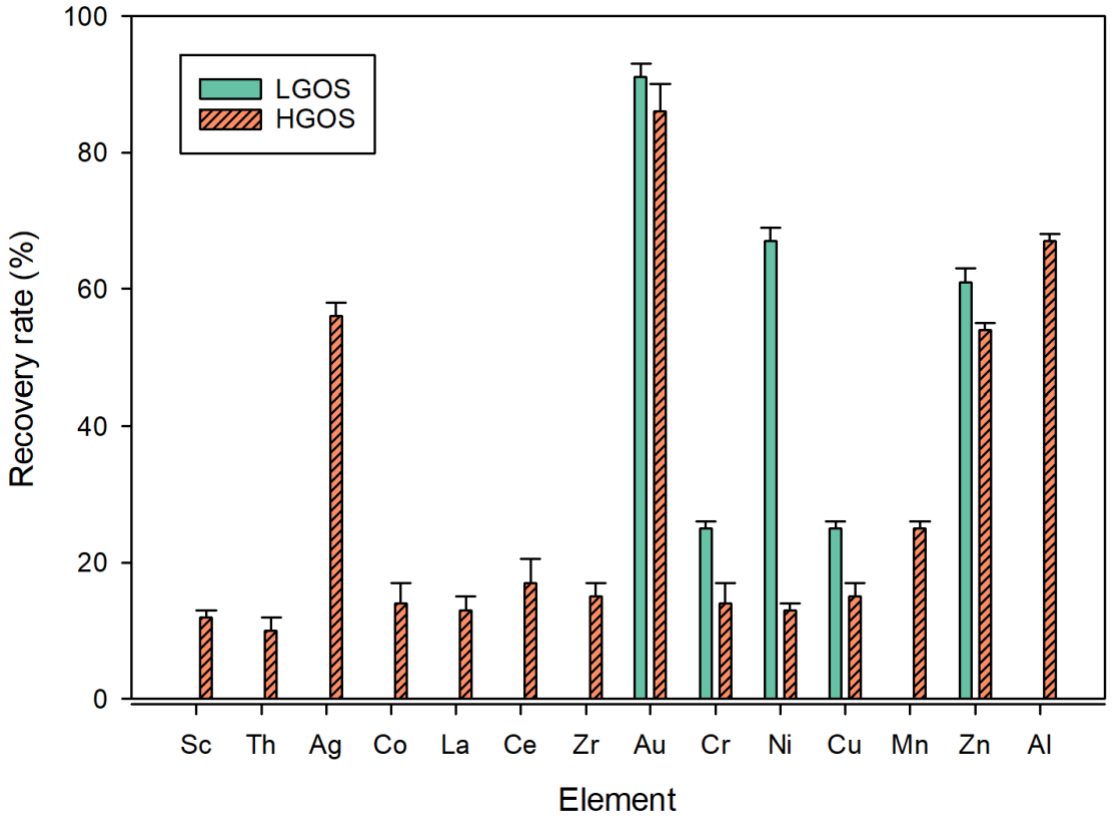

Figure 6.6. Plot of gold recovery using cyanidation for LGOS and HGOS at maximum pyrite dissolution using EnBiTe.

Figure 6.6 presents the results of an ICP (Inductively Coupled Plasma) test on the leachate solution following the cyanidation process, showing the recovery of various elements. The results indicate that the HGOS generally leads to higher recovery rates for most elements, especially Ag, Au, Zr, Cu, Mn, and Zn, compared to the LGOS. This suggests that EnBiTe provides more effective exposure and liberation of these elements, enhancing their recovery during the cyanidation process.

A comparison of gold recovery efficiency between the pretreatment methods from various approaches and the EnBiTe process is presented in **Table 6.1**. The results of this study clearly showcase a significant improvement in gold recovery rates when compared to other biooxidation processes reported in the literature. In this research, the gold recovery for High-Grade Ore Samples (HGOS) and Low-Grade Ore Samples (LGOS) surpassed 80%, with values of 84% and 92%, respectively. These recovery rates not only highlight the effectiveness of the enzymatic biooxidation technology employed but also outshine the methods reported by Xu et al. (2020), where *A. ferrooxidans* and *L. ferrooxidans* achieved gold recovery rates of 61% and 65%, respectively, over a much longer treatment period of 8 days. The stark difference in both recovery efficiency and treatment duration underscore the advanced capability of the enzymatic approach utilized in this study, making it highly efficient for gold recovery from refractory ores.

A key advantage of this study is the remarkably short pretreatment time of 180 minutes, which is substantially faster than the extended durations required by other methods. For example, McNeice et al. (2021) documented biooxidation processes using *L. ferrooxidans* that required up to 15 days to achieve a maximum gold recovery of 79%. Similarly, Azizitorghabeh et al. (2022) reported in-situ biooxidation processes with recovery rates as high as 86.9%, but these required 60 days of treatment. By achieving higher or comparable recovery rates within just three hours, this study demonstrates a breakthrough in reducing process time while maintaining exceptional efficiency. The shortened timeline has significant implications for industrial scalability and cost-effectiveness, making enzymatic biooxidation a promising alternative to traditional methods.

Moreover, the enzymatic biooxidation process in this study achieves superior results even when compared to neutral atmospheric oxidation methods combined with biooxidation. McNeice et al. (2021) documented gold recovery rates of 84% for RC3 ore with neutral atmospheric oxidation, but this process required a pretreatment period of 87 hours, followed by additional biooxidation steps. In contrast, the enzymatic method used in this study achieved a comparable recovery rate of 84% for HGOS and an even higher recovery of 92% for LGOS within just 180 minutes. This substantial improvement in both recovery and efficiency further emphasize the potential of enzymatic biooxidation as a more sustainable and time-effective solution for gold recovery.

Overall, the findings of this study present a compelling case for the adoption of enzymatic biooxidation technology in industrial gold recovery. The ability to recover gold from both high-

grade and low-grade ore samples with recovery rates exceeding 80%, coupled with a significantly reduced pretreatment time, positions this method as a superior alternative to traditional biooxidation techniques. By combining high efficiency with reduced time and potentially lower operating costs, this method has the potential to revolutionize the gold recovery process, making it more sustainable, economical, and practical for industrial-scale applications. These results pave the way for further exploration and optimization of enzymatic biooxidation in the field of refractory ore processing.

Table 6.1. Comparison of Gold Recovery Efficiency and Pretreatment Times Under Various Methods.

Operations	Sources (ore)	Recovery (%)	Treatment time	References
1- Untreated 2- Neutral Atmospheric oxidation 3- Biooxidation (*L. ferrooxidans*)	RC1: Au: 1.18, Pyrite: 20.33%	1- Au: 31% 2- Au: 76% 3- Au: 75%	1- 0 2- 87 hr 3- 15 days	(McNeice et al., 2021)
1- Untreated 2- Neutral Atmospheric oxidation 3- Biooxidation (*L. ferrooxidans*)	RC3: Au: 0.92 g/t, Pyrite: 17.42%	1- Au: 38% 2- Au: 84% 3- Au: 79%	1- 0 2- 87 hr 3- 15 days	(McNeice et al., 2021)
1- Untreated 2- Neutral Atmospheric oxidation 3- Biooxidation (*L. ferrooxidans*)	RC2: Au: 1.25 g/t, Pyrite: 20.02%	1- Au: 44% 2- Au: 82% 3- Au: 72%	1- 0 2- 87 hr 3- 15 days	(McNeice et al., 2021)
A. thiooxidans: A. ferrooxidans: L. ferrooxidans = 1:1:1	1- Leaching of non-oxidized ore, 2- Leaching after control test, 3- Leaching of biooxidized ore with ferric iron addition, 4- In-situ leaching of biooxidised ore 5- In-situ leaching of biooxidised ore with ferric iron addition	1- Au: 16.1% 2- Au: 51.8% 3- Au: 66.4% 4- Au: 86.9% 5- Au: 64.5%	60 days	(Azizitorghabeh et al., 2022)
A. Ferrrooxidans *L. Ferrrooxidans*	High Gold Grade Sample: 18.05 g/t	*A. Ferrrooxidans*: Au: 61%, *L. Ferrrooxidans*: Au: 65%	8 days	(Xu, Li, et al., 2020b)
Enzymatic Biooixdation Technology (Enbite)	High Grade Ore Sample (HGOS), Low Grade Ore Sample (LGOS)	HGOS; Ag: 57%, Au: 84%, Zn: 54%, Al: 64% LGOS: Au: 92%, Ni:63%, Zn:61%	180 min	This Study

6.4. Conclusion

This study highlights the efficacy of Enzymatic Biooxidation Technology (EnBiTe) in addressing the challenges of gold recovery from refractory sulfide ores in low-temperature environments. The optimized conditions—5 g immobilized glucose oxidase (GO) enzyme, 100 mM substrate concentration, 1 g/l iron (II), and 20% ore content—enabled an impressive 89.2% pyrite dissolution for high-grade ore (HGOS) and 73.4% for low-grade ore (LGOS) within maximum 180 minutes of reaction time. Notably, citric acid-based carboxylation pretreatment of the enzyme support yielded higher enzymatic activity (80 µmol/min) compared to other methods, enhancing the biooxidation process. The enzyme demonstrated optimal activity at 20–24°C and pH 5–6, emphasizing its adaptability to low-temperature conditions.

The cyanidation step further validated the effectiveness of EnBiTe, achieving maximum gold recovery within 20 hours at pH 10–11, with HGOS showing superior recovery rates for gold and other elements such as silver and copper. These findings confirm EnBiTe as a robust and eco-friendly alternative to traditional microbial-driven biooxidation, offering a sustainable solution for the mining industry, particularly in regions with cold climates where traditional methods are less effective. Future research could explore scaling up the process and further optimizing enzyme immobilization to enhance industrial applicability.

Interface 4: This phase of study recovers gold from refractory sulphide ores using the innovative low-temperature Enzymatic Biooxidation Technology (EnBiTe). Immobilizing glucose oxidase (GO) on modified sawdust increases pyrite decomposition and gold liberation. Citric acid carboxylation boosted enzyme activity to 80 µmol/min at 1 wt.% glutaraldehyde, peaking hydrogen peroxide production at 20-24°C. Optimised biooxidation conditions—100 mM substrate, 5 g immobilised enzyme, 1 g/Liron (II), and 20% ore content—dissolved 89.2% pyrite for HGOS and 73.4% for low-grade samples. Cyanidation recovered the most gold at pH 10–11 in 20 hours, with HGOS recovering most. This suggests that EnBiTe might replace traditional pretreatment processes in colder areas as an effective and ecologically friendly alternative.

To prove EnBiTe's commercial viability, particularly under operationally relevant flow conditions, the following research phase deployed enzymatic modules to column systems modelling heap leach settings.

Chapter 7: Enzymatic Biooxidation Technology (EnBiTe): catalase and glucose oxidase modules configuration*

*Mohammad Hossein Karimi Darvanjooghi, Sara Magdouli, Satinder Kaur Brar, *Process Safety and Environmental Protection Journal*, submitted.

Abstract

In this chapter the modular enzymatic systems were used and assessed to investigate the application of Enzymatic Biooxidation Technology (EnBiTe) for gold recovery from refractory sulfide ores. The biooxidation process was optimized under various conditions, including substrate flow rates of 5–10 ml/h, circulation flow rates of 50–200 ml/h, and aeration flow rates of 1.0–2.0 l/min. The EnBiTe system utilized two immobilized enzyme modules: a glucose oxidase (GO) module to produce oxidizing agents and a catalase (CAT) module to mitigate oxidative stress by consuming excess hydrogen peroxide. These modules were organized in parallel and series configurations, within this parallel configuration have demonstrate a superior performance. Pyrite dissolution reached a maximum of 91% under optimized conditions with a substrate flow rate of 10 ml/h and a circulation flow rate of 100 ml/h. The recovery rate of gold (Au) using cyanidation was higher (90%) in the parallel configuration with a circulation flow rate of 100 ml/h. This research highlights the efficacy of modular EnBiTe systems as controllable and efficient solutions for enhancing gold recovery, offering significant advantages over conventional microorganism-assisted biooxidation methods.

7.1. Introduction

Psychrophilic bacteria such as *Acidithiobacillus ferrivorans* and *Leptospirillum spp.* may facilitate bio-oxidation at temperatures below 10 °C; however, biooxidation at low temperatures (below 5°C) encounters considerable obstacles owing to two main causes. Initially, decreased temperatures diminish the rates of chemical bioreactions, which might negatively affect the generation of ferric ions causing low pace biooxidation rate (D'Amico et al., 2006; Duku, 2011b). Second, while psychrophilic microorganisms exhibit higher metabolic activity under such conditions, they are highly sensitive to temperature fluctuations and become less effective as temperatures change (Jin et al., 2022). The use of mesophilic and psychrophilic microorganisms for biooxidation adds complication because of their different growth and activity needs. Integrating these two microbial populations in a single biooxidation process requires carefully regulated temperature, nutrition and supply, and acidity of environment, to balance their metabolic activity, which is usually difficult to accomplish. Conflicts occur when temperature circumstances favor one group, reducing the efficiency of the other. This discrepancy in physiological demands hampers the design of biooxidation systems, especially in places with changing or high temperatures (Ercolini et al., 2009; García-Descalzo et al., 2022; Ingraham & Bailey, 1959). Maintaining the heap at a targeted low temperature during biooxidation poses significant challenges due to the massive scale of crushed ore typically involved, often ranging from 100,000 to 300,000 tons. The sheer volume of material introduces substantial thermal inertia, making it difficult to regulate and sustain the desired temperature throughout the heap. Furthermore, the operational complexities of ensuring consistent aeration, moisture distribution, and heat dissipation across such a large heap further complicate the process (Bhakta & Arthur, 2002b; Darvanjooghi et al., 2022; Y. Jia et al., 2024). Furthermore, the growth of these microorganisms is notably affected by their interactions with mineral surfaces, which plays a crucial role in the efficiency of biooxidation alongside the impact of low temperatures on their overall performance (Kleber et al., 2021). Nevertheless, elevated levels of certain ions and the occurrence of toxic minerals can adversely influence this interaction (W. Qin et al., 2020).

To address the challenges associated with microorganism-based biooxidation of sulfide-iron refractory gold ores at low temperatures, this research chapter explores the implementation of Enzymatic Biooxidation Technology (EnBiTe) as a novel technology based on the highly oxidative byproducts of Glucose Oxidase (GO) reaction with suitable substrate. GO catalyzes the

oxidation of monosaccharides, generating hydrogen peroxide as a byproduct, which enhances the biooxidation process by promoting sulfide mineral dissolution. The modular design of EnBiTe enhances the controllability of the biooxidation process, as temperature regulation is required only for the EnBiTe module, simplifying operational requirements compared to the thermal management of entire ore heaps. However, the production of highly oxidative components by the GO enzyme leads to partial enzyme degradation over time, necessitating the inclusion of a system to manage excess oxidative byproducts. This study focuses on the combined implementation of immobilized Glucose Oxidase (GO) and immobilized Catalase (CAT) modules, where the catalase module is designed to mitigate oxidative stress by consuming surplus oxidative compounds, thereby improving enzyme stability and overall process efficiency.

To evaluate the effectiveness of the EnBiTe module in reducing the biooxidation time, a Low-Grade Ore Sample (LGOS) was utilized for assessment in column tests. LGOS typically requires an extended duration for biooxidation when using microorganism-assisted methods, making it an ideal candidate to demonstrate the operational differentiation offered by the EnBiTe approach. The investigation included testing various configurations of the glucose oxidase (GO) and catalase (CAT) modules, such as parallel or series arrangements, while also exploring different flow ratios to the GO and CAT modules. These configurations were analyzed to identify the optimal setup for enhancing the biooxidation process and minimizing operational time.

7.2. Materials and Methods

GO enzyme was extracted from *Aspergillus Niger* (**Chapter 2, Section 6.2.3**). Natural sugar source (molasses) was used as substrate for enzyme test. Catalase enzyme from bovine liver with specific enzyme activity of 5000 units/mg proteins was purchased from Merck Inc., Canada. For the surface modification of the support and to optimize carboxylation, citric acid (95% purity, sourced from Merck Inc., Canada), sulfuric acid (99.6% purity, obtained from Merck Inc., Canada), and hydrochloric acid (99.99% purity, sourced from Merck Inc., Canada) were employed. Glutaraldehyde, with a purity of 99.9% and obtained from Merck Inc., was employed as the linking agent for immobilizing glucose oxidase (GO) and catalase (CAT) on the pretreated support.

In this study, mining ore was utilized to make up the solid components in the column biooxidation process. The sample exhibited a low pyrite concentration at 1.5 wt.% and a gold grade of 0.5 g/t.

A sample of low-grade ore (LGOS). In conclusion, sodium cyanide was acquired (with a purity of 98%, received from Merck Inc. Germany) and employed for the dissolution of gold following the pretreatment process. Sodium hydroxide and sulfuric acid were employed to modify the pH levels in all the experiments. For all experiments, a buffer solution was prepared using acetic acid (purity 99.9%, Merck Inc.) and sodium acetate (99.9%, also from Merck Inc.) to achieve optimal GO and CAT enzyme activity. Standard samples were prepared from SigmaAldrich with purity of higher than 99.99% for measuring the gold content in solution after cyanidation.

7.2.1. Characterization

Fourier Transform Infrared Spectroscopy (FT-IR) test was used for confirmation of enzyme immobilization over the surface of support. ICP was used to find out how much gold and other metals were in the ore at first. Using a Microwave Plasma Atomic Emission Spectrometer (MP-AES) with a standard absorption curve made it possible to precisely find out the amount of iron and gold in the solution after cyanidation so that the total recovery could be calculated.

7.2.2. Enzyme immobilization

7.2.2.1. Incubation

Sawdust was utilized as a support material for the immobilization of both glucose oxidase (GO) and catalase (CAT), following the same procedure for both enzymes. Briefly, the sawdust was pretreated and functionalized using glutaraldehyde as a crosslinking agent at varying concentrations (0.001, 0.005, 0.01, 0.05, 0.1, 0.5, 1, and 5 wt.%). Subsequently, the enzymes were washed and stored, awaiting further experiments. The optimum glutaraldehyde concentration for immobilization was determined experimentally by assessing enzyme activity and stability.

7.2.3. Process design

The initial phase involved running the process without the CAT module, aerating only the GO module to facilitate oxidizing agent production essential for pyrite dissolution. During this phase, the substrate flow rate was set at 10 and 5 ml/h with a substrate concentration of 80 mg/. Two initial iron concentrations, 0.1 g/l and 1 g/l, were used to investigate their effect on the biooxidation process. To enhance substrate and oxidizing agent distribution, circulation flow rates were set on

50, 100, and 200 ml/h; and to optimize oxygen availability for enzymatic activity, aeration flow rates of 1 and 2 l/min were tested. To completely isolate the CAT module from the system throughout the experiment, valve-1 and valve-4 were closed, thus ensuring the observed biooxidation efficiency was solely attributable to conditions within the GO module. The setup presented in **Figure 7.1** allowed for a comprehensive assessment of the parameters influencing biooxidation efficiency under controlled aeration and flow conditions.

The GO module is cylindrical, with a diameter of 3 cm, a height of 10 cm, and a porosity of 35%, allowing for efficient flow and reaction within the module. The modular design facilitates rapid replacement and minimizes downtime, ensuring sustained biooxidation performance. The total ratio of dry immobilized enzyme volume per module to the total volume of ore sample in column was 60, indicating low amount of enzyme usage compared to the ore sample.

In the subsequent phase of the experiment, the combination of CAT and GO modules was investigated to optimize the process for maximum pyrite dissolution. Two parallel and series configurations——were considered to study their effects on biooxidation efficiency. In the parallel configuration, only valve-4 was kept closed, allowing the flow to split between the CAT and GO modules. Various flow rate ratios (CAT to GO) of 0.25, 0.5, and 0.75 were tested to determine the optimal distribution of flow between the two modules. For the series configuration, valve-1 and valve-5 were closed, directing the flow sequentially through the GO module followed by the CAT module. To simulate the temperature conditions of cold regions, the columns in the experimental setup were maintained at temperatures below 7°C, while the enzymatic modules (GO and CAT modules) were kept at room temperature to preserve their activity and functionality. This arrangement allowed for the investigation of biooxidation efficiency under a gradient of environmental conditions resembling natural cold-region settings. The pyrite dissolution in the circulation line was monitored using **Eq. 4.1**.

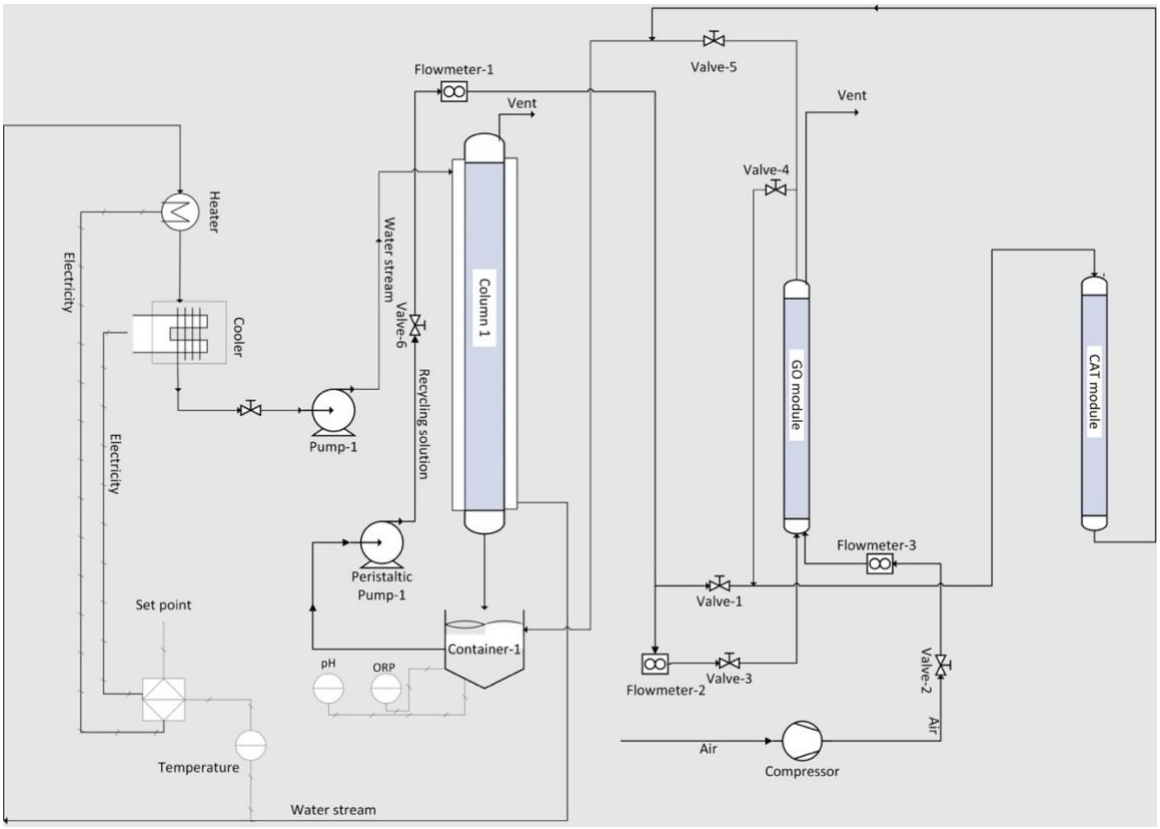

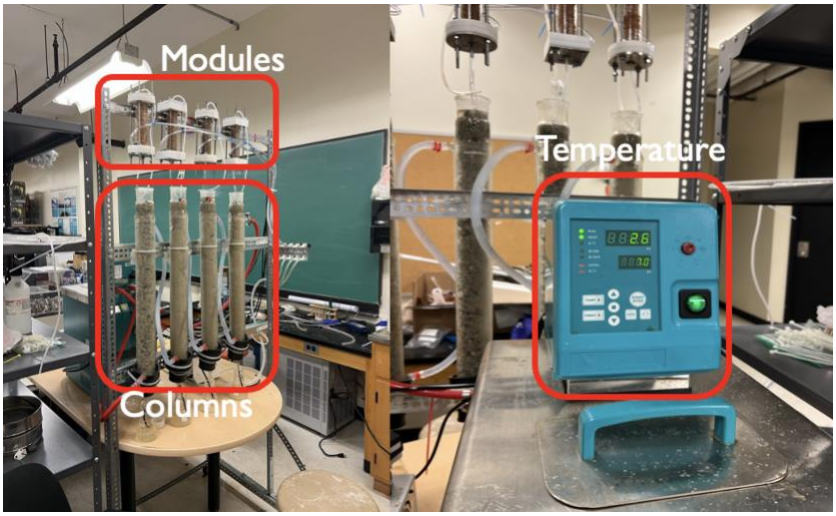

Figure 7.1. Process flow diagram and laboratory experimental set-up.

7.3. Results and discussion

7.3.1. Characterization

Low grade refractory ore sample was employed in this research chapter for enzymatic biooxidation. The sample of low-grade ore (LGOS) was characterized, revealing 1.5 wt.% pyrite and 0.5 g/ton of gold in pyrite inclusions from previous chapter **(Chapter 6 section 6.3.1)**.

7.3.2. Immobilization approach

The carboxylation of spruce sawdust was carried out using a combination of NaClO and H_2O_2 to introduce functional groups suitable for enzyme immobilization. Glutaraldehyde was then employed as a cross-linking agent to attach the enzymes to the modified support. Both Glucose Oxidase (GO) and Catalase (CAT) enzymes were immobilized on the carboxylated sawdust to study the effect of varying glutaraldehyde concentrations on the specific activity of each enzyme.

The FTIR spectra presented in **Figure 7.2** provide compelling evidence of the successful immobilization of glucose oxidase (GO) and catalase (CAT) onto the hydrolyzed spruce sawdust support. The spectral analysis reveals key functional groups associated with both the enzymes and the support, with distinct peaks confirming their structural integrity post-immobilization. Notably, characteristic peaks corresponding to amide I (~1665 cm^{-1}) and amide II (~1555 cm^{-1}) bands are present in both the immobilized glucose oxidase (Imm-GO) and immobilized catalase (Imm-CAT) spectra, indicating the presence of protein structures (Adochitei & Drochioiu, 2011). These peaks are also observed in the pure enzyme spectra, further reinforcing the successful attachment of the biomolecules onto the support material.

Additional confirmation of immobilization is provided by the presence of peaks at ~1261 cm^{-1}, attributed to C-N stretching of amide bonds, and the absorption band at ~2905 cm^{-1}, which corresponds to C-H stretching vibrations. However, there is a peak at ~2800 cm^{-1} indicating the presence of same hydrocarbon structure in the Imm-GO sample. These peaks, which appear in both the free enzyme and immobilized enzyme spectra, suggest that the fundamental chemical structure of the enzymes remains intact after immobilization (Chey et al., 2012; Kaushal et al., 2018). Furthermore, the hydrolyzed support (HYD) spectrum exhibits distinct peaks at ~1623 cm^{-1} and ~1665 cm^{-1}, which are retained in the immobilized enzyme samples, demonstrating that the

interaction between the enzyme and the support does not significantly alter the spectral features of the support material (Łojewska et al., 2005).

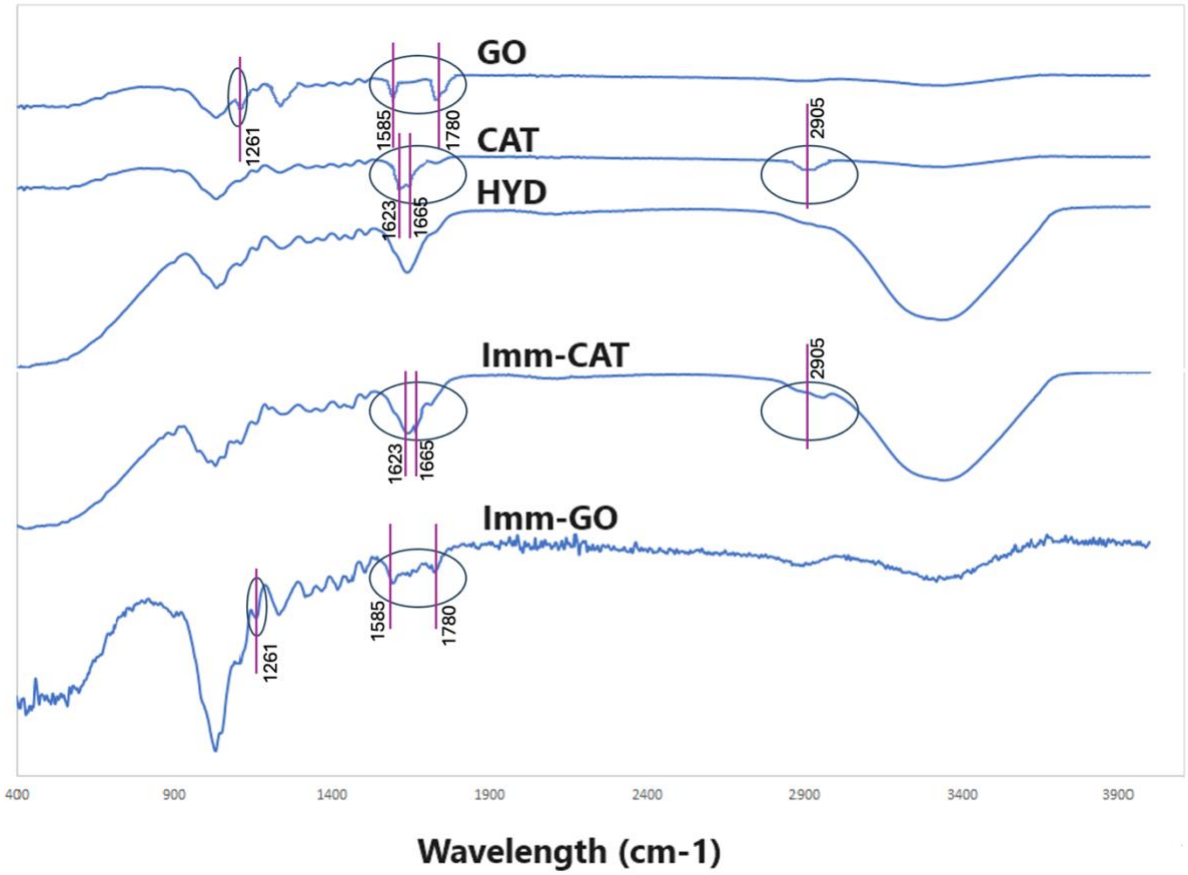

Figure 7.2. FTIR spectrum for Glucose oxidase (GO), Catalase (CAT), Hydrolyzed support (HYD), Immobilized glucose oxidase on support (Imm-GO), Immobilized catalase on support (Imm-CAT).

The specific enzyme activity analysis revealed distinct optimal glutaraldehyde concentrations for immobilizing Glucose Oxidase (GO) and Catalase (CAT) (**Figure 7.3**). For GO, the highest specific activity was observed at a glutaraldehyde concentration of 0.1 wt.%, while CAT demonstrated peak activity at a lower concentration of 0.05 wt.%. These results suggested that GO required a higher level of cross-linking to achieve stability without compromising flexibility, whereas CAT was more sensitive to excessive cross-linking, which can hinder active site accessibility or alter its conformational dynamics. Further increases in glutaraldehyde concentration beyond the optimal levels resulted in a decline in specific enzyme activity for both

GO and CAT. This reduction can be attributed to the oxidative nature of glutaraldehyde, which can cause enzyme denaturation or inactivation when present at high concentrations.

The immobilization of enzymes onto modified supports is a critical process in enhancing their stability and reusability for various applications. In the study by Olstad (2018), glucose oxidase (GO) was immobilized on platinum electrodes using glutaraldehyde as a cross-linking agent. The research demonstrated that the concentration of glutaraldehyde significantly influenced the enzyme's specific activity. Specifically, a 2.5% glutaraldehyde solution used for a 10-minute soaking period post-immobilization resulted in the highest final current density after multiple heat treatments, indicating optimal enzyme activity and stability under these conditions (Olstad, 2018).

Conversely, excessive cross-linking with glutaraldehyde can adversely affect enzyme activity. A study on the immobilization of β-galactosidase on chitosan beads found that higher concentrations of glutaraldehyde led to a decrease in enzyme activity. This reduction was attributed to the rigidification of the enzyme structure, which hindered substrate accessibility to the active sites. The findings underscore the importance of optimizing glutaraldehyde concentration to balance enzyme stability and activity (H. Chen et al., 2013).

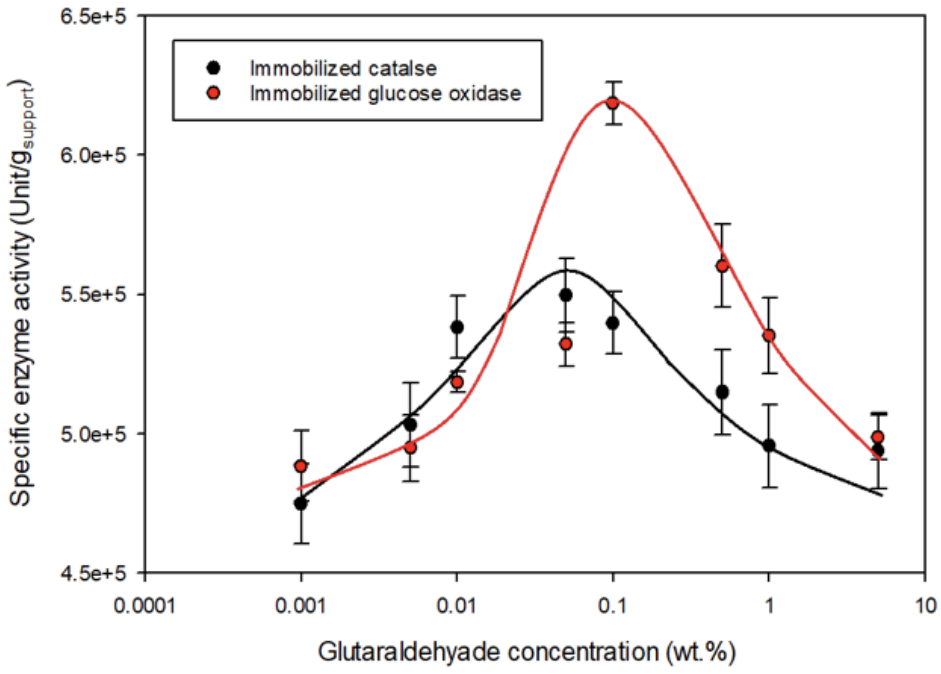

Figure 7.3. Effect of glutaraldehyde concentration on enzyme activity (80 mM D-β-glucose as substrate and 1.3 g of immobilized enzyme on support) for both GO and CAT enzyme modules.

7.3.2. Biooxidation

Figure 7.4 indicates a consistent reduction in pH across all tested conditions, which is attributed to the enzymatic activity of the Glucose Oxidase (GO) module. The GO enzyme catalyzes the oxidation of glucose, producing gluconic acid as a byproduct (Bankar et al., 2009a). The accumulation of gluconic acid in the circulation line lowers the pH, creating an acidic environment. The rate of pH reduction was more pronounced under higher substrate flow rates (e.g., 80 mg/L), highlighting the role of increased glucose availability in enhancing the enzymatic reaction.

Figure 7.4 also indicates an increase in oxidation-reduction potential (ORP) over time, reflecting the oxidative environment generated by the GO module. The rise in ORP is primarily due to the production of hydrogen peroxide. Hydrogen peroxide acts as a potent oxidizing agent, facilitating the breakdown of pyrite in the column tests (Antonijević et al., 1997; Chiriţă, 2009). The ORP profiles demonstrate that higher aeration flow rates (e.g., 2 l/min) and circulation flow rates (e.g., 100 ml/h) result in a steeper ORP increase, as these conditions improve oxygen availability and mass transfer.

Variations in operational parameters significantly (p-values<0.02) influence both pH and ORP trends. Higher substrate flow rates (e.g., 80 mg/l) accelerated the pH reduction and ORP increase, suggesting that elevated glucose levels enhance gluconic acid and hydrogen peroxide production. Additionally, circulation flow rates (e.g., 100 ml/h) promoted better mixing and mass transfer, further supporting these processes. The interplay between aeration, substrate concentration, and circulation flow rate is critical in optimizing the performance of the GO module.

Similar to microorganism-assisted biooxidation, where microbial growth leads to a progressive increase in oxidation-reduction potential (ORP) and a corresponding pH decline, enzymatic biooxidation with the GO module achieves similar effects through glucose oxidation. In microbial biooxidation, acidophilic bacteria such as *Acidithiobacillus ferrooxidans* and *Leptospirillum ferrooxidans* facilitate sulfide mineral dissolution by generating sulfuric acid as a metabolic byproduct, lowering the pH and promoting metal solubilization (Rawlings et al., 2003; Rohwerder et al., 2003). The elevated ORP observed in microbial systems results from ferric ion regeneration and sulfide oxidation, enhancing the oxidative breakdown of refractory gold ores (Sand et al., 2001).

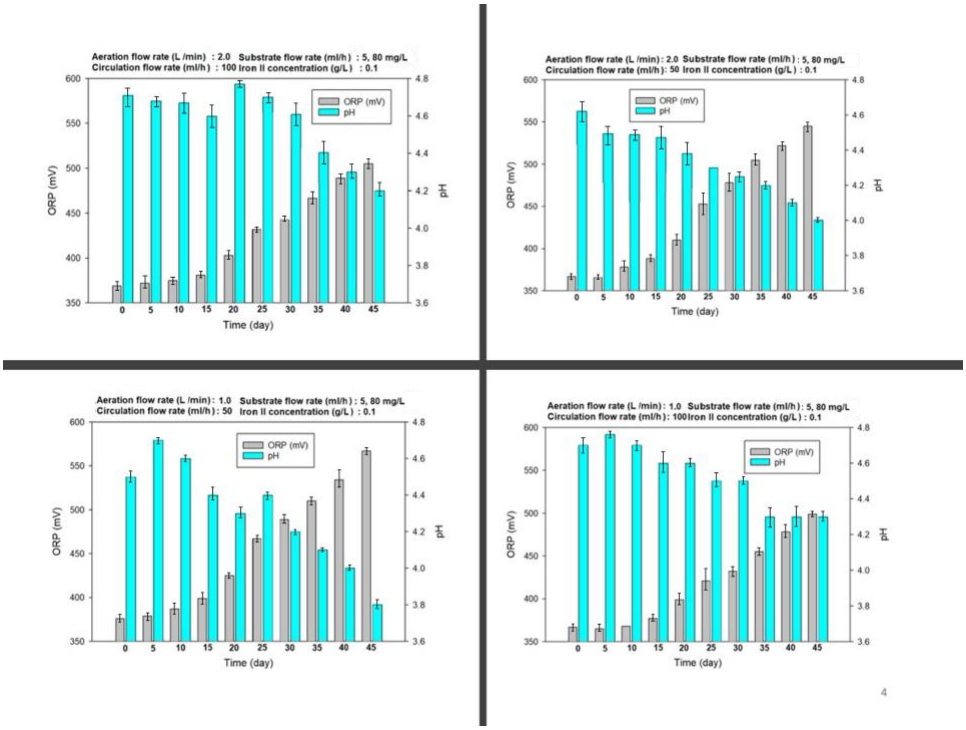

Figure 7.4. pH and ORP variations on circulation flow for different aeration flow rates, substrate flow rate, circulation flow rate, and total iron concentrations.

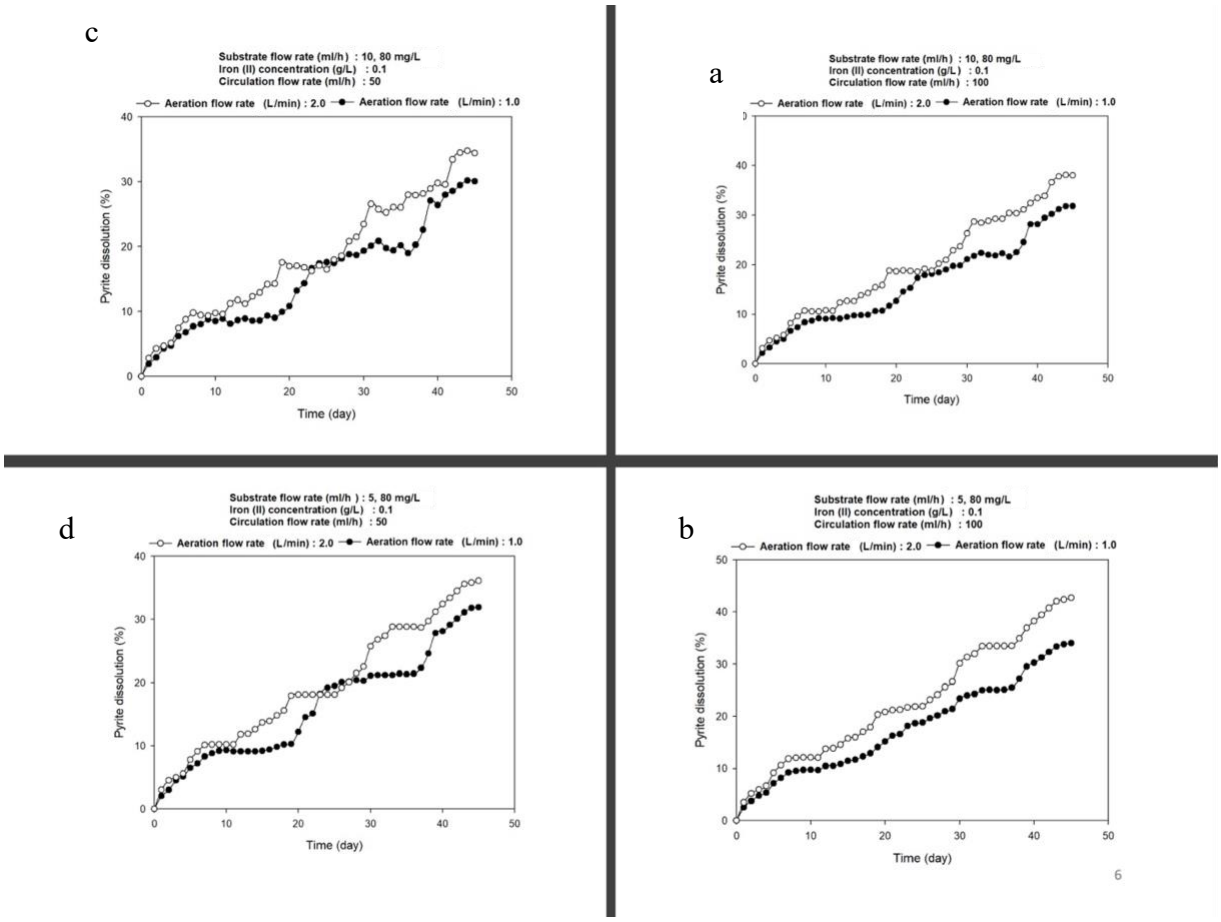

Figure 7.5. Pyrite dissolution vs time for different aeration flow rate, substrate flow rate, circulation flow rate, and total iron concentration.

Figure 7.5 a shows the pyrite dissolution over time for a substrate flow rate of 10 ml/h, an aeration flow rate of 1.0 L/min and 2.0 l/min, and a circulation flow rate of 100 ml/h. The results indicate that the dissolution rate steadily increases throughout the experiment for both aeration flow rates. The higher aeration flow rate of 2.0 l/min demonstrates consistently better performance compared to 1.0 l/min, as higher oxygen availability facilitates oxidation. At the end of the experiment, the maximum pyrite dissolution achieved is approximately 47% for 2.0 l/min and around 42% for 1.0 l/min.

This graph indicates two and three plateaus during the experiment for aeration flow rates of 2.0 l/min and 1.0 l/min. These plateaus represent periods where enzyme inactivation occurred, requiring the replacement of the enzyme module. The higher aeration flow rate of 2.0 l/min shows

slightly delayed plateau formation compared to 1.0 l/min, suggesting a slower rate of enzyme degradation due to less hydrogen peroxide production (Y. Zhang & Wilson, 1993).

Figure 7.5 b evaluates the performance at a lower substrate flow rate of 5 ml/h with the same aeration flow rates of 1.0 l/min and 2.0 l/min and a circulation flow rate of 100 ml/h. Here, the trends are similar, with the higher aeration flow rate (2.0 l/min) resulting in greater pyrite dissolution. However, the dissolution rates are slightly reduced compared to the higher substrate flow condition due to the limited availability of substrate for enzymatic oxidation. By the end of the experiment, maximum pyrite dissolution reaches approximately 36% for 2.0 l/min and 30% for 1.0 l/min. Three plateaus are observed over the course of the experiment for both aeration flow rates.

Figure 7.5 c represents the same substrate flow rate of 10 ml/h but with a lower circulation flow rate of 50 mL/h. As expected, the lower circulation flow rate results in slower pyrite dissolution due to reduced mass transfer efficiency. Nevertheless, the higher aeration flow rate (2.0 l/min) continues to outperform the lower aeration flow rate (1.0 l/min), with dissolution rates steadily increasing over time. The maximum pyrite dissolution achieved is approximately 40% for 2.0 l/min and 35% for 1.0 l/min at the end of the experiment. This graph shows two plateaus for both aeration flow rates.

Figure 7.5 d shows the pyrite dissolution for a substrate flow rate of 5 ml/h and a circulation flow rate of 50 mL/hr. Under these conditions, the dissolution rates are the lowest among all tested configurations, likely due to the combined effects of reduced substrate availability and lower circulation flow (Donaldson et al., 1987; S. Zhang et al., 2022). The aeration flow rate of 2.0 l/min still leads to slightly better performance than 1.0 l/min. At the end of the experiment, the maximum pyrite dissolution is approximately 28% for 2.0 l/min and 24% for 1.0 l/min.

In this figure also, four distinct plateaus are observed for both aeration flow rates, the highest among all configurations. The combination of a low substrate flow rate (5 ml/h) and a low circulation flow rate (50 ml/h) results in the most frequent enzyme inactivation, likely due to overproduction of hydrogen peroxide exacerbating oxidative stress. This condition leads to the highest enzyme turnover, requiring frequent module replacement.

Table 7.1 provides the ratio of active days to inactive days (indicative ratio A) during the biooxidation process under various operational conditions. This ratio serves as a measure of enzyme stability and effectiveness throughout the experiment.

The maximum A value is observed at 1.78 for the condition with a substrate flow rate of 10 ml/h, a circulation flow rate of 200 ml/h, and an aeration flow rate of 1.0 l/min. This high ratio indicates prolonged enzyme activity with minimal inactivation, likely due to optimal oxygen availability, effective substrate delivery, and sufficient mass transfer of hydrogen peroxide to the targeted ore (Mantle et al., 2001; Rase, 2013), all of which reduce oxidative stress on the enzyme. The combination of high circulation flow and substrate flow ensures steady reactant availability and removal of excess oxidizing agents, enhancing enzyme stability.

The minimum A value is observed at 1.21 for the condition with a substrate flow rate of 5 mL/h, a circulation flow rate of 100 ml/h, and an aeration flow rate of 1.0 l/min. This low ratio suggests frequent enzyme inactivation due to limited substrate availability, which could lead to inefficient enzymatic turnover and the accumulation of oxidizing byproducts. The insufficient substrate and suboptimal flow conditions likely exacerbate enzyme degradation, necessitating frequent module replacement.

Table 7.1. Indicative ratio A (Active days/inactive days) for GO module in column biooixdation.

		Aeration flow rate (l/min): 2.0	**Aeration flow rate (l/min): 1.0**
Substrate flow rate (ml/h): 5, 80 mg/L	Iron (II) concentration (g/l) : 0.1 Circulation flow rate (ml/h) : 50	EnBiTe: 1.29 Control: 0.07	EnBiTe: 1.53 Control: 0.00
	Iron (II) concentration (g/l) : 0.1 Circulation flow rate (ml/h) : 100	EnBiTe: 1.64 Control: 0.04	EnBiTe: 1.21 Control: 0.01
Substrate flow rate (ml/h): 10, 80 mg/L	Iron (II) concentration (g/l) : 1.0 Circulation flow rate (ml/h) : 50	EnBiTe: 1.44 Control: 0.00	EnBiTe: 1.51 Control: 0.02
	Iron (II) concentration (g/l) : 1.0 Circulation flow rate (ml/h) : 100	EnBiTe: 2.04 Control: 0.02	EnBiTe: 1.52 Control: 0.01
Substrate flow rate (ml/h): 10, 80 mg/L	Iron (II) concentration (g/l) : 1.0 Circulation flow rate (ml/h) : 200	EnBiTe: 1.61 Control: 0.01	EnBiTe: 1.69 Control: 0.00
	Iron (II) concentration (g/l) : 1.0 Circulation flow rate (ml/h) : 200	EnBiTe: 1.74 Control: 0.02	EnBiTe: 1.78 Control: 0.06

Table 7.2 provides the average pyrite dissolution per active day for the GO module under various operational conditions. This metric indicates the efficiency of pyrite dissolution during periods when the enzyme module is active.

The maximum average pyrite dissolution per active day is observed at 2.04 for the condition with a substrate flow rate of 10 ml/h, a circulation flow rate of 100 ml/h, and an aeration flow rate of 2.0 l/min. This high dissolution rate suggests that these conditions optimize oxygen supply, substrate availability, and hydrogen peroxide mass transfer, enhancing the enzymatic activity of the GO module and its ability to sustain high rates of pyrite oxidation during active periods.

The minimum average pyrite dissolution per active day is 1.21, which occurs under the condition of a substrate flow rate of 5 ml/h, a circulation flow rate of 100 ml/h, and an aeration flow rate of 2.0 l/min. The suboptimal flow rates may also limit mass transfer and the removal of inhibitory byproducts.

Higher substrate flow rates (10 ml/h) generally result in greater average pyrite dissolution, emphasizing the importance of sufficient glucose availability for effective enzyme activity. Furthermore, circulation flow rates of 100–200 ml/h improve dissolution efficiency compared to 50 ml/hr, as higher flow rates enhance mass transfer and oxygen delivery to the system. Interestingly, while aeration flow rates of 2.0 l/min generally provided good performance, certain conditions (e.g., lower substrate flow rates) see improved efficiency with 1.0 l/min, possibly due to excessive oxidative stress at higher oxygen levels.

Table 7.2. Average pyrite dissolution in only active days for GO module in biooxidation column.

		Aeration flow rate (l/min) : 2.0	Aeration flow rate (l/min) : 1.0
Substrate flow rate (ml/h) : 5, 80 mg/L	Iron (II) concentration (g/l) : 0.1 Circulation flow rate (ml/h) : 50	EnBiTe: 1.29 Control: 0.02	EnBiTe: 1.53 Control: 0.03
	Iron (II) concentration (g/l) : 0.1 Circulation flow rate (ml/h) : 100	EnBiTe: 1.64 Control: 0.04	EnBiTe: 1.21 Control: 0.01
Substrate flow rate (ml/h) : 10, 80 mg/L	Iron (II) concentration (g/l) : 1.0 Circulation flow rate (ml/h) : 50	EnBiTe: 1.44 Control: 0.04	EnBiTe: 1.51 Control: 0.03
	Iron (II) concentration (g/l) : 1.0 Circulation flow rate (ml/h) : 100	EnBiTe: 2.04 Control: 0.04	EnBiTe: 1.52 Control: 0.05
Substrate flow rate (ml/hr) : 10, 80 mg/Lit	Iron (II) concentration (g/l) : 1.0 Circulation flow rate (ml/h) : 200	EnBiTe: 1.61 Control: 0.06	EnBiTe: 1.69 Control: 0.03
	Iron (II) concentration (g/l) : 1.0 Circulation flow rate (ml/h) : 200	EnBiTe: 1.74 Control: 0.04	EnBiTe: 1.78 Control: 0.03

Figure 7.5 a and **b** shows the pyrite dissolution efficiency under parallel configurations of Glucose Oxidase (GO) and Catalase (CAT) modules, with two circulation flow rates: 50 ml/h (left graph) and 100 ml/h (right graph). The substrate flow rate was 10 ml/h with a sucrose concentration of 80 mg/l iron (II) concentration of 1.0 g/l, and aeration flow rate of 2.0 l/min, which was chosen based on optimal conditions identified for the GO-only system.

The **Figure 7.5 a** illustrates pyrite dissolution for the same conditions but with a higher circulation flow rate of 100 ml/h. This increased flow enhances mass transfer and mixing, leading to improved pyrite oxidation efficiency. The stream ratio of 0.25 demonstrates the lowest pyrite dissolution, which reaches a maximum of approximately 39.4% by the end of the experiment. The increased circulation flow provides better oxygen and substrate delivery, amplifying the efficiency of both GO and CAT modules. Stream ratios of 0.50 and 0.75 result in higher dissolution rates, reinforcing the importance of balanced flow distribution. For the ratio of 0.75 the maximum pyrite dissolution of 91% achieved in just 14 days which is comparable to the previous researches (Bailey & Hansford, 1993; BOUFFARD & DIXON, 2004b).

The series configuration, shown in the table at the bottom, results in lower maximum pyrite dissolution compared to the parallel setup. At a circulation flow rate of 50 ml/h, the series configuration achieves 32.4% dissolution, while the parallel configuration achieves the same value at stream ratio of 0.25. For 100 ml/h, the series configuration results in 39.4% dissolution, matching the parallel configuration's maximum dissolution rate at a stream ratio of 0.25. This

demonstrates that both configurations can achieve similar efficiencies under optimal flow conditions, but the parallel configuration provides more flexibility for balancing oxidizing and detoxifying agents.

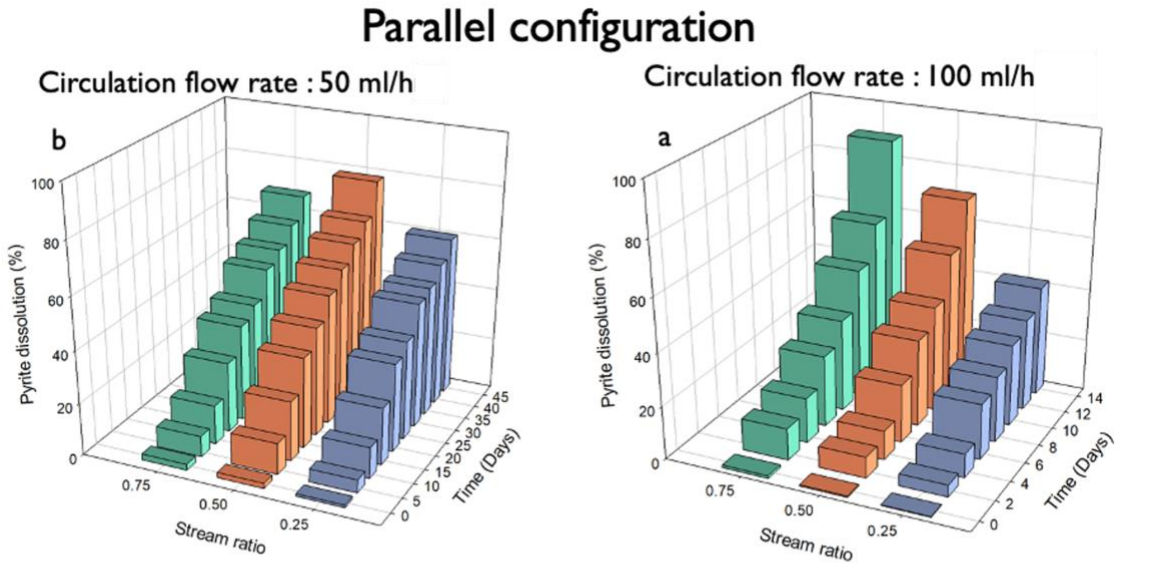

	Circulation flow rate: 50 ml/h	Circulation flow rate: 100 ml/h
	Maximum pyrite dissolution (%)	
Series configuration	32.4	39.4

Figure 7.5. Pyrite dissolution vs time for different circulation flow rates for parallel and series configuration of CAT and GO modules.

The observed differences in pyrite dissolution efficiency between parallel and series configurations of Glucose Oxidase (GO) and Catalase (CAT) modules can be attributed to the distinct ways these configurations manage the by-products of enzymatic reactions. In the parallel configuration, both enzymes operate simultaneously, allowing for immediate decomposition of hydrogen peroxide (H_2O_2) by CAT as it is produced by GO. This immediate action prevents the accumulation of H_2O_2, which is known to inactivate enzymes like GO if not promptly removed. In contrast, the series configuration may lead to a delay in H_2O_2 decomposition, resulting in higher local concentrations of H_2O_2 and subsequent enzyme inactivation. This difference likely contributes to the lower pyrite dissolution observed in the series setup (Prenosil, 1979).

The circulation flow rate plays a crucial role in enhancing mass transfer and mixing within the reactor system. A higher circulation flow rate of 100 ml/h improves the delivery of oxygen and substrates to the enzymes, thereby increasing the efficiency of the oxidative reactions involved in pyrite dissolution. Efficient mixing ensures that both GO and CAT have adequate access to their respective substrates, facilitating optimal enzymatic activity. This enhanced mass transfer likely accounts for the improved pyrite dissolution efficiency observed at the higher circulation flow rate (L. A. H. Petersen et al., 2017).

The stream ratio in the parallel configuration determines the distribution of flow between the GO and CAT modules. An optimal stream ratio ensures a balanced supply of substrates and efficient removal of by-products, maintaining enzyme activity and stability. Deviations from this optimal ratio can lead to imbalances, such as insufficient H_2O_2 decomposition or inadequate substrate availability, resulting in decreased pyrite dissolution rates. Therefore, fine-tuning the stream ratio is essential for maximizing the efficiency of the parallel enzyme system (Britton et al., 2018).

The X-ray diffraction (XRD) patterns in **Figure 7.6** illustrate a comparative analysis of ore samples before and after (parallel configuration with stream ratio of 0.75 and circulation flow rate of 100 ml/h) the biooxidation process. The untreated ore (before biooxidation) exhibits distinct peaks at 2θ values of 14.2°, 36.5°, 39.4°, 77.6°, and 87.2°, which are characteristic of the pyrite (FeS_2) crystal structure (Pourghahramani & Akhgar, 2015). These peaks indicate a significant presence of pyrite in the raw ore sample, confirming its mineralogical composition before undergoing biooxidation treatment.

In contrast, the XRD pattern of the treated ore (after biooxidation) reveals a notable disappearance of these characteristic pyrite peaks. This disappearance strongly suggests the effective decomposition and removal of pyrite as a result of the biooxidation process. Additionally, the overall reduction in peak intensity in the treated sample implies a significant alteration in the mineralogical composition of the ore, further supporting the efficiency of biooxidation in breaking down and leaching sulfide minerals.

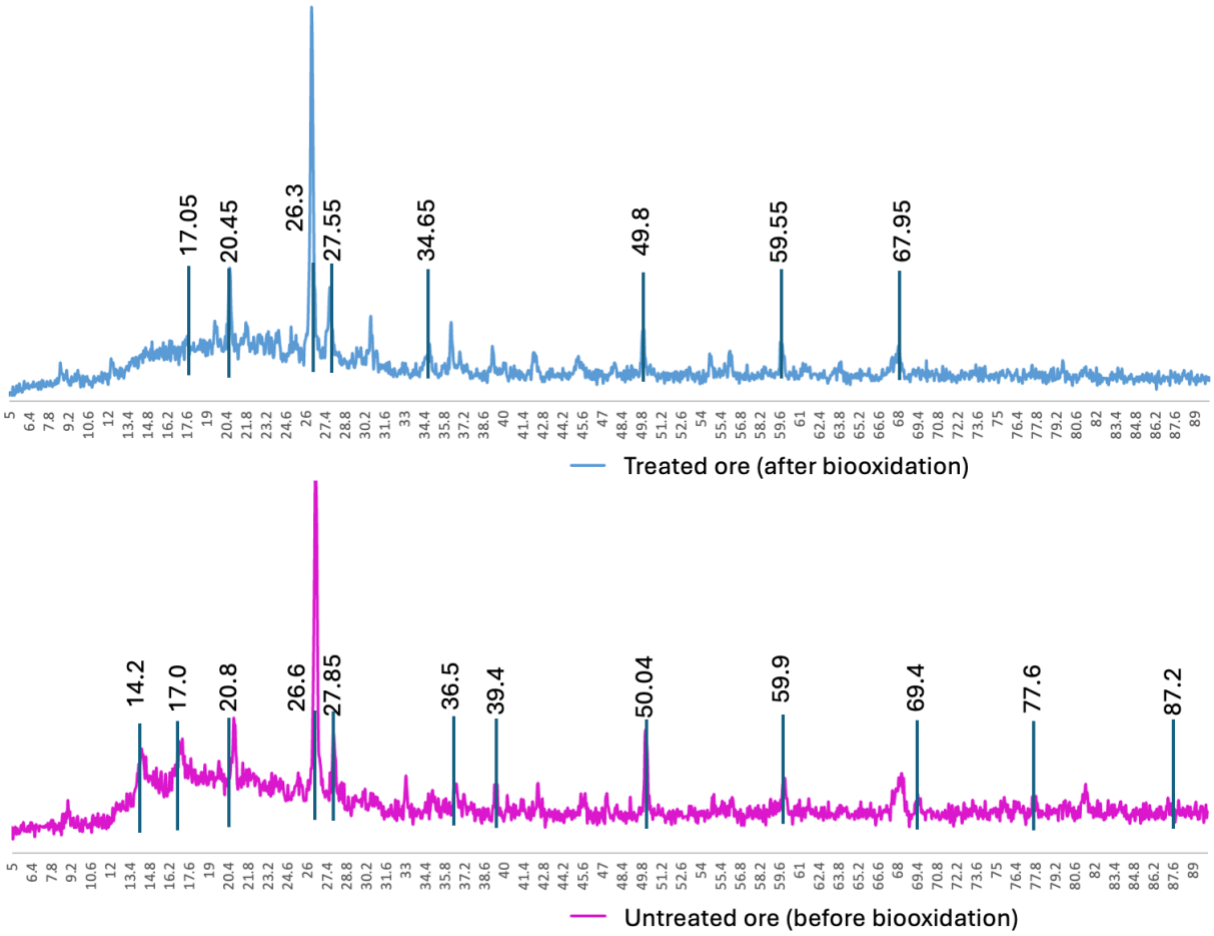

Figure 7.6. XRD test for both untreated (before biooxidation) and treated (after biooxidation sample)**.**

7.3. Gold recovery

The optimized time for cyanidation in gold recovery is detailed in the supplementary information, providing critical insights into process efficiency. According to the reported data, the maximum duration for effective cyanidation is approximately 25 hours, conducted under alkaline conditions with a pH range of 10-11.

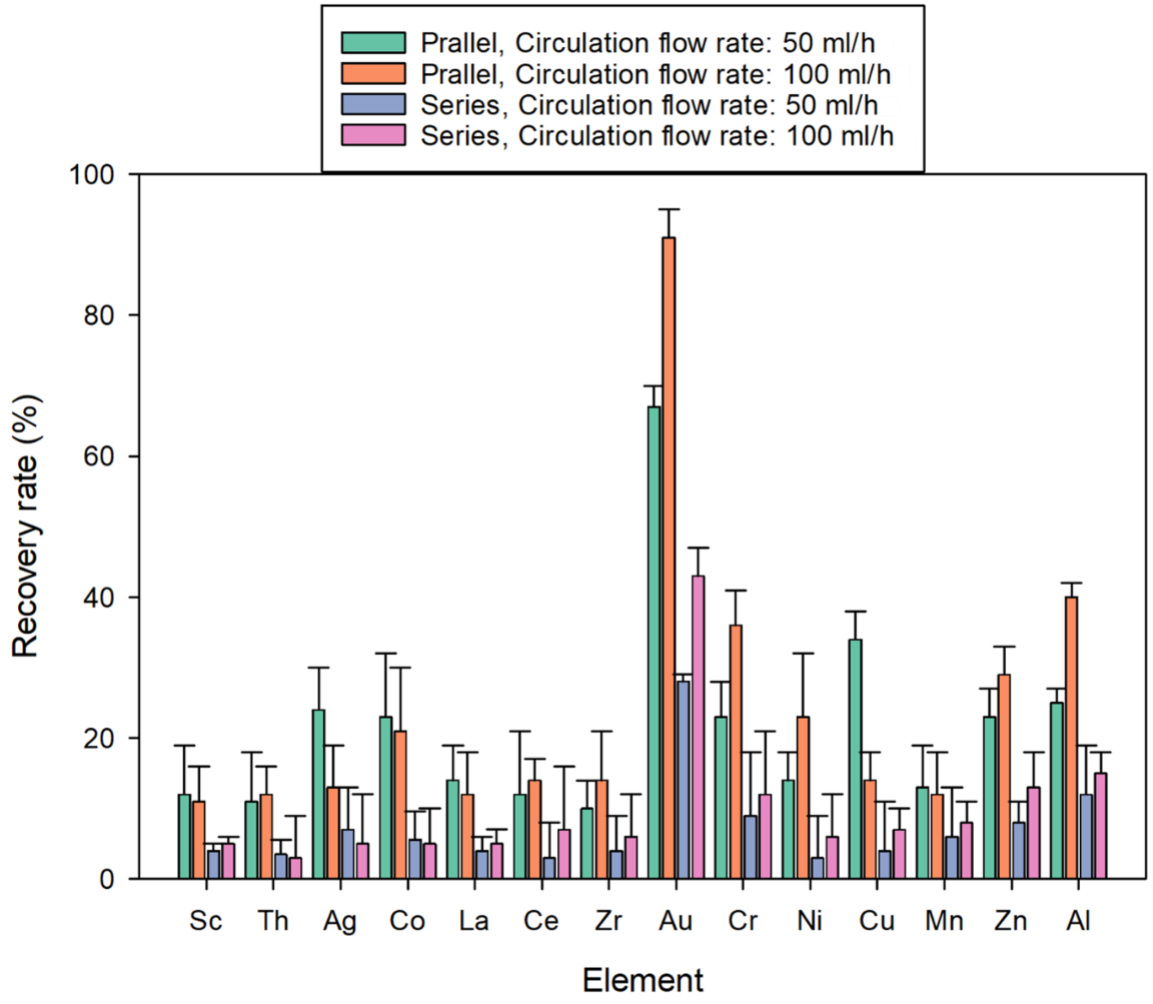

Figure 7.7. Plot of gold recovery using cyanidation for LGOS at various operational conditions.

The recovery rates of various elements after biooxidation followed by cyanidation were analyzed under different configurations (parallel and series) and circulation flow rates (50 ml/h and 100 ml/h) (**Figure 7.7**). The results indicate that the highest gold (Au) recovery, approximately 90%, was achieved under the parallel configuration with a circulation flow rate of 100 ml/h. However, the amount of gold recovery for untreated ore sample was less than 20%. The higher circulation flow ensures effective mixing and reduces localized enzyme inactivation or the accumulation of inhibitory byproducts, thereby maximizing Au recovery.

In comparison, the parallel configuration at 50 ml/h achieved a moderately high Au recovery of approximately 75%, while the series configuration at 100 ml/h resulted in a lower recovery rate of

around 65%. The series configuration with 50 ml/h circulation flow demonstrated the lowest Au recovery, approximately 50%, due to reduced mixing efficiency and suboptimal management of enzymatic activity. These findings highlight the superiority of the parallel configuration, particularly at higher circulation flow rates, in achieving efficient biooxidation and maximizing Au recovery through cyanidation.

The biooxidation of refractory gold ores has been a widely studied method for enhancing gold recovery, especially for ores with high sulfide and iron content. Conventional heap biooxidation processes typically employ bacterial oxidation to break down sulfide matrices, liberating gold particles for subsequent extraction through cyanidation or other leaching techniques. While these methods have been successful, they often require extended treatment times. For instance, as shown in the **Table 7.3**, treatment durations range from 62 days to 365 days, with varying gold recovery rates from 41% to 84%. Such long durations not only increase operational costs but also limit the scalability of these methods for large-scale applications.

When comparing conventional heap biooxidation methods to the enzymatic biooxidation technology presented in the last row of the table, it becomes evident that the enzyme-based approach offers significant advantages. The enzymatic biooxidation process, utilizing GO+CAT enzyme modules in column tests, achieved recovery rates of 64% and 91% within a remarkably short period of just 45 days. This high recovery rate in a fraction of the time required by traditional methods highlights the efficiency of enzyme-mediated biooxidation as a pretreatment strategy. In particular, the shorter pretreatment time is crucial for operations targeting rapid gold extraction and cost reduction.

The effectiveness of the enzymatic biooxidation approach stems from its ability to accelerate the breakdown of sulfide and organic matrices in the ore through the targeted action of enzymes. Unlike microbial processes that rely on slow bacterial growth and activity, enzymes act as direct catalysts, facilitating faster chemical reactions without requiring extensive acclimation periods. This efficiency is particularly important for low-grade ores, such as the LGOS sample tested in this study, where maximizing recovery within a limited timeframe is a priority. Furthermore, the circulation flow rate optimization (50 ml/h and 100 ml/h) in this method ensures uniform contact between the enzymes and the ore, enhancing the overall reaction kinetics.

The enzymatic biooxidation technology demonstrates a clear superiority over conventional heap biooxidation methods in terms of recovery rate and treatment time. Its ability to achieve up to 91% gold recovery within 45 days represents a significant advancement, particularly for industries seeking sustainable and cost-effective gold extraction solutions. This study establishes a foundation for further exploration and scaling of enzymatic technologies in the field of metallurgical processing, offering a promising alternative for the biooxidation of refractory gold ores.

Table 7.3. Comparison of gold recovery processes using heap ore column microorganisms-assisted biooxidation and EnBiTe.

Operation	Sources (ore)	Recovery (%)	Treatment time	References
Heap Biooxidation	Gold grade in ore: 2.64 g/t Sulfide content: 1.58%	Milling process with average gold recovery of 53.6%	164 days	(Logan et al., 2007)
Heap Biooxidation	Gold grade in ore: 0.84 g/t Sulfide content: - Iron content: 14%	Cyanidation process with average gold recovery of 41%	62 days	(Mihaylov & Hendrix, 1993)
Heap Biooxidation	Gold grade in ore: 3.2 g/t Sulfide content: 0.8 % Iron content: 1.4 %	Cyanidation process with average gold recovery of 50%	300 days	(Langhans et al., 1995)
Heap Biooxidation	Gold grade in ore: - g/t Sulfide content: 2.5 % Iron content: 8.7 %	Thiourea process with average gold recovery of 84%	365 days	(Groudev, Spasova, & Ivanov, 1995)
Heap Biooxidation	Gold grade in ore: 4.2 g/t Sulfide content: - Iron content: -	Cyanidation process with average gold recovery of 52%	180 days	(Holtum & Murray, 1994b)
Heap Biooxidation	Gold grade in ore: - Sulfide content: - Iron content: -	Cyanidation process with average gold recovery of 55-75%	90 days	(Burbank et al., 1990)
Enzymatic Biooixdation Technology (Enbite: GO+CAT enzyme modules)+clumns tests: 1-Circulation flow rate: 50 mL/h 1-Circulation flow rate: 100 mL/h	Low Grade Ore Sample (LGOS)	1- Au: 64% 2- Au: 91%	45 days	This Study

7.4. Conclusion

This research successfully demonstrated the efficacy of Enzymatic Biooxidation Technology (EnBiTe) as a modular approach for recovering gold from refractory sulfide ores. The study highlighted the potential of immobilized enzyme systems, specifically Glucose Oxidase (GO) and

Catalase (CAT) modules, in enhancing pyrite dissolution and subsequent gold recovery. Under optimized conditions, a substrate flow rate of 10 ml/h, a circulation flow rate of 100 ml/h, and an aeration flow rate of 2.0 l/min resulted in a maximum pyrite dissolution of 47%. The use of modular enzyme systems allowed for greater control over operational parameters, minimizing enzyme inactivation and improving the overall efficiency of the biooxidation process compared to conventional microorganism-assisted methods.

The investigation into different configurations of the GO and CAT modules revealed that the parallel configuration consistently outperformed the series configuration. At a circulation flow rate of 100 ml/h, the parallel configuration achieved a maximum pyrite dissolution of 39.4%, compared to 32.4% in the series configuration under the same flow conditions. Similarly, the highest gold recovery rate of 90% was obtained in the parallel configuration at a circulation flow rate of 100 ml/h, while the series configuration under the same conditions achieved only 65%. These results underscore the importance of optimizing flow distribution and module configuration to maximize the efficiency of the EnBiTe system.

Overall, this study demonstrates that EnBiTe offers a scalable and efficient alternative to traditional biooxidation approaches, particularly in challenging operational environments. The modular design facilitates the replacement of enzyme modules, maintaining continuous operation and minimizing downtime. With a pyrite dissolution efficiency of up to 47% and a gold recovery rate of 90% under optimized conditions, EnBiTe presents a promising solution for the extraction of gold from refractory ores, offering both operational and economic advantages. Future studies could further explore the long-term stability of immobilized enzymes and the potential for integration of EnBiTe into industrial-scale gold recovery processes.

Chapter 8: Summary and future recommendations

8.1. Summary

Biooxidation prospects via stirred tank reactors or piles remain problematic, despite successful deployments throughout the globe. A greater knowledge of biological activity, process engineering, and mathematical modelling is needed. Thus, breakthroughs and improvements in microbiology and genomics may be directed toward enhancing biooxidation processes while maintaining processing speeds and process scalability. Geographic, microbiological, and mineralogical characteristics all provide significant obstacles and concerns for the biooxidation of low-grade sulfide ore in a Nordic environment, which provides a higher level of complexity. To maximize value recovery and support the transition to Autonomous Mine, modelling, life cycle analysis, process simulations including implementation of machine learning and artificial intelligence in the field of biomining, and novel biooxidation technologies, must be considered.

The attachment of microorganisms to surfaces and the influencing parameters is crucial in biomining pretreatment. This research examined the influence of monosaccharides on the adaptability and adhesiveness of *Ferroplasma acidiphilum* in the oxidation of sulfide-bearing ore containing pyrite, which encapsulates 98% of gold within its crystal lattice. D-sucrose enhanced EPS synthesis, achieving the highest pyrite dissolving rate of 69% compared to other monosaccharides. The incorporation of 0.8 wt. % D-sucrose increased ferric ion production by 65% for a 20 wt.% ore load, whereas the inclusion of 0.4 wt.% resulted in a maximum ferric ion concentration of 95%. The findings showed that including both yeast extract and D-sucrose at a concentration of 0.4 wt.% increased the EPS (Extracellular Polymeric Substances) biovolume fraction from 7.5 to 32.5 v/v%.

The associated effects of monosaccharides, ore content, pyrite content, and duration on the activity and growth rate of *Ferroplasma acidiphilum* from native Acid Mine Drainage (AMD) were examined during biooxidation, while also identifying the optimal machine learning method for predicting process efficiency utilizing the independent variables. The findings indicated that the ideal conditions for achieving maximum pyrite dissolution (~75%) are 15 days of operational duration, a pyrite concentration of 7.2 wt.%, an ore concentration of 5 wt.%, a pH of 1.47, and concentrations of D-+-sucrose, D-+-galactose, and D-+-fructose at 0.52, 0.09, and 0.12 wt.%,

respectively. The model comparison results demonstrated that the Artificial Neural Network (ANN) model predicted the experimental outcomes of this study with satisfactory accuracy, surpassing both Genetic Programming (GP) and Polynomial Regression informed by Response Surface Methodology (PR-RSM) based on experimental data. The results indicated that variations in D-+-fructose and D-+-galactose concentrations do not considerably affect ferric ion concentration and pyrite dissolving content, however changes in D-+-sucrose concentration have a markedly significant impact.

Preliminary Microorganism-based Biooxidation Pretreatment techniques included stirred tank reactors and column tests with *Ferroplasma Acidiphilum*. The results indicated that the stirred tank reactor had superior recovery rates for essential elements, with gold recovery attaining 55% for HGOS in contrast to 40% for LGOS as determined by the column test. Optimal conditions for biooxidation were determined, comprising aeration flow rates of 1.0-1.5 l/min and agitation speeds of 300-450 rpm, which promoted efficient microbial activity and pyrite dissolution. In cyanidation, optimal gold recovery occurred at a pH of 10.5, achieving up to 60% recovery with 8 g/L NaCN. At pH levels exceeding 11, gold recovery diminished to around 40% because of competing chemical species and the precipitation of metal hydroxides.

This research also presented a novel low-temperature-adapted method, Enzymatic Biooxidation Technology (EnBiTe), for the extraction of gold from refractory sulphide ores. The application of glucose oxidase (GO) immobilized on modified sawdust improves pyrite dissolution and gold extraction for conventional biooxidation techniques. Experiments revealed that citric acid carboxylation enhanced enzyme activity, reaching a maximum of 80 μmol/min at a 1 wt.% glutaraldehyde concentration, whereas hydrogen peroxide production peaked at 20–24°C. Optimized biooxidation parameters—100 mM substrate, 5 g immobilized enzyme, 1 g/Liron (II), and 20% ore content—yielded 89.2% pyrite dissolution for the high-grade ore sample (HGOS) and 73.4% for the low-grade ore sample (LGOS). Following cyanidation, optimal gold recovery was attained within 20 hours at a pH of 10–11, with HGOS demonstrating enhanced gold recovery. These findings highlight EnBiTe's potential as an efficient and environmentally sustainable alternative to conventional pretreatment procedures, especially in colder climates.

The research found that immobilized enzyme systems, such as Glucose Oxidase (GO) and Catalase (CAT) modules, improved pyrite dissolving and gold recovery. Under optimal circumstances, 10 mL/h substrate flow, 100 ml/h circulation, and 2.0 l/min aeration resulted in 47% pyrite

breakdown. Compared to microorganism-assisted approaches, modular enzyme systems simplified operating parameters, reduced enzyme inactivation, and increased biooxidation efficiency.

The parallel setup outperformed the sequential configuration in GO and CAT module tests. A maximum pyrite dissolution of 39.4% was reached in the parallel setup at 100 ml/h, compared to 32.4% in the series arrangement. The parallel setup at 100 ml/h had the greatest gold recovery rate of 90%, whereas the series configuration had 65%. These findings emphasize the need of adjusting flow distribution and module setup for EnBiTe system efficiency.

This research shows that EnBiTe is scalable and efficient compared to existing biooxidation methods, even under adverse operating conditions. Modular enzyme module replacement reduces downtime and maintains functioning. EnBiTe offers operational and economic benefits for gold extraction from refractory ores with pyrite dissolving efficiency of up to 47% and gold recovery rate of 90% under optimal circumstances. Immobilized enzyme stability and EnBiTe incorporation into industrial-scale gold recovery systems might be studied in the future.

8.2. Recommendations

- **Scale-Up Pilot Trials for Industrial Validation**, semi-pilot and pilot-scale testing of the GO-CAT modular system needs to be conducted in real mining conditions (e.g., open-pit or underground mines) to validate the enzymatic performance under variable temperature and humidity profiles.

- **Life Cycle and Technoeconomic Analysis (LCA & TEA)**, a comprehensive TEA and LCA needs to be developed for enzymatic biooxidation versus microbial and traditional methods. This will assess not only capital and operational costs but also GHG emissions, sustainability, and regulatory feasibility in cold climates.

- **Improved Immobilization Techniques**, novel immobilization matrices (e.g., biochar, hydrogel composites, nanocellulose) must be explored that offer better porosity, mechanical stability, and long-term enzyme activity under fluctuating redox and pH environments and different linking agent with the minimum environmental adverse impacts.

- **Integration with Cyanide-Free Gold Recovery**, coupling EnBiTe with environmentally benign leaching agents (e.g., thiosulfate, glycine) could be investigated to establish a **fully green gold recovery circuit**, eliminating dependency on cyanide.

- **Dynamic Modeling of Enzyme Kinetics**, real-time GO/CAT enzyme kinetics modeling integrated with AI/machine learning tools in biooxidation (e.g., ANN or GP) could be implemented to predict enzyme degradation, optimize input parameters, and develop autonomous control systems for enzymatic reactors.

- **Microbial-Enzyme Hybrid Systems**, the feasibility of hybrid bioreactors that use microbial consortia during warmer periods and enzyme modules during colder seasons could be explored—allowing year-round gold recovery in temperate zones.

Bibliography

Abdollahi, A., Darvanjooghi, M. H. K., Karimipour, A., & Safaei, M. R. (2018). Experimental study to obtain the viscosity of CuO-loaded nanofluid: effects of nanoparticles' mass fraction, temperature and basefluid's types to develop a correlation. *Meccanica*, *53*(15), 3739–3757. https://doi.org/https://doi.org/10.1007/s11012-018-0916-1

Abdollahi, H., Maleki, S., Sayahi, H., Gharabaghi, M., Darvanjooghi, M. H. K., Magdouli, S., & Brar, S. K. (2021). Superadsorbent Fe3O4-coated carbon black nanocomposite for separation of light rare earth elements from aqueous solution: GMDH-based Neural Network and sensitivity analysis. *Journal of Hazardous Materials*, 125655. https://doi.org/https://doi.org/10.1016/j.jhazmat.2021.125655

Adochitei, A., & Drochioiu, G. (2011). Rapid characterization of peptide secondary structure by FT-IR spectroscopy. *Rev. Roum. Chim*, *56*(8), 783–791.

Aguirre, P., Guerrero, K., Sanchez-Rodriguez, A., Gentina, J. C., & Schippers, A. (2018). Making sticky cells: effect of galactose and ferrous iron on the attachment of Leptospirillum ferrooxidans to mineral surfaces. *Research in Microbiology*, *169*(10), 569–575.

Aguirre, P., Saavedra, A., Moncayo, E., Hedrich, S., Guerrero, K., & Gentina, J. C. (2021). Sticky Bacteria: Understanding the Behavior of a D-Galactose Adapted Consortium of Acidophilic Chemolithotroph Bacteria and Their Attachment on a Concentrate of Polymetallic Mineral. *Frontiers in Microbiology*, *12*, 767639.

Ahmadi, A., Ranjbar, M., & Schaffie, M. (2012). Catalytic effect of pyrite on the leaching of chalcopyrite concentrates in chemical, biological and electrobiochemical systems. *Minerals Engineering*, *34*, 11–18.

Aitimbetov, T., White, D. M., & Seth, I. (2005). Biological gold recovery from gold–cyanide solutions. *International Journal of Mineral Processing*, *76*(1–2), 33–42.

Akcil, A., & Gahan, C. S. (2015). Application of industrial waste in biohydrometallurgy: A review on its use as neutralising agent and potential source for metal recovery, microbiology for minerals, metals, materials and the environment. *Microbiology for Minerals, Metals, Materials and the Environment (Abhilash P., Pandey BD and Natarajan KA, Eds.). CRC Press, Taylor Francis, Boca Raton, USA*, 185–208.

Amar, M. N., Ouaer, H., & Ghriga, M. A. (2022). Robust smart schemes for modeling carbon dioxide uptake in metal− organic frameworks. *Fuel*, *311*, 122545.

Antonijević, M. M., Dimitrijević, M., & Janković, Z. (1997). Leaching of pyrite with hydrogen peroxide in sulphuric acid. *Hydrometallurgy*, *46*(1–2), 71–83.

Astudillo, C., & Acevedo, F. (2009). Effect of CO2 air enrichment in the biooxidation of a refractory gold concentrate by Sulfolobus metallicus adapted to high pulp densities. *Hydrometallurgy*, *97*(1–2), 94–97.

Aylmore, M. G., & Muir, D. M. (2001). Thiosulfate leaching of gold—A review. *Minerals Engineering*, *14*(2), 135–174.

Azizitorghabeh, A., Mahandra, H., Ramsay, J., & Ghahreman, A. (2022). A sustainable approach for gold recovery from refractory source using novel BIOX-TC system. *Journal of Industrial and Engineering Chemistry*, *115*, 209–218.

Azizitorghabeh, A., Wang, J., Ramsay, J. A., & Ghahreman, A. (2021). A review of thiocyanate gold leaching–Chemistry, thermodynamics, kinetics and processing. *Minerals Engineering*, *160*, 106689.

Bacelar-Nicolau, P., & Johnson, D. B. (1999). Leaching of pyrite by acidophilic heterotrophic iron-oxidizing bacteria in pure and mixed cultures. *Appl. Environ. Microbiol.*, *65*(2), 585–590.

Bailey, A. D., & Hansford, G. S. (1993). Factors affecting bio-oxidation of sulfide minerals at high concentrations of solids: A review. *Biotechnology and Bioengineering*, *42*(10), 1164–1174.

Baker, B. J., & Banfield, J. F. (2003). Microbial communities in acid mine drainage. *FEMS Microbiology Ecology*, *44*(2), 139–152.

Baker, W. E. (1973). The role of humic acids from Tasmanian podzolic soils in mineral degradation and metal mobilization. *Geochimica et Cosmochimica Acta*, *37*(2), 269–281.

Ballester, A., Blázquez, M. L., González, F., & Muñoz, J. A. (2007). Catalytic role of silver and other ions on the mechanism of chemical and biological leaching. In *Microbial Processing of Metal Sulfides* (pp. 77–101). Springer.

Bampole, D. L., & Mulaba-Bafubiandi, A.-F. (2020). Mesophilic bioleaching performance of copper, cobalt and nickel with emphasis on complex orebodies of the Democratic Republic of Congo: a review of dynamic interactions between solids loading, microbiota activity and growth. *Energy, Ecology and Environment*, 1–23.

Banerjee, I., Burrell, B., Reed, C., West, A. C., & Banta, S. (2017). Metals and minerals as a biotechnology feedstock: engineering biomining microbiology for bioenergy applications. *Current Opinion in Biotechnology*, *45*, 144–155.

Bankar, S. B., Bule, M. V, Singhal, R. S., & Ananthanarayan, L. (2009a). Glucose oxidase—an overview. *Biotechnology Advances*, *27*(4), 489–501.

Bankar, S. B., Bule, M. V, Singhal, R. S., & Ananthanarayan, L. (2009b). Glucose oxidase—an overview. *Biotechnology Advances*, *27*(4), 489–501.

Barreto, M., Gehrke, T., Harneit, K., Sand, W., Jedlicki, E., & Holmes, D. (2005). Unexpected insights into biofilm formation by Acidithiobacillus ferrooxidans revealed by genome analysis and experimental approaches. *Proceedings of the 16th International Biohydrometallurgy Symposium, Cape Town, South Africa*, 817–825.

Barreto, M., Jedlicki, E., & Holmes, D. S. (2005). Identification of a gene cluster for the formation of extracellular polysaccharide precursors in the chemolithoautotroph Acidithiobacillus ferrooxidans. *Applied and Environmental Microbiology*, *71*(6), 2902–2909.

Bartlett, R. W. (1996). Biooxidation heap pretreatment of sulfide refractory gold ore. *Mineral Processing and Extractive Metullargy Review*, *16*(2), 89–124.

Bartlett, R. W. (1998). *Solution mining: Leaching and fluid recovery of materials*. Psychology Press.

Bartlett, R. W., & Prisbrey, K. A. (1996). Convection and diffusion limited aeration during biooxidation of shallow ore heaps. *International Journal of Mineral Processing*, *47*(1–2), 75–91.

Bauer, J. A., Zámocká, M., Majtán, J., & Bauerová-Hlinková, V. (2022a). Glucose oxidase, an enzyme "Ferrari": Its structure, function, production and properties in the light of various industrial and biotechnological applications. *Biomolecules*, *12*(3), 472.

Bauer, J. A., Zámocká, M., Majtán, J., & Bauerová-Hlinková, V. (2022b). Glucose oxidase, an enzyme "Ferrari": Its structure, function, production and properties in the light of various industrial and biotechnological applications. *Biomolecules*, *12*(3), 472.

Beech, I. B., & Cheung, C. W. S. (1995). Interactions of exopolymers produced by sulphate-reducing bacteria with metal ions. *International Biodeterioration & Biodegradation*, *35*(1–3), 59–72.

Bellenberg, S., Leon-Morales, C.-F., Sand, W., & Vera, M. (2012). Visualization of capsular polysaccharide induction in Acidithiobacillus ferrooxidans. *Hydrometallurgy*, *129*, 82–89.

Bennett, C. R., McBride, D., Cross, M., & Gebhardt, J. E. (2012a). A comprehensive model for copper sulphide heap leaching: Part 1 basic formulation and validation through column test simulation. *Hydrometallurgy*, *127*, 150–161.

Bennett, C. R., McBride, D., Cross, M., & Gebhardt, J. E. (2012b). A comprehensive model for copper sulphide heap leaching: Part 1 basic formulation and validation through column test simulation. *Hydrometallurgy*, *127*, 150–161.

Bhakta, P., & Arthur, B. (2002a). Heap bio-oxidation and gold recovery at Newmont mining: first-year results. *Jom*, *54*(10), 31–34.

Bhakta, P., & Arthur, B. (2002b). Heap bio-oxidation and gold recovery at Newmont mining: first-year results. *Jom*, *54*(10), 31–34.

Bhaskar, P. V, & Bhosle, N. B. (2006). Bacterial extracellular polymeric substance (EPS): a carrier of heavy metals in the marine food-chain. *Environment International*, *32*(2), 191–198.

Bobadilla-Fazzini, R. A., & Poblete-Castro, I. (2021). Biofilm formation is crucial for efficient copper bioleaching from bornite under mesophilic conditions: unveiling the lifestyle and catalytic role of sulfur-oxidizing bacteria. *Frontiers in Microbiology*, *12*, 761997.

Bonnefoy, V., & Holmes, D. S. (2012). Genomic insights into microbial iron oxidation and iron uptake strategies in extremely acidic environments. *Environmental Microbiology*, *14*(7), 1597–1611.

Boon, M., & Heijnen, J. J. (1998a). Gas–liquid mass transfer phenomena in bio-oxidation experiments of sulphide minerals: a critical review of literature data. *Hydrometallurgy*, *48*(2), 187–204.

Boon, M., & Heijnen, J. J. (1998b). Gas–liquid mass transfer phenomena in bio-oxidation experiments of sulphide minerals: a critical review of literature data. *Hydrometallurgy*, *48*(2), 187–204.

Bouffard, S. C., & Dixon, D. G. (2002). On the rate-limiting steps of pyritic refractory gold ore heap leaching: results from small and large column tests. *Minerals Engineering*, *15*(11), 859–870.

Bouffard, S. C., & Dixon, D. G. (2003). Mathematical modeling of pyritic refractory gold ore heap biooxidation: model development and isothermal column simulations. *Hydrometallurgy 2003: 5 Th International Symposium Honoring Professor Ian M. Ritchie*, 275–288.

Bouffard, S. C., & Dixon, D. G.. (2004a). Heap biooxidation of refractory gold ores: current state of the art. *Mineral Processing and Extractive Metallurgy Review*, *25*(3), 159–192.

Bouffard, S. C., & Dixon, D. G. (2004b). Heap biooxidation of refractory gold ores: current state of the art. *Mineral Processing and Extractive Metallurgy Review*, *25*(3), 159–192.

Bouffard, S. C., Tshilombo, A., & West-Sells, P. G. (2009). Use of lignosulfonate for elemental sulfur biooxidation and copper leaching. *Minerals Engineering*, *22*(1), 100–103.

Brandl, H. (2001a). Microbial leaching of metals. *Biotechnology*, *10*, 191–224.

Brandl, H. (2001b). Microbial leaching of metals. *Biotechnology*, *10*, 191–224.

Brar, K. K., Magdouli, S., Etteieb, S., Zolfaghari, M., Fathollahzadeh, H., Calugaru, L., Komtchou, S.-P., Tanabene, R., & Brar, S. K. (2020). Integrated Bioleaching-Electrometallurgy for Copper Recovery-A Critical Review. *Journal of Cleaner Production*, 125257.

Brehm, U., Gorbushina, A., & Mottershead, D. (2005). The role of microorganisms and biofilms in the breakdown and dissolution of quartz and glass. In *Geobiology: Objectives, Concepts, Perspectives* (pp. 117–129). Elsevier.

Brierley, C. L. (2008). How will biomining be applied in future? *Transactions of Nonferrous Metals Society of China*, *18*(6), 1302–1310.

Brierley, C. L., & Brierley, J. A. (1973). A chemoautotrophic and thermophilic microorganism isolated from an acid hot spring. *Canadian Journal of Microbiology*, *19*(2), 183–188.

Brierley, C. L., & Brierley, J. A. (2013). Progress in bioleaching: part B: applications of microbial processes by the minerals industries. *Applied Microbiology and Biotechnology*, *97*(17), 7543–7552.

Brierley, J. (2000). Expanding role of microbiology in metallurgical processes. *Mining Engineering(Colorado)*, *52*(11), 49–53.

Brierley, J. A., & Kulpa Jr, C. F. (1993). *Biometallurgical treatment of precious metal ores having refractory carbon content*. Google Patents.

Britton, J., Majumdar, S., & Weiss, G. A. (2018). Continuous flow biocatalysis. *Chemical Society Reviews*, *47*(15), 5891–5918.

Bromfield, L. (2011). *Factors affecting the attachment of Metallosphaera hakonensis during the colonisation of low grade mineral sulphide heaps*.

Bulaev, A., Belyi, A., Panyushkina, A., Solopova, N., & Pivovarova, T. (2017). Microbial population of industrial biooxidation reactors. *Solid State Phenomena*, *262*, 48–52.

Bulaev, A. G. (2020a). Effect of organic carbon source on pyrite biooxidation by moderately thermophilic acidophilic microorganisms. *Microbiology*, *89*, 301–308.

Bulaev, A. G. (2020b). Effect of organic carbon source on pyrite biooxidation by moderately thermophilic acidophilic microorganisms. *Microbiology*, *89*, 301–308.

Bulaev, A., Nechaeva, A., Elkina, Y., & Melamud, V. (2021a). Effect of carbon sources on pyrite-arsenopyrite concentrate bio-oxidation and growth of microbial population in stirred tank reactors. *Microorganisms*, *9*(11), 2350.

Bulaev, A., Nechaeva, A., Elkina, Y., & Melamud, V. (2021b). Effect of carbon sources on pyrite-arsenopyrite concentrate bio-oxidation and growth of microbial population in stirred tank reactors. *Microorganisms*, *9*(11), 2350.

Burbank, A., Choi, N., & Prisbrey, K. (1990). Biooxidation of refractory gold ores in heaps. *Advances in Gold and Silver Processing*, 151–159.

Burford, E. P., Fomina, M., & Gadd, G. M. (2003). Fungal involvement in bioweathering and biotransformation of rocks and minerals. *Mineralogical Magazine*, *67*(6), 1127–1155.

Busch, A. W., MYRICK, N., McKinney, K. W., & Peterson, J. W. (1961). Bench-Scale Bio-Oxidation Studies, Batch vs. Continuous Systems. *International Journal of Air and Water Pollution*, *5*(2–4), 199–203.

Castro, C., Donati, E. R., & Vera, M. (2023a). Characterization of extracellular polymeric substances produced by an Acidianus species and their relevance to bioleaching. *Minerals*, *13*(3), 310.

Castro, C., Donati, E. R., & Vera, M. (2023b). Characterization of extracellular polymeric substances produced by an Acidianus species and their relevance to bioleaching. *Minerals*, *13*(3), 310.

Chaerun, S. K., Winarko, R., & Yushandiana, F. (2023). Biohydrometallurgy: paving the way for a greener future of mineral processing in Indonesia-A mini review. *Current Research on Bioscences and Biotechnology*, *5*(1), 299–307.

Chakraborty, S., & Mali, K. (2020). An overview of biomedical image analysis from the deep learning perspective. *Applications of Advanced Machine Intelligence in Computer Vision and Object Recognition: Emerging Research and Opportunities*, 197–218.

Chapman, J. T., Marchant, P. B., Lawrence, R. W., & Knopp, R. (1993). Bio-oxidation of a refractory gold bearing high arsenic sulphide concentrate: A pilot study. *FEMS Microbiology Reviews*, *11*(1–3), 243–252.

Chen, H., Zhang, Q., Dang, Y., & Shu, G. (2013). The effect of glutaraldehyde cross-linking on the enzyme activity of immobilized β-galactosidase on chitosan bead. *Adv. J. Food Sci. Technol*, *5*(7), 932–935.

Chen, J., Liu, Y., Diep, P., & Mahadevan, R. (2022). Genetic engineering of extremely acidophilic Acidithiobacillus species for biomining: Progress and perspectives. *Journal of Hazardous Materials*, *438*, 129456.

Chen, M., & Schlömann, M. (2022). Mineral Bioleaching in Brackish and Saline Environments. In *Biomining Technologies: Extracting and Recovering Metals from Ores and Wastes* (pp. 229–238). Springer.

Chen, S.-Y., & Cheng, Y.-K. (2019). Effects of sulfur dosage and inoculum size on pilot-scale thermophilic bioleaching of heavy metals from sewage sludge. *Chemosphere*, *234*, 346–355.

Chey, C. O., Ibupoto, Z. H., Khun, K., Nur, O., & Willander, M. (2012). Indirect determination of mercury ion by inhibition of a glucose biosensor based on ZnO nanorods. *Sensors*, *12*(11), 15063–15077.

Chiriţă, P. (2009). Hydrogen peroxide decomposition by pyrite in the presence of Fe (III)-ligands. *Chemical and Biochemical Engineering Quarterly*, *23*(3), 259–265.

Choi, Y., & Gharelar, A. G. (2020). *Method for pre-treatment of gold-bearing oxide ores*. Google Patents.

Chowdhury, F., & Ojumu, T. V. (2014). Investigation of ferrous-iron biooxidation kinetics by Leptospirillum ferriphilum in a novel packed-column bioreactor: Effects of temperature and jarosite accumulation. *Hydrometallurgy*, *141*, 36–42.

Christel, S., Herold, M., Bellenberg, S., Buetti-Dinh, A., El Hajjami, M., Pivkin, I. V, Sand, W., Wilmes, P., Poetsch, A., & Vera, M. (2018). Weak iron oxidation by Sulfobacillus thermosulfidooxidans maintains a favorable redox potential for chalcopyrite bioleaching. *Frontiers in Microbiology*, *9*, 3059.

Chung, T. H., Shahidi, M., Mezbahuddin, S., & Dhar, B. R. (2023). Ensemble machine learning approach for examining critical process parameters and scale-up opportunities of microbial electrochemical systems for hydrogen peroxide production. *Chemosphere*, *324*, 138313.

Clark, D. A., & Norris, P. R. (1996). Acidimicrobium ferrooxidans gen. nov., sp. nov.: mixed-culture ferrous iron oxidation with Sulfobacillus species. *Microbiology*, *142*(4), 785–790.

Clark, M. E., Batty, J. D., Van Buuren, C. B., Dew, D. W., & Eamon, M. A. (2006). Biotechnology in minerals processing: Technological breakthroughs creating value. *Hydrometallurgy*, *83*(1–4), 3–9.

Colmer, A. R., & Hinkle, M. E. (1947). The role of microorganisms in acid mine drainage: a preliminary report. *Science*, *106*(2751), 253–256.
Coram, N. J., & Rawlings, D. E. (2002). Molecular relationship between two groups of the genus Leptospirillum and the finding that Leptospirillum ferriphilum sp. nov. dominates South African commercial biooxidation tanks that operate at 40 C. *Appl. Environ. Microbiol.*, *68*(2), 838–845.
Counts, J. A. (2019). *Determinants for Hot Acid Microbial Lifestyles: Chemolithoautorophic Physiology of the Extremely Thermoacidophilic Archaeal Lineage Sulfolobales*.
Coupland, K., & Johnson, D. B. (2008). Evidence that the potential for dissimilatory ferric iron reduction is widespread among acidophilic heterotrophic bacteria. *FEMS Microbiology Letters*, *279*(1), 30–35.
Cruz, K., Guézennec, J., & Barkay, T. (2017). Binding of Hg by bacterial extracellular polysaccharide: a possible role in Hg tolerance. *Applied Microbiology and Biotechnology*, *101*, 5493–5503.
D'Amico, S., Collins, T., Marx, J., Feller, G., Gerday, C., & Gerday, C. (2006). Psychrophilic microorganisms: challenges for life. *EMBO Reports*, *7*(4), 385–389.
Darvanjooghi, M. H. K., Kaur, K., Magdouli, S., & Brar, S. K. (2023a). Extracellular polymeric substances overproduction strategy in Ferroplasma acidiphilum growth for biooxidation of low-grade gold bearing ore: Role of monosaccharides. *Bioresource Technology*, *369*, 128476.
Darvanjooghi, M. H. K., Kaur, K., Magdouli, S., & Brar, S. K. (2023b). Extracellular polymeric substances overproduction strategy in Ferroplasma acidiphilum growth for biooxidation of low-grade gold bearing ore: Role of monosaccharides. *Bioresource Technology*, *369*, 128476.
Darvanjooghi, M. H. K., Khan, U. T., Magdouli, S., & Brar, S. K. (2024). Biooxidation of refractory sulfide-bearing ore using feroplasma acidophilum: Efficiency assessment and machine learning based prediction. *Current Research in Biotechnology*, *7*, 100179.
Darvanjooghi, M. H. K., Magdouli, S., Brar, S. K., Abdollahi, H., & Zolfaghari, M. (2021). Bio-oxidation of Gold from Refractory Sulfide Ores: A Journey Ahead. *Geomicrobiology Journal*, 1–17.
Darvanjooghi, M. H. K., Magdouli, S., Brar, S. K., Abdollahi, H., & Zolfaghari, M. (2022). Bio-oxidation of gold from refractory sulfide ores: a journey ahead. *Geomicrobiology Journal*, *39*(3–5), 399–415.
Dave, S. R., & Tipre, D. R. (2019). Diversity of Iron and Sulphur Oxidizers in Sulphide Mine Leachates. In *Microbial Diversity in Ecosystem Sustainability and Biotechnological Applications* (pp. 293–317). Springer.
Deng, T. L., Liao, M. X., Wang, M. H., Chen, Y.-W., & Belzile, N. (2000). Investigations of accelerating parameters for the biooxidation of low-grade refractory gold ores. *Minerals Engineering*, *13*(14–15), 1543–1553.
Donaldson, T. L., Strandberg, G. W., Hewitt, J. D., Shields, G. S., & Worden, R. M. (1987). Biooxidation of coal gasification wastewaters using fluidized-bed bioreactors. *Environmental Progress*, *6*(4), 205–211.
du Plessis, C. A., Batty, J. D., & Dew, D. W. (2007). Commercial applications of thermophile bioleaching. In *Biomining* (pp. 57–80). Springer.
Duku, P. (2011a). *Biooxidation kinetics of Leptospirillum Ferriphilum attached to a defined solid substrate*.

Duku, P. (2011b). *Biooxidation kinetics of Leptospirillum Ferriphilum attached to a defined solid substrate*. University of Cape Town.

EFSA Panel on Food Contact Materials Flavourings and Processing Aids (CEF), E., Silano, V., Bolognesi, C., Castle, L., Chipman, K., Cravedi, J., Fowler, P., Franz, R., Grob, K., & Gürtler, R. (2018). Safety evaluation of the food enzyme glucose oxidase from a genetically modified Aspergillus oryzae (strain NZYM-KP). *EFSA Journal*, *16*(7), e05319.

Ehrlich, H. L. (2004). Beginnings of rational bioleaching and highlights in the development of biohydrometallurgy: A brief history. *European Journal of Mineral Processing & Environmental Protection*, *4*(2).

Elomaa, H., Sinisalo, P., Rintala, L., Aromaa, J., & Lundström, M. (2020). Process simulation and gate-to-gate life cycle assessment of hydrometallurgical refractory gold concentrate processing. *The International Journal of Life Cycle Assessment*, *25*(3), 456–477.

Epiforov, A. V, Seleznev, A. N., Emelyanov, Y. Y., Balikov, S. V, Shketova, L. Y., & Kopylova, N. V. (2017). Heap Biooxidation of Gold-Sulphide and Polymetallic Ores and Tailings. *Solid State Phenomena*, *262*, 122–125.

Ercolini, D., Russo, F., Nasi, A., Ferranti, P., & Villani, F. (2009). Mesophilic and psychrotrophic bacteria from meat and their spoilage potential in vitro and in beef. *Applied and Environmental Microbiology*, *75*(7), 1990–2001.

Erüst, C., Akcil, A., Gahan, C. S., Tuncuk, A., & Deveci, H. (2013). Biohydrometallurgy of secondary metal resources: a potential alternative approach for metal recovery. *Journal of Chemical Technology & Biotechnology*, *88*(12), 2115–2132.

Escobar, B., Buccicardi, S., Morales, G., & Wiertz, J. (2010). Biooxidation of ferrous iron and sulphide at low temperatures: Implications on acid mine drainage and bioleaching of sulphide minerals. *Hydrometallurgy*, *104*(3–4), 454–458.

Fazzini, R. A. B., & Valdecantos, P. P. (2016). *Bacterial strain, cutipay, isolated from the sulfobacillus thermosulfidooxidans species, bacterial inoculum comprising same, and method for the bioleaching of minerals where said bacterial inoculum is inoculated*. Google Patents.

Feng, D., & Van Deventer, J. S. J. (2001). Preg-robbing phenomena in the thiosulphate leaching of gold ores. *Minerals Engineering*, *14*(11), 1387–1402.

Fernando, W. A. M., De Silva, P. C. P., Guatame-Garcia, A., Vriens, B., & Fernando, C. A. N. (2024). Mineral Processing in Bioreactors: Fundamentals and Design Aspects. In *Biotechnological Innovations in the Mineral-Metal Industry* (pp. 207–228). Springer.

Ferrer, M., Golyshina, O. V, Beloqui, A., Golyshin, P. N., & Timmis, K. N. (2007). The cellular machinery of Ferroplasma acidiphilum is iron-protein-dominated. *Nature*, *445*(7123), 91–94.

Forney, L. J., Reddy, C. A., Tien, M., & Aust, S. D. (1982). The involvement of hydroxyl radical derived from hydrogen peroxide in lignin degradation by the white rot fungus Phanerochaete chrysosporium. *Journal of Biological Chemistry*, *257*(19), 11455–11462.

Fowler, T. A., Holmes, P. R., & Crundwell, F. K. (1999). Mechanism of Pyrite Dissolution in the Presence ofThiobacillus ferrooxidans. *Appl. Environ. Microbiol.*, *65*(7), 2987–2993.

Fowler, T. A., Holmes, P. R., & Crundwell, F. K. (2001). On the kinetics and mechanism of the dissolution of pyrite in the presence of Thiobacillus ferrooxidans. *Hydrometallurgy*, *59*(2–3), 257–270.

Free, M. L. (2024). Principles of Biohydrometallurgy. In *Treatise on Process Metallurgy* (pp. 507–514). Elsevier.

Ganjkhanlou, Y. (2012). Optimizing of iron bioleaching from a contaminated kaolin clay by the use of artificial neural network. *International Journal of Engineering*, *25*(2), 81–88.
García-Descalzo, L., García-López, E., & Cid, C. (2022). Comparative proteomic analysis of psychrophilic vs. mesophilic bacterial species reveals different strategies to achieve temperature adaptation. *Frontiers in Microbiology*, *13*, 841359.
Garcia-Ochoa, J., Khalfet, R., Poncin, S., & Wild, G. (1997). Hydrodynamics and mass transfer in a suspended solid bubble column with polydispersed high density particles. *Chemical Engineering Science*, *52*(21–22), 3827–3834.
Garrido-Cardenas, J. A., Esteban-García, B., Agüera, A., Sánchez-Pérez, J. A., & Manzano-Agugliaro, F. (2020). Wastewater treatment by advanced oxidation process and their worldwide research trends. *International Journal of Environmental Research and Public Health*, *17*(1), 170.
Gehrke, T., Telegdi, J., Thierry, D., & Sand, W. (1998). Importance of extracellular polymeric substances from Thiobacillus ferrooxidans for bioleaching. *Appl. Environ. Microbiol.*, *64*(7), 2743–2747.
Geyik, A. G., & Çeçen, F. (2015). Variations in extracellular polymeric substances (EPS) during adaptation of activated sludges to new feeding conditions. *International Biodeterioration & Biodegradation*, *105*, 137–145.
Ghadiri, M. (2020). *Investigating variables affecting heap (bio) leaching through determining access to sub-surface mineral grains by micro-scale X-ray tomography*.
Ghadiri, M., Harrison, S. T. L., & Fagan-Endres, M. A. (2019). Effect of surfactant on the growth and activity of microorganisms in a heap bioleaching system. *Minerals Engineering*, *138*, 43–51.
Ghorbani, Y., Becker, M., Mainza, A., Franzidis, J.-P., & Petersen, J. (2011). Large particle effects in chemical/biochemical heap leach processes–A review. *Minerals Engineering*, *24*(11), 1172–1184.
Ghosh, S., Bal, B., & Das, A. P. (2018). Enhancing manganese recovery from low-grade ores by using mixed culture of indigenously isolated bacterial strains. *Geomicrobiology Journal*, *35*(3), 242–246.
Ghosh, S., & Das, A. P. (2018). Metagenomic insights into the microbial diversity in manganese-contaminated mine tailings and their role in biogeochemical cycling of manganese. *Scientific Reports*, *8*(1), 1–12.
Golyshina, O. V, Pivovarova, T. A., Karavaiko, G. I., Kondratéva, T. F., Moore, E. R., Abraham, W.-R., Lünsdorf, H., Timmis, K. N., Yakimov, M. M., & Golyshin, P. N. (2000a). Ferroplasma acidiphilum gen. nov., sp. nov., an acidophilic, autotrophic, ferrous-iron-oxidizing, cell-wall-lacking, mesophilic member of the Ferroplasmaceae fam. nov., comprising a distinct lineage of the Archaea. *International Journal of Systematic and Evolutionary Microbiology*, *50*(3), 997–1006.
Golyshina, O. V, Pivovarova, T. A., Karavaiko, G. I., Kondratéva, T. F., Moore, E. R., Abraham, W.-R., Lünsdorf, H., Timmis, K. N., Yakimov, M. M., & Golyshin, P. N. (2000b). Ferroplasma acidiphilum gen. nov., sp. nov., an acidophilic, autotrophic, ferrous-iron-oxidizing, cell-wall-lacking, mesophilic member of the Ferroplasmaceae fam. nov., comprising a distinct lineage of the Archaea. *International Journal of Systematic and Evolutionary Microbiology*, *50*(3), 997–1006.

Golyshina, O. V, & Timmis, K. N. (2005). Ferroplasma and relatives, recently discovered cell wall-lacking archaea making a living in extremely acid, heavy metal-rich environments. *Environmental Microbiology*, *7*(9), 1277–1288.

Groudev, S. N., Spasova, I. I., Groudeva, V. I., & Ivanov, I. M. (1995). Pilot scale microbial heap leaching of gold from a refractory ore at the Zlata Mine, Bulgaria. *Biohydrometallurgical Processing*, *1*, 425–435.

Groudev, S. N., Spasova, I. I., & Ivanov, I. M. (1995). Microbial heap leaching of refractory sulfide gold-bearing ore. *International Scientific Conference Precious Metals, Kosice*.

Guo, Z., Ren, J., & Song, C. (2025). Enhanced Thermal and Storage Stability of Glucose Oxidase via Encapsulation in Chitosan-Coated Alginate and Carboxymethyl Cellulose Gel Particles. *Foods*, *14*(4), 664.

Hallberg, K. B., & Johnson, D. B. (2001). *Biodiversity of acidophilic prokaryotes*.

Hallberg, K. B., & Lindström, E. B. (1994). Characterization of Thiobacillus caldus sp. nov., a moderately thermophilic acidophile. *Microbiology*, *140*(12), 3451–3456.

Hamad, H., Alma, M., Ismael, H., & Göçeri, A. (2014). The effect of some sugars on the growth of Aspergillus niger. *KSÜ Doğa Bilimleri Dergisi*, *17*(4), 7–11.

Hansford, G. S., & Miller, D. M. (1993). Biooxidation of a gold-bearing pyrite-arsenopyrite concentrate. *FEMS Microbiology Reviews*, *11*(1–3), 175–181.

Haque, K. E. (1992). The role of oxygen in cyanide leaching of gold ore. *CIM Bulletin*, *85*(963), 31–38.

Hol, A., van der Weijden, R. D., Van Weert, G., Kondos, P., & Buisman, C. J. N. (2011). Processing of arsenopyritic gold concentrates by partial bio-oxidation followed by bioreduction. *Environmental Science & Technology*, *45*(15), 6316–6321.

Hold, C., Andrews, B. A., & Asenjo, J. A. (2009). A stoichiometric model of Acidithiobacillus ferrooxidans ATCC 23270 for metabolic flux analysis. *Biotechnology and Bioengineering*, *102*(5), 1448–1459.

Holmes, P. R., & Crundwell, F. K. (2000). The kinetics of the oxidation of pyrite by ferric ions and dissolved oxygen: an electrochemical study. *Geochimica et Cosmochimica Acta*, *64*(2), 263–274.

Holtum, D. A., & Murray, D. M. (1994a). Bacterial heap leaching of refractory gold/sulphide ores. *Minerals Engineering*, *7*(5–6), 619–631.

Holtum, D. A., & Murray, D. M. (1994b). Bacterial heap leaching of refractory gold/sulphide ores. *Minerals Engineering*, *7*(5–6), 619–631.

Ingraham, J. L., & Bailey, G. F. (1959). Comparative study of effect of temperature on metabolism of psychrophilic and mesophilic bacteria. *Journal of Bacteriology*, *77*(5), 609–613.

Jennings, S. R., Dollhopf, D. J., & Inskeep, W. P. (2000). Acid production from sulfide minerals using hydrogen peroxide weathering. *Applied Geochemistry*, *15*(2), 235–243.

Jerez Guevara, C. (2011). *Bioleaching and Biomining for the Industrial Recovery of Metals*.

Jia, T., Kapelan, Z., de Vries, R., Vriend, P., Peereboom, E. C., Okkerman, I., & Taormina, R. (2023). Deep learning for detecting macroplastic litter in water bodies: A review. *Water Research*, *231*, 119632.

Jia, Y., Ruan, R., Qu, J., Tan, Q., Sun, H., & Niu, X. (2024). Multi-Scale and Trans-Disciplinary Research and Technology Developments of Heap Bioleaching. *Minerals*, *14*(8), 808.

Jin, S., Wang, Y., & Zhao, X. (2022). Cold-adaptive mechanism of psychrophilic bacteria in food and its application. *Microbial Pathogenesis*, *169*, 105652.

Johnson, D. B. (1998a). Biodiversity and ecology of acidophilic microorganisms. *FEMS Microbiology Ecology*, *27*(4), 307–317.
Johnson, D. B. (1998b). Biodiversity and ecology of acidophilic microorganisms. *FEMS Microbiology Ecology*, *27*(4), 307–317.
Johnson, D. B. (1998c). Biodiversity and ecology of acidophilic microorganisms. *FEMS Microbiology Ecology*, *27*(4), 307–317.
Johnson, D. B. (2006). Biohydrometallurgy and the environment: intimate and important interplay. *Hydrometallurgy*, *83*(1–4), 153–166.
Johnson, D. B. (2007). Physiology and ecology of acidophilic microorganisms. In *Physiology and biochemistry of extremophiles* (pp. 257–270). American Society of Microbiology.
Johnson, D. B. (2008). Biodiversity and interactions of acidophiles: Key to understanding and optimizing microbial processing of ores and concentrates. *Transactions of Nonferrous Metals Society of China*, *18*(6), 1367–1373.
Johnson, D. B. (2013). Development and application of biotechnologies in the metal mining industry. *Environmental Science and Pollution Research*, *20*(11), 7768–7776.
Johnson, D. B. (2014). Biomining—biotechnologies for extracting and recovering metals from ores and waste materials. *Current Opinion in Biotechnology*, *30*, 24–31.
Johnson, D. B., & Bangor, U. K. (2009). Extremophiles: acidic environments. In *The Desk Encyclopedia of Microbiology* (pp. 463–482). Academic Press of Elsevier Oxford.
Johnson, D. B., Kanao, T., & Hedrich, S. (2012). Redox transformations of iron at extremely low pH: fundamental and applied aspects. *Frontiers in Microbiology*, *3*, 96.
Jung, H., Inaba, Y., & Banta, S. (2022). Genetic engineering of the acidophilic chemolithoautotroph Acidithiobacillus ferrooxidans. *Trends in Biotechnology*, *40*(6), 677–692.
Kaksonen, A. H., Mudunuru, B. M., & Hackl, R. (2014). The role of microorganisms in gold processing and recovery—A review. *Hydrometallurgy*, *142*, 70–83.
Kang, J.-K., Cho, K.-H., Kim, S.-B., & Choi, N.-C. (2020). Artificial Neural Network Modeling for Prediction of Dynamic Changes in Solution from Bioleaching by Indigenous Acidophilic Bacteria. *Applied Sciences*, *10*(21), 7569.
Karavaiko, G. I., Tat'yana, I. B., Tat'yana, P. T., Kondrat'eva, T. F., Tsaplina, I. A., Egorova, M. A., Krasil'nikova, E. N., & Zakharchuk, L. M. (2005). Reclassification of 'Sulfobacillus thermosulfidooxidans subsp. thermotolerans' strain K1 as Alicyclobacillus tolerans sp. nov. and Sulfobacillus disulfidooxidans Dufresne et al. 1996 as Alicyclobacillus disulfidooxidans comb. nov., and emended description. *International Journal of Systematic and Evolutionary Microbiology*, *55*(2), 941–947.
Karimi Darvanjooghi, M. H., Magdouli, S., & Brar, S. K. (2024a). Recent challenges in biological cyanidation and oxidation of sulfide-based refractory gold ore. *World Journal of Microbiology and Biotechnology*, *40*(2), 67.
Karimi Darvanjooghi, M. H., Magdouli, S., & Brar, S. K. (2024b). Recent challenges in biological cyanidation and oxidation of sulfide-based refractory gold ore. *World Journal of Microbiology and Biotechnology*, *40*(2), 67.
Karimi Darvanjooghi, M. H., Magdouli, S., & Brar, S. K. (2025a). Column and stirred tank reactor test on the biooxidation of refractory gold ore using Ferroplasma acidiphilum: a case study. *Article in Press*.

Karimi Darvanjooghi, M. H., Magdouli, S., & Brar, S. K. (2025b). Enzymatic Biooxidation Technology (EnBiTe) as a low-temperature adapted method for recovery of gold from refractory sulfide ores. *Article in Press*.

Karimi, P., Abdollahi, H., Amini, A., Noaparast, M., Shafaei, S. Z., & Habashi, F. (2010). Cyanidation of gold ores containing copper, silver, lead, arsenic and antimony. *International Journal of Mineral Processing*, *95*(1–4), 68–77.

Karimipour, A., Ghasemi, S., Darvanjooghi, M. H. K., & Abdollahi, A. (2018). A new correlation for estimating the thermal conductivity and dynamic viscosity of CuO/liquid paraffin nanofluid using neural network method. *International Communications in Heat and Mass Transfer*, *92*, 90–99.

Karthikeyan, O. P., Rajasekar, A., & Balasubramanian, R. (2015). Bio-oxidation and biocyanidation of refractory mineral ores for gold extraction: a review. *Critical Reviews in Environmental Science and Technology*, *45*(15), 1611–1643.

Kaushal, J., Singh, G., & Arya, S. K. (2018). Immobilization of catalase onto chitosan and chitosan–bentonite complex: a comparative study. *Biotechnology Reports*, *18*, e00258.

Kelly, D. P., & Wood, A. P. (2000). Reclassification of some species of Thiobacillus to the newly designated genera Acidithiobacillus gen. nov., Halothiobacillus gen. nov. and Thermithiobacillus gen. nov. *International Journal of Systematic and Evolutionary Microbiology*, *50*(2), 511–516.

Khatami, S. H., Vakili, O., Ahmadi, N., Soltani Fard, E., Mousavi, P., Khalvati, B., Maleksabet, A., Savardashtaki, A., Taheri-Anganeh, M., & Movahedpour, A. (2022a). Glucose oxidase: Applications, sources, and recombinant production. *Biotechnology and Applied Biochemistry*, *69*(3), 939–950.

Khatami, S. H., Vakili, O., Ahmadi, N., Soltani Fard, E., Mousavi, P., Khalvati, B., Maleksabet, A., Savardashtaki, A., Taheri-Anganeh, M., & Movahedpour, A. (2022b). Glucose oxidase: Applications, sources, and recombinant production. *Biotechnology and Applied Biochemistry*, *69*(3), 939–950.

Kimura, S., Bryan, C. G., Hallberg, K. B., & Johnson, D. B. (2011). Biodiversity and geochemistry of an extremely acidic, low-temperature subterranean environment sustained by chemolithotrophy. *Environmental Microbiology*, *13*(8), 2092–2104.

Kleber, M., Bourg, I. C., Coward, E. K., Hansel, C. M., Myneni, S. C. B., & Nunan, N. (2021). Dynamic interactions at the mineral–organic matter interface. *Nature Reviews Earth & Environment*, *2*(6), 402–421.

Konadu, K. T., Mendoza, D. M., Huddy, R. J., Harrison, S. T. L., Kaneta, T., & Sasaki, K. (2020). Biological pretreatment of carbonaceous matter in double refractory gold ores: A review and some future considerations. *Hydrometallurgy*, *196*, 105434.

Kondrat'eva, T. F., Pivovarova, T. A., Tsaplina, I. A., Fomchenko, N. V, Zhuravleva, A. E., Murav'ev, M. I., Melamud, V. S., & Bulayev, A. G. (2012). Diversity of the communities of acidophilic chemolithotrophic microorganisms in natural and technogenic ecosystems. *Microbiology*, *81*(1), 1–24.

Konishi, Y., Kogasaki, K., & Asai, S. (1997). Bioleaching of pyrite by Acidianus brierleyi in a continuous-flow stirred-tank reactor. *Chemical Engineering Science*, *52*(24), 4525–4532.

Konishi, Y., Yoshida, S., & Asai, S. (1995). Bioleaching of pyrite by acidophilic thermophile Acidianus brierleyi. *Biotechnology and Bioengineering*, *48*(6), 592–600.

Kovalenko, E. V, & Malakhova, P. T. (1983). THE SPORE-FORMING IRON-OXIDIZING BACTERIUM SULFOBACILLUS-THERMOSULFIDOOXIDANS. *Microbiology*, *52*(6), 760–763.

Krebs, W., Brombacher, C., Bosshard, P. P., Bachofen, R., & Brandl, H. (1997). Microbial recovery of metals from solids. *FEMS Microbiology Reviews*, *20*(3–4), 605–617.

Kremser, K., Thallner, S., Schoen, H., Weiss, S., Hemmelmair, C., Schnitzhofer, W., Aldrian, A., & Guebitz, G. M. (2020a). Stirred-tank and heap-bioleaching of shredder-light-fractions (SLF) by acidophilic bacteria. *Hydrometallurgy*, *193*, 105315.

Kremser, K., Thallner, S., Schoen, H., Weiss, S., Hemmelmair, C., Schnitzhofer, W., Aldrian, A., & Guebitz, G. M. (2020b). Stirred-tank and heap-bioleaching of shredder-light-fractions (SLF) by acidophilic bacteria. *Hydrometallurgy*, *193*, 105315.

Kubara, M., & Kopczewska, K. (2024). Akaike information criterion in choosing the optimal k-nearest neighbours of the spatial weight matrix. *Spatial Economic Analysis*, *19*(1), 73–91.

Kumar, P. S., & Yaashikaa, P. R. (2020). Recent trends and challenges in bioleaching technologies. In *Biovalorisation of Wastes to Renewable Chemicals and Biofuels* (pp. 373–388). Elsevier.

Langhans, D., Lord, A., Lampshire, D., Burbank, A., & Baglin, E. (1995). Biooxidation of an arsenic-bearing refractory gold ore. *Minerals Engineering*, *8*(1–2), 147–158.

Larsson, L., Olsson, G., Holst, O., & Karlsson, H. T. (1990). Pyrite oxidation by thermophilic archaebacteria. *Appl. Environ. Microbiol.*, *56*(3), 697–701.

LeCun, Y., Bengio, Y., & Hinton, G. (2015). Deep learning. *Nature*, *521*(7553), 436–444.

Li, H., Li, S., Ma, P., Zhou, Z., Long, H., Peng, J., & Zhang, L. (2020). Evaluation of a cleaner production for cyanide tailings by chlorination thermal treatments. *Journal of Cleaner Production*, 124195.

Li, J., Tong, L., Xia, Y., Yang, H., Sand, W., Xie, H., Lan, B., Zhong, S., & Auwalu, A. (2020). Microbial synergy and stoichiometry in heap biooxidation of low-grade porphyry arsenic-bearing gold ore. *Extremophiles*, 1–10.

Li, J., Tong, L., Zhang, H., Chen, Q., Yang, H., Shen, L., Zhai, Y., & Yao, R. (2024). Pool bio-oxidation and fitting analysis of low-grade arsenic-containing refractory gold ore. *Green Chemical Engineering*.

Li, J., Zhong, S., Tong, L., Zhang, D., Bao, D., & Yang, H. (2020). Modeling heap biooxidation of arsenic-bearing gold ore. *Journal of Central South University*, *27*(5), 1424–1431.

Li, Z., Xin, X., Xiong, B., Zhao, D., Zhang, X., & Bi, C. (2020). Engineering the Calvin–Benson–Bassham cycle and hydrogen utilization pathway of Ralstonia eutropha for improved autotrophic growth and polyhydroxybutyrate production. *Microbial Cell Factories*, *19*, 1–9.

Limoli, D. H., Jones, C. J., & Wozniak, D. J. (2015). Bacterial extracellular polysaccharides in biofilm formation and function. *Microbial Biofilms*, 223–247.

Liu, F. W., Qiao, X. X., Xing, K., Shi, J., Zhou, L. X., Dong, Y., Bi, W. L., & Zhang, J. (2020). Effect of Nitrate Ions on Acidithiobacillus ferrooxidans-Mediated Bio-oxidation of Ferrous Ions and Pyrite. *Current Microbiology*, 1–11.

Logan, T. C., Seal, T., & Brierley, J. A. (2007). Whole-ore heap biooxidation of sulfidic gold-bearing ores. In *Biomining* (pp. 113–138). Springer.

Łojewska, J., Miśkowiec, P., Łojewski, T., & Proniewicz, L. M. (2005). Cellulose oxidative and hydrolytic degradation: In situ FTIR approach. *Polymer Degradation and Stability*, *88*(3), 512–520.

Magdouli, S., Brar, S. K., & Blais, J. F. (2018). Morphology and rheological behaviour of Yarrowia lipolytica: impact of dissolved oxygen level on cell growth and lipid composition. *Process Biochemistry*, *65*, 1–10.

Mahmood, Q., Zheng, P., Wu, D.-L., Wang, X.-S., Yousaf, H., Ulislam, E., Hassan, M. J., Jilani, G., & Azim, M. R. (2007). Prediction of Anoxic Sulfide Biooxidation Under Various HRTs Using Artificial Neural Network. *Biomedical and Environmental Sciences*, *20*(5), 398.

Mahmoud, A., Cézac, P., Hoadley, A. F. A., Contamine, F., & d'Hugues, P. (2017). A review of sulfide minerals microbially assisted leaching in stirred tank reactors. *International Biodeterioration & Biodegradation*, *119*, 118–146.

Makaula, D. X., Huddy, R. J., Fagan-Endres, M. A., & Harrison, S. T. L. (2020). Cross-correlating analyses of mineral-associated microorganisms in an unsaturated packed bed flow-through column test; cell number, activity and EPS. *Research in Microbiology*, *171*(7), 222–229.

Mäkinen, J., Bachér, J., Kaartinen, T., Wahlström, M., & Salminen, J. (2015). The effect of flotation and parameters for bioleaching of printed circuit boards. *Minerals Engineering*, *75*, 26–31.

Mandal, S., Mahapatra, S. S., Adhikari, S., & Patel, R. K. (2015). Modeling of arsenic (III) removal by evolutionary genetic programming and least square support vector machine models. *Environmental Processes*, *2*, 145–172.

Mantle, M. D., Sederman, A. J., & Gladden, L. F. (2001). Single-and two-phase flow in fixed-bed reactors: MRI flow visualisation and lattice-Boltzmann simulations. *Chemical Engineering Science*, *56*(2), 523–529.

Martell-Nevárez, M. A., Medina-Torres, L., Ríos-Fránquez, F. J., Alba-Fierro, C. A., González-Lozano, M. A., Escobedo-Bretado, M. Á., Rojas Montes, J. C., Bernad-Bernad, M. J., Núñez-Ramírez, D. M., & Manero, O. (2025). Bio-Oxidation Process of a Polymetallic Sulfide Mineral Concentrate for Silver Recovery. *Minerals*, *15*(3), 261.

Martinez, P., Vera, M., & Bobadilla-Fazzini, R. A. (2015). Omics on bioleaching: current and future impacts. *Applied Microbiology and Biotechnology*, *99*(20), 8337–8350.

Mayel, M., Abah, M. A., & Ayo, G. F. (2025a). Production of glucose oxidase from Aspergillus Niger using yam peels as carbon source. *Int J Mol Biol Open Access*, *8*(1), 1–6.

Mayel, M., Abah, M. A., & Ayo, G. F. (2025b). Production of glucose oxidase from Aspergillus Niger using yam peels as carbon source. *Int J Mol Biol Open Access*, *8*(1), 1–6.

Mazuelos, A., Carranza, F., Palencia, I., & Romero, R. (2000). High efficiency reactor for the biooxidation of ferrous iron. *Hydrometallurgy*, *58*(3), 269–275.

Mazuelos, A., Moreno, J. M., Carranza, F., Palomino, C., Torres, A., & Villalobo, E. (2012). Biotic factor does not limit operational pH in packed-bed bioreactor for ferrous iron biooxidation. *Journal of Industrial Microbiology & Biotechnology*, *39*(12), 1851–1858.

McNeice, J., Marzoughi, O., Kim, R., & Ghahreman, A. (2021). Gold extraction from refractory sulfide gold concentrates: a comparison of bio-oxidation and neutral atmospheric pre-treatment and economic implications. *Journal of Sustainable Metallurgy*, *7*(3), 1354–1367.

Mihaylov, B. V, & Hendrix, J. L. (1993). Gold recovery from a low-grade ore employing biological pretreatment in columns. *Biohydrometallurgical Technologies.*, *1*, 499–511.

Miri, S., Davoodi, S. M., Darvanjooghi, M. H. K., Brar, S. K., Rouissi, T., & Martel, R. (2021). Precision Modelling of Co-metabolic Biodegradation of Recalcitrant Aromatic Hydrocarbons in conjunction with experimental data. *Process Biochemistry*, *105*, 113–127. https://doi.org/https://doi.org/10.1016/j.procbio.2021.03.026

Mohanty, S., Ghosh, S., Bal, B., & Das, A. P. (2018). A review of biotechnology processes applied for manganese recovery from wastes. *Reviews in Environmental Science and Bio/Technology*, *17*(4), 791–811.
Mohanty, S., Ghosh, S., Nayak, S., & Das, A. P. (2017a). Bioleaching of manganese by Aspergillus sp. isolated from mining deposits. *Chemosphere*, *172*, 302–309.
Mohanty, S., Ghosh, S., Nayak, S., & Das, A. P. (2017b). Isolation, identification and screening of manganese solubilizing fungi from low-grade manganese ore deposits. *Geomicrobiology Journal*, *34*(4), 309–316.
Moncayo, E. A., Debut, A., Vizuete, K., Jumbo-Flores, D., & Aguirre, P. (2022). Sticky bacteria: Combined effect of galactose and high ferric iron concentration on extracellular polymeric substances production and the attachment of Acidithiobacillus ferrooxidans on a polymetallic sulfide ore surface. *Frontiers in Microbiology*, *13*, 951402.
Mousaid, I., & Kaya, A. (2020). Experimental Mines: Research Platforms for Sustainable Development. *Available at SSRN 3591959*.
Muravyov, M. I., & Bulaev, A. G. (2013). Two-step oxidation of a refractory gold-bearing sulfidic concentrate and the effect of organic nutrients on its biooxidation. *Minerals Engineering*, *45*, 108–114.
Muravyov, M., & Panyushkina, A. (2020). Distinct Roles of Acidophiles in Complete Oxidation of High-Sulfur Ferric Leach Product of Zinc Sulfide Concentrate. *Microorganisms*, *8*(3), 386.
Nanthakumar, B., Pickles, C. A., & Kelebek, S. (2007). Microwave pretreatment of a double refractory gold ore. *Minerals Engineering*, *20*(11), 1109–1119.
Naseri, T., Beigi, V., Namdar, A., Behbahan, A. K., & Mousavi, S. M. (2022). Biohydrometallurgical recycling approaches for returning valuable metals to the battery production cycle. In *Nano Technology for Battery Recycling, Remanufacturing, and Reusing* (pp. 217–246). Elsevier.
Ndlovu, S. (2008). Biohydrometallurgy for sustainable development in the African minerals industry. *Hydrometallurgy*, *91*(1–4), 20–27.
Ng, W. S., Wang, Q., & Chen, M. (2020). A review of Preg-robbing and the impact of chloride ions in the pressure oxidation of double refractory ores. *Mineral Processing and Extractive Metallurgy Review*, 1–28.
Noguchi, H., & Okibe, N. (2020). The role of bioleaching microorganisms in saline water leaching of chalcopyrite concentrate. *Hydrometallurgy*, 105397.
Norris, P. R. (1997). Thermophiles and bioleaching. In *Biomining* (pp. 247–258). Springer.
Norris, P. R. (2007a). Acidophile diversity in mineral sulfide oxidation. In *Biomining* (pp. 199–216). Springer.
Norris, P. R. (2007b). Acidophile diversity in mineral sulfide oxidation. In *Biomining* (pp. 199–216). Springer.
Norris, P. R., & Barr, D. W. (1988). *Bacterial oxidation of pyrite in high temperature reactors*.
Norris, P. R., Barr, D. W., & Hinson, D. (1988). *Iron and mineral oxidation by acidophilic bacteria: Affinities for iron and attachment to pyrite*.
Norris, P. R., Clark, D. A., Owen, J. P., & Waterhouse, S. (1996). Characteristics of Sulfobacillus acidophilus sp. nov. and other moderately thermophilic mineral-sulphide-oxidizing bacteria. *Microbiology*, *142*(4), 775–783.

Ofori-Sarpong, G., Adam, A.-S., Asamoah, R. K., & Amankwah, R. K. (n.d.). *Characterisation of Biooxidation Feed and Products for Improved Understanding of Biooxidation and Gold Extraction Performance*.
Ofori-Sarpong, G., Osseo-Asare, K., & Tien, M. (2011). Fungal pretreatment of sulfides in refractory gold ores. *Minerals Engineering*, *24*(6), 499–504.
Okibe, N., Gericke, M., Hallberg, K. B., & Johnson, D. B. (2003). Enumeration and characterization of acidophilic microorganisms isolated from a pilot plant stirred-tank bioleaching operation. *Appl. Environ. Microbiol.*, *69*(4), 1936–1943.
Oktay, B., Öztunç, H., & Serin, Z. V. (2016). Determinants of gold reserves: An empirical analysis for G-7 countries. *Procedia Economics and Finance*, *38*, 8–16.
Olson, G. J. (1994). Microbial oxidation of gold ores and gold bioleaching. *FEMS Microbiology Letters*, *119*(1–2), 1–6.
Olson, G. J., Brierley, C. L., Briggs, A. P., & Calmet, E. (2006). Biooxidation of thiocyanate-containing refractory gold tailings from Minacalpa, Peru. *Hydrometallurgy*, *81*(3–4), 159–166.
Olson, G. J., Brierley, J. A., & Brierley, C. L. (2003). Bioleaching review part B. *Applied Microbiology and Biotechnology*, *63*(3), 249–257.
Olson, G. J., & Clark, T. R. (2008). Bioleaching of molybdenite. *Hydrometallurgy*, *93*(1–2), 10–15.
Olstad, H. E. (2018). *Increased stability of glucose oxidase biosensors using high hydrostatic pressure and cross-linking with glutaraldehyde*. University of Georgia.
Ongendangenda, H. N., & Ojumu, T. V. (2011). The effect of initial pH on the kinetics of ferrous-iron biooxidation at low temperature. *African Journal of Biotechnology*, *10*(9), 1679–1683.
Ouyang, K., Yu, X.-Y., Zhu, Y., Gao, C., Huang, Q., & Cai, P. (2017). Effects of humic acid on the interactions between zinc oxide nanoparticles and bacterial biofilms. *Environmental Pollution*, *231*, 1104–1111.
Pakostova, E., Johnson, D. B., Bao, Z., MacKenzie, P. M., Ptacek, C. J., & Blowes, D. W. (2020). Bacterial and Archaeal Diversity in Sulfide-Bearing Waste Rock at Faro Mine Complex, Yukon Territory, Canada. *Geomicrobiology Journal*, *37*(6), 511–519.
Panda, S., Akcil, A., Pradhan, N., & Deveci, H. (2015). Current scenario of chalcopyrite bioleaching: a review on the recent advances to its heap-leach technology. *Bioresource Technology*, *196*, 694–706.
Panda, S., Mishra, S., Pradhan, N., Mohaptra, U., Sukla, L. B., & Mishra, B. K. (2015). Application of Microbes for Metal Extraction from Mining Wastes. *AND THE ENVIRONMENT*, 209.
Petersen, J. (2010). Determination of oxygen gas–liquid mass transfer rates in heap bioleach reactors. *Minerals Engineering*, *23*(6), 504–510.
Petersen, J., & Dixon, D. G. (2002). Thermophilic heap leaching of a chalcopyrite concentrate. *Minerals Engineering*, *15*(11), 777–785.
Petersen, L. A. H., Villadsen, J., Jørgensen, S. B., & Gernaey, K. V. (2017). Mixing and mass transfer in a pilot scale U-loop bioreactor. *Biotechnology and Bioengineering*, *114*(2), 344–354.
Pham, V. H. T., Kim, J., Chang, S., & Chung, W. (2022). Bacterial biosorbents, an efficient heavy metals green clean-up strategy: prospects, challenges, and opportunities. *Microorganisms*, *10*(3), 610.

Pourghahramani, P., & Akhgar, B. N. (2015). Characterization of structural changes of mechanically activated natural pyrite using XRD line profile analysis. *International Journal of Mineral Processing*, *134*, 23–28.
Prenosil, J. E. (1979). Immobilized glucose oxidase–catalase and their deactivation in a differential-bed loop reactor. *Biotechnology and Bioengineering*, *21*(1), 89–109.
Qin, M., Su, C.-W., Lobonţ, O.-R., & Moldovan, N.-C. (2023). Does global supply chain pressure motivate the gold market? *Economic Research-Ekonomska Istraživanja*, *36*(3), 2183229.
Qin, W., Wang, C., Ma, Y., Shen, M., Li, J., Jiao, K., Tay, F. R., & Niu, L. (2020). Microbe-mediated extracellular and intracellular mineralization: environmental, industrial, and biotechnological applications. *Advanced Materials*, *32*(22), 1907833.
Rafie, S. F., Abdollahi, H., Sayahi, H., Ardejani, F. D., Aghapoor, K., Darvanjooghi, M. H. K., Brar, S. K., & Magdouli, S. (2023). Genetic algorithm-assisted artificial neural network modelling for remediation and recovery of Pb (II) and Cr (VI) by manganese and cobalt spinel ferrite super nanoadsorbent. *Chemosphere*, *321*, 138162.
Rao, M. D., Singh, K. K., Morrison, C. A., & Love, J. B. (2020). Challenges and opportunities in the recovery of gold from electronic waste. *RSC Advances*, *10*(8), 4300–4309.
Rase, H. F. (2013). *Fixed-bed reactor design and diagnostics: gas-phase reactions*. Butterworth-Heinemann.
Rathna, R., & Nakkeeran, E. (2020). Biological treatment for the recovery of minerals from low-grade ores. In *Current Developments in Biotechnology and Bioengineering* (pp. 437–458). Elsevier.
Rawlings, D. E. (2002a). Heavy metal mining using microbes. *Annual Reviews in Microbiology*, *56*(1), 65–91.
Rawlings, D. E. (2002b). Heavy metal mining using microbes. *Annual Reviews in Microbiology*, *56*(1), 65–91.
Rawlings, D. E. (2005). Characteristics and adaptability of iron-and sulfur-oxidizing microorganisms used for the recovery of metals from minerals and their concentrates. *Microbial Cell Factories*, *4*(1), 13.
Rawlings, D. E., Dew, D., & du Plessis, C. (2003). Biomineralization of metal-containing ores and concentrates. *Trends in Biotechnology*, *21*(1), 38–44.
Rawlings, D. E., & Johnson, D. B. (2007a). *Biomining*. Springer.
Rawlings, D. E., & Johnson, D. B. (2007b). The microbiology of biomining: development and optimization of mineral-oxidizing microbial consortia. *Microbiology*, *153*(2), 315–324.
Renman, R., Jiankang, W., & Jinghe, C. (2006). Bacterial heap-leaching: Practice in Zijinshan copper mine. *Hydrometallurgy*, *83*(1–4), 77–82.
Rohwerder, T., Gehrke, T., Kinzler, K., & Sand, W. (2003). Bioleaching review part A: progress in bioleaching: fundamentals and mechanisms of bacterial metal sulfide oxidation. *Applied Microbiology and Biotechnology*, *63*, 239–248.
Rossi, G. (1990). *Biohydrometallurgy*. McGraw-hill.
Run, G. J., & Clark, T. R. (2004a). Fundamentals of metal sulfide biooxidation. *Mining Engineering(Colorado)*, *56*(8), 40–46.
Run, G. J., & Clark, T. R. (2004b). Fundamentals of metal sulfide biooxidation. *Mining Engineering(Colorado)*, *56*(8), 40–46.

Saavedra, A., Aguirre, P., & Gentina, J. C. (2020). Biooxidation of iron by Acidithiobacillus ferrooxidans in the presence of D-galactose: understanding its influence on the production of EPS and cell tolerance to high concentrations of iron. *Frontiers in Microbiology*, *11*, 759.

Sadowski, Z., & Pawlowska, A. (2018). Hydrometallurgy and Bio-crystallization of Metals by Microorganisms. *Recent Advances in Trace Elements*, 277.

Sajjad, W., Zheng, G., Din, G., Ma, X., Rafiq, M., & Xu, W. (2019a). Metals extraction from sulfide ores with microorganisms: the bioleaching technology and recent developments. *Transactions of the Indian Institute of Metals*, *72*(3), 559–579.

Sajjad, W., Zheng, G., Din, G., Ma, X., Rafiq, M., & Xu, W. (2019b). Metals extraction from sulfide ores with microorganisms: the bioleaching technology and recent developments. *Transactions of the Indian Institute of Metals*, *72*(3), 559–579.

Saldaña, M., Jeldres, M., Galleguillos Madrid, F. M., Gallegos, S., Salazar, I., Robles, P., & Toro, N. (2023). Bioleaching Modeling—A Review. *Materials*, *16*(10), 3812.

Salimpour, M. R., Darvanjooghi, M. H. K., Abdollahi, A., Karimipour, A., & Goodarzi, M. (2019). Providing a model for Csf according to pool boiling convection heat transfer of water/ferrous oxide nanofluid using sensitivity analysis. *International Journal of Numerical Methods for Heat & Fluid Flow*, *30*(6), 2867–2881. https://doi.org/https://doi.org/10.1108/HFF-01-2019-0009

Salo-Zieman, V. L. A., Sivonen, T., Plumb, J. J., Haddad, C. M., Laukkanen, K., Kinnunen, P. H. M., Kaksonen, A. H., Franzmann, P. D., & Puhakka, J. A. (2006). Characterization of a thermophilic sulfur oxidizing enrichment culture dominated by a Sulfolobus sp. obtained from an underground hot spring for use in extreme bioleaching conditions. *Journal of Industrial Microbiology and Biotechnology*, *33*(12), 984–994.

Sand, W., Gehrke, T., Jozsa, P.-G., & Schippers, A. (2001). (Bio) chemistry of bacterial leaching—direct vs. indirect bioleaching. *Hydrometallurgy*, *59*(2–3), 159–175.

Sanket, A. S., Ghosh, S., Sahoo, R., Nayak, S., & Das, A. P. (2017). Molecular identification of acidophilic manganese (Mn)-solubilizing bacteria from mining effluents and their application in mineral beneficiation. *Geomicrobiology Journal*, *34*(1), 71–80.

Sara, M., Rouissi, T., Brar, S. K., & Blais, J. F. (2016). Life cycle analysis of potential substrates of sustainable biorefinery. In *Platform Chemical Biorefinery* (pp. 55–76). Elsevier. https://doi.org/https://doi.org/10.1016/B978-0-12-802980-0.00004-3

Schippers, A. (2007a). Microorganisms involved in bioleaching and nucleic acid-based molecular methods for their identification and quantification. In *Microbial processing of metal sulfides* (pp. 3–33). Springer.

Schippers, A. (2007b). Microorganisms involved in bioleaching and nucleic acid-based molecular methods for their identification and quantification. In *Microbial processing of metal sulfides* (pp. 3–33). Springer.

Schippers, A. (2007c). Microorganisms involved in bioleaching and nucleic acid-based molecular methods for their identification and quantification. In *Microbial processing of metal sulfides* (pp. 3–33). Springer.

Schippers, A., Breuker, A., Blazejak, A., Bosecker, K., Kock, D., & Wright, T. L. (2010). The biogeochemistry and microbiology of sulfidic mine waste and bioleaching dumps and heaps, and novel Fe (II)-oxidizing bacteria. *Hydrometallurgy*, *104*(3–4), 342–350.

Schneider, D., & Greenberg, M. R. (2023). Remediating and Reusing Abandoned Mining Sites in US Metropolitan Areas: Raising Visibility and Value. *Sustainability*, *15*(9), 7080.

Segerer, A., Neuner, A., Kristjansson, J. K., & Stetter, K. O. (1986). Acidianus infernus gen. nov., sp. nov., and Acidianus brierleyi comb. nov.: facultatively aerobic, extremely acidophilic thermophilic sulfur-metabolizing archaebacteria. *International Journal of Systematic and Evolutionary Microbiology*, *36*(4), 559–564.

Shen, L., Wang, J., Liu, H., Yin, H., Liu, X., Qiu, G., & Liu, Y. (2020). Effect of introduction of exogenous strain Leptospirillum ferriphilum YSK on functional gene expression, structure, and function of indigenous consortium during pyrite bioleaching. *Journal of Central South University*, *27*(5), 1453–1465.

Sheng, G.-P., Xu, J., Luo, H.-W., Li, W.-W., Li, W.-H., Yu, H.-Q., Xie, Z., Wei, S.-Q., & Hu, F.-C. (2013). Thermodynamic analysis on the binding of heavy metals onto extracellular polymeric substances (EPS) of activated sludge. *Water Research*, *47*(2), 607–614.

Shiers, D. W., Ralph, D. E., Bryan, C. G., & Watling, H. R. (2013). Substrate utilisation by Acidianus brierleyi, Metallosphaera hakonensis and Sulfolobus metallicus in mixed ferrous ion and tetrathionate growth media. *Minerals Engineering*, *48*, 86–93.

Silver, M., Margalith, P., & Lundgren, D. G. (1967). Effect of glucose on carbon dioxide assimilation and substrate oxidation by Ferrobacillus ferrooxidans. *Journal of Bacteriology*, *93*(6), 1765–1769.

Stott, M. B., Watling, H. R., Franzmann, P. D., & Sutton, D. (2000). The role of iron-hydroxy precipitates in the passivation of chalcopyrite during bioleaching. *Minerals Engineering*, *13*(10–11), 1117–1127.

Street, L., Gopaul, K., Kumar, M., Lu, C., & Hewitt, A. (2015). Gold Demand Trends. *Technology*, *11*, 2.

Tavakoli, H. Z., Abdollahy, M., Ahmadi, S. J., & Darban, A. K. (2017). Kinetics of uranium bioleaching in stirred and column reactors. *Minerals Engineering*, *111*, 36–46.

Thiel, R., & Smith, M. E. (2004). State of the practice review of heap leach pad design issues. *Geotextiles and Geomembranes*, *22*(6), 555–568.

Tributsch, H. (2001). Direct versus indirect bioleaching. *Hydrometallurgy*, *59*(2–3), 177–185.

Trivedi, A., & Hait, S. (2023). Metal bioleaching from printed circuit boards by bio-Fenton process: Optimization and prediction by response surface methodology and artificial intelligence models. *Journal of Environmental Management*, *326*, 116797.

Ulya, F. (2022). Isolation and Selection of Sulfuric Acid Bacteria from Kejayan River as Bio-oxidation Agents. *Jurnal Pembelajaran Dan Biologi Nukleus*, *8*(2), 419–429.

Van Aswegen, P. C., & Van Niekerk, J. (2004). New developments in the bacterial oxidation technology to enhance the efficiency of the BIOX process. *Proceedings of the BacMin Conference, Bendigo*, 181–190.

van Niekerk, J. A., van Buuren, C. B., & Olivier, J. W. (2022). Bioprocessing of refractory gold ores: The BIOX, MesoTHERM, and ASTER processes. In *Biomining Technologies: Extracting and Recovering Metals from Ores and Wastes* (pp. 67–88). Springer.

Vardanyan, A. K., Vardanyan, N. S., & Markosyan, L. M. (2013). Peculiarities of adhesion and bioleaching of pyrite by new isolated Leptospirillum spp. bacteria. *Universal Journal of Microbiology Research*, *1*(2), 22–25.

Vardanyan, N., Badalyan, H., Markosyan, L., Vardanyan, A., Zhang, R., & Sand, W. (2020). Newly isolated Acidithiobacillus sp. Ksh from Kashen copper ore: peculiarities of EPS and colloidal exopolysaccharide. *Frontiers in Microbiology*, *11*, 1802.

Vera, M., Schippers, A., & Sand, W. (2013). Progress in bioleaching: fundamentals and mechanisms of bacterial metal sulfide oxidation—part A. *Applied Microbiology and Biotechnology*, *97*(17), 7529–7541.

Vogt, S., Schneider, M., Schäfer-Eberwein, H., & Nöll, G. (2014). Determination of the pH dependent redox potential of glucose oxidase by spectroelectrochemistry. *Analytical Chemistry*, *86*(15), 7530–7535.

Vriens, B., Plante, B., Seigneur, N., & Jamieson, H. (2020). Mine Waste Rock: Insights for Sustainable Hydrogeochemical Management. *Minerals*, *10*(9), 728.

Vyas, S., Das, S., & Ting, Y.-P. (2020). Predictive modeling and response analysis of spent catalyst bioleaching using artificial neural network. *Bioresource Technology Reports*, *9*, 100389.

Wan, R. Y., Luinstra, L., & Brierley, J. (1995). Gold recovery from refractory sulfidic-carbonaceous ore. II. Thiourea leaching following biooxidation-heap pretreatment. *EPD Congress 1995*, 165–173.

Wang, J., Faraji, F., Ramsay, J., & Ghahreman, A. (2021). A review of biocyanidation as a sustainable route for gold recovery from primary and secondary low-grade resources. *Journal of Cleaner Production*, *296*, 126457.

Wang, M., Huang, Y., & Liu, H. (2023). Removal of trichloroethene by glucose oxidase immobilized on magnetite nanoparticles. *RSC Advances*, *13*(17), 11853–11864.

Wang, Y., Cao, X., Jiang, S., Gao, L., Han, X., Qu, J., Jiang, X., Liu, G., & Qu, Y. (2024). Engineering the substrate preference of glucose oxidase for the enzymatic oxidation of xylose. *Green Chemistry*, *26*(8), 4851–4859.

Wenbin, N., Dejuan, Z., Feifan, L., Lei, Y., Peng, C., Xiaoxuan, Y., & Hongyu, L. (2011). Quorum-sensing system in Acidithiobacillus ferrooxidans involved in its resistance to Cu2+. *Letters in Applied Microbiology*, *53*(1), 84–91.

Weremfo, A., Abassah-Oppong, S., Adulley, F., Dabie, K., & Seidu-Larry, S. (2023). Response surface methodology as a tool to optimize the extraction of bioactive compounds from plant sources. *Journal of the Science of Food and Agriculture*, *103*(1), 26–36.

Wu, B., Shang, H., Wen, J., Liu, M., Zhang, Q., & Cui, X. (2020a). Well-controlled stirring tank leaching to improve bio-oxidation efficiency of a high sulfur refractory gold concentrate. *Journal of Central South University*, *27*(5), 1416–1423.

Wu, B., Shang, H., Wen, J., Liu, M., Zhang, Q., & Cui, X. (2020b). Well-controlled stirring tank leaching to improve bio-oxidation efficiency of a high sulfur refractory gold concentrate. *Journal of Central South University*, *27*(5), 1416–1423.

Wu, Z. L., Huang, Z. S., Ruan, R. M., Zhong, S. P., & Chan, B. K. C. (2013). Effect of temperature on column bioleaching of a refractory gold ore. *Advanced Materials Research*, *825*, 352–355.

Xing, D., Magdouli, S., Zhang, J., & Koubaa, A. (2020). Microbial remediation for the removal of inorganic contaminants from treated wood: Recent trends and challenges. *Chemosphere*, 127429. https://doi.org/https://doi.org/10.1016/j.chemosphere.2020.127429

Xu, R., Li, Q., Meng, F., Yang, Y., Xu, B., Yin, H., & Jiang, T. (2020a). Bio-Oxidation of a Double Refractory Gold Ore and Investigation of Preg-Robbing of Gold from Thiourea Solution. *Metals*, *10*(9), 1216.

Xu, R., Li, Q., Meng, F., Yang, Y., Xu, B., Yin, H., & Jiang, T. (2020b). Bio-Oxidation of a Double Refractory Gold Ore and Investigation of Preg-Robbing of Gold from Thiourea Solution. *Metals*, *10*(9), 1216.

Xu, R., Nan, X., Meng, F., Li, Q., Chen, X., Yang, Y., Xu, B., & Jiang, T. (2020). Analysis and prediction of the thiourea gold leaching process using grey relational analysis and artificial neural networks. *Minerals*, *10*(9), 811.

Yadollahi, A., Abdollahi, H., Ardejani, F. D., Mirmohammadi, M., & Magdouli, S. (2021). Bio-oxidation behavior of pyrite, marcasite, pyrrhotite, and arsenopyrite by sulfur-and iron-oxidizing acidophiles. *Bioresource Technology Reports*, *15*, 100699.

Yen, W.-T., Amankwah, R. K., & Choi, Y. (2009). *Microbial pre-treatment of double refractory gold ores*. Google Patents.

Young, K. D. (2006). The selective value of bacterial shape. *Microbiology and Molecular Biology Reviews*, *70*(3), 660–703.

Yu, R., Jing, L. I. U., An, C., Zhong, D., Qian, L. I., Qin, W., Qiu, G., & Gu, G. (2013). Interaction mechanism of Cu2+, Fe3+ ions and extracellular polymeric substances during bioleaching chalcopyrite by Acidithiobacillus ferrooxidans ATCC2370. *Transactions of Nonferrous Metals Society of China*, *23*(1), 231–236.

YU, R., TAN, J., Peng, Y., Jing, S. U. N., OUYANG, X., & DAI, Y. (2008). EPS-contact-leaching mechanism of chalcopyrite concentrates by A. ferrooxidans. *Transactions of Nonferrous Metals Society of China*, *18*(6), 1427–1432.

Yu, Z., Yu, R., LIU, A., Jing, L. I. U., Zeng, W., Liu, X., & Qiu, G. (2017). Effect of pH values on extracellular protein and polysaccharide secretions of Acidithiobacillus ferrooxidans during chalcopyrite bioleaching. *Transactions of Nonferrous Metals Society of China*, *27*(2), 406–412.

Yuan, M., Ning, C., Yang, S., Liang, Q., Mou, H., & Liu, Z. (2020a). A new cold-active glucose oxidase from Penicillium: High-level expression and application in fish preservation. *Frontiers in Microbiology*, *11*, 606007.

Yuan, M., Ning, C., Yang, S., Liang, Q., Mou, H., & Liu, Z. (2020b). A new cold-active glucose oxidase from Penicillium: High-level expression and application in fish preservation. *Frontiers in Microbiology*, *11*, 606007.

Yuan, X., Xie, X., Fan, F., Zhu, W., Na, L. I. U., & Liu, J. (2013). Effects of mutation on a new strain Leptospirillum ferriphilum YXW and bioleaching of gold ore. *Transactions of Nonferrous Metals Society of China*, *23*(9), 2751–2758.

Zahari, M. A. K. M., Jaapar, J., Bunyok, M. A., Sohor, S. H., & Ahmad, W. A. (n.d.). *Biooxidation of mine tailings using a mixed bacterial population*.

Zhang, D., Chen, H., Xia, J., Nie, Z., Fan, X., Liu, H., Zheng, L., Zhang, L., & Yang, H. (2020). Humic acid promotes arsenopyrite bio-oxidation and arsenic immobilization. *Journal of Hazardous Materials*, *384*, 121359.

Zhang, R. (2016). *Biofilm formation and extracellular polymeric substances of acidophilic metal/sulfur-oxidizing archaea*.

Zhang, S., Yang, H., Ma, P., Luan, Z., Tong, L., Jin, Z., & Sand, W. (2022). Column bio-oxidation of low-grade refractory gold ore containing high-arsenic and high-sulfur: Insight on change in microbial community structure and sulfide surface corrosion. *Minerals Engineering*, *175*, 107201.

Zhang, Y., & Wilson, G. S. (1993). In vitro and in vivo evaluation of oxygen effects on a glucose oxidase based implantable glucose sensor. *Analytica Chimica Acta*, *281*(3), 513–520.

Zhao, H., Yang, H., Tong, L., Zhang, Q., & Kong, Y. (n.d.). Biooxidation-Thiosulfate Leaching of Refractory Gold Concentrate. *International Journal of Minerals, Metallurgy and Materials*, 0.

Zhao, H., Yang, H., Tong, L., Zhang, Q., & Kong, Y. (2020). Biooxidation-thiosulfate leaching of refractory gold concentrate. *International Journal of Minerals, Metallurgy and Materials*, *27*(8), 1075–1082.

Zhou, J. Y., & Cabri, L. J. (2004). Gold process mineralogy: Objectives, techniques, and applications. *Jom*, *56*(7), 49–52.

Zhou, X., Li, Z., Feng, X., Yan, H., Chen, D., & Yang, C. (2022). *A hybrid deep learning framework driven by data and reaction mechanism for predicting glycolic acid production*.

Zolfaghari, M., Magdouli, S., Tanabene, R., Komtchou, S. P., Martial, R., & Saffar, T. (2020). Pragmatic strategy for the removal of ammonia from gold mine effluents using a combination of electro-coagulation and zeolite cation exchange processes: A staged approach. *Journal of Water Process Engineering*, *37*, 101512.

Appendices

Appendix A

In the first method of biooxidation, the membranes of bacterial directly interact with the mineral sulfide particles through a direct mechanism which is presented in **Fig. S1**. On the other hand, indirect mechanism is enhanced following the biooxidation of ferrous ions to ferric ions in the mineral matrix which is also presented in **Fig. S1**. In this mechanism, the ferric ion can directly oxidize metal sulfides while being transformed to ferrous ions (iron directly carries electron).

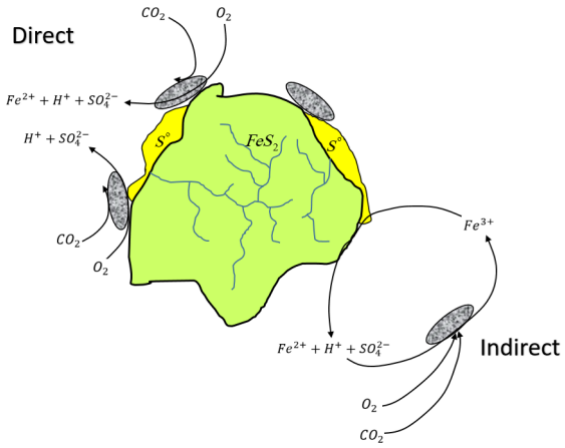

Figure A1. *Schematic of reactions for both direct and indirect biooxidation of pyrite (FeS_2).*

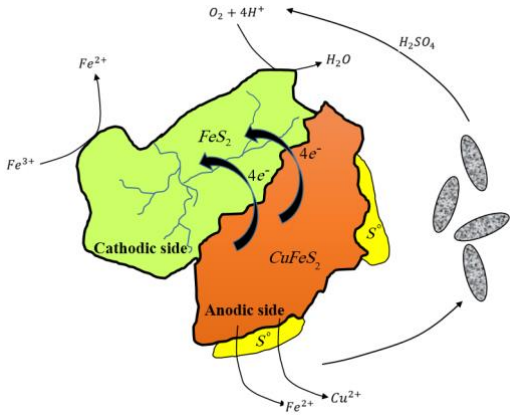

Figure A2. *Schematic of reactions for galvanic interaction between chalcopyrite/pyrite in biooxidation.*

The combination of both “contact” and “non-contact” (named as cooperative mechanism) effectively enhances the dissolution of the sulfide minerals and colloids planktonic cells (**Fig. S3**).

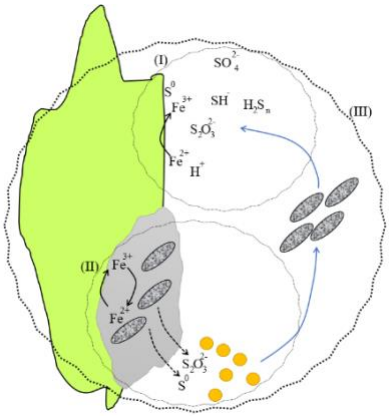

Figure A3. *Schematic of reactions for non-contact (I), contact (II), and cooperative mechanism (III).*

Appendix B

Table B1. XRF (in wt.%) and ICP (in ppm) analysis data for the ore sample (LGOS) composition.

XRF analysis data						
SiO_2	**Al_2O_3**	**Fe_2O_3**	**CaO**	**K_2O**	**LOI**	**Na_2O**
66.20	13.20	5.56	4.01	2.61	2.58	2.49
MgO	**SO_3**	**TiO_2**	**P_2O_5**	**MnO**	**BaO**	
1.69	1.04	0.37	0.12	0.08	0.05	
ICP analysis data						
Na	**Ti**	**Sr**	**Zr**	**Zn**	**Ni**	**Cu**
2.0×10^4	1.4×10^3	2.0×10^2	1.1×10^2	668	56	54
Ce	**Cr**	**V**	**La**	**Pb**	**Mo**	**Co**
49	46	46	25	21	8.5	14
Th	**Sc**	**Li**	**U**	**As**	**Y**	**Sb**
10	5.7	5	<5	4.1	4	3
Be	**Yb**	**Ag**	**Cd**	**Au**		
1	0.7	0.36	0.3	447 ppb		

Table B2. XRD analysis data for mineral characterization for original and Bromoform-assisted concentrated samples (LGOS).

XRD results of the original sample.			
Phases		Crystal system	Semi-quantitative (%)
Name	Chemical Formula		
Quartz, syn	SiO_2	Hexagonal	44.6
Plagioclase	$NaAlSi_3O_8$	Triclinic	22.5
Mica	$Kal_2(Si_3Al)O_{10}(OH,F)_2$	Monoclinic	20
Chlorite	$(Mg,Al,Fe)_6(Si,Al)_4O_{10}(OH)_8$	Monoclinic	7.9
Ankerite	$Ca(Fe^{+2},Mg)(CO_3)_2$	Rhombo.H.axes	3.5
Calcite	$CaCO_3$	Rhombo.H.axe	1.5

XRD results of the sample concentrated by Bromoform.			
Phases		Crystal system	Semi-quantitative (%)
Name	Chemical Formula		
Ankerite	$a(Mg_{0.67}Fe_{0.33}^{+2})(CO_3)_2$	Rhombo.H.axes	58.1
Quartz, syn	SiO_2	Hexagonal	10.5
Chlorite	$(Mg,Fe)_6(Si,Al)_4O_{10}(OH)_8$	Monoclinic	10.4
Mica	$Kal_2(Si_3Al)O_{10}(OH,F)_2$	Monoclinic	8.3
Mixed layered clay mineral	$Kal_4(Si,Al)_8O_{10}(OH)_4 \cdot 4H_2O$		7.2
Plagioclase	$NaAlSi_3O_8$	Triclinic	2.8
Alkali feldspar	$K(AlSi_3O_8)$	Monoclinic	1.5
Pyrite	FeS_2	Cubic	1.2

Table B3. Gold Association with Gangue Minerals (LGOS).

Gold type association	Quantity (%)	
Gold associated with non-opaque gangue	0.4	
Gold partly associated with sulfide	10.9	
Gold associated with sulfide	88.7	
Mode of gold occurrence in minerals	Distribution based on the numbers of occurrences (%)	Distribution based on Cumulative grain area (%)
Inclusion in mineral 	42.7	24.2
Grain boundaries/ included 	1.2	0.02
Along fracture 	12.2	17.4
Grain Boundaries 	43.9	58.3

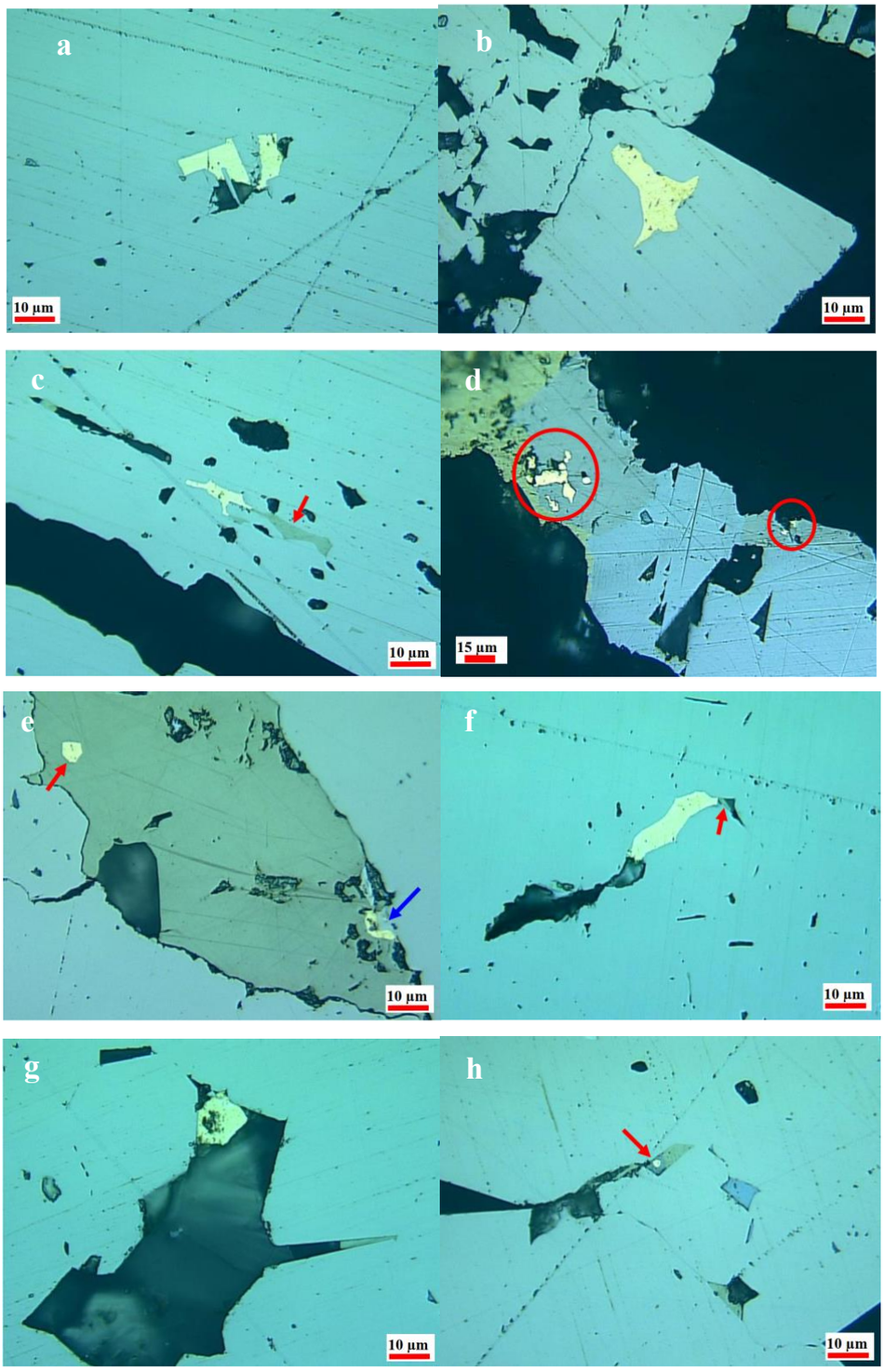

Figure B4. Images of gold inclusion in different minerals in the ore sample. (a, native gold inclusion in pyrite, b, native gold inclusion in pyrite and associated with chalcopyrite (red arrow) partly occurs at pyrite cleavage limit, c, native gold (red circle) in lead-sulfosalt at sulfosalt silicate grain boundaries (circle on the right) and associated with gold is galena and chalcopyrite, d, native gold at pyrite-silicate grain boundaries, e, Electrum (red arrow) inclusion in galena (or Au-Pb Telluride), f, Uncommon occurrence of gold occurring as inclusion in chalcopyrite (red arrow), g, native gold inclusion in pyrite and here gold is associated with chalcopyrite (red arrow), h, native gold inclusion in pyrite.

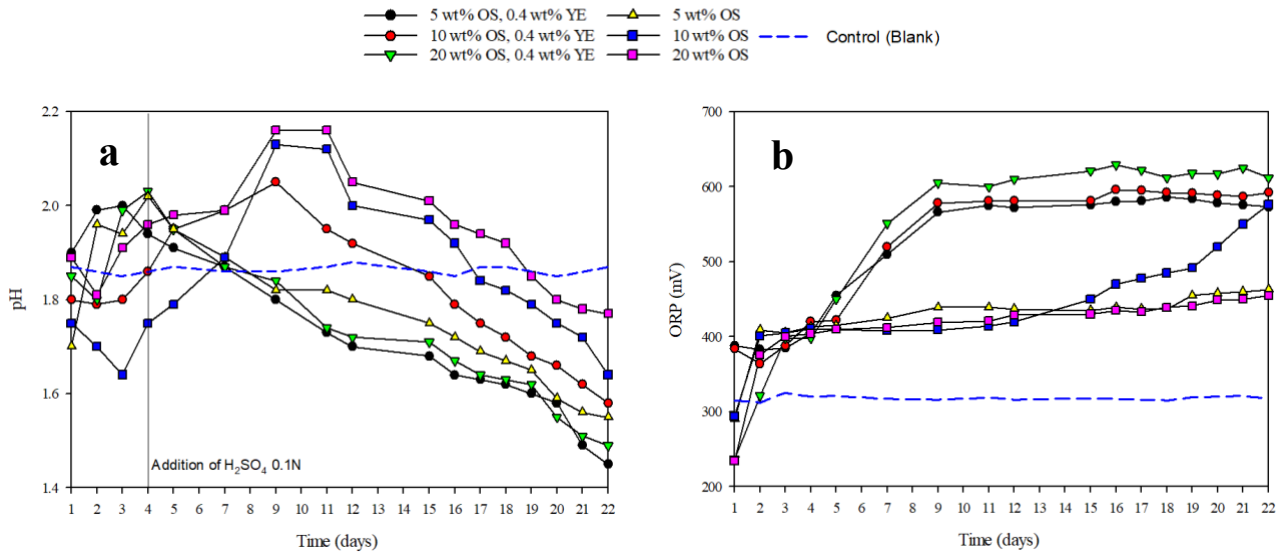

Figure B5. a, pH and b, ORP of biooxidation of ore sample in the presence and absence of yeast extract without the addition of monosaccharides (OS: ore sample, YE: yeast extract)-reference condition: Ag/AgCl 1 M KCl: 228 mV.

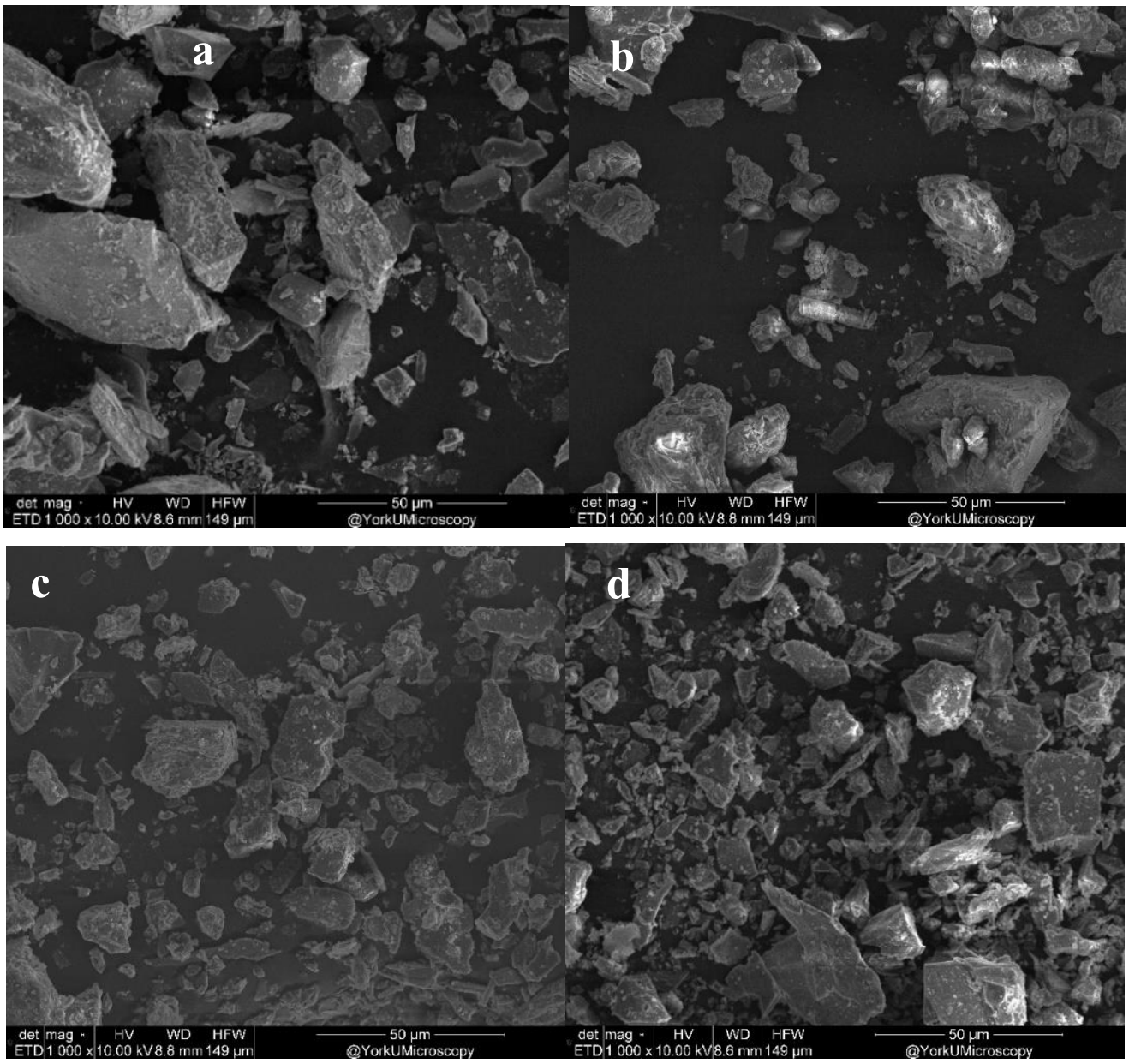

No Yeast Extract	0.4 wt.% Yeast Extract	0.4 wt.% Yeast Extract and 0.4 wt.% D-+-Sucrose
e	i	m
f	j	n
g	k	o
h	l	p

Figure B6. SEM images of a, raw sample, b, after biooxidation in absence of yeast extract, c, after biooxidation in presence of 0.4wt.% of yeast extract, d, after biooxidation in presence of 0.4 wt.% D-+-sucrose and yeast extract as well as CLSM results of, e, i, m, the 3D image of the cells and EPS, f, j, n, carbohydrates inside the microorganisms, g, k, o nucleic acids inside the microorganism's cell, and h, l, p, the carbohydrate inside the produced EPS.

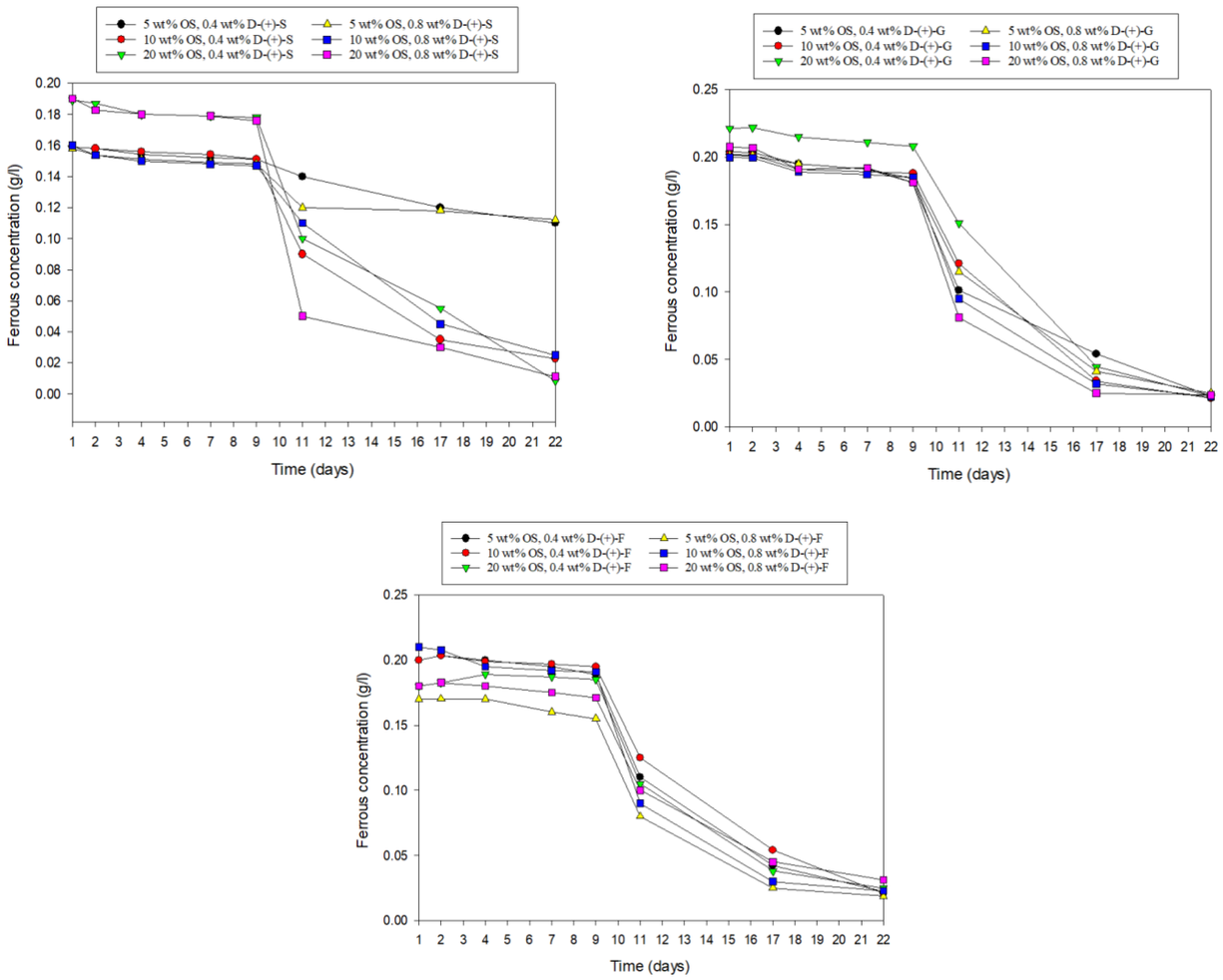

Figure B7. The concentration of ferrous ions in the solution during biooxidation (D-+-G: D-galactose, D-+-F: D-fructose, D-+-S: D-sucrose).

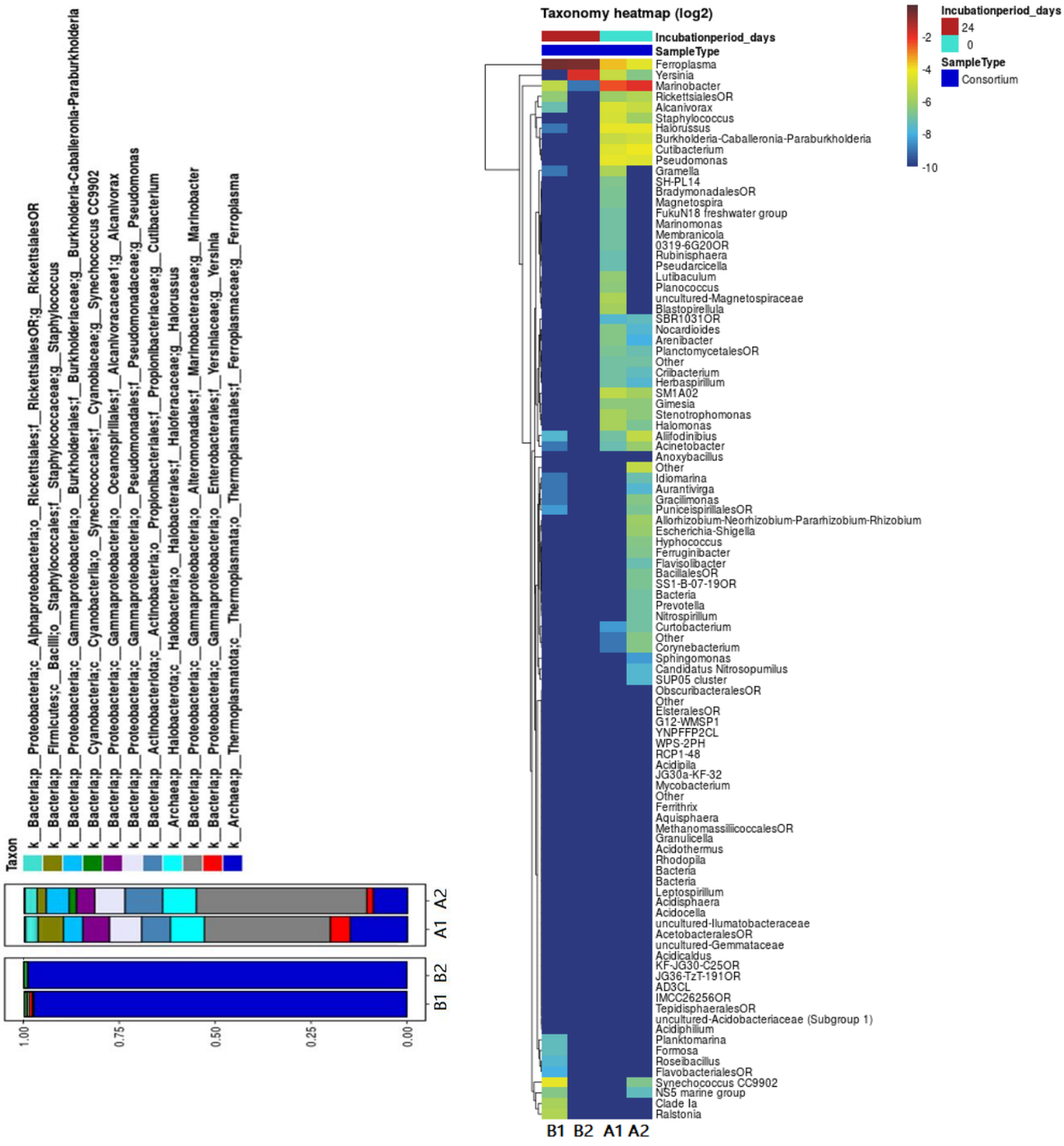

Figure B8. Results of microorganisms' community profiling before (A1, A2) and after (B1, B2) biooxidation in the presence of D-sucrose (0.4 wt.%) and yeast extract (0.4 wt.%).

Appendix C

By considering the dimensionless parameters for inputs and outputs (ξ_i), the proposed correlation for PR-RSM are provided as follows (**Eq. C.1** and **Eq. C2**, here $i = 1$ to 8 indicates pyrite content, ore content, D-+-sucrose, D-+-galactose, D-+-fructose, pyrite dissolution, and ferric ions concentration, respectively):

$$\begin{aligned}\xi_7 = {} & 2.17 \times 10^{-17} + 0.477\xi_1 + 0.234\xi_2 - 0.133\xi_3 + 0.396\xi_4 + 0.132\xi_5 + 0.109\xi_6 \\ & - 0.969\xi_1^2 + 0.218\xi_2^2 - 0.155\xi_3^2 + 0.048\xi_4^2 + 0.143\xi_5^2 + 0.121\xi_6^2 \\ & - 0.446\xi_1\xi_2 - 0.012\xi_1\xi_3 + 0.021\xi_1\xi_4 + 0.060\xi_1\xi_5 + 0.040\xi_1\xi_6 \\ & - 0.031\xi_2\xi_3 - 0.033\xi_2\xi_4 - 0.044\xi_2\xi_5 - 0.020\xi_2\xi_6 - 0.012\xi_3\xi_4 \\ & + 0.044\xi_3\xi_5 + 0.043\xi_3\xi_6 - 0.036\xi_4\xi_5 + 0.050\xi_4\xi_6 - 0.027\xi_5\xi_6\end{aligned} \quad \text{(C.3)}$$

$$\begin{aligned}\xi_8 = {} & 1.16 \times 10^{-16} + 0.204\xi_1 + 0.447\xi_2 + 0.182\xi_3 - 0.014\xi_4 + 0.008\xi_5 - 0.004\xi_6 \\ & - 0.452\xi_1^2 + 0.415\xi_2^2 + 0.179\xi_3^2 - 0.011\xi_4^2 - 0.005\xi_5^2 - 0.011\xi_6^2 \\ & + 0.125\xi_1\xi_2 + 0.343\xi_1\xi_3 + 0.067\xi_1\xi_4 + 0.132\xi_1\xi_5 + 0.130\xi_1\xi_6 \\ & + 0.079\xi_2\xi_3 + 0.021\xi_2\xi_4 + 0.034\xi_2\xi_5 + 0.043\xi_2\xi_6 + 0.021\xi_3\xi_4 \\ & - 0.013\xi_3\xi_5 - 0.015\xi_3\xi_6 + 0.021\xi_4\xi_5 - 0.004\xi_4\xi_6 + 0.030\xi_5\xi_6\end{aligned} \quad \text{(C.4)}$$

Table C.1. The levels and the symbols for representing the parameters in Box-Behnken design of experiment.

Parameters	Symbols	Levels		
-	-	-1.0	0.0	1.0
Time (day)	T	1	12	24
Pyrite content (wt.%)	PO	1.5	16.8	30.6
Ore content in solution (wt.%)	OC	5	12.5	20
D-+-galactose (wt.%)†	DG	-2	-1	0
D-+-sucrose (wt.%)†	DS	-2	-1	0
D-+-fructose (wt.%)†	DF	-2	-1	0

†In Log_{10} format

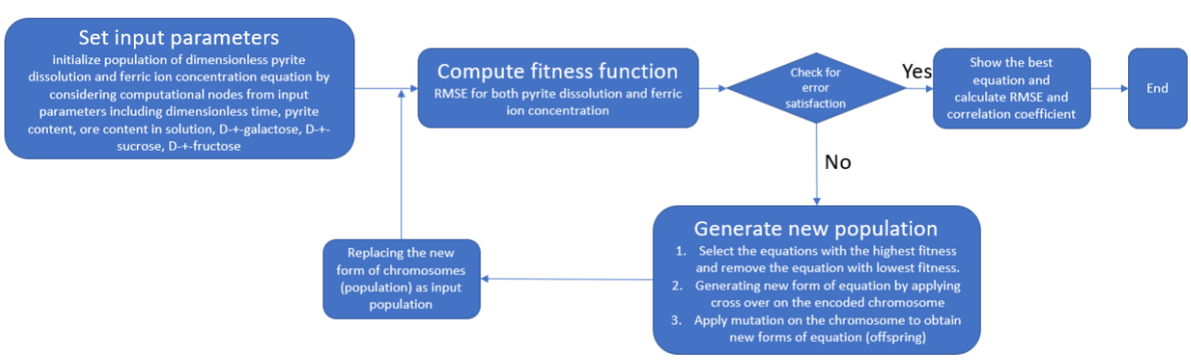

Figure C1. Schematic illustrating the Genetic Programing method used to develop the model for pyrite dissolution and ferric ions concentration as input parameters.

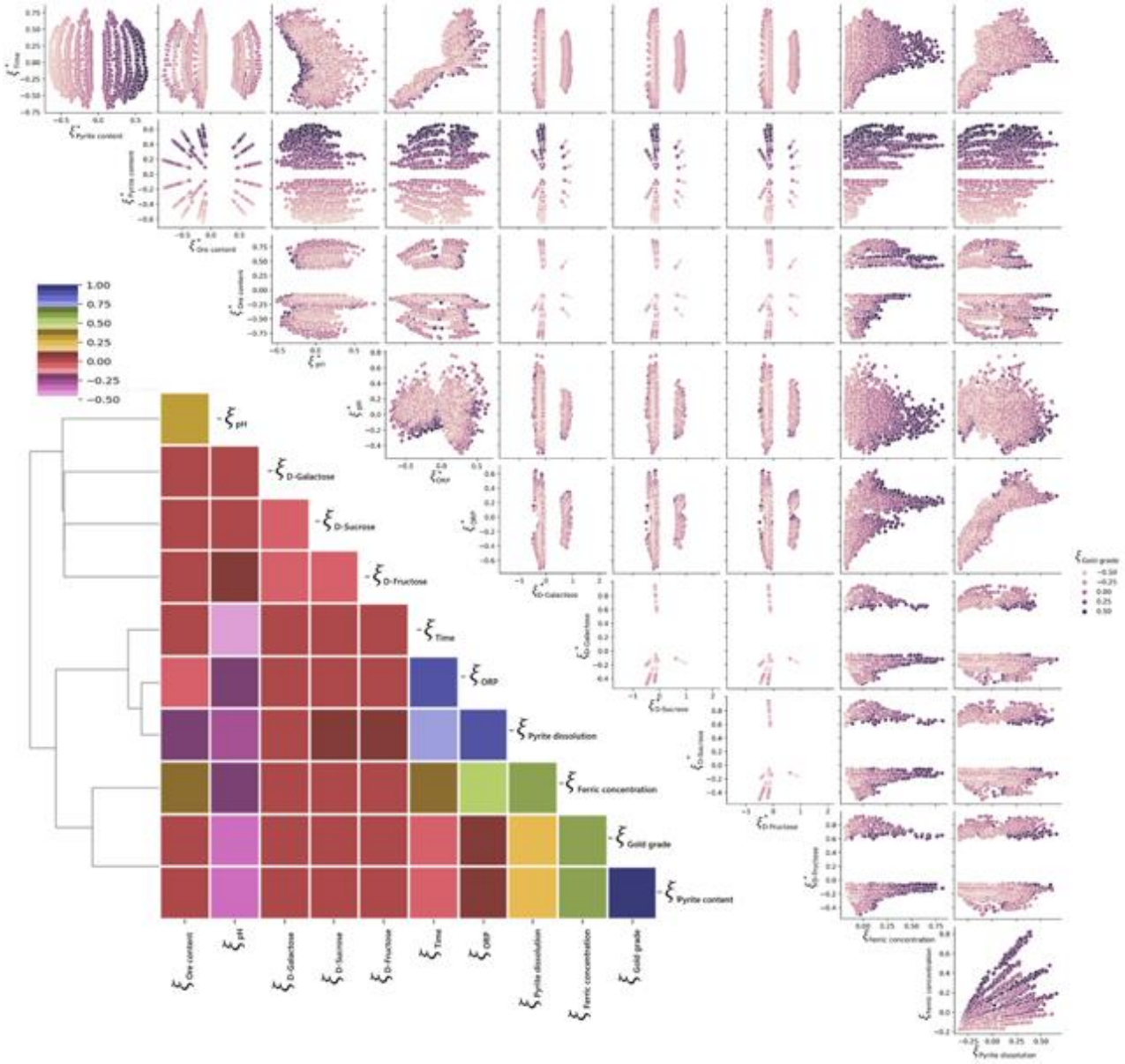

Figure C2. Cluster map for the inter-item correlation factor (p-values<0.05) and dimensionless parameters plots ($\xi_i^* = \frac{\xi_l}{(\sum_l \xi_l)^2}, i \neq$ *pyrite dissolution*, *ferric concentratio*).

Table C2. Input parameters selection.

✓ Data set No. 1

No.	Input variables	No.	Output (Target)
X1	Time (day)	Y1	Pyrite dissolution (%)
X2	Gold content in ore sample (g/ton)	Y2	Ferric (Fe^{3+}) ions concentration (g/l)

✓ Data set No. 2

No.	Input variables	No.	Output (Target)
X1	Time (day)	Y1	Pyrite dissolution (%)
X2	Pyrite content in ore sample (wt.%)	Y2	Ferric (Fe^{3+}) ions concentration (g/l)
X3	Ore content in contact with microorganisms (wt.%)		
X4	pH		

✓ Data set No. 3

No.	Input variables	No.	Output (Target)
X1	Time (day)	Y1	Pyrite dissolution (%)
X2	Pyrite content in ore sample (wt.%)	Y2	Ferric (Fe^{3+}) ions concentration (g/l)
X3	Ore content in contact with microorganisms (wt.%)		
X4	pH		
X5	ORP (as an indicator for measuring the ratio of ferric ions concentration to ferrous ions concentration, Fe^{3+}/Fe^{2+} (mV)		

✓ Data set No. 4

No.	Input variables	No.	Output (Target)
X1	Time (day)	Y1	Pyrite dissolution (%)
X2	Pyrite content in ore sample (wt.%)	Y2	Ferric (Fe^{3+}) ions concentration (g/l)
X3	Ore content in contact with microorganisms (wt.%)		
X4	pH		
X5	ORP (as an indicator for measuring the ratio of ferric ions concentration to ferrous ions concentration, Fe^{3+}/Fe^{2+} (mV)		
X6	Concentration of D-Galactose (wt.%)		
X7	Concentration of D-Sucrose (wt.%)		
X8	Concentration of D-Fructose (wt.%)		

Table C3. Elemental analysis data (contents are in ppm) for two types of ore samples (results are from ICP).

HPC ore sample						
Fe	**As**	**Al**	**Zn**	**K**	**Ca**	**Mn**
2.4×10^5	5.9×10^4	2.1×10^4	7.7×10^3	6.4×10^3	5.4×10^3	2.5×10^3
Mg	**Na**	**Cu**	**Ni**	**Cr**	**Cd**	**Au**
2.4×10^3	2.1×10^3	900	710	65.9	35.7	25.2
LPC ore sample						
Na	**Ti**	**Sr**	**Zr**	**Zn**	**Ni**	**Cu**
2.0×10^4	1.4×10^3	2.0×10^2	1.1×10^2	668	56	54
Ce	**Cr**	**V**	**La**	**Pb**	**Mo**	**Co**
49	46	46	25	21	8.5	14
Th	**Sc**	**Li**	**U**	**As**	**Y**	**Sb**
10	5.7	5	<5	4.1	4	3
Be	**Yb**	**Ag**	**Cd**	**Au**		
1	0.7	0.36	0.3	447 ppb		

Table C4. Results of XRD analysis HPC and LPC samples.

XRD results of the HPC sample.			
Phases		Crystal system	Semi-quantitative (%)
Name	Chemical Formula		
Quartz, syn	SiO_2	Hexagonal	62.5
-	$Bi_{39}InTe_{58.6}S$	Rhombo.H.axes	0.5
-	As_5Te_7I	Monoclinic	6.5
Pyrite	FeS_2	Cubic	30.6
XRD results of the LPC sample concentrated by Bromoform.			
Phases		Crystal system	Semi-quantitative (%)
Name	Chemical Formula		
Ankerite	$a(Mg_{0.67}Fe_{0.33}^{+2})(CO_3)_2$	Rhombo.H.axes	58.1
Quartz, syn	SiO_2	Hexagonal	10.5
Chlorite	$(Mg, Fe)_6(Si,Al)_4O_{10}(OH)_8$	Monoclinic	10.4
Mica	$Kal_2(Si_3Al)O_{10}(OH,F)_2$	Monoclinic	8.3
Mixed layered clay mineral	$Kal_4(Si,Al)_8O_{10}(OH)_4 \cdot 4H_2O$	-	7.2
Plagioclase	$NaAlSi_3O_8$	Triclinic	2.8
Alkali feldspar	$K(AlSi_3O_8)$	Monoclinic	1.5
Pyrite	FeS_2	Cubic	1.5

Table C5. Distribution of data for the parameters.

Parameters	Mean	Standard Deviation	Distribution				
			Min	25%	50%	75%	Max
Time (min)	12.5	6.9	1	6.8	12.5	18.3	24
Gold grade (g/ton)	12.8	8.4	0.5	5.4	12.8	20.2	25.2
Pyrite content (wt.%)	15.8	10	1.5	6.8	15.7	24.7	30.6
Ore content (wt.%)	11.7	6.2	5	5	10	20	20
pH	2.3	0.3	1.4	2.1	2.3	2.6	3.5
ORP (mV)	432.6	91.9	222	355	475	508	575
D-+-Galactose (wt.%)	0.2	0.3	0	0	0	0.1	1
D-+-Sucrose (wt.%)	0.2	0.3	0	0	0	0.1	1
D-+-Fructose (wt.%)	0.2	0.3	0	0	0	0.1	1
Ferric (g/lit)	3.8	4.1	0	0.4	2.6	5.8	21.5
Pyrite dissolution (%)	18.2	12.9	0	5.3	17.9	29.1	53.6

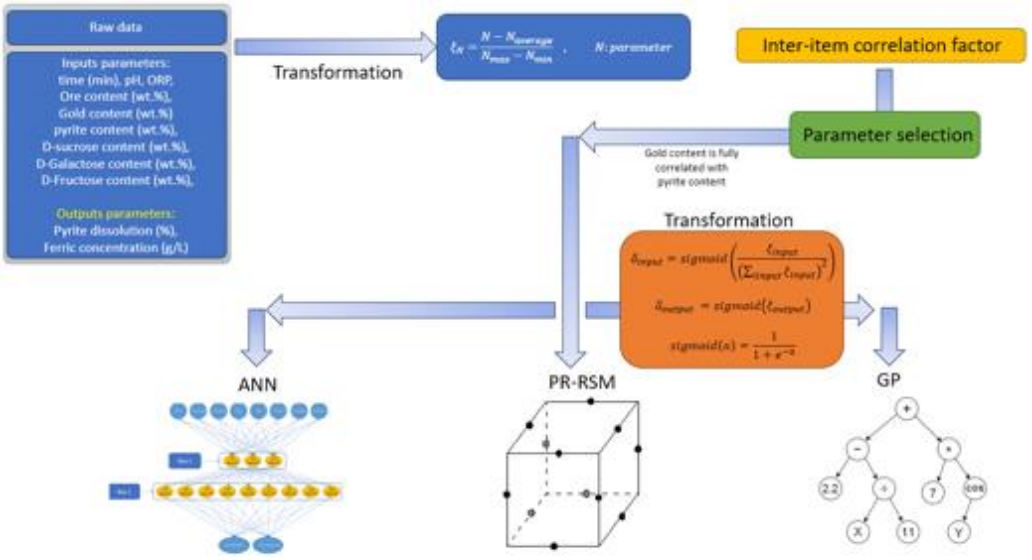

Figure C3. Schematic illustrating the preprocessing of the data for use in ANN, PR-RSM, and GP modeling.

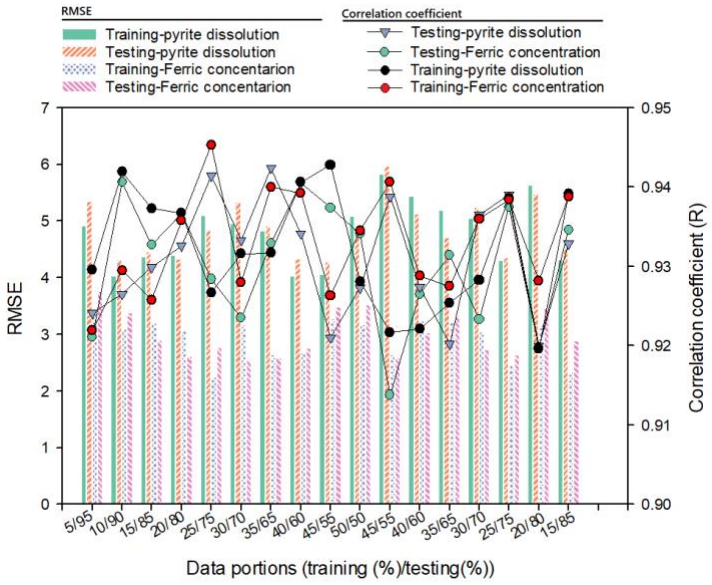

Figure C4. Data portioning study for selection of best correlation for pyrite dissolution and ferric concentration using Genetic Programming.

Table C6. Levels and the output data (Pyrite dissolution and Ferric concentration) for RSM-Box-Behnken Design of Experiment.

Experiment No.	Time	Pyrite content	Ore content	D-Gal	D-Suc	D-Fruc	Pyrite dissolution (%)	Ferric concentration (g/L)
1	-1	-1	0	0	0	0	0.4	0.005
2	1	-1	0	0	0	0	14	0.196
3	-1	1	0	0	0	0	18.2	1.11
4	1	1	0	0	0	0	0.4	10.543
5	-1	0	-1	0	0	0	14	0.322
6	1	0	-1	0	0	0	1.7	3.392
7	-1	0	1	0	0	0	27	0.683
8	1	0	1	0	0	0	1.6	7.756
9	-1	0	0	-1	0	0	31.3	0.452
10	1	0	0	-1	0	0	1.1	5.304
11	-1	0	0	1	0	0	22.3	0.463
12	1	0	0	1	0	0	1.3	5.195
13	-1	0	0	0	-1	0	26.3	0.446
14	1	0	0	0	-1	0	1.5	5.294
15	-1	0	0	0	1	0	27.9	0.528
16	1	0	0	0	1	0	1.3	5.4
17	-1	0	0	0	0	-1	25.9	0.447
18	1	0	0	0	0	-1	1.8	5.302
19	-1	0	0	0	0	1	32.9	0.53
20	1	0	0	0	0	1	1.3	5.281
21	0	-1	-1	0	0	0	26	0.183
22	0	1	-1	0	0	0	1.8	6.373
23	0	-1	1	0	0	0	31.8	0.98
24	0	1	1	0	0	0	15.6	15.012
25	0	-1	0	-1	0	0	30.2	0.208
26	0	1	0	-1	0	0	10.2	10.688
27	0	-1	0	1	0	0	24.2	0.273
28	0	1	0	1	0	0	13.6	10.876
29	0	-1	0	0	-1	0	25.5	0.209
30	0	1	0	0	-1	0	15	10.512
31	0	-1	0	0	1	0	27.2	0.304
32	0	1	0	0	1	0	13.4	12.2
33	0	-1	0	0	0	-1	25.1	0.213
34	0	1	0	0	0	-1	17.1	10.554
35	0	-1	0	0	0	1	31.3	0.263
36	0	1	0	0	0	1	13.4	12.122
37	0	0	-1	-1	0	0	25.2	3.242
38	0	0	1	-1	0	0	17.2	7.693
39	0	0	-1	1	0	0	30.3	3.316
40	0	0	1	1	0	0	30.2	7.809
41	0	0	-1	0	-1	0	21.9	3.2
42	0	0	1	0	-1	0	31.8	7.594
43	0	0	-1	0	1	0	23.4	3.837
44	0	0	1	0	1	0	29.7	8.581

45	0	0	-1	0	0	-1	21.5	3.226
46	0	0	1	0	0	-1	36.1	7.621
47	0	0	-1	0	0	1	27.1	3.608
48	0	0	1	0	0	1	29.9	8.544
49	0	0	0	-1	-1	0	21.6	4.911
50	0	0	0	1	-1	0	34.6	4.915
51	0	0	0	-1	1	0	26.8	5.401
52	0	0	0	1	1	0	26.1	5.421
53	0	0	0	-1	0	-1	28	4.938
54	0	0	0	1	0	-1	33	4.939
55	0	0	0	-1	0	1	34.7	5.233
56	0	0	0	1	0	1	26.2	5.283
57	0	0	0	0	-1	-1	28.1	4.896
58	0	0	0	0	1	-1	32	5.369
59	0	0	0	0	-1	1	33.9	5.174
60	0	0	0	0	1	1	25.7	5.941
61	0	0	0	0	0	0	32.6	4.956
62	0	0	0	0	0	0	31.6	4.956
63	0	0	0	0	0	0	37.9	4.956
64	0	0	0	0	0	0	26.9	4.956
65	0	0	0	0	0	0	26.9	4.956
66	0	0	0	0	0	0	26.9	4.956

Table C7. ANOVA and impact tests for pyrite dissolution and ferric ions concentration.

Source	ξ_7 (Pyrite dissolution)				ξ_8 (Ferric concentration)			
	$\frac{SSB}{DoF_1}$	$\frac{SSW}{DoF_2}$	$F\ ratio$	$Prob > F$	$\frac{SSB}{DoF_1}$	$\frac{SSW}{DoF_2}$	$F\ ratio$	$Prob > F$
Model	132.6	208.3	0.6	0.9010	14.8	2.0	7.4	0.00001*
Lack of fit	60.7	47.4	1.27	0.4371	6.7	4.8	1.41	0.3811
ξ_1	103.9	10.0	10.34	0.00013*	2180.5	62.5	34.9	0.00001*
ξ_2	238.8	5.8	41.4	0.00001*	741.7	108.2	6.9	0.0020*
ξ_3	46.1	11.9	3.88	0.0257*	92.2	128.8	0.7	0.4927
ξ_4	0.25	13.3	0.02	0.9817	61.5	129.8	0.5	0.6247
ξ_5	2.21	13.3	0.17	0.8441	73.6	129.4	0.6	0.5692
ξ_6	1.59	13.3	0.12	0.8871	210.0	125.1	1.7	0.1947
$\xi_1\xi_2$	90.3	2	43.4	0.0001*	896.6	19.8	45.3	0.0001*
$\xi_1\xi_3$	37.9	9.4	4	0.0008*	573	65.1	8.8	0.0001*
$\xi_1\xi_4$	26	11.1	2.4	0.0295*	566	66.2	8.6	0.0001*
$\xi_1\xi_5$	26.2	11.1	2.4	0.0280*	558	67.3	8.3	0.0001*
$\xi_1\xi_6$	26.1	11.1	2.3	0.0288*	583	63	9.2	0.0001*
$\xi_2\xi_3$	73.5	4.4	16.6	0.0001*	220	114.6	1.9	0.0731
$\xi_2\xi_4$	59.7	6.3	9.5	0.0001*	198	117	1.7	0.1211
$\xi_2\xi_5$	60.7	6.2	9.8	0.0001*	197	117.9	1.7	0.1248
$\xi_2\xi_6$	60.7	6.2	9.7	0.0001*	226	113.9	2.0	0.0647
$\xi_3\xi_4$	11.7	13.1	0.9	0.5285	67.3	136.9	0.5	0.8554
$\xi_3\xi_5$	12.3	13	0.9	0.4856	47.4	138.9	0.3	0.9458
$\xi_3\xi_6$	12.2	13	0.9	0.4964	88.5	133.2	0.7	0.7199
$\xi_4\xi_5$	0.8	13.9	0.06	0.9974	72.3	132.3	0.5	0.7406
$\xi_4\xi_6$	0.7	13.9	0.05	0.9985	133	127.2	1.0	0.3994
$\xi_5\xi_6$	1.7	13.9	0.1	0.9869	134	127	1.0	0.3939

SSB: Sum of Squares Between the levels

SSW: Sum of Squares Within the levels

DOF_1=Levels -1

DOF_1=Observations-Levels

*Statistically significant

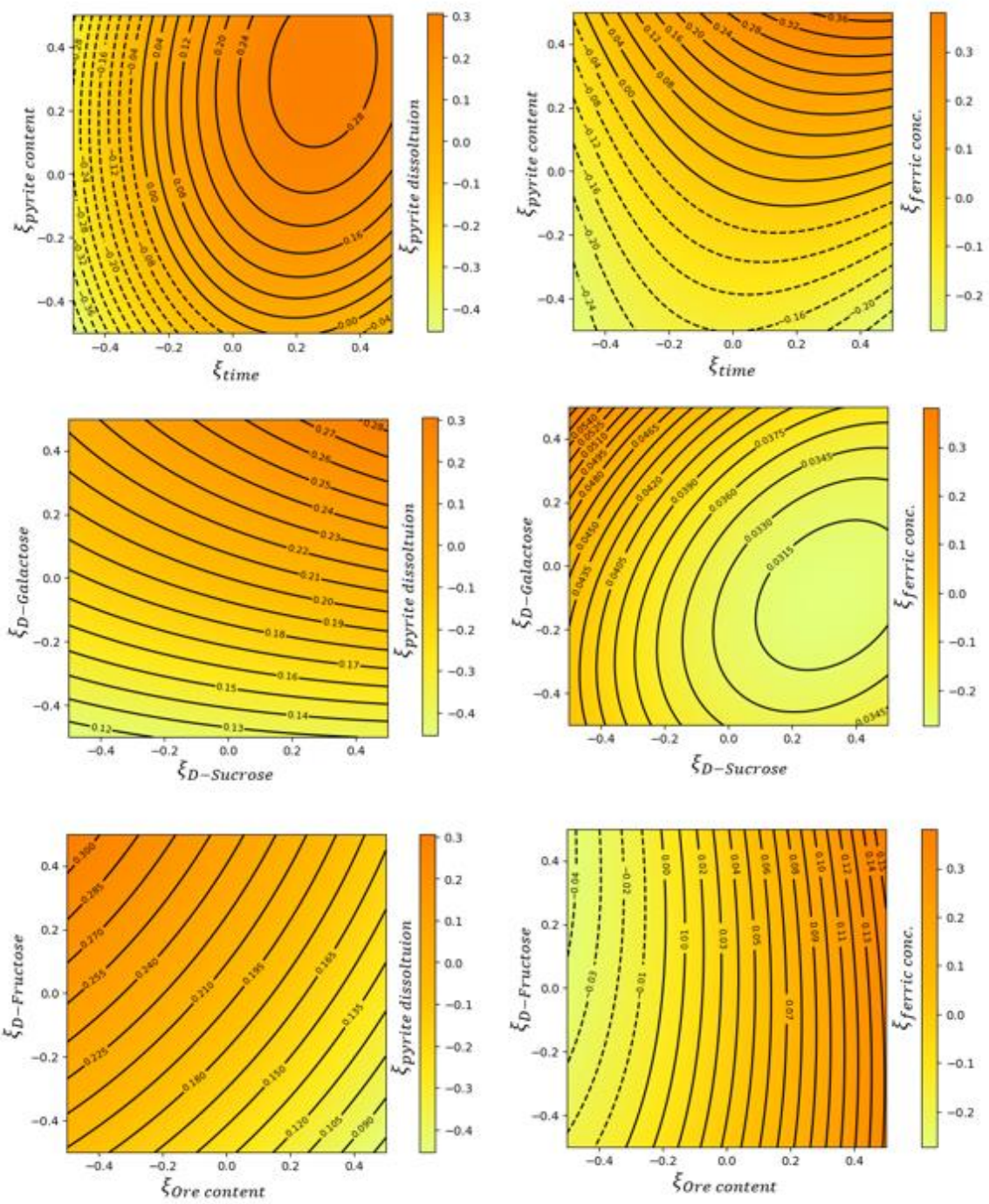

Figure C5. Results of model prediction obtained using RSM. For each graph the values of other parameters (i) are set to average values (ξ_i=0, $i \neq$ parameters presented in each graph).

Table C8. The results of model architecture for considering input variable set.

Neuron # in second layer	Model No.1	Model No.2	Model No.3	Model No.4
1	R=0.760 RMSE=0.1245 AIC= 1.19×10^4	R=0.923 RMSE=0.0752 AIC=7.87×10^3	R=0.944 RMSE=0.0567 AIC=5.99×10^3	R=0.925 RMSE=0.0560 AIC=5.97×10^3
2	R=0.812 RMSE=0.1218 AIC=1.18×10^4	R=0.949 RMSE=0.0765 AIC=7.17×10^3	R=0.970 RMSE=0.0675 AIC=5.32×10^3	R=0.965 RMSE=0.0554 AIC=5.12×10^3
3	R=0.844 RMSE=0.1132 AIC=1.15×10^4	R=0.956 RMSE=0.0592 AIC=4.45×10^3	R=0.982 RMSE=0.0568 AIC=5.12×10^3	R=0.989 RMSE=0.0455 AIC=3.34×10^3
4	R=0.849 RMSE=0.1175 AIC=1.13×10^4	R=0.986 RMSE=0.0685 AIC=5.38×10^3	R=0.983 RMSE=0.0598 AIC=3.11×10^3	R=0.981 RMSE=0.0749 AIC=4.15×10^3
5	R=0.812 RMSE=0.0989 AIC=1.13×10^4	R=0.977 RMSE=0.0573 AIC=4.34×10^3	R=0.978 RMSE=0.0658 AIC=2.90×10^3	R=0.980 RMSE=0.0544 AIC=3.61×10^3
6	R=0.833 RMSE=0.1218 AIC=1.13×10^4	R=0.945 RMSE=0.0630 AIC=3.96×10^3	R=0.944 RMSE=0.0655 AIC=3.27×10^3	R=0.975 RMSE=0.0541 AIC=3.69×10^3
7	R=0.845 RMSE=0.1027 AIC=1.13×10^4	R=0.948 RMSE=0.0593 AIC=4.77×10^3	R=0.964 RMSE=0.0657 AIC=2.18×10^3	R=0.965 RMSE=0.0496 AIC=2.99×10^3
8	R=0.855 RMSE=0.0981 AIC=1.11×10^4	R=0.944 RMSE=0.0453 AIC=2.77×10^3	R=0.987 RMSE=0.0567 AIC=2.61×10^3	R=0.971 RMSE=0.0478 AIC=2.94×10^3
9	R=0.843 RMSE=0.0967 AIC=1.13×10^4	R=0.981 RMSE=0.0591 AIC=2.12×10^3	R=0.987 RMSE=0.0543 AIC=1.86×10^3	R=0.996 RMSE=0.0335 AIC=1.41×10^3
10	R=0.831 RMSE=0.0989 AIC=1.12×10^4	R=0.978 RMSE=0.0731 AIC=2.57×10^3	R=0.988 RMSE=0.0463 AIC=2.21×10^3	R=0.987 RMSE=0.0356 AIC=2.18×10^3

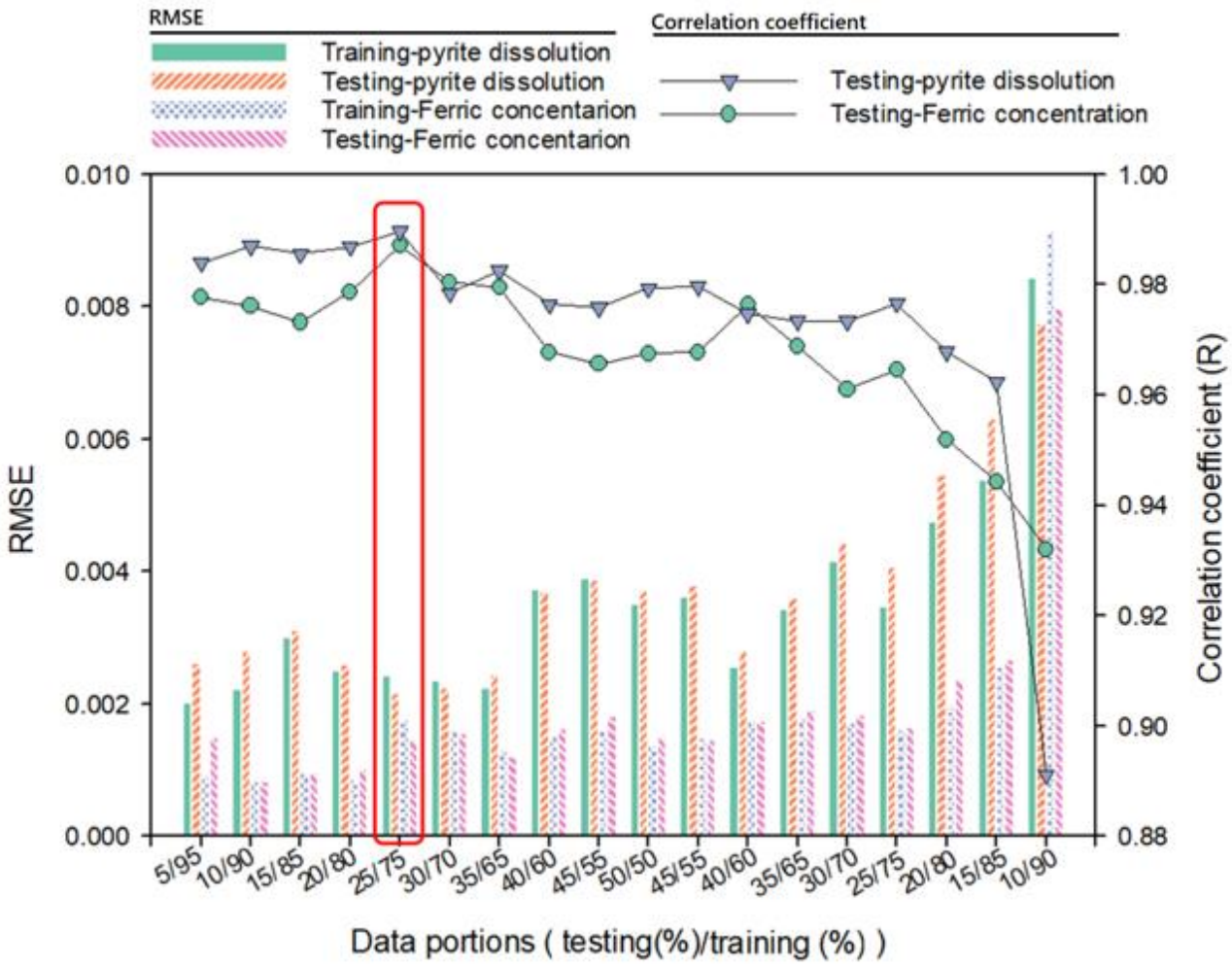

Figure C6. Results for optimization (RMSE and Correlation coefficient) of data portioning in ANN model.

Table C9. Weights and biases for nodes of calculation in ANN model ($n_{\text{layer number, node number}}$).

First hidden layer									
nodes \ inputs	ξ_{time}	$\xi_{pyrite\ content}$	$\xi_{Ore\ content}$	ξ_{pH}	ξ_{ORP}	ξ_{D-gal}	ξ_{D-suc}	ξ_{D-fru}	Bias
$n_{1,1}$	0.7276	-25.4817	0.0691	0.4623	3.7543	-0.4294	-0.4742	-0.5566	-9.7483
$n_{1,2}$	0.6564	1.9102	0.9047	1.0493	4.8260	-0.1747	0.2211	0.0710	-2.8403
$n_{1,3}$	0.5030	0.1766	-0.3540	0.7945	5.4305	-0.1822	0.1949	0.0636	-2.0042

Second hidden layer				
nodes \ inputs	$n_{1,1}$	$n_{1,2}$	$n_{1,3}$	Bias
$n_{2,1}$	1.2076	1.0300	-2.6943	-1.5863
$n_{2,2}$	-2.0414	14.4376	1.5439	0.7578
$n_{2,3}$	-1.4280	1.7079	1.0750	-1.4594
$n_{2,4}$	-0.9759	3.8010	-1.8038	-1.7446
$n_{2,5}$	0.9065	1.3440	1.0677	-0.9521
$n_{2,6}$	-2.4843	6.5506	-7.0258	-2.1124
$n_{2,7}$	7.3655	-4.0543	0.3281	1.4472
$n_{2,8}$	1.3833	-1.0805	0.0908	0.5946
$n_{2,9}$	-7.7253	-9.1630	-1.4995	-0.3642

Output layer										
outputs \ inputs	$n_{2,1}$	$n_{2,2}$	$n_{2,3}$	$n_{2,4}$	$n_{2,5}$	$n_{2,6}$	$n_{2,7}$	$n_{2,8}$	$n_{2,9}$	Bias
$\xi_{pyrite\ dissoultion}$	1.4682	-1.0303	-0.2917	1.2843	0.9457	-1.0383	-0.2846	0.6214	-1.4167	0.2150
$\xi_{Ferric\ conc.}$	-0.9115	0.4363	-0.3578	1.0139	-0.5425	0.9709	-0.7661	0.6277	-0.7382	0.1575

Appendix D

Table D1. Elemental analysis data (contents are in g/ton) for two types of ore samples (results are from ICP).

HGOS ore sample						
Fe	**As**	**Al**	**Zn**	**K**	**Ca**	**Mn**
4.8×10^4	1.16×10^4	6.5×10^3	2.05×10^3	1.8×10^3	1.3×10^3	735
Mg	**Na**	**Cu**	**Ni**	**Cr**	**Cd**	**Au**
654	1.6×10^4	225	195	52	7.5	5.4
LGOS ore sample						
Na	**Ti**	**Sr**	**Zr**	**Zn**	**Ni**	**Cu**
2.0×10^4	1.4×10^3	2.0×10^2	1.1×10^2	668	56	54
Ce	**Cr**	**V**	**La**	**Pb**	**Mo**	**Co**
49	46	46	25	21	8.5	14
Th	**Sc**	**Li**	**U**	**As**	**Y**	**Sb**
10	5.7	5	<5	4.1	4	3
Be	**Yb**	**Ag**	**Cd**	**Au**		
1	0.7	0.36	0.3	447 ppb		

Table D2. Results of XRD analysis HGOS and LGOS samples.

XRD results of the HGOS sample.			
Phases		Crystal system	Semi-quantitative (%)
Name	Chemical Formula		
Quartz, syn	SiO_2	Hexagonal	23
Ankerite	$a(Mg_{0.67}Fe_{0.33}^{+2})(CO_3)_2$		48
Chlorite	$(Mg, Fe)_6(Si,Al)_4O_{10}(OH)_8$		9
Mica	$KAl_2(Si_3Al)O_{10}(OH,F)_2$		7.7
Plagioclase	$NaAlSi_3O_8$		2.2
Alkali feldspar	$K(AlSi_3O_8)$		1.2
-	$Bi_{39}InTe_{58.6}S$	Rhombo.H.axes	0.2
-	As_5Te_7I	Monoclinic	1.5
Pyrite	FeS_2	Cubic	7.2
XRD results of the LGOS sample (concentrated by Bromoform for accurate detection).			
Phases		Crystal system	Semi-quantitative (%)
Name	Chemical Formula		
Ankerite	$a(Mg_{0.67}Fe_{0.33}^{+2})(CO_3)_2$	Rhombo.H.axes	58.1
Quartz, syn	SiO_2	Hexagonal	10.5
Chlorite	$(Mg, Fe)_6(Si,Al)_4O_{10}(OH)_8$	Monoclinic	10.4
Mica	$Kal_2(Si_3Al)O_{10}(OH,F)_2$	Monoclinic	8.3
Mixed layered clay mineral	$Kal_4(Si,Al)_8O_{10}(OH)_4 \cdot 4H_2O$	-	7.2
Plagioclase	$NaAlSi_3O_8$	Triclinic	2.8
Alkali feldspar	$K(AlSi_3O_8)$	Monoclinic	1.5
Pyrite	FeS_2	Cubic	1.5

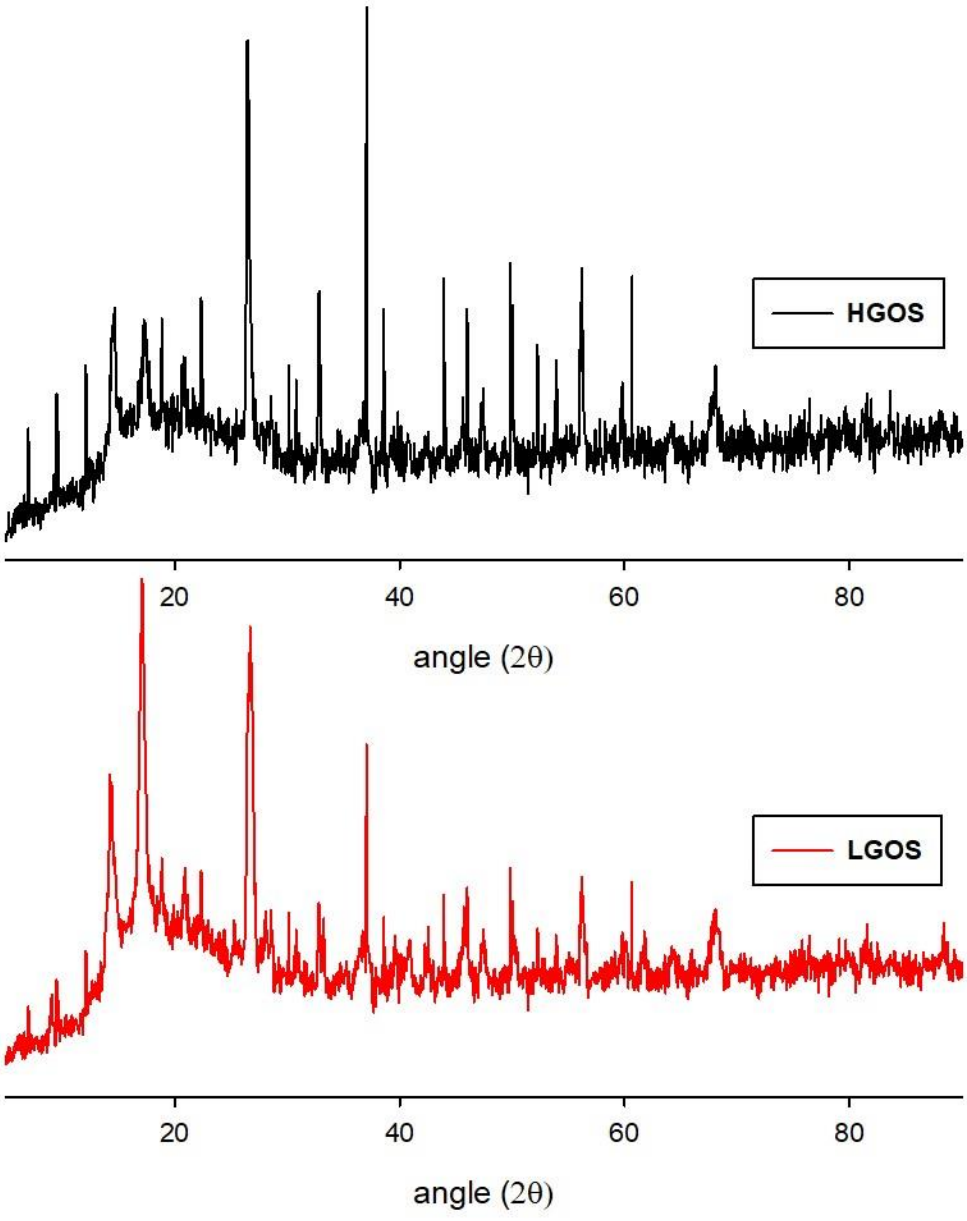

Figure D1. Plot of XRD for both HGOS and LGOS.

Table D3. Results of XRF analysis HGOS and LGOS samples (wt.%).

XRF results of the LGOS						
SiO_2	**Al_2O_3**	**BaO**	**CaO**	**Fe_2O_3**	**K_2O**	**MgO**
66.20	13.20	0.05	4.01	5.56	2.61	1.69
MnO	**Na_2O**	**P_2O_5**	**SO_3**	**TiO_2**	**LOI**	
0.08	2.49	0.12	1.04	0.37	2.58	
XRF results of the HGOS						
SiO_2	**Al_2O_3**	**BaO**	**CaO**	**Fe_2O_3**	**K_2O**	**MgO**
36.93	7.61	0.03	2.33	12.02	5.84	9.55
MnO	**Na_2O**	**P_2O_5**	**SO_3**	**TiO_2**	**LOI**	
0.33	11.02	0.14	1.5	0.86	11.85	

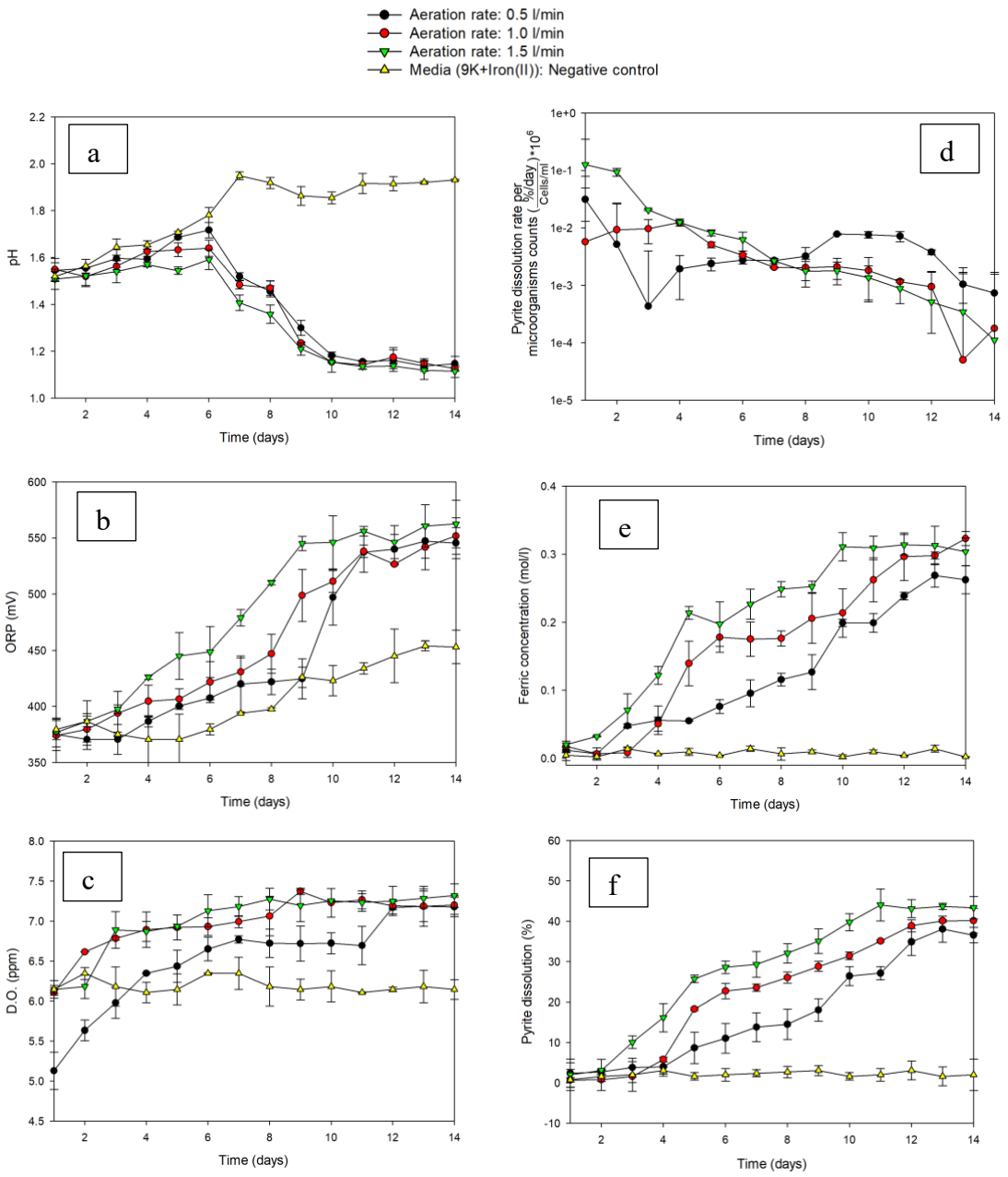

Figure D2. Plot of a, pH, b, ORP, c, D.O. and d, pyrite dissolution rate per microorganisms count, e, ferric concentration, and f, pyrite dissolution vs time for HGSO sample under stirred tank reactor biooxidation (aeration rate of negative control: 1.5 L/min).

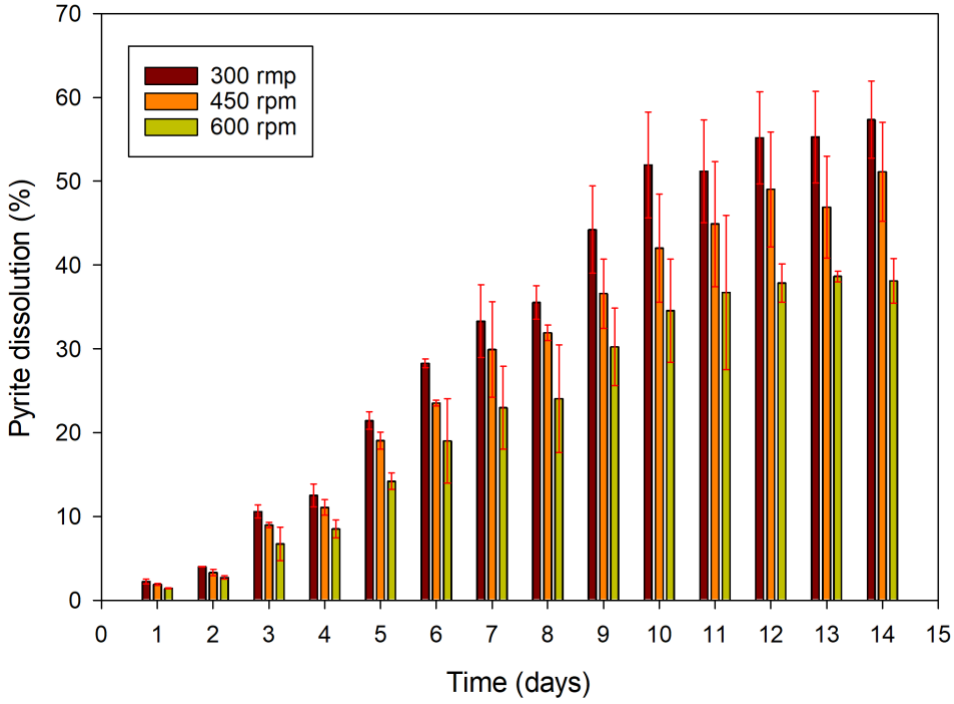

Figure D3. Pyrite dissolution vs time at different agitation rates for HGOS in stirred tank reactor.

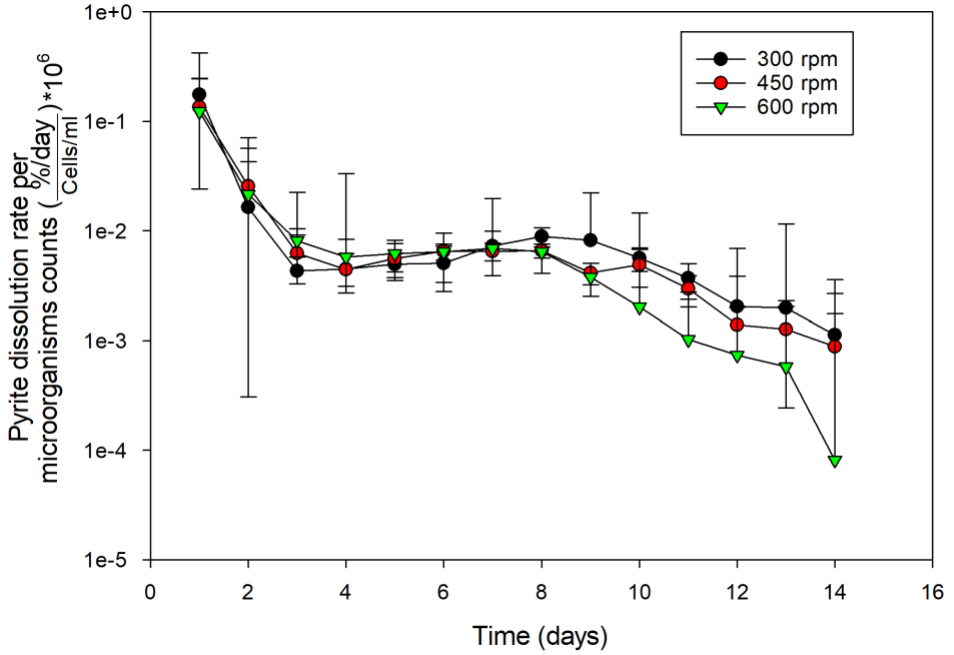

Figure D4. Plot of pyrite dissolution rate per microorganisms counts vs time at different agitation rate for HGOS in stirred tank reactor.

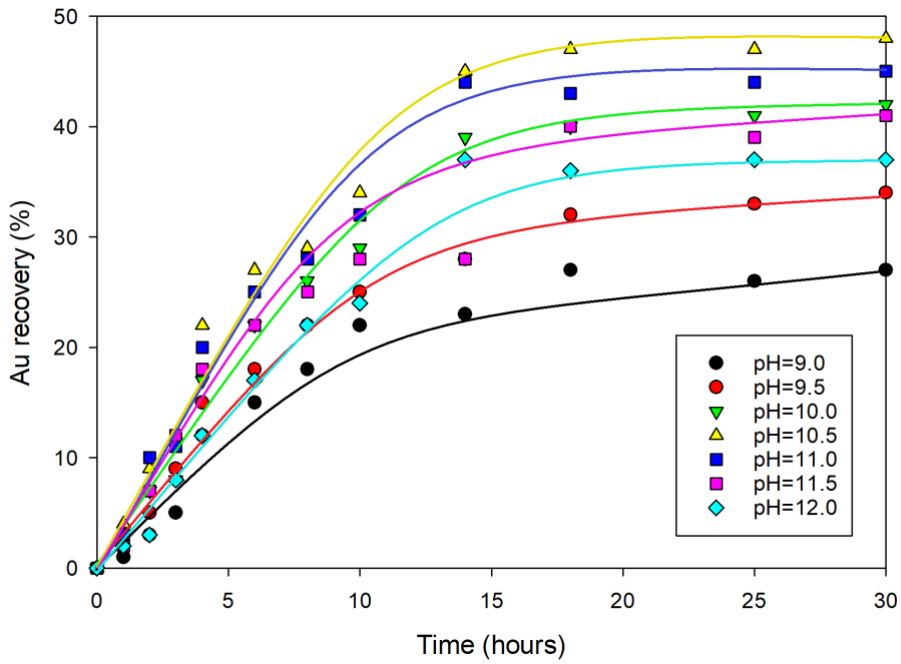

Figure D5. Plot of gold recovery using cyanidation (2000 ppm sodium cyanide) vs time at different pH.

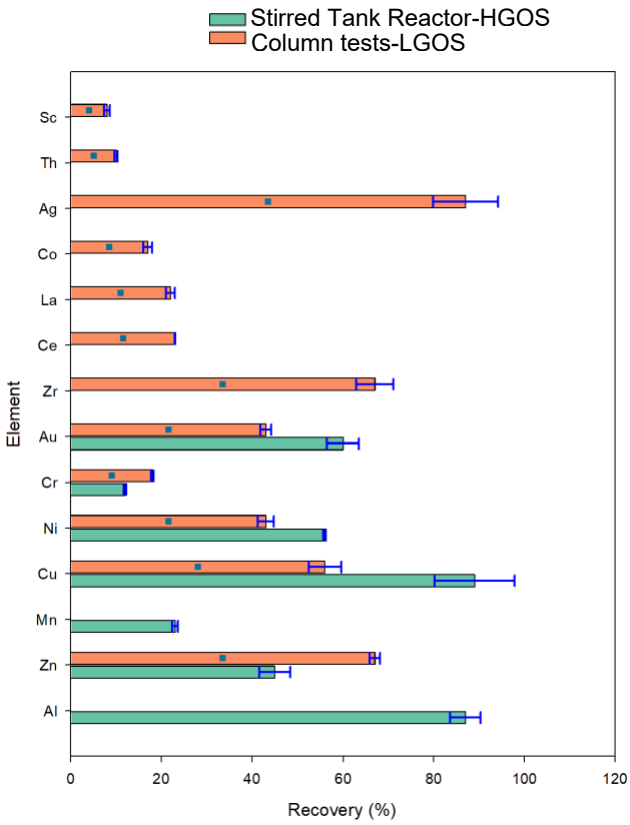

Figure D6. Plot of gold recovery using cyanidation vs pH and NaCN concentration for pretreated, a, LGOS using column test, b, HGOS using stirred tank reactor. c, other metal recovery using cyanidation and after both pretreatment methods.

Appendix E

Table E1. Average size distribution of saw dust spruce.

Mesh	Size (mm)	Fraction (%)	Cumulative (%)
3	6.73	5	15
7	2.83	8	13
10	2.00	19	32
18	1.00	22	54
35	0.50	24	78
40	0.40	15	93
50	0.30	7	100

Figure E1. *Incubation of Aspergillus niger for production of enzyme.*

The enzyme activity is measured by using ABTS in presence of Horseradish peroxidase using the following reaction. In this reaction the color of solution change from bright green to blue-green and the reaction rate and hydrogen peroxide production is quantized by using UV-Visible spectroscopy at wavelength of 420 nm.

$$O_2 + D - Galactose \xrightarrow{GOD} \beta - D - Glucono - \delta Lactone + H_2O_2$$

$$ABTS + 2H_2O_2 \xrightarrow{Horseradish\ Peroxidase} ABTS_{oxadized} + H_2O$$

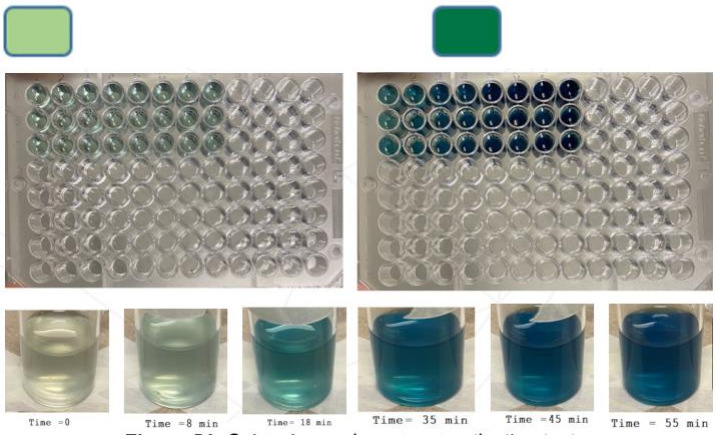

Figure E2. *Enzyme activity assay.*

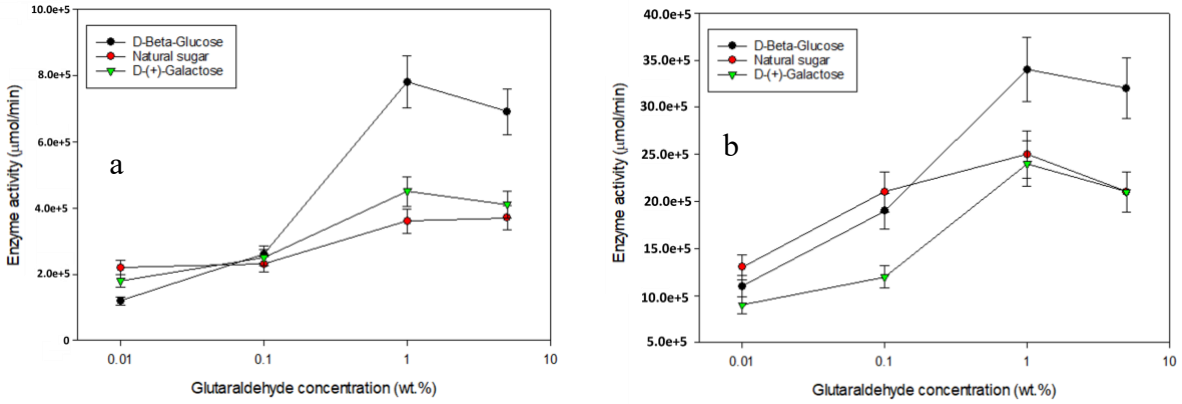

Figure E3. Effect of glutaraldehyde concentration on enzyme activity (80 mM D-b-golucose as substrate and 1.5 g of immobilized enzyme on support) for a, citric acid and b,$NaClO/H_2O_2$-assisted method of surface modification. Here natural sugar is molasses that contain mixture of sugar types including sucrose, glucose, and fructose).

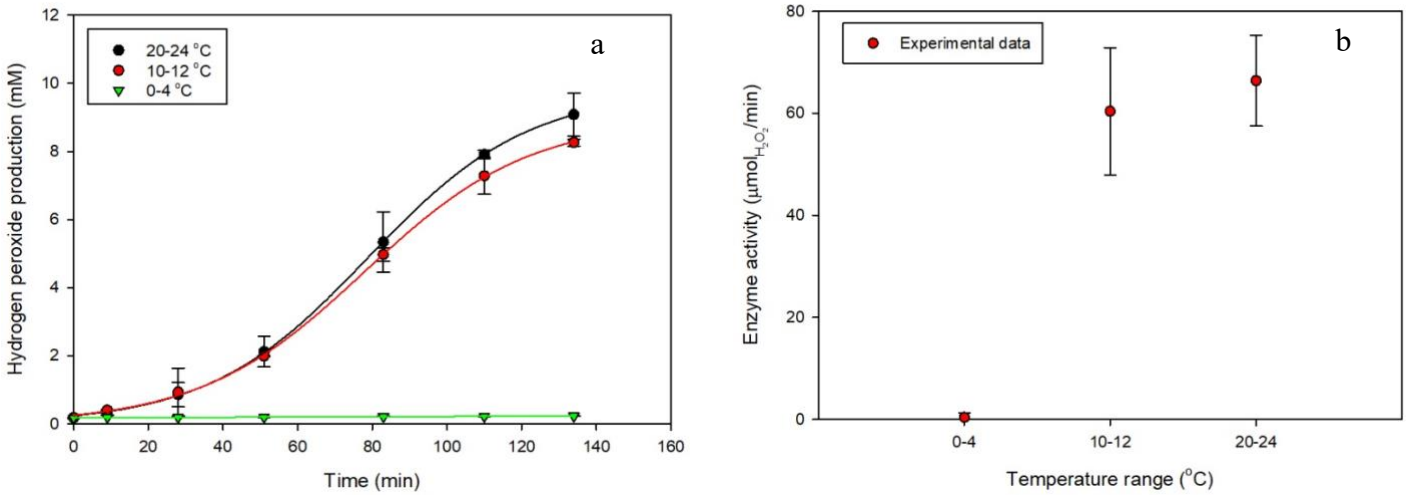

Figure E4. a) Hydrogen peroxide production vs time for different temperatures; b) enzyme activity for different temperatures (substrate: 80 mM) for natural sugar.

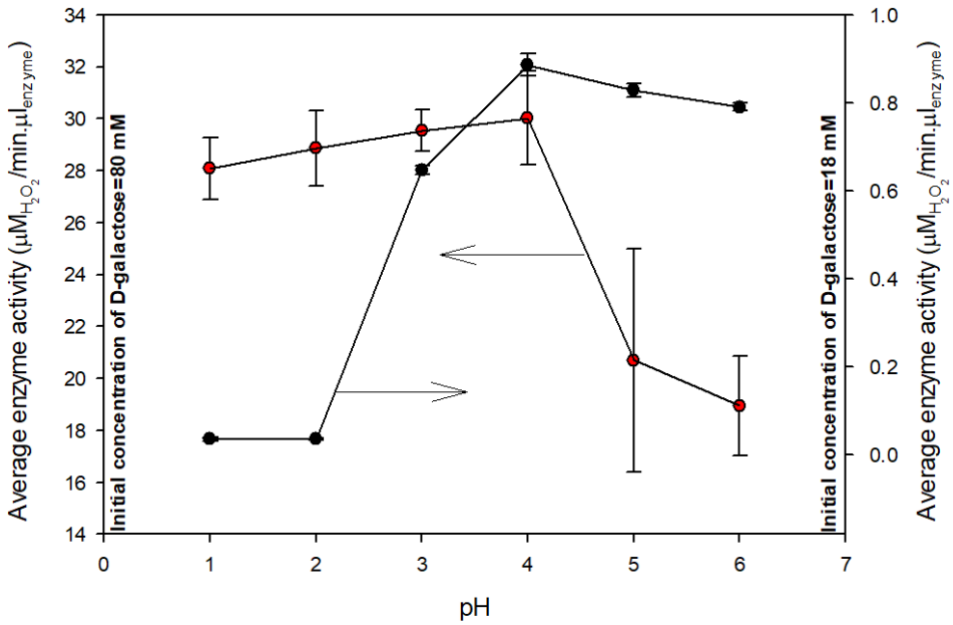

Figure E5. Enzyme activity vs pH and initial D-galactose concentration of 18 and 80 mM (100 ml of enzyme cocktail) for natural sugar.

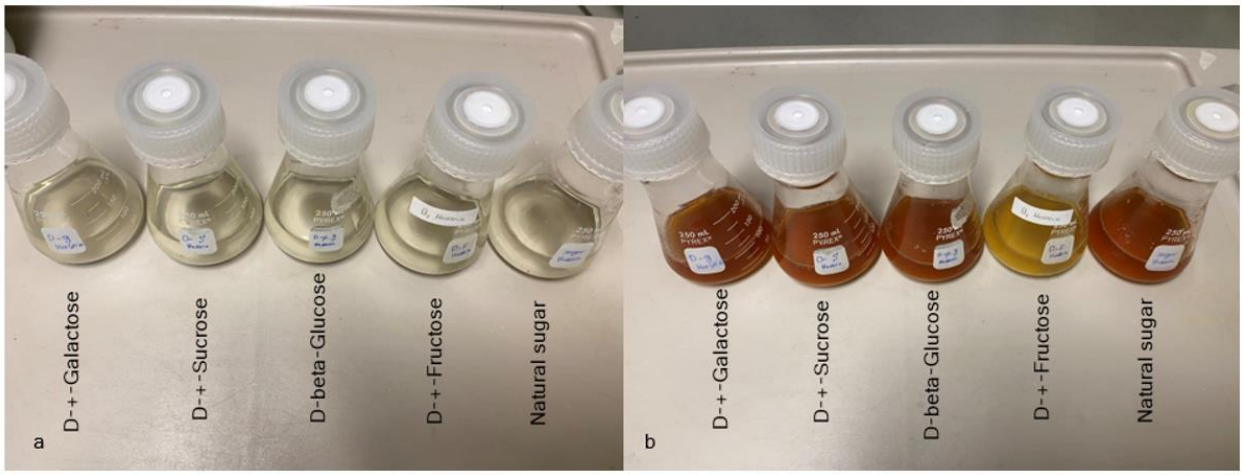

Figure E6. Images of the addition of different substrate (80 mM substrate and 1 ml of enzyme cocktail in 100 ml of solution) for iron (III) production in presence of ferrous ions a, before starting bio-Fenton reaction and b, after completion of bio-Fenton reaction.